

**The Application of Geophysical Wireline Logs for Porosity and Permeability
Characterisation of Coal Seams for Coal Bed Methane Evaluation: Waterberg
Basin, South Africa**

A Thesis in Petroleum Geosciences

By

ACHU TEUMAHJI NIMUNO

**Submitted in partial fulfilment of the requirements for the degree of
Magister Scientiae in the Department of Earth Sciences,
University of the Western Cape**



**UNIVERSITY of the
WESTERN CAPE**

Supervised by Dr. Mimonitu Opuwari

Co- Supervised by Prof. Jan Van Bever Donker

ABSTRACT

The Application of Geophysical Wireline Logs for Porosity and Permeability Characterisation of Coal Seams for Coal Bed Methane Evaluation: Waterberg Basin, South Africa

T. N. ACHU

The fracture porosity and permeability of the Beaufort Seam 1 (BS1) and Ecca coal seams of the Waterberg Basin have been comprehensively characterised with the aid of geophysical wire-line logs. The main aim of the thesis was to estimate the porosity and permeability of the coal seams using down-hole wire-line data; comparing results from injection falloff test to establish the validity of the technique as a fast and effective method.

The study area is the largely under explored Karoo-aged, fault bounded Waterberg basin Located in the Limpopo Province of South Africa.

The study employed mainly the density and dual lateral resistivity logging data (Las format) from eight wells (WTB45, WTB48, WTB56, WTB58, WTB62, WTB65, WTB70 and WTB72). Density logging data was used for coal identification and fracture porosity estimation while fracture permeability was estimated from dual laterallog resistivity data. Analysis of fracture porosity required coal cementation indices and fracture width as an input parameter. These were estimated with the aid of water pump out test data, coal quality and gas analysis data provided by Anglo Coal in addition to the above mention logs.

The collection of sheet coal model was used to represent anisotropic coal reservoirs with non-uniform fracture system was used to represent these coals. The mathematical formulas used to estimate both fracture porosity and permeability took into account the above coal model. The theoretical formulas are a modification from both Darcy's equation and Archie's equations.

The coal seams were encountered at depths ranging from 198m to 385m in the wells and were marked by low density and very high resistivity. From the estimated results the coal reservoirs are characterised by high cementation indices ranging from 0.82 to 2.42, very low fracture porosity and low fracture permeability. Estimated results show that coal reservoir fracture porosity ranged from 0.0002% to 0.33% for both BS1 and Ecca seams. Estimated results also show that coal reservoir permeability ranged from 0.0045mD to 6.05mD in the BS1 formation and from 0.01 to 0.107mD in the Ecca. Results when compared with those of injection falloff test shows that the estimated permeability is slightly lower as expected since the model did not account for coal anisopropy. The fracture permeability was found to decrease with increase in vitrinite content, coal rank, coal burial depth and increases with increase in inertinite content. On a basinal scale the model estimated permeability was

found to increase slightly from the east to the west of the basin. The porosity decreases with increase cementation index for deeper coal seams and increases with increase cementation index for shallower coal seams.



DECLARATION

I declare that The Application of Geophysical Wireline Logs for Porosity and Permeability Characterisation of Coal Seams for Coal Bed Methane Evaluation: Waterberg Basin, South Africa is my own work, that it has not been submitted before for any degree or examination in any other university, and that all the sources I have used or quoted have been indicted and acknowledged by means of complete references.”

Achu Teumahji Nimuno

November 2011

.....

Sign



Acknowledgment

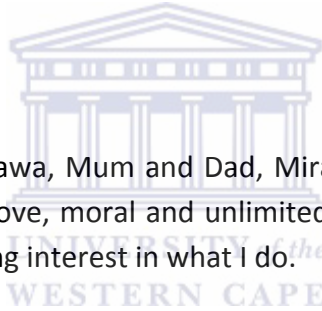
My profound gratitude goes to my Supervisor Dr. Mimonitu Opuwari for his time and effort in reading through my work, criticizing and making corrections and suggestions even on tight datelines.

Prof. Jan Van Bever Donker my co-supervisor thanks for securing funding for my work.

To Inkaba ye Africa for their financial support to the project during my last year of Study.

Many thanks to Anglo Coal for data provision; most especially to Johan Koekermoer, Chief geologist at Waterberg CBM project and his team for their warmth welcome during my stay at Lephalale, for taking out time to sort out my data and for the constructive input offered whenever needed.

To my family (Mr and Mrs Tichaawa, Mum and Dad, Mirabel and Cornel), I will be forever grateful for your unconditional Love, moral and unlimited financial support throughout my studies. Thanks for always showing interest in what I do.




To my Niece Mercy Tichaawa for always giving me a good reason not to sleep in the office.

To my Colleagues, Emmanuel, Thierry, Christopher and Shaun for their academic guidance.

To God Almighty for the strength to carry me through till the end.

TABLE OF CONTENT

TITLE PAGE.....	I
ABSTRACT.....	II
DECLARATION.....	IV
ACKNOWLEDGEMENT.....	V
TABLE OF CONTENTS.....	VI
LIST OF TABLES.....	XII
LIST OF FIGURES.....	XIII
LIST OF APPENDICES.....	VIV
KEYWORDS.....	XIV
	
CHAPTER 1: GENERAL INTRODUCTION.....	1
1.1 Introduction.....	1
1.2 Rationale.....	4
1.3 Objectives/Scope.....	5
1.4 Location of Study area.....	6
CHAPTER 2: GEOLOGY OF THE STUDY AREA.....	8
2.1 Geological Setting.....	8
2.2 Tectonic Setting and Basin Evolution.....	8
2.3 Stratigraphic Setting.....	12
2.3.1 Karoo Sequence.....	12
2.3.1.1 Depositional System of Karoo.....	13
2.3.1.2 Karoo Stratigraphy.....	14
2.3.1.2.1 The Dwyka.....	14
2.3.1.2.2 The Ecca.....	16

2.3.1.2.3 The Beaufort.....	17
2.3.1.2.4 The Stormberg.....	18
2.3.1.2.5 The Drakensberg Volcanics.....	18
2.3.1.3 Stratigraphy of Ellisras Basin.....	19
2.3.1.3.1 Dwyka of Ellisras Basin.....	20
2.3.1.3.1.1 The Lower Dwyka.....	21
2.3.1.3.1.2 The Upper Dwyka.....	21
2.3.1.3.2 The Ecca of the Ellisras Basin.....	22
2.3.1.3.2.1 The Lower Ecca of the Ellisras Basin.....	22
2.3.1.3.2.1.1 The Goedgedacht Formation.....	23
2.3.1.3.2.2 The Middle Ecca of the Elisras Basin.....	23
2.3.1.3.2.3 The Upper Ecca of the Ellisras Basin.....	24
2.3.1.3.3 The Beaufort Formation.....	25
2.3.1.3.4 The Stormberg Group.....	26
2.3.1.3.4.1 The Greenwich Formation of the Ellisras Basin.....	26
2.3.1.3.4.2 The Lisbon Formation of the Ellisras Basin.....	26
2.3.1.3.4.3 The Clarens Formation of the Ellisras Basin.....	26
2.3.1.4 Coal Petrography of the Ellisras Basin.....	27
2.3.1.4.1 Paleao – Flora Distribution in Karoo.....	27
2.3.1.4.2 Maceral Content.....	28
2.3.1.5 Coal Ranking.....	29
CHAPTER 3: LITERATURE REVIEW.....	33
3.1 Review of Coal Geology.....	33
3.1.1 Formation of Coal.....	33
3.1.2 Coal Rank.....	34
3.1.3 Coal Type of Lithotype.....	36

3.1.3.1 Humic Coal.....	36
3.1.3.2 Sapropelic Coal.....	37
3.1.4 Coal Maceral.....	38
3.1.4.1 Vitrinite Group.....	39
3.1.4.2 Liptinite (Exenite) Group.....	39
3.1.4.3 Inertinite Group.....	40
3.1.5 Micro Lithotype.....	40
3.1.6 Moisture and Volatile Material in Coal.....	41
3.1.7 Carbon and Hydrogen.....	42
3.1.8 Fixed Carbon.....	42
3.1.9 Coal Distribution and Age.....	42
3.2 Coal Bed Methane Resource.....	44
3.2.1 Recent Trends.....	45
3.2.2 Coal Bed Methane Production.....	47
3.2.4 Coal Petrophysical Parameters.....	49
3.2.4.1 Coal Fractures or Cleats.....	49
3.2.4.1.1 Origin of Cleats.....	50
3.2.5 Porosity and Permeability of Coal.....	51
3.2.5.1 Coal Porosity.....	51
3.2.5.1.1 Coal Pore Structure.....	52
3.2.5.2 Gas Adsorption in Coal.....	53
3.2.5.2.1 Preferential Adsorption of Carbondioxide to Methane	54
3.2.5.2.2 Coal Type and Adsorption Capacity.....	55
3.2.5.2.3 Maceral Content and Adsorption Capacity.....	55
3.2.5.2.4 Mineral Matter and Gas Adsorption.....	56
3.2.5.2.5 Ash Content and Gas Adsorption.....	56



3.2.5.2.6 Grain Size and Gas Adsorption.....	56
3.2.5.2.7 Physical Parameters Affecting Gas Adsorption Experiments.....	56
3.2.5.2.7.1 Grain Size.....	57
3.2.5.2.7.2 Temperature.....	57
3.2.5.2.7.3 Moisture Content.....	57
3.2.5.3 Coal Permeability and Fluid Flow.....	58
3.2.5.3.1 Gas Diffusion in Coal and Fick’s Law.....	60
3.2.5.3.2 Darcy Flow/Cleat Permeability.....	61
3.2.5.3.2.1 Permeability and Rank Variation.....	62
3.2.5.3.2.2 Permeability and Organic matter Variation.....	62
3.2.5.3.2.3 Permeability and Pressure Variation.....	62
3.2.5.3.2.4 Variation in Permeability due to Gas Sorption.....	63
3.4 Coal Porosity and Permeability Measurements.....	64
3.4.1 Laboratory Based Simulation Experiments.....	64
3.4.1.1 Porosity Measurements.....	65
3.4.1.1.1 Miscible Drive Technique.....	65
3.4.1.1.2 Multi Scale Imaging.....	66
3.4.1.1.3 Other porosity measurement Technique.....	67
3.4.1.2 Permeability Measurement.....	68
3.4.1.2.1 Laboratory Measurement of Permeability.....	68
3.4.1.2.1.1 Steady State Method.....	69
3.4.1.2.1.1 Unsteady State Method.....	69
3.4.1.2.2 Field Permeability Measurements.....	70
3.4.1.2.2.1 Multi Well Interference Test.....	71
3.4.1.2.2.2 Pressure Build Up Test (PBU).....	71
3.4.1.2.2.3 Drill Stem Test.....	71

3.4.1.2.2.4 Slug Test.....	71
3.4.1.2.2.5 Injection Fall off Test.....	72
3.4.1.2.2.5.1 Tank Test.....	72
3.4.1.2.2.5.2 Below Fracture Pressure Falloff Test (BFP-IFT).....	72
3.4.1.2.2.5.3 Diagnostic Fracture Injection Test (DFIT).....	72
3.5 Geophysical Wire-line Logs.....	74
3.5.1 Classification of well Logs.....	75
3.5.2 Principles and Characteristics of Interested Wire-line Logs.....	75
3.5.2.1 Nuclear or Radioactive Logs.....	75
3.5.2.1.1 Natural Gamma Ray Log (GR).....	76
3.5.2.1.2 Density Log (RHOB).....	76
3.5.2.1.3 Neutron Log.....	77
3.5.2.2 Electrical Logs.....	78
3.5.2.2.1 Self Potential (SP).....	78
3.5.2.2.2 Electrical Resistivity Logs.....	79
3.5.2.2.2.1 Dual Laterologs.....	79
3.5.2.2.2.3 Acoustic Log/Sonic Log	80
CHAPTER 4: ANALYSIS AND RESULTS	81
4.1 Well Selection.....	81
4.1.1 Zone Delineation.....	81
4.2 Petrographic Maceral Analysis.....	84
4.2.1. Results of Petrographic Maceral Analysis.....	85
4.3 Permeability Pressure Transient Well Test Analysis.....	86
4.3.1. Equipment and Experimental Procedure.....	87
4.4 Geophysical Wire-Line Log Analysis.....	90

4.4.1 Coal Identification.....	91
4.4.2 Fracture Permeability Estimation from Logging Data.....	99
4.4.2.1 Coal Permeability models.....	100
4.4.3 Fracture Porosity estimation from logging data.....	101
4.4.3.1 Formation Water Analysis.....	102
4.4.3.2 Gas and Coal Quality Analysis.....	103
4.4.3.3 Fracture Width Estimation from Resistivity Logging Data.....	107
4.4.3.4 Cementation Exponent estimation from Logging Data.....	110
4.4.4 Results of Cementation Exponent, Fracture Width, Fracture porosity and Fracture Permeability Analysis.....	111
CHAPTER 5: DISCUSSION AND INTERPRETATION.....	119
5.1 Burial Depth and coal Thickness.....	119
5.1.1 Depth controlled Permeability and Porosity.....	123
5.2 Maceral Content and Vitrinite reflectance controlled Permeability.....	130
5.3 Reservoir Porosity and permeability – Fracture width and Cementation Variation.....	136
5.3.1 Cementation index vs fracture width variation.....	136
5.3.2 Permeability vs Cementation Index Variation.....	140
5.3.3 Permeability vs resistivity relationship.....	144
5.3.4 Log derived permeability and field derived Permeability Comparison.....	152
CHAPTER 6: CONCLUSION.....	154
REFERENCES.....	155
APPENDIX.....	170

List of Tables

Table 3.1	ASTM Coal rank.35
Table 3.2	Stoope's Heerlen Classification of Maceral Groups, Macerals and Sub-macerals of Hard Coal.38
Table 3.3	Micro-lithotype Composition.41
Table 3.4	Main Difference between conventional and Coalbed Methane Reservoir48
Table 3.5	Summary of Main Advantages and Disadvantages of the Different Field Permeability Methods.73
Table 4.1	Summary of Petrographic Maceral Analysis.85
Table 4.2	Pressure transient test Results summary.89
Table 4.3	Coal Thickness derived from Density Logs.92
Table 4.4	Grain matrix and Residual hydrocarbon saturation.104
Table 4.5	Density log derived fracture porosity.106
Table 4.6	Results obtained from geophysical Logging Data116
Table 4.7	Comparison between Log and field derived permeabilities.118

List of Figures

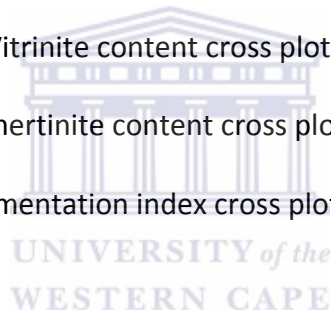
Figure 1.1	South Africa's historical and projected GHG emissions.2
Figure 1.2	Regional location of the Waterberg coalfield in Southern Africa.6
Figure 1.3	Drawing of Waterberg Coalfield illustrating main Faults.7
Figure 2.1	Gondwanaland reconstruction during late Palaeozoic displaying associated foreland Basin. (b) Generalised cross section of the main Karoo foreland Basin.9
Figure 2.2	Gravity map and N-S gravity profile of Ellisras Basin showing the main faults that bound the basin forming half and Graben structure of the Basin.10
Figure 2.3	Stratigraphic chart with the major litho-stratigraphic subdivisions of the Karoo Super-group in the main Karoo Basin of South Africa.15
Figure 2.4	Main Formations in the Ellisras Basin compared to Main Karoo Basin.20
Figure 2.5	Lithostratigraphy of the Ellisras Basin.21
Figure 2.6	Succession of coal seams in the Upper Ecca, Middle Ecca and Molteno Stage in some coalfields in South Africa.25
Figure 2.7	Maceral distribution in the Grootegeluk Formation at different relative density floats.30
Figure 3.1	Coal rank depends on thermal maturity.35
Figure 3.2	Locations of Currently Producing CBM Basins in USA.46
Figure 3.3	Typical Langmuir Isotherm.48

Figure 3.4	Relationship between different cleats in Coal.50
Figure 3.5	Sorption sites of each gas at one given fixed surface coverage (fixed P, T) and the intersection for multi-component sorption isotherms.58
Figure 3.6	Different fluid flow systems in coal (modified after Fourie, 2000), sourced from Anglo Coal Data base.60
Figure 3.7a	Quantification of connected porosity in 3D, (left) Bituminous coal, (right) Connected porosity map (darker grey = higher porosity)67
Figure 3.7b	Investigation of open and occluded porosity 3D, (top left) μ CT image, (top right) SEM image.67
Figure 4.1	Well Location Map.82
Figure 4.2	Coal zone delineation.83
Figure 4.3	Banded coal from BS1; Alternating bright and dull bands.84
Figure 4.4	Experimental setup for pressure transient test.88
Figure 4.5	Analysed Pressure Data from Zone 10 and 11 WTB45 pressure transient test.89
Figure 4.6a	Composite Log plot for WTB4595
Figure 4.6b	Composite Log plot for WTB4896
Figure 4.6c	Composite Log plot for WTB5697
Figure 4.6d	Composite Log plot for WTB5898
Figure 4.7	Collection of cubes, b) Collection of Sheets used for evaluating coal reservoir permeability100
Figure 4.8	Dual Laterolog response of zone 11 and 9 for wells: WTB45, WTB48, WTB56, WTB62, WTB65, WTB70, and WTB72.115
Figure 5.1	East – West cross section linking WTB56, WTB72, WTB70, WTB45.121
Figure 5.2	North – South cross section linking WTB48, WTB58, WTB45.122
Figure 5.3	Permeability depth plots for WTB45, WTB56, WTB62, WTB65, and WTB70. Plots show negative correlation with depth.125
Figure 5.4	Porosity depth plot for WTB45, WTB48, WTB56, WTB62, WTB70, and WTB72.128
Figure 5.5	Permeability vs Vitrinite Reflectance cross plots for WTB45, WTB56, WTB62, WTB65 and WTB70132
Figure 5.6	Permeability vs vitrinite content cross plots WTB45, WTB62, WTB56 and WTB65. Plots show positive correlation.134
Figure 5.7	Permeability vs Inertinite content cross plots for WTB45, WTB56 and WTB65. Plots show negative correlation for these wells.136
Figure 5.8	Cementation index vs Fracture width cross plots for WTB45, WTB48, WTB56, WTB62, WTB65, WTB70 and WTB72. All show decreasing cementation indices with fracture width.140
Figure 5.9	Permeability vs cementation index variation for WTB48, WTB56, WTB62, WTB65, and WTB72.144

Figure 5.10	Deep resistivity vs cementation index plots for WTB45, WTB48, WTB56, WTB62, WTB65 and WTB70.148
Figure 5.11	Shallow resistivity vs cementation index plots for WTB45, WTB48, WTB56, WTB62, WTB65 and WTB70.151

Appendix

Appendix 1	Results of Vitrinite Reflectance Analysis170
Appendix 2	Results of Petrographic Maceral Analysis172
Appendix 3	Composite Log plots for WTB62, WTB65, WTB70 and WTB72174
Appendix 4	Water Analysis178
Appendix 5	Gas and Coal Quality Data179
Appendix 6	Permeability-Depth plots for WTB48 and WTB72180
Appendix 7	Porosity-Depth plots for WTB65181
Appendix 8	Cross Plots of Vitrinite content, Liptinite content, Inertinite content and Vitrinite Reflectance vs Depth (zones)182
Appendix 9	permeability - Vitrinite reflectance cross plots for WTB48 and WTB72184
Appendix 10	Permeability – Vitrinite content cross plots WTB48, WTB70 and WTB72185
Appendix 11	Permeability – Inertinite content cross plots for WTB48, WTB62, WTB70, WTB72.187
Appendix 12	Permeability-cementation index cross plots for WTB45 and WTB70.189



Keywords

Waterberg Basin

Porosity

Permeability

Coal Bed Methane

Geophysical Wireline Logs

Cleats

CHAPTER 1: INTRODUCTION

1.1. Introduction

With the coming of industrialisation, the earth has witnessed a progressive increase in the concentration of greenhouse gases (GHG) in the atmosphere. Canadell et al., (2007) report that Global average atmospheric CO₂ rose from 280 ppm at the start of the industrial revolution to 381 ppm in 2006. Anthropogenic Carbon dioxide is a major component of GHG; progressive increased concentration of atmospheric carbon dioxide is globally accepted to pose serious environmental problems such as global warming which may in turn alter other dependent systems like general rise in sea level, weather and precipitation patterns. The two main anthropogenic CO₂ sources as reported by Canadell et al., (2007) are emissions from the combustions of fossil fuels and net emissions from land use changes. Focus on anthropogenic CO₂ emissions have been on Annex B countries or developed nations (countries committed to the Kyoto protocol GHG reduction programme) and emerging developing nations like China. The UNEP and ALGAS concluded that CO₂ emissions will grow with an average annual rate of 3–5% for most of the countries until 2020, with a tendency to expect highest growth rates for Asian countries (Halsnaes, 2008). Due to rapid population and developmental growth, there is an upward trend in CO₂ emission from fossil fuels in Africa and other developing countries. The international energy agency estimated that energy demands will rise by 45% by 2030 (Oxburgh, 2010) accompanied by progressive increase in carbon dioxide emissions. DEAT(2004) reports south Africa's national CO₂ emission for 1990, 1994 and 2000 at 347, 380, 435 mt respectively while a more extensive study by Letete et al., (2009) estimates South Africa's historical and future emission from 1970 to 2055 projecting an increase by a factor of four in the next forty years illustrated in figure 1. As such although South Africa and other African countries have no GHG reduction commitment in the Kyoto Protocol, it is of great importance for such countries to engage in GHG emission reduction programmes.

With such concerns interest have been stimulated in governments and other organisations to develop and design new strategies to help trap and reduce carbon dioxide emission. As such there is greater demand for cleaner energy sources. Despite all attempts, the cost of limiting emission and developing new reduction technology is still a major drawdown.

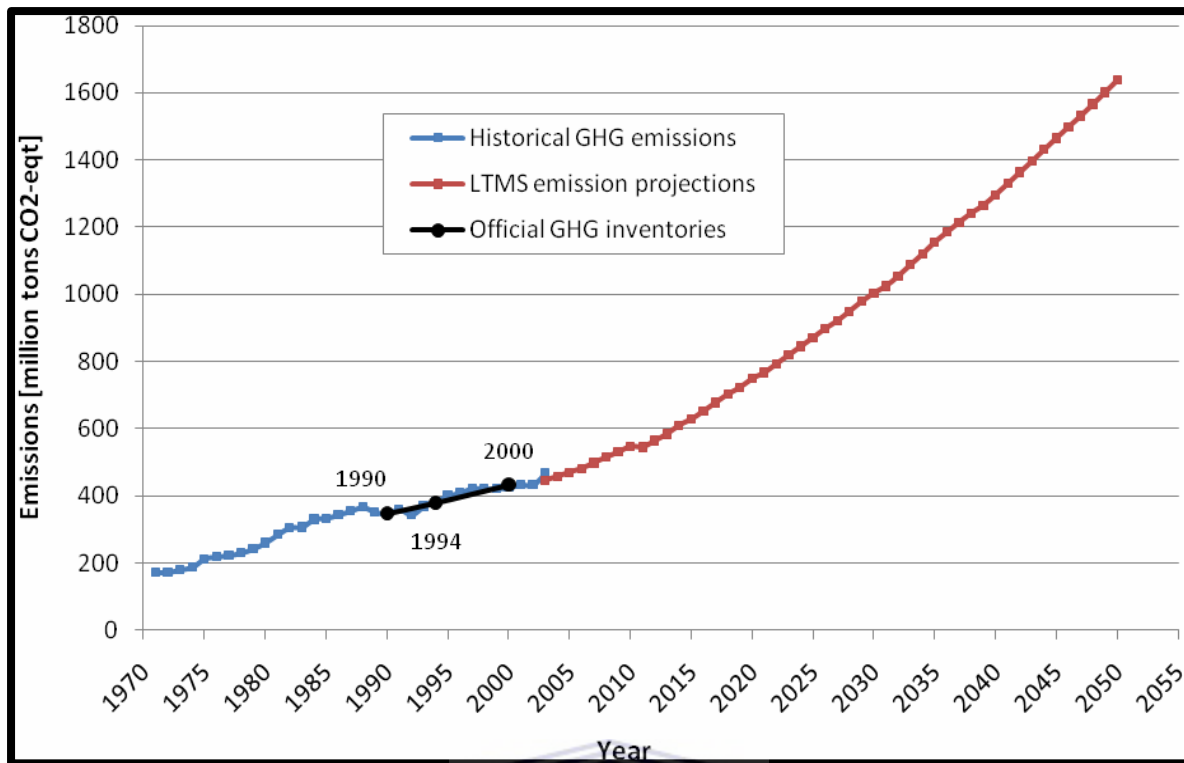


Figure 1.1: South Africa's historical and projected GHG emissions (Letete et al., 2009)

Based on a coordinated study effort by the ALGAS and UNEP the marginal costs of GHG emission reduction projects in developing countries in the energy sector is in the order of magnitude of 10–15% of future baseline emissions at a cost of US\$ 25 per tonne of CO₂. This cost estimate for all developing countries (DC's) excludes reduction cost potential related to power production with the exception of Estonia with a projected reduction cost potential of 65% by 2030 at a cost of US\$42 per tonne of CO₂ that includes options related to power production such as nuclear power, reduction in electricity exportation, wind turbines. The big question is *"how do we maintain an efficient and adequate supply of energy while keeping our atmosphere carbon free?"*

Most environmentalists have prescribed the use of non-fossil fuel sources of energy, nevertheless the world still rely greatly on fossil fuel which as of now is cost effective than non- fossil fuel energy sources. In an attempt to reduce atmospheric concentration of carbon dioxide, research focused on the sequestration of carbon dioxide have been carried out, proven and implemented in plants around the world however a lot of work is still to be done particularly in practical engineering issues and characterisation of the various storage mechanisms for Carbon dioxide. Carbon dioxide sequestration may be considered as the

long term capture and storage of anthropogenic carbon dioxide. Sequestration technologies include Biological sequestration (reforestation), chemical sequestration, ocean sequestration and geological sequestration (storage in saline aquifers, depleted oil fields, abandon mines and in unmineable coal seams. During the past two decades as concentration of carbon dioxide increases in the atmosphere, the production of Coal Bed Methane (CBM) during CO₂ sequestration in unmineable coal seam appear as a value added stream for cost reduction in sequestering CO₂. Thus CBM provides the energy industry with two broad advantages:

- A medium to store anthropogenic carbon dioxide.
- Cleaner energy source compared to oil. Methane burns to release less toxic material than crude oil. Most CBM production sides cause very little damage to the environment than Oil wells.

Methane associated with coal is an old issue but still constitutes one of the miner's most horrifying nightmare, however Coal Bed Methane (CBM) and Enhance Coal Bed Methane (ECBM) remain an evolutionary new concept in the energy industry as CBM from both mineable and unmineable coal seam becomes a significant resource on its own. During coalification large amounts of gases (methane, carbon dioxide, carbon monoxide, hydrogen and Nitrogen) are adsorbed on the coal surface with methane forming a greater part of the whole. While mining for coal the confining pressure within the coal seam is dropped forcing the methane gas to diffuse into the fracture system and subsequently into the mine. Methane being an inflammable gas is consequently a prime cause of most mine explosions. Top on the mining engineer's priority list is to quantify the amount of gas present within the coal seam, estimate the porosity and permeability of the coal seam as well as the rate of gas diffusion from coal seam. This will enable an efficient design of mine degasification techniques. Degasification techniques range from mine ventilation with large fans to CBM evacuation wells yet very limited success has been registered. Most methane recovered from coal mines have been reused as an energy source for the mines.

Unlike conventional oil and gas reservoirs where fluids storage and flow occur in the pores and radial flow through connected pore spaces, the flow of gas within the coal seam occurs by diffusion in the coal matrix and Darcy flow in the natural fracture system (cleats) which

controls CBM reservoir deliverability (Aminian, 2007 and Robertson et al., 2005). Due to molecular size differences there is a preferential adsorption of carbon dioxide over methane on the matrix coal block. Peterson et al., (1992) argues that the discovery of coal with adequate natural permeability is the most significant issue in the coal bed methane (CBM) industry. The Permeability of coal, coal matrix sorption capacity of carbon dioxide and methane, preferential adsorption of CO₂ over (CH₄) (Mahajan, 1991 and Schroede et al, 2001), and induced swelling and shrinkage (Reichle et al., 1999) of coal caused by sorption of CO₂ and CH₄ are some of the most important properties in the Enhance Coal Bed Methane (ECBM) industry.

Robertson (2005) describes coal as an elastic sorptive medium that has the ability to adsorb or desorbs large amounts of gas causing it to swell or shrink. This swelling and shrinking of the matrix block brings about a change in the permeability pattern of the coal. To understand and properly model permeability of coal, all the factors that directly or indirectly affect the dynamism of coal fracture geometry must be taken into consideration. Such factors include coal properties, coal seam confining and over burden pressures, moduli of elasticity (Young's modulus, Poisson's ratio, and constrained axial modulus), sorption strain and seam porosity. In order to design an effective methane production or carbondioxide injection plan, the storage and flow characteristic of the coal seam must be well understood.

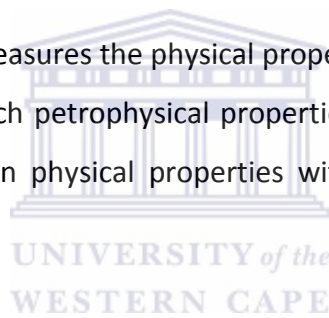
1.2. Rationale

Coal Bed Methane (CBM) exploration and production is still in its very early stages in South Africa. There is therefore limited qualitative and quantitative data as well as literature on CBM reservoir characterisation on South Africa coals. Reservoir characterisation techniques widely used in oil and gas sector for conventional oil and gas analysis includes; measurements from Core Sample, historical simulation using production data, Injection/falloff well test and recently geophysical wire line logging. With the coming of unconventional industry particularly CBM and shale gas, these techniques have been widely applied but for geophysical wire-line logging. However most of these techniques need to be modified to accommodate for the vast heterogeneous nature of coal particularly conventional core analysis.

Measurements from core samples and field test analyses though considered most effective techniques because of their direct measurement on reservoir rock are none the less very expensive due to coring and the lengthy procedures involved. Core measurements however do not provide parameters at in situ reservoir conditions. Historical simulations make use of production data from pre-production basins or wells.

With proper understanding of the bore hole environment, the principles and application of down-hole geophysical along with proper data processing and a thorough knowledge of the geology of the rock. Wire-line geophysical data can provide a fast and accurate means of evaluating the reservoir. In frontier regions like South Africa with no CBM methane production projects to date and thousands of coal exploration bore holes but very limited preserved cores available, geophysical wire line logging stands as a quick reservoir analytical technique.

Geophysical well logging tools measures the physical properties of rock matrix and the fluids that occupy the pores from which petrophysical properties can be obtained or calculated. These logs measure variations in physical properties within the formation and between different formations.



1.3. Objectives/Scope

The aim of this study is to apply the use of geophysical wire-line logging data to determine the porosity and permeability for the Beaufort Seam 1 and Ecca formation coals from eight wells in the Waterberg basin. The calculated CBM reservoir parameters will be compared to values derived from Injection falloff test for same wells to establish the correlation between logging derived permeability and field derived permeability for these coals. A CBM reservoir according to this thesis is a coal seam or a group of coal seams with appreciable thickness and contains appropriate organic matter, buried at sufficient depths to be able to produce and store gas.

Specific Objectives include:

- Identify coal units and calculate their net thicknesses using geophysical logging data.
- Calculate coal cementation index and fracture width using geophysical logging data.

- Calculate Reservoir fracture permeability and fracture porosity using geophysical logging data.
- Make a comparison between logs derived permeability and field test derived permeability.
- To confirm the relationship between estimated coal reservoir permeability and porosity and the degree of cementation of the coal as well as the fracture width.
- To determine the extent to which coal burial depth, type of maceral and degree of coalification of the coal affects the permeability and porosity of coals.

1.4. Location of Study Area

The Waterberg coalfield is found in the Waterberg or Ellisras Basin located west to Lephalale in the Limpopo province (North East of South Africa) (Figure1.2).

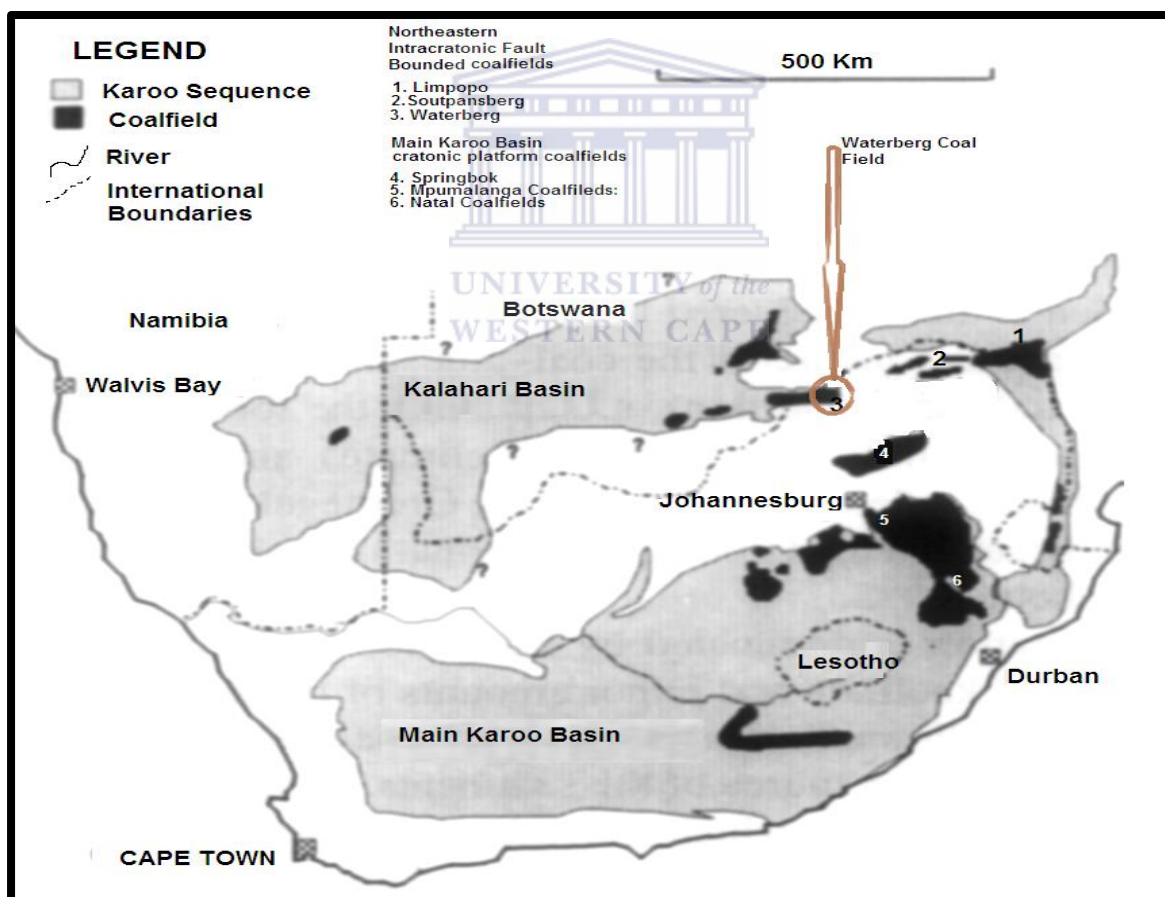


Figure 1.2: Regional location of the Waterberg coalfield in Southern Africa. Relative position of the Waterberg coalfield compared to other South African coalfields. Waterberg coalfield considered as an embayment of the Kalahari Basin rather than part of the Main Karoo Basin (modified after Seipker, 1986).

The Basin extends into Botswana to the West where it is called the Kalahari Basin. The basin strikes East - West and is approximately 90km long with a 50km N-S width and a total surface area of 4500km² in South Africa, bounded by Latitude 27E and 28E. The coalfield covers a relatively small area in relation to other coalfields in South Africa (Faure, 1996). Structurally referred to as a Graben, the basin is bordered by two East-West striking faults, the Zoetfontein fault to the North, Eenzaamheid Fault to the south with the Daarby fault in the centre (Figure 1.3). The coalfield is drained by two rivers; to the east by River Lephalela and River Mokolo that empties into River Limpopo to the North (Mtimkulu, 2009).

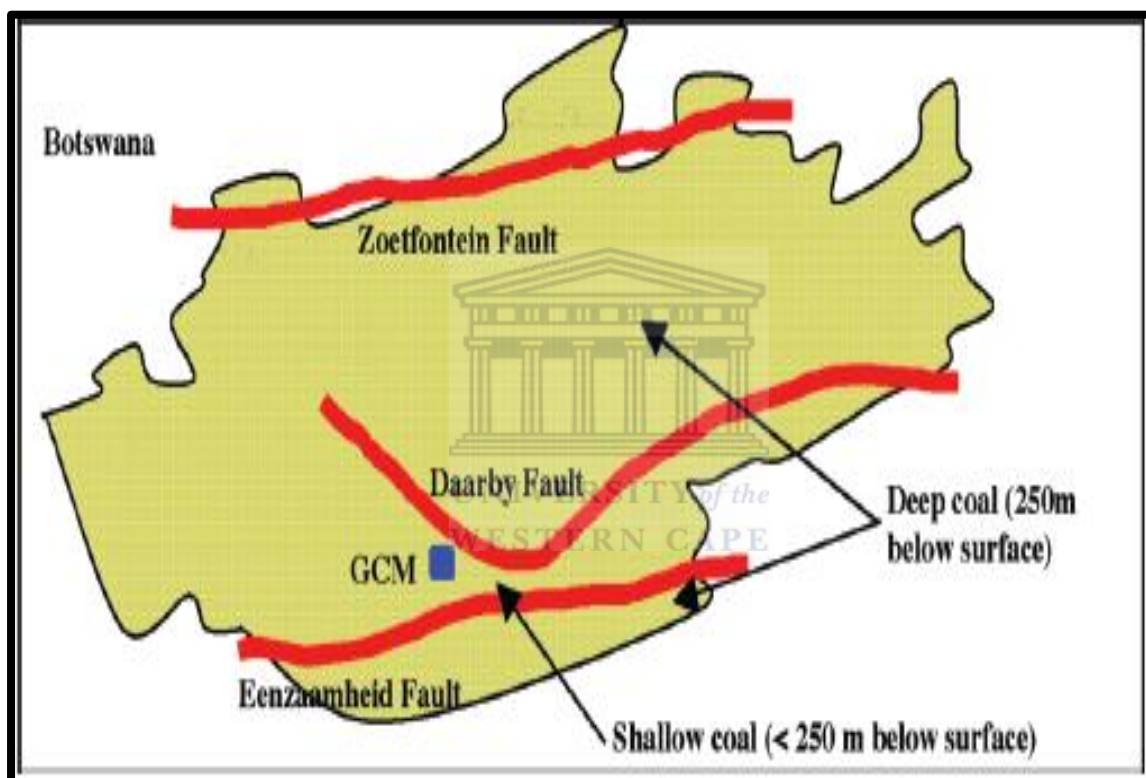


Figure 1.3: Drawing of Waterberg Coalfield illustrating main Faults (Jeffrey, 2005).

CHAPTER 2: GEOLOGY OF STUDY AREA

2.1. Geological Setting

In this section we shall look at tectonic events that led to the formation or structural evolution of the Waterberg Basin. We shall also discuss the lithostratigraphic units of the basin making reference to the main Karoo Basin as well as neighbouring sub basins. A vivid description of the petrography and petrology of the coal bearing succession is also paramount for related study.

A wide majority of the coal beds in South Africa are associated to the Late Carboniferous to Early Jurassic Karoo deposits (South African Committee for Stratigraphy (SACS), 1980). The Waterberg Coalfield is part of the Ellisras Basin which is also Karoo in age. In South Africa the main Karoo basin covers more than half of the country (Faure et al, 1996) and host a vast majority of the coal beds which occur in the early to late Permian Ecca group of the Karoo sequence (Synman, 1998; Faure et al, 1996). Most mining activities for coal in South Africa are concentrated on the Eastern part of the main Karoo Basin with activities prominent in the Witbank, Highveld and Ermelo sub basins. Figure 1.2 shows the relative position of the main Karoo Basin with superimposed sub basins.

Coal was discovered in the Waterberg Basin since 1920 (Fourie et al., 2009). Nevertheless exploration and production of these coals compared to the main Karoo basin (MKB) is not yet advanced. The area coverage of the Waterberg basin is small when compared to other MKB's although it contains approximately 44% of in situ reserves of bituminous coal according to Dreyer (2006). The western margins of the basin extends into neighbouring Botswana where extensive coal exploration is currently being done (Fourie et al., 2009) hence this basin can be considered as an extension of the Karoo aged Kalahari Basin in Botswana (Figure 1.2). The coalfield has an east west orientation (Haughton, 1963) and is 260-190 million years old (Wagner et al., 2012).

2.2. Tectonic Setting and Basin Evolution

The plate tectonic theory identifies a variation in basin types for Karoo coals. According to Snyman and Botha (1993), the coal deposits of Southern Africa, South of the Kalahari occur in two distinct tectonic settings; the cratonic platform in which the main Karoo group is

found and the rifted fault Bounded Basin in which setting the Waterberg Basin Belongs. The nature of these basins along with their sedimentary fill seems to have been affected by the chain of tectonic activities that led to the creation of Africa today. Tectonic activities in the main Karoo Basin of South Africa started in the Devonian, increased gradually in the late Carboniferous and Permian, reaching its climax in the Triassic (Hobday, 1987) . Figure 2.1 (a) shows Gondwanaland continental reconstruction during the late Palaeozoic illustrating subduction zones and associated foreland basin while (b) is a cross section of the main Karoo Foreland Basin. Further to the North-East the coalfield of this basin was developed within the greater intracratonic Soutpanberg trough (Arnott and Williams, 2007) which was reactivated during the Permian to early Triassic time (Seipker, 1986; Mtikulu 2009). Most MKB sedimentation occurs in a foreland basin or deposition was on the flanks of the Kaapvaal Craton as described by Falcon (1989) while most north Eastern Karoo Basins (Waterberg, Limpopo and Soutspenberg) sedimentation occurred in a relative subsiding graben structures (Figure 2.2).

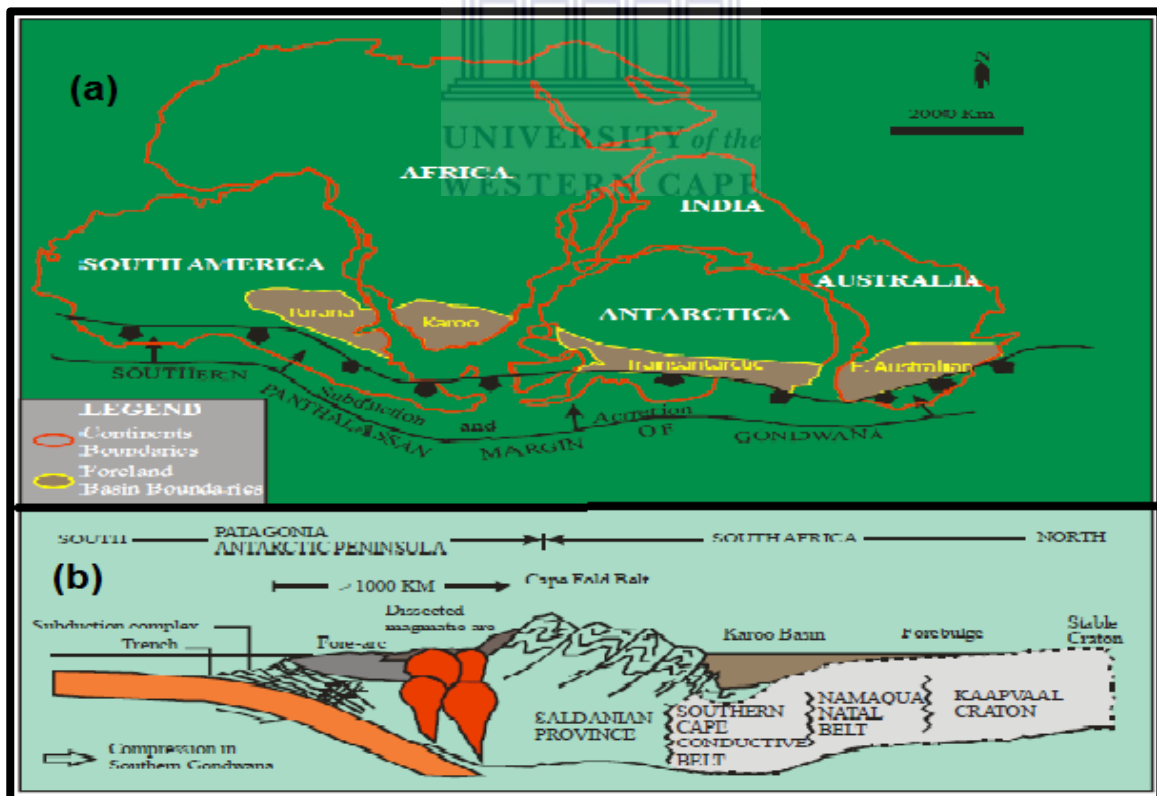


Figure 2.1: Gondwanaland reconstruction during late Palaeozoic displaying associated foreland Basin. (b) Generalised cross section of the main Karoo foreland Basin (Turner et al., 1983).

The structural features of the Waterberg Basin are very complex and have not been fully studied to date. However a couple of articles on the structure of the Waterberg Basin have been written which includes those of Mtikulu (2009), Fourie et al. (2009) with the most recent attempt by Fourie et al (2011) in a geophysics basinal study of the Waterberg basin sponsored by COALTECH Research Association. Mtikulu's (2009) basinal study of the Waterberg Basin provides detail information into the structural and tectonic history of the basin.

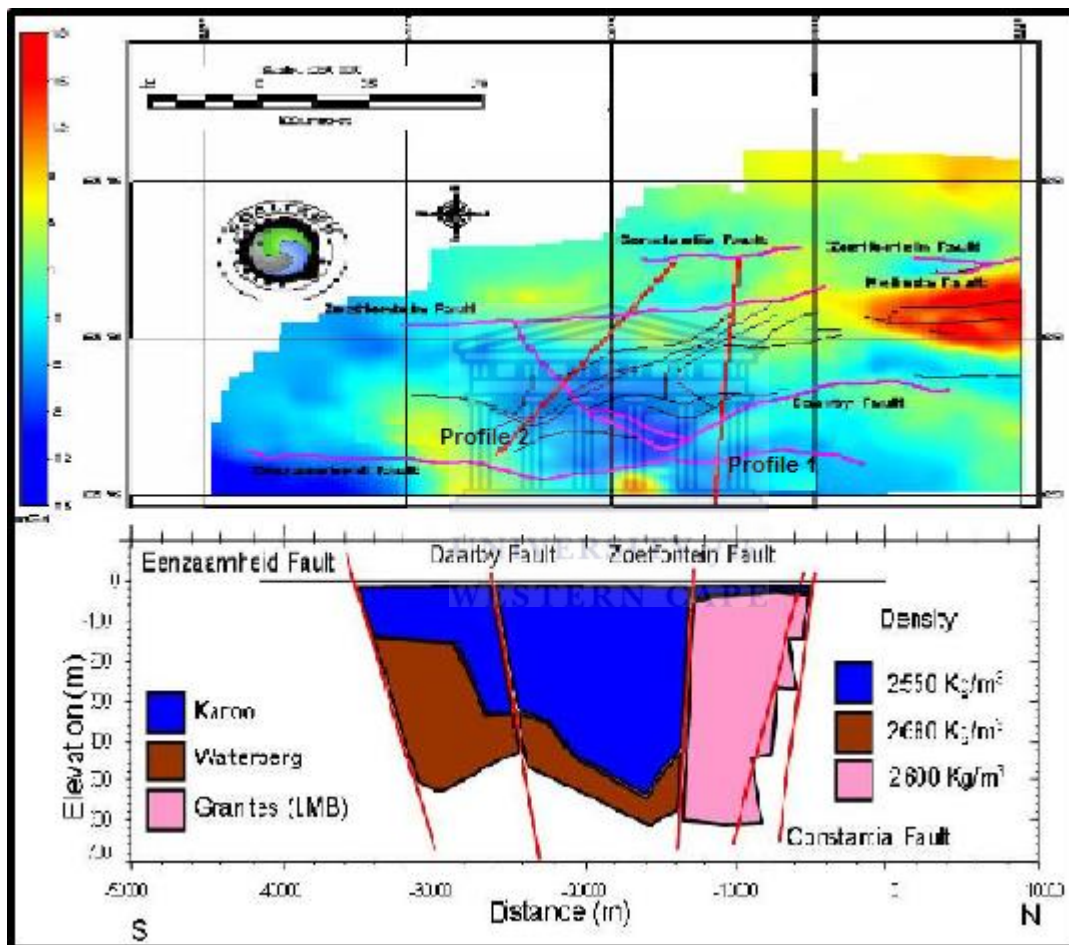


Figure 2.2: Gravity map and N-S gravity profile of Waterberg Basin showing the main faults that bound the basin forming half and Graben structure of the Basin (Fourie et al., 2011).

Though the Karoo sequence in the Waterberg Basin as well as the MKB date as far back as the Carboniferous, the structural and basinal development started at a much earlier time. The series of orogenic activities that led to the formation of Limpopo mobile Belt form the foundation of the structural evolution of the Waterberg Basin.

Johnson et al (2006a) describe the Limpopo Mobile Belt as a highly metamorphosed sedimentary, Volcanic and Igneous unit created from a loop of orogenic activities that occurred around 2690 – 2560Ma and 2000Ma. The Belt is divided into three major zones; the Northern Marginal zone (NMZ) that borders Zimbabwean Craton, the Central Zone (CZ) and the Southern Marginal Zone (SMZ) that borders the Kaapvaal Craton (KC). Separating the SMZ and the CZ is the Palala Shear Zone (PSZ) (Bumby and Van Der Merwe, 2004) which along with its WSW extension (the Melinda Fault Zone) has a sinistral sense of shear though reactivated locally in opposite sense (Mtikulu, 2009). The Zeotfontein fault that borders the basin to the North is located in the Malinda Fault Zone. According to Mtikulu (2009), it is probably movements along and between the SMZ and CZ during the Permian time that reactivated the Palala shear zone and causes the formation of the Zeotfontein fault. The PSZ is made up of mylonised CZ and Bushveld complex rocks (Bumby, 2000). There Waterberg Basin formation comes from the reactivation of the Intracratonic Soutpansberg trough.

Early stages in the formation of the Limpopo Belt were characterised by crustal folding from compressive forces caused by the collision of the KC and the ZC during the Neoproterozoic time that led to the metamorphism of supracrustal rocks followed by the intrusion of granitic gneiss (Barker, 1983). Notwithstanding the age of the Limpopo Belt is highly contest by other writers. Bumby and Van Der Merwe (2004) proposed a much older event while other writers think the granitic gneiss from this belt are much younger in age. According to Barker (1983) the development of plutonic bodies within the crust in the CZ stimulated uplift and resultant crustal thinning. He further proposed that during 2300 – 2200 Ma the ZC and KC experienced a net pull apart movement along the CZ resulting in the formation of fractures, crustal thinning and uplift causing erosion. These fractures generation form the structural basis of the Soutpansberg trough in which magma from partial melting of the mantle during 2100 – 2000Ma settled. This event may correspond to that proposed by De Wit et al., (1992) with a southward directional thrusting of the CZ along with an East West transcurrent faulting associated with the opening of the Soutpansberg Graben The Melinda fault which is a dextral strike-slip fault with a 17km total displacement was then formed by late stage re-activation of the Palala shear zone (Bumby, 2000).

The Eenzaamheid fault in the South Boundary of the basin has a total vertical displacement of up to 250km in some areas and downthrows to the North (Brandl, 1996). It also forms a northern boundary of the Waterberg rocks towards the east of the Basin. The waterberg group rocks to the south exclusively form two-third to three quarter of floor of the Waterberg Basin while to the Southeast as earlier seen, Karoo rocks lie on the Villa Roralope of the Bushveld Complex (Fourie et al., 2009). The Villa Roralope contains both layered basic rocks and granite and is in faulted contact with the Mesina suite to the Northeast.

2.3. Stratigraphic Setting

In this section we shall discuss the rock succession of the Waterberg Basin. We will first start by discussing the stratigraphy of the Karoo Supper group in South Africa making references to the Karoo sequence of some coal fields in the main Karoo basin. Furthermore we shall examine the depositional environment in which these rocks were laid.

The Karoo supper group is considered the largest stratigraphic unit in South Africa. A bulk of the sedimentology and stratigraphic studies carried out on the Karoo made use of bore-hole data. Principal authors and researchers include Van Vuuren et al., (1979), Cairncross (1979 and 1986) Le Black Smith (1980), Winter (1985), Haughton (1963).

Haughton (1963) discusses the stratigraphic history of rock sequences of Africa, South of the Sahara in which he makes particular references to the Karoo system of Southern Africa. The name Karoo according to Haughton was derived from the wide area in the Cape Province of South Africa where we have almost flat –lying sandstones and shales that are intersected by sheets of Doleritic dykes. The system therefore consist of a series of wide spread rocks deposited throughout Africa probably under similar conditions that span from the Carboniferous to the Lower Jurassic. Consequently one will therefore wonder for a possible explanation to the cause of the varied nature and distribution of Karoo coal sequences in South Africa.

2.3.1. Karoo Sequence

Cairncross (1989) blames the control of the distribution of Karoo coals in South Africa primarily on four factors; the tectonic setting, the nature of pre – Karoo basement lithologies, the basement paleogeography and the paleo-depositional environment

associated with the peat formation. In the Northern and North-eastern Karoo Basins a stable intra-cratonic shelf provided a suitable tectonic setting for coal deposition and the Archean granite basement terrain provided residual topographic depression for sedimentary filling. The coal sequences in the Paleo-valleys or depressions (grabens) are much thicker in the centre and thin out into finer units towards the adjacent valley flanks or basement highs.

2.3.1.1. Depositional Systems for Karoo

Hobday (1987) records four depositional systems for the coals in the Karoo of South Africa. These includes Alluvial fan and fan-delta systems, Fluvial System, Delta plain system and Back – Barrier system According to Falcon (1989), the most significant feature of the Karoo time was the early Karoo (Dwyka) glaciations which was continental in extent but appear to have had several phases Of glacial advances and retreats towards the end of the period (Falcon, 1973). During the latter stages of the Palaeozoic the climate in South Africa changed from glacial to paraglacial (Snyman and Botha, 1993) suggesting that cold climate prevailed in South African or Gondwanaland coals contrary to tropical rain forest of the Carboniferous Laurasian coals (Stach et al. 1982). This may also be deduced from the flora assemblages seen during this period.

The alluvial fan and fan-delta systems could be identified in the basal Ecca sediments that coarsen up from Valve shales into cross bedded sandstones and conglomerate of broad deglaciated palaeo-valleys along the northern flanks of the Karoo Basin (Witbank and Highveld)(Le blanc Smith, 1980, Cadle, 1982). The coarsing upward sequences are bounded from above by the seam 1, 2, 3 and 4 coals. The system is initiated by the erosion of nearby deglaciated highlands with high runoff of glacial melt water. The fluvial systems are characterised by dip-oriented channel-fill sandstones separated by lenticular but locally very thick coal seams (Hobday, 1987). These channel fills are characterised by mixed bedloads which are gradational and show cross bedding, plannar-tubular foresets indicative of braided streams and are sometimes overlaid by suspended load fluvial systems. The coal seams overlying the channel fill sandstones are high in ash value (Cairncross, 1979). There is a gradational boundary between the fluvial system and the delta plain system of the Karoo. Hobday (1973), Van Vuuren and Cole (1979) and Le Blanc Smith (1979, 1980) all agree that

the Karoo Delta plain facies can be identified by their relationship to underlying thick, upward-coarsening pro-delta through delta front sequences with the delta plain facies characterised by mixed-load and suspended load channel facies, burrowed shales, and upward coarsening bayfill sequences with sandy and silty crevasse splays and the coals usually overly and infringe with the upper parts of the bayfill sequences (Hobday, 1987). The coals of the back-barrier system of the Karoo Basin are thin, very persistent along deposition strikes and have low ash content locally (Cadle, 1979).

The Karoo succession in South Africa is representative in the Cape, Orange Free State, Natal, Transvaal provinces and Limpopo province. At the centre of the Transvaal lies the Springbok flats, more to the north is the Soutpansberg Coalfield and the Waterberg to the Northeast. At the base of the Succession is the Dwyka Series. This series is succeeded by the Ecca, Beaufort and Stormberg Series (figure 2.3). In the Cape, Natal and Free State the Karoo system is estimated to reach a total thickness of 35000ft (10 668m) while in the Springbok flats the succession has a maximum thickness of 2200ft off which 1000ft are Volcanics (Haughton, 1963). Haughton (1963) describes the Karoo of the provinces in detail.

2.3.1.2. Karoo Stratigraphy

2.3.1.2.1. The Dwyka

In the main Basin, the Dwyka group is divided into the Northern Mbizane formation and the Southern Elandsvlei Formation and averages attains a maximum thickness of 800m while in the Kalahari of Botswana the sediments are thickest in the South West (Mtikulu, 2009). In the north of the main Basins, the Dwyka lie on the Precambrian basement and to the east it overlies the Phanerozoic Natal group and Msikaba formation while to the South it unconformably or paraconformably on the Cape Supper group (Mtikulu, 2009).

The base of the succession as described by Haughton (1963) is made up of compacted fine grained glacial originated Dwyka Tillite. They are blue or green in colour made up of fine grain sand in an argillaceous rock that carry pebbles and boulders of assorted rock type

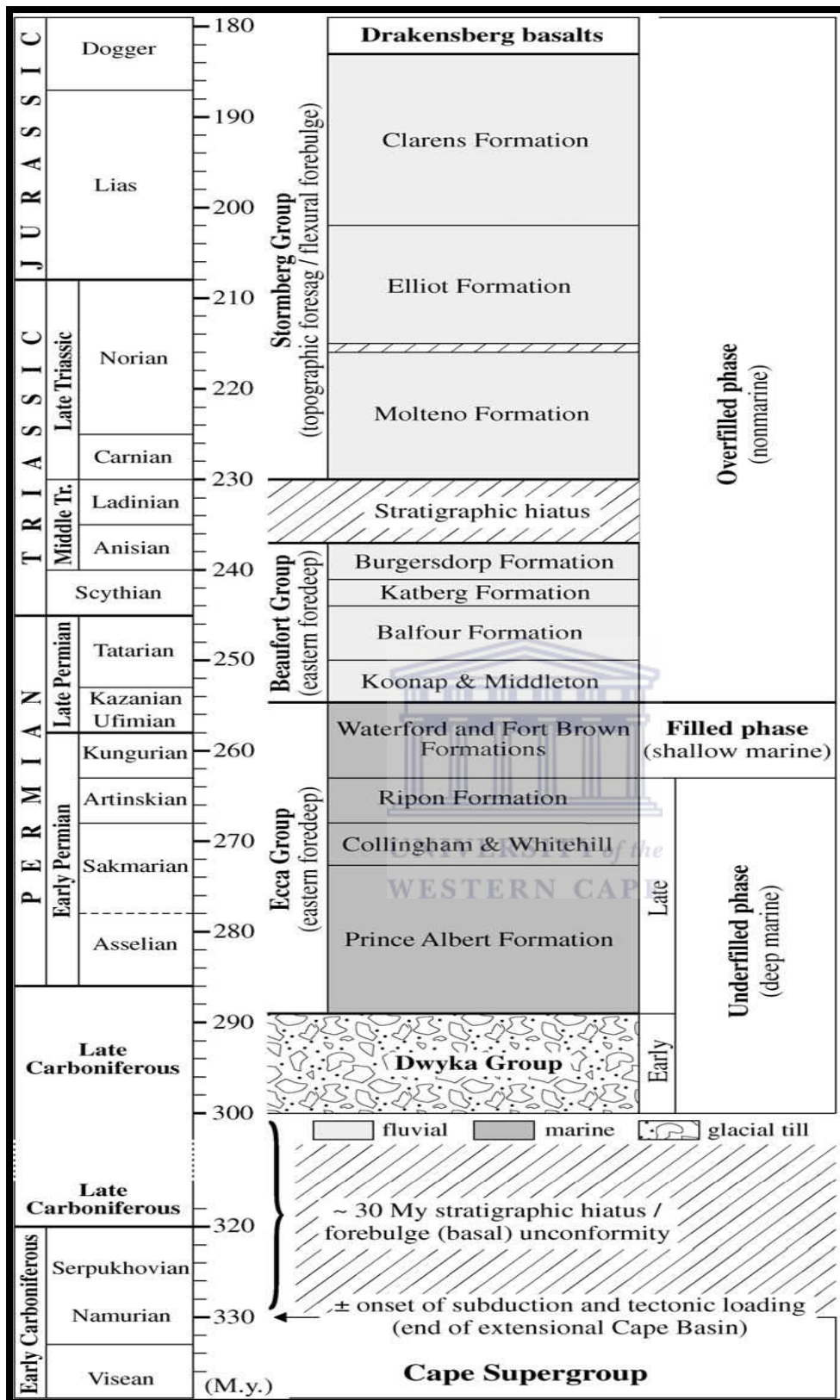


Figure 2.3: Stratigraphic chart with the major litho-stratigraphic subdivisions of the Karoo Supergroup in the main Karoo Basin of South Africa (based on the time scale of Palmer, 1983, and compiling information from Rubidge, 2005 and Catuneanu, 2004a).

whose nature varies from place to place with the finer grains being angular in shape. At the border of the Cape Mountain ranges close to Laingsburg the tillite show maximum development to a thickness greater than 2000ft and are intercalated with thin partings of shale while in the Southern and South eastern region of the Transvaal where the Dwyka series is represented by fine and asymmetrical patches of tillite. Unlike in the South, the tillite is overlaid by conglomerates with pebbles of grit and sandstone. In the Springbok basin, but for a few points where the Dwyka conglomerates have been registered, the Eccca group lie directly on an irregular pre-Karoo rocks. The Upper Dwyka Shales lie on the tillite and varies in thickness from 300 to 700fts and has a maximum thickness in the south but has not yet been identified in the Natal succession. The rock units of the Dwyka shales are composed of olive-green finely bedded shales intercalated by dark fine sandstones and lenses of dolomitic limestone concretions. Johnson et al., (2006) describe the tillites to be made up of conglomerates that may represent outwash gravels and also mudrocks that are probably glacio-marine or lacustrine deposits with occasional coal seams that which are indicative of warmer climates. The laminated shales grade into black carbonaceous shales.

2.3.1.2.2. The Eccca

The Eccca series which is mainly Permian in age lies conformably on Dwyka rocks. Caincross (1989) reports that most of the coals in the Northern Karoo Basins are contained in the Vryheid formation of the Eccca group. The Eccca series is differentiated into the Price Albert formation at the base followed by the Collingham, Whitehill, Ripon Waterford and Port Brown formation (Catuneanu et al, 2005). The description of the Eccca series here is into three stages, the lower, upper and middle stages, follows from that done by Haughton (1963). The Eccca series is divided into three stages; the lower, middle and upper Eccca succession. In the Cape province the Eccca series has thicknesses ranging from 6500fts close to Prince Albert and up to 10 000ft north of Grahamstown. Here the lower, middle and upper stages are folded and are characterised by; arenaceous shales and sandstones of the lower Eccca, shales with minor sandstone that laterally grade into black and carbonaceous form the middle Eccca and the Upper stage is made up of sandstones with mudstones and shales that become argillaceous towards the top. In Natal the lower Eccca Shales lies on the Dwyka and is made up of unfossiliferous dark blue or green shales with some flagstones, rare lenses of limestone or clayband ironstones, succession have maximum thickness of

1400fts in the south but progressively reduce to zero northwards. The middle Ecca in Natal as well as most of the other coal fields is completely different from that of the Cape Province in that they contain the coal measures of South Africa. They have a maximum thickness of 1700fts in Natal but thin out towards the South. They are characterised by an alternation of thick bands of yellow to whitish sandstones and grits with coal. The top layers have dark shales with few bands of impure limestone. The coal measures are contained within 180fts of strata. Blue shales that contain hard nodules characterised the Upper Ecca of Natal. In the Southern and South-eastern region of the Transvaal the lower Ecca units are absent. The middle Ecca lie directly on the Dwyka and are not more than 400ft thick in the Witbank coalfield but are generally thicker than those from Natal. The middle Ecca units here are intruded by dolerite but are less common than in the Natal. The Coal seams of the Middle Ecca in the Springbok are poor in quality but have considerable thickness and most often form the basal component of the system. The Upper Ecca is made up of shales that reach a thickness of 250 - 300fts. They are carbonaceous at their base and successively become grey or blue carrying bands and lenses of fibrous Limestones.

2.3.1.2.3. The Beaufort

Succeeding conformably on the Ecca series is the Beaufort group which is late Permian to early Triassic and divided successively into the Koonap and Middleton, Balfour, Katberg and Burgersdorp formation according to Catuneanu et al., (2005). The succeeding Stormberg Group is early Triassic to Jurassic in age and contains the Molteno, Elliot, and Clarens formations overlain by the Drakensberg basalts. These rocks are composed of thick successions of shales, mudstones, sandstones and coal. In the Cape, Orange Free State and Natal Provinces the sediments are characterised by preserved reptilian remain sand are generally intruded by doleritic dykes and sills. The base of the system is differentiated from the upper Ecca by a reddish or purplish shales unit which is void of reptilian fossils. In the south, at the Cape Province the rock units are very thick and the lower beds even reach thicknesses of 9000fts. The succession thins laterally towards north and north eastward into natal and Orange Free State. In East London, the rocks of the lower Beaufort series are composed of pebbles bearing sandstones and conglomerates. The middle and Upper Beaufort series are similar but only different by the presence of yellow to brown sandstone units in the Upper Beaufort series. Both series are characterised by bright to red maroon

and purple mudstones that alternates with bluish green varieties with sandstones bands which are capped by outstanding beds of felspathic sandstones. The Beaufort series is absent in rock successions of the Springbok field.

2.3.1.2.4. The Stormberg

The Stormberg Series stratigraphically is divided into the Molteno, Red Beds, Cave Sandstones and Drakensberg Volcanics. According to Haughton (1963) the lower part of the series (Molteno) is spotted. The beds appear to lie conformably on the Ecca in the major areas of the Cape, Basutoland and Natal. They have a maximum thickness of 2000ft in the south where they occur in the form of a wedge tapering and are reduced to a single thin band 300miles to the north. Rocks of the Molteno include coarse-grained glittering sandstones, grey to blue shales and infrequent coal intercalations. The red beds like the Molteno show a decrease in thicknesses from north to south with maximum thicknesses of 1600ft in the Elliot district and approximately 300ft in Harrismith of the Orange free state where they appear to lie disconformably on the Beaufort but conformably in the South. Just like their name the red beds are made up of purple and red mudstones and shales and red sandstone along with thick beds of yellow and White felspathic sandstones. The rock units have abundant calcareous nodules. The boundary between the cave Sandstone and the Red Beds is abrupt. The sandstones are massive, fine-grained, light in colour but sometimes show coarse false bedding with occasional fairly large lenses of dark shale. The Stormberg in the Springbok is characterised and correlated to the Bushveld Marl that lie unconformably on the Ecca marking an absence of the Beaufort series in the Springbok. The rocks are made up of soft red, purplish or greenish clays and mudstones and occasional sandstone layers that are rarely exposed. These rocks are overlain by pinkish and yellowish Bushveld sandstones that form surface features.

2.3.1.2.5. The Drakensberg Volcanics

The Drakensberg Volcanics affected a greater portion in Southern Africa and forms the final event of the Karoo. Generally they are composed of wide area coverage of lava flow, sometimes intercalated with tuffs, agglomerates, volcanic breccias and Aeolian sandstones. The most southerly exposures are in Port Elizabeth within the Cape folded belt where the lava

has a thickness of 500fts. In the central Transvaal the lava rise up to 2000fts and rest on the Bushveld sandstones.

2.3.1.3. Stratigraphy of Ellisras Basin

In recent years there has been numerous attempts to create a stratigraphic nomenclature for the Waterberg Basin which is been flawed by the fact that there is no clear connection between the Waterberg and the main basins resulting in difficulty during correlation of lithologies and stratigraphic positioning (MacRae, 1988); nevertheless many similarities exist between lithologic units and their occurrences. Figure 2.4 compares the Waterberg stratigraphic nomenclature to that of the MKB while figure 2.5 illustrates the lithostratigraphic division of the Waterberg Basin. Stratigraphically the Karoo succession lies unconformably on the Waterberg sandstones, a succession of sedimentary fills in the paleo-proterozoic from where the basin derived its name. Contrasting views exist as to what name to use for the basin, some authors use Waterberg basin while others use Ellisras Basin. Nevertheless a gross half of the authors use the name Waterberg basin when referring to the sedimentary fill of the Waterberg group i.e. pre Karoo and the others use Ellisras Basin when making reference to the Karoo succession that hold the coal seams.

The coal bearing sequences of the Waterberg Basin belong to the Karoo supper group that was deposited between 260ma to 190Ma (Fourie and Henry, 2009). Contrary to coals mined in the main Karoo basin with relative thicknesses of 0.5-7m the Waterberg Basin holds distinct coal seams with thickness ranging from tens of mm to a few metres and are intercalated with carbonaceous mudstones that usually persist laterally covering several Kilometres and occur predominantly in the Grootegeluk formation (a replacement to MKB's Volksrust formation which does not have any coal registered to it) (Faure et al., 1996). Figure 2.6 compares coal development in different South African coal fields. The description of the stratigraphic units discussed here closely for the Genetic Unit of Sedimentation (GUS) proposed in Siepker's Lithostratigraphic nomenclatures (Siepker, 1986) as rewritten by Mtikulu (2009).

2.3.1.3.1. Dwyka of Ellisras Basin

The presence of the Dwyka series according to Haughton (1963) is doubtful in the Waterberg Basin with some tillite occurrences on the western extension of Bechuanaland and mudstones lie on pre-Karoo rocks on the Limpopo River. Similar to the main Karoo basin, the Dwyka is divided into the lower Dwyka (Waterkloof formation) and Upper Dwyka (Wellington Formation).

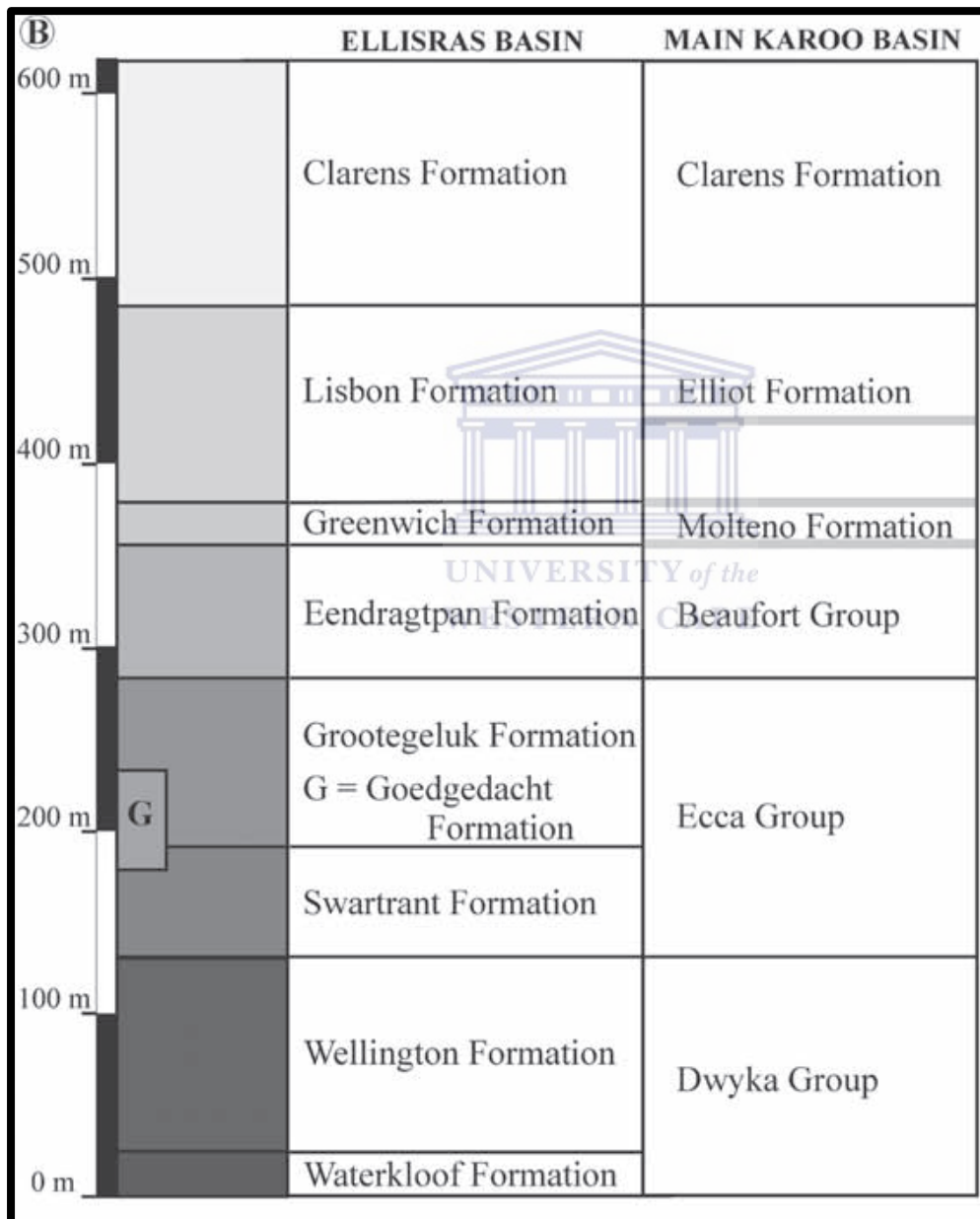


Figure 2.4: Main Formations in the Ellisras Basin compared to Main Karoo Basin (Modified from Bordy et al., 2010.)

2.3.1.3.1.1. The Lower Dwyka

Mtikulu (2009) described the lower Dwyka to be made up of Diamictite, mudstone and conglomerates and as related also by Houghton they are distributed towards the north and western margins of the Basin. The diamictites are over 9m thick and contain local sandstones and mudstone beds. The deposit are thought to have been subaqueous outwash from reworked glacial till while the formation mudstones reach a total thickness of 17m and are interpreted as glacio-lacustrine deposits.

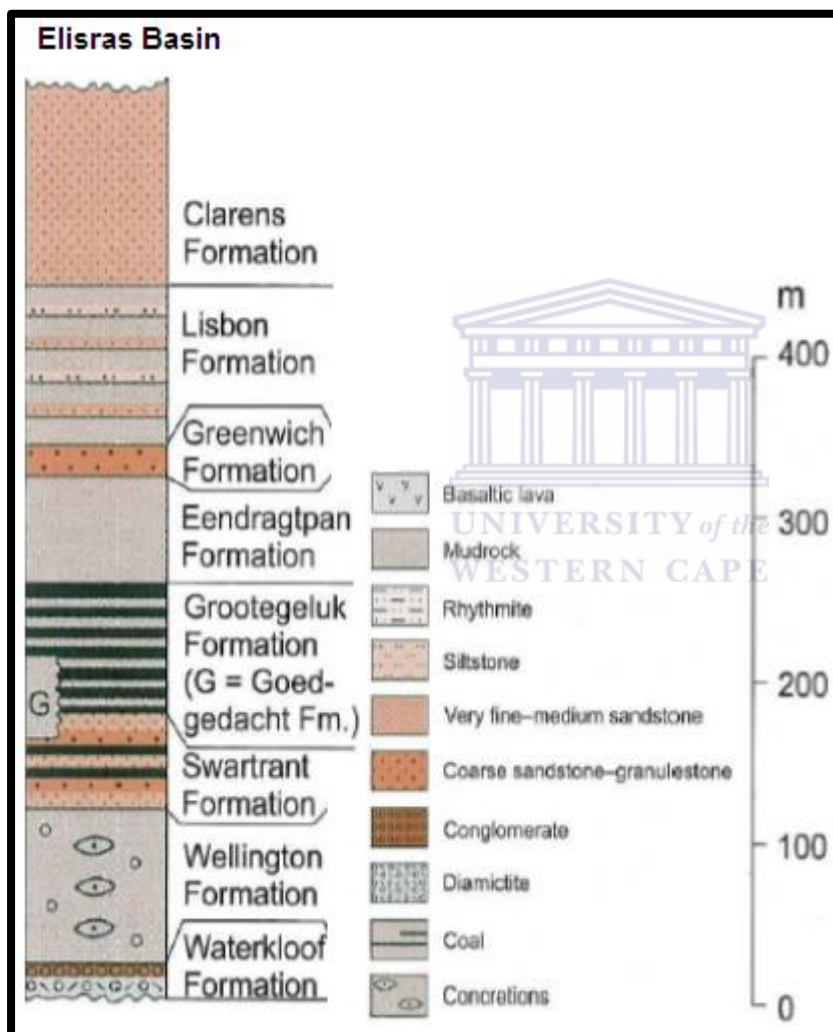


Figure 2.5: Lithostratigraphy of the Elisras Basin (modified after Johnson et al., 2006)

2.3.1.3.1.2. The Upper Dwyka

The overlying Wellington formation is generally 20-30m thick with a maximum thickness of 180m experienced in the South West and is developed only in the south of the basin. The

rocks are anticipated to have been deposited in brackish or salty water and are predominantly mudrocks, sandy lenses and small dropstones at the base that coarsen upward into silty or sandy rocks with some scanty localised occurrence of limestones, sandy shales and feldspathic sandstones at the base (Mtikulu, 2009).

2.3.1.3.2. The Ecca of the Ellisras Basin

Haughton (1963) divides the Ecca into the lower, middle and Upper Ecca, a differentiation he used for the main Karoo Basins. Other authors preferentially subdivide the group as well as other groups into various formations.

2.3.1.3.2.1. The Lower Ecca of the Ellisras Basin

Haughton's Lower Ecca division corresponds to the Vryheid formation as classified by SACS (1980) and the Siepkers Swartrants formation (GUS 1-3) which in most areas of the basin forms the base of the Karoo Supper group. Generally the coal seams of the Vryheid Formation in the Waterberg Basin and those of the main Karoo Basin have similar lithologic characteristics as those of Vryheid of the main Karoo Basin (De Jager, 1976, 1983, 1986; Falcon, 1986; Mac Rae, 1988). Haughton estimates a maximum thickness of 540ft and minimum of 20ft while Siepker reports minimum thickness of 2m in the north and 130m maximum thickness in the centre.

The lower Ecca is further divided into the lower, middle and upper zones (Mtikulu, 2009). The lower zone hosts the No. 1 coal seam and sandstones. The rock units show flaser structures, ripple cross-laminations, cross-bedding with embedded plant imprints which he interpreted to be deposited in a delta plain. The middle zone is characterised by sandstones, mudstones, coaly shales and host the No. 2 coal seam and is anticipated to be glacio-lacustrine. The sediments of the upper zone conformably overlie the No. 2 coal seam and are made up of Sandstones, cross bedded feldspathic sandstones, flaser bedded and wavy laminated mudstones and coal seam (No. 3). These sediments are thought to be from braided or meandering streams that migrated onto a delta or flood plain (Siepker, 1976) nevertheless Faure et al. (1996) studied the facies, palaeoenvironment and thermal history of the Grootegeluk formation using organic and clastic material and came to the conclusion that the sediments and the organic matter of the Grootegeluk Formation were deposited in

a rapidly subsiding basin unlike the coal deposits from the other coalfields that were formed in high standing mires in relatively stable basins.

2.3.1.3.2.1.1. The Goedgedacht Formation

The Goedgedacht Formation (GUS 4) when correlated with the main Karoo Basin according to Siepker (1986) has no equivalent and is only present in the North and Northwest with a maximum thickness of 80m that decreases southwards and eventually infringes with the Swartrant Formation with sharp contact marked by impure coal. It lies non-conformably on the Constantia Suite granitoids-gneiss-mafic rocks in the North and is made up of graded bedded mudstones and capped by thin impure vitrinite coal. The units also show local upward coarsening cycles from coaly mudstones-mudstones-siltstone-medium to coarse-grained sandstone with general sharp but in-erosive contacts. The mudstones are massive with localized sandstones which are interpreted to be deposited in a braided fluvial environment. However the overall depositional system is assumed to be an alluvial fan in a pro-glacial setting where the water is stagnant or retreating.

2.3.1.3.2.2. The middle Ecca of the Ellisras Basin

The Grootegeluk Formation which according to Siepker (1986) is a GUS 5 unit represents the middle Ecca succession and as described by Haughton (1963) to hold the main and mineable coal seams present in this basin that alternates with successions of carbonaceous shales and coal. Faure et al. (1996) estimates the thickness of the Grootegeluk in the Waterberg Basin at 70m while Siepker (1986) reports a 110m thickness in the South, 40-60m in the NW, 50m in the SE and 10 – 20m in the NE and conformably overlies the Swartrant Formation in the East and South while in the Central and the north of the Basin the formation apparently interfingers the Goedgedacht Formation.

The sediments at the base of the Grootegeluk are considered to have been relatively more distal and those at the upper portion are more proximal to the source (Faure et al., 1996). The formation is made up of repeated cycles of basal coal layers with sharp basal contacts, carbonaceous shales which are prominent (plus coal) in the lower parts of the formation and mudstones with siderite lenses, concretions and nodules along with fracture filling of calcite and pyrite common throughout the succession. The base of the formation is unique

as explained by Faure et al. (1896) in that the associated mudstone contain a 2m thick tonstein dominated by crystallised kaolinite, organic matter (app. wt40%), siderite calcite plus major proportions of apatite. The mudstones are dark, laminated and carbon rich but also vary to lighter colours which are slightly massive and lightly carbonaceous. In the completed section of the succession it is divided into 38 zones with the basal zones 1-6 made up of dark, highly carbonaceous mudstone and dull coal while the overlying zones 7-28 comprise carbonaceous shales alternating with dark and bright coals. Mtikulu (2009) relays that some microcycles exist within these zones which are made up of alternating laminae of 0.2m of vitrinite, mudstone, exinite and detrital material. Zones 29 – 38 are made of 88% vitrinite rich bright coal and carbonaceous shales.

The only operational mine within the basin is the Grootegeluk mine which probably derives its name from the mineable coal seam located in the Grootegeluk formation of the Waterberg Basin. The description of the lithostratigraphy of the Grootegeluk mine was done by the mine geologist who classified the coal seams into 11 zones. De Jager (1976) originally divided the Ecca from bottom to top into seams 1, 2, 3, 4A, 4, 5A, 5B, 5C, 6A, 6B, 6C, and 7 and the Geoscience, South Africa further retained the numbering of coal seam 1, 2, 3, 4 and 4A assigning them to the Vryheid formation which according to Siepker forms part of the Lower Ecca and middle Ecca formation. This classification was adopted by the geologist of the mine who further reclassified the other seams into seam 5 to 11.

Faure et al. (1996) established that the seam 1 and 2 coal seams are often overlain by a thin conglomerate film, nevertheless seam 1 reaches a total thickness of 2m but is general thin and contains bright coal bands at the base that grade into dull coal with shale partings at the top while seam 2 show uniform thickness of 1 - 4.5m in the west and 5.2m in the centre. The two seams are separated by a 5m interval of impure fine to medium grained cross bedded sandstone. The lower part of seam 3 contains a mixture of dull and bright bands of coal while the upper part is predominantly dull coal.

2.3.1.3.2.3. The Upper Ecca of the Ellisras Basin

Seam 4 and 4A mark the transition between middle and Upper Ecca succession in the field and are 4m to 9m respectively above seam 3. Seams 5 to 9 are made up of alternations of bright coals with massive carbonaceous shales which according to the Council of Geoscience

are also inter-bedded with siltstone and mudstones of the Upper Ecça division according to De Jager (1996) and belong primarily to the Grootegeluk formation.

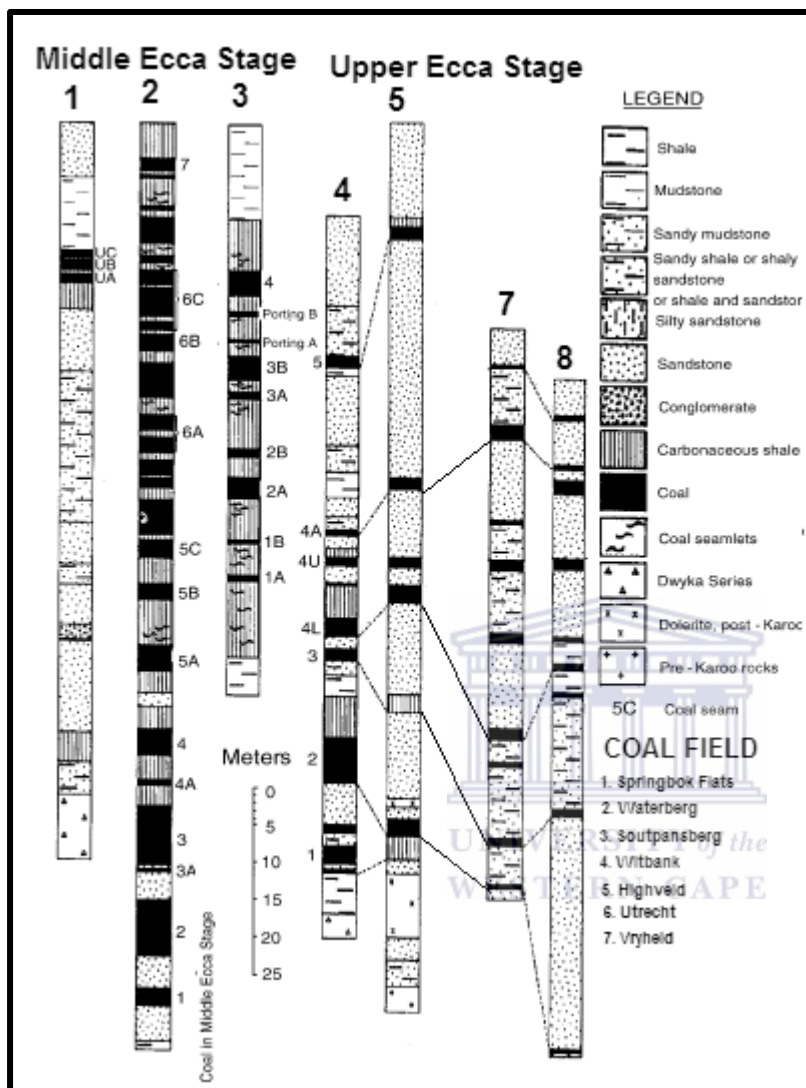


Figure 2.6: Succession of coal seams in the Upper Ecça, Middle Ecça and Molteno Stage in some coalfields in South Africa (modified after Jager, 1996)

2.3.1.3.3. The Beaufort Formation of the Ellisras Basin

The Beaufort formation of the Grootegeluk coal mine can be equated to Siepker's GUS 6 classification of the Eendragtpan Formation and lie unconformably on the Limpopo gneisses to the east and Northeast and conformably on the Grootegeluk Formation in other areas in the basin. The Formations' lithology is 110m thick in the central part and decreases to 40m wards the NE and is made up entirely of bluish grey, purple, yellow and red variegated mudstones that grades into silty mudstones in the lower third of the succession

with each colour lithology separated from the other by a sharp boundary. Siepker (1986) interpreted the Eendragtpan formation to be deposited within a floodplain.

2.3.1.3.4. The Stormberg Group

The post Beaufort Stratigraphy of late Triassic to Jurassic in the Waterberg basin is represented by the Stormberg group which according to Seipker (1986) and Johnson et al (2006) is represented by the Greenwich, Lisbon, Clarens and Drakensberg formations. These formations are correlated to the Molteno, Elliot, Clarens and Drakensberg formations as well as Molteno, Red Bed, Cave Sandstone and Drakensberg formations described by SACS (1980).

2.3.1.3.4.1. The Greenwich Formation of the Ellisras Basin

The Greenwich formation lies unconformably on the Eendragtpan formation with thicknesses of 7m-33m, narrower sections located in the North and East. Medium to coarse – grained purple-red-green-white cross bedded felspathic sandstones with lenses of grit, conglomerates and laminated mudstones characterise this formation. The formation is anticipated to be braided stream deposits.

2.3.1.3.4.2. The Lisbon Formation of the Ellisras Basin

The overlying Lisbon (GUS 8) or Elliot formation has a uniform thickness of 100m to 110m thick and is extensive throughout the Karoo of this basin with the succession made up of predominantly red massive mudrock with calcareous concretions, lenticular fine to coarse sandstones. The basal contact is sharp or gradational and depositional setting is interpreted to be meandering rivers and flood plain.

2.3.1.3.4.3. The Clarens Formation of the Ellisras Basin

The cream to off-white, well sorted, fine-grained massive sandstones of the Clarens formation mark the last sedimentary deposits of the Karoo time in the Waterberg Basin. This unit has a maximum thickness of 130m as inferred by Seipker (1986) and is characterised by large visible planar cross-beds which he inferred to be deposited in a palaeo-desert.

2.3.1.4. Coal Petrography of the Ellisras Basin

It has already been established that the Carboniferous to Jurassic coal deposits in Laurentia were deposited in a relatively warmer climatic conditions than those of the then South Pangaea or Gondwanaland. Consequently the organic material encountered in the coals of these two regions is different in content, type and volume. Cadle et al. (1993) reports that a prime difference between the Permian Gondwana coals and the northern Hemisphere Laurentian coals is the characteristic high content of inertinite in Gondwana coal particularly in the semifusinite group than those of the Northern Laurentian coals. Cold climatic conditions, fungal activities and atmospheric exposure of peat results to oxidation which is the main factor necessary for formation of inertinite (Snyman and Botha, 1993) which were prevailing during the Permian of Gondwana.

2.3.1.4.1. Paleao-Flora Distribution in the Karoo

Reports on the floral distribution in the Southern Africa's chronostratigraphic column show a distinct change in floral assemblages throughout the Carboniferous to the Triassic. Early literature on macro-palaeobotanics on South African stratigraphy was written by Plumstead (1957, 1966); Falcon, (1975b, 1978b, 1989) and Falcon et al., (1984a).

The Pre Karoo Cape super group acts as host to the "Lycopod Flora" which according to Plumstead is the earliest flora record in southern Africa. The late Carboniferous to early Permian Dwyka glaciation came along with a change in vegetation characterised by Conifers and moss in the early Karoo sequence (Falcon, 1986b; 1989) which were mainly deposited under cold temperatures while their pre- karoo counterparts were deposited in Arctic conditions. Falcon (1989) further established that the middle to upper Ecca in Southern Africa was characterised by repeated fluctuations of cold to cool temperatures in the Middle Ecca that gradually changed into fluctuations of cool to warm temperatures in the Upper Ecca while the early Ecca was succeeded by abundant gangamopterids which was quickly followed by a diversified mixture of Glossopteris- Gangamopteris, herbaceous Glossopteridophyta with minor proportions of lycopods, ferns, cordaites and early gymnosperms.

The late Ecca and early Beaufort formations (Late Permian) are characterised mainly by woody upland flora with swampy grown *Glossopteris* which is the predominant plant genre (Plumstead 1957, 1966). The Upper Triassic Molteno sediments are characterised by *Dicrodium* which is a fern like flora succeeded by fossilised woody sediments in the Clarens formation (Plumstead 1957, 1966).

The macro flora changes in southern Africa was representative of microfloras present i.e. the miospores. Falcon (1986) used the Saccate pollen miospore group to illustrate the vegetational changes in the South African Karoo stratigraphy since the saccate plants are less affected by minor changes in water level. He proposed six biostratigraphic zones for Karoo succession beginning with the Dwyka monosaccate rich micro-flora which was followed by the non-striated disaccate-rich microspore of the lower and mid Ecca. The Upper Ecca and Beaufort time was characterised by striated disaccate rich microspores which gave way to the non –striated disaccate microspores of the molteno i.e. Early Triassic time. It is therefore apparent that the vertical variation of micro flora and macroflora assemblages as well as the climatic conditions experienced during the deposition of the Karoo sequence in Southern Africa may be a reason for the variation of maceral associations within the various basins and the various strata of the Karoo.

2.3.1.4.2. Maceral Content

The petrography of South African Coals as well as related studies has so far been widely studied by Falcon (1986), Hagelskamp and Snyman (1988), Snyman and Botha (1993), Snyman et al., (1983), Krystyna (2003), Daniel et al. (2008) and Daniel et al. (2010). According to these authors coals from the MKB are generally rich in Inertinite maceral while those from the North Eastern Basins i.e. the Waterberg and Soutspanberg are rich in Vitrinite with minor proportions of the other maceral groups present for both MKB and NE Basins. Generally South African Permian coals characteristically have minor proportions of liptinite (less than 7% by volume) when compared to carboniferous coals (Cairncross, 2001; Snyman and Botha, 1993; Walker, 2000; Krystyna, 2003) but with considerable amounts, up to 60% of semifusinite (Hagelskamp and snyman, 1988).

The thick coal seams of the MKB are enriched with inertinite particularly in the lower part of the succession nevertheless the upper coal seams of the Witbank Basin are rich in vitrinite

content and register up to 60% for the number 5 seam (Monika et al., 2003) . In related studies Daniel et al. (2008) recorded contents of up to 88% inertinite for Highveld coal samples but pointed out that the dominating maceral type for this coalfield was Semifusinite with liptinite representing as low as < 3% by volume. These results follow closely with those derived by Daniel et al (2010) but reported that the identification of inertinite for the Highveld coals was hindered by the presence of low reflecting semifusinite and inertodetrinite. This is due to the fact that semifusinite and inertodetrinite has slightly higher reflectance than the accompanying vitrinite, visual recognition is highly subjective.

In the Waterberg coalfield, the coals are enriched with high vitrinite content. Daniel et al., (2003), Faure et al., (1996) accounts for up to 92% vol. of vitrinite for Waterberg coals with inertinite, liptinite and reactive semi-fusinite occurring in minor proportions. However the high vitrinite proportions decreases towards the base with corresponding increase in inertinite to 60% at the base but relative stable liptinite content. According to petrographic analysis carried out on 3 Permian samples from the Waterberg basin and 1 from the Soutspansberg basin by Monika et al. (2003), the results confirm those of Daniel et al. (2003) for predominant vitrinite rich north eastern Basins coals with an average of 75% by volume of Vitrinite. The results also established the presence of 4-12% of Pseudovitrinite as well as some minor dark vitrinite constituents. Pseudovitrinite is a more homogenous type of vitrinite with higher reflectivity (Daniel et al., 2010). The upward increase of vitrinite content is associated to an increase in the energy of the depositional environment which considerably was an important factor in the preservation of vitrinite (Faure et al., 1996).

The organic material in the Grootegeluk formation which holds majority of the coal seams in the Waterberg basin have widely different origins but where deposited in the same physical and chemical conditions and buried to same temperatures. Faure et al. (1996) stated that the major variation of maceral in the Grootegeluk Formation is principally between vitrinite and Inertinite which seem to be manifested in the varied extend of maceral degradation. He concluded that the high proportions of inertinite and reactive semifusinite (as illustrated in figure 2.7) at the base of the Grootegeluk formation coals and mudstones suggest that these coals were subjected to higher degradation than the organic material in the upper parts of the formation.

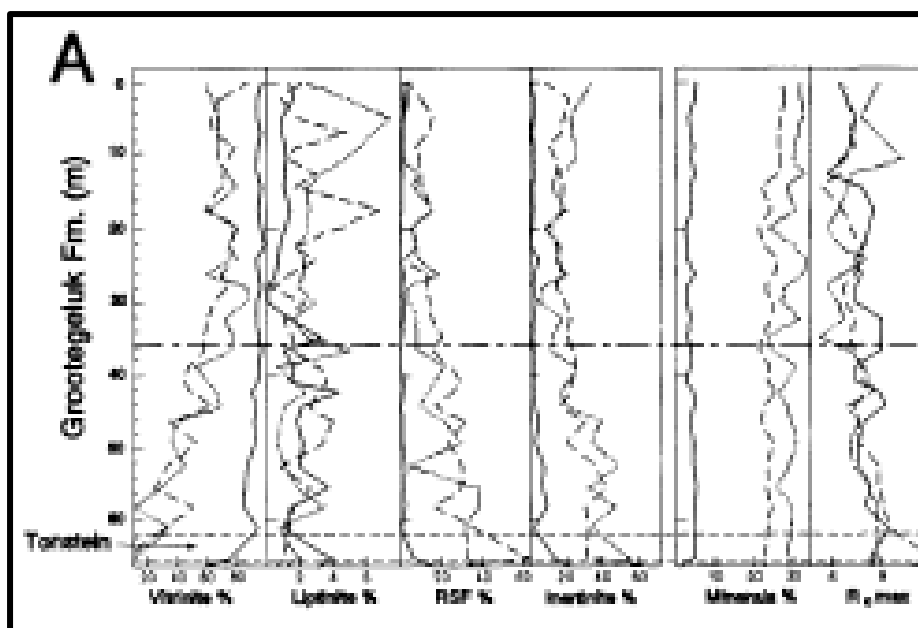


Figure 2.7: Maceral distribution in the Grootegeluk Formation at different relative density floats. Fairly stable liptinite conc., increasing vitrinite with corresponding decreasing inertinite towards the top (Faure et al., 1996).

Like all other South African Coals, the Liptinite content rarely exceeds 7% by volume even for Waterberg coals (Krystyna, 2003). Figure 2.7 shows fairly stable proportion of liptinite from the base to the top of the Grootegeluk formation coal but reduced values for liptinite in mudstone samples. Most techniques used for the quantification and identification of macerals are carried out in white light. Krystyna (2003) study on fluorescing macerals in South Africa coals made use of the fluorescence techniques and recorded much higher liptinite content for South African coals when compared to results of routine maceral analysis in white light. The difference he explained to be due to the difficulty in the identification of fine liptodetrinite particles under illumination by the halogen lamp. Krystyna records liptinite contents of up to 12% in the coals of the Greetegeluk formation contrary to results presented by Faure et al., (1996). Major sub liptinite maceral groups include sporininites, cutinite, liptodetrinite and resinite. Faure et al. suggested that the minor proportion of liptinite macerals are highly variable and show different trends in coal and mudstone groups which may be as a result of enrichment of liptinite in mudstone by degradation and the increase in liptinite in the coal due to the destruction of tissue cells by fusination rather than vitrinitisation.

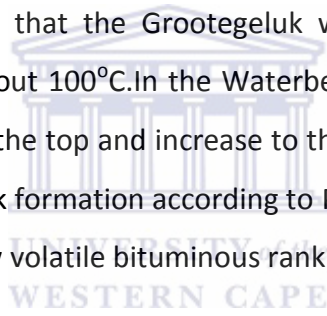
2.3.1.5. Coal Ranking

Coal rank as earlier seen defines the degree of coalification. It has already been established that an increase in coal rank is dependent on the temperature, pressure, degree of burial and resident time of a coal sample. Consequently the paleo-tectonic setting of a basin which determines the paleo-geothermal gradient should be taken into account when considering the coalification process of a particular coal sample. In the gently sloping MKB the Ecca coals generally show an increase in rank from west to east (De Jager, 1983) while those of the Beaufort-Molteno Formation increases in the South-eastward direction (Saggerson, 1991). The North eastern coal fields of the country, located in fault bounded basins generally vary from low to high ranks dependent on their initial depth of burial with associated greater heat flow related to fairly thin crust in these active tectonic settings (Cairncross and Langford, 1991).

Previously the generally consensus on the variation of rank of South African coals centre around the intrusions of dolerite sills and Dykes (Blignaut, 1952; Du Toit, 1954). Blignaut (1952) established that doloritic intrusions in South Africa affect coal seams over a distance that is equal to their thickness. Snyman and Barclay (1989) argues that this may not be true, questioning the absence of true anthracite formed close to dykes in South African coalfields where the coal ranks are generally low. In the Natal Coalfield, the entire range of ranks from high volatile bituminous coals to anthracite is present with higher ranks bounding dolerite sills, while in the coalfields of the Orange Free State and Transvaal commercially viable anthracite has not been discovered close to dykes and transgressive sills of dolerite (Snyman and Barclay, 1989). From their study, Snyman and Barclay concluded that the dolerite intrusive dykes or sills in South Africa affect the coals to variable distances, generally from 0.6 to 2 times the thickness of the intrusion whereby this distance is dependent on the rank of the coal outside the metamorphic aureole. They further stated that where the metamorphism of the coal is caused by dolorite intrusions, the specific metamorphic effect is defined by the maximum temperature of the intrusion, the period of cooling of the magma, the period of cooling of the magma, the rank of the coal prior to intrusion and the thermal diffusivity of the coal and rocks. Consequently the rank of South African coal is dependent on contact metamorphism from intrusive bodies as well as the superimposed burial metamorphism and that the regional increase in paleo-geothermal gradient

eastwardly probably related to the large-scale magmatic activity that culminated in the extrusion of the Drakensberg basalt resulting in the formation of anthracite in the far eastern Transvaal and Natal.

Very little information is provided for the quality of the coals in the Waterberg basin. Jeffrey (2005) suggested most of the information on the rank of the coalfield is drawn from the Grootegeluk Coal mine which is the only one located in the region and that by assumption rank variation is similar to the West-East increase in rank proposed by De Jager (1983). Although the coal in these basin is bounded in a small area, according to Dreyer (2006) they form 50% of South Africa's Bituminous coal reserves. He further reported vitrinite reflectance of 0.72% for the Grootegeluk formation which corresponds to medium ranked C bituminous coal. Faure et al. (1996) infers same value for average vitrinite reflectance for the Grootegeluk formation but reports that it ranges from 0.52% to 1.06% and that palynological evidence indicates that the Grootegeluk was subjected to maximum post depositional temperatures of about 100°C. In the Waterberg Basin, the vitrinite reflectance of the coal samples are lower at the top and increase to the highest value at the base. Most of the coals from the Grootegeluk formation according to Pinheiro et al. (1998) and Krystyna (2003) are of medium rank C (low volatile bituminous rank).



CHAPTER 3: LITERATURE REVIEW

3.1. Review of Coal Geology

Coal is a sedimentary rock formed from the accumulation, burial and transformation of plant debris in specific depositional environments. Thomas (2002) also describe coal as a sediment, organoclastic in nature, composed of lithified plant remains, which has the important distinction of being a combustible material. For centuries now coal has been a major source of energy in the world use for generation of electricity, steel and cement manufacturing and domestic consumption. In recent years the global coal consumption has witness an increase in growth with additional uses as liquid fuel, in pharmaceuticals, coal bed methane and most recent attempts to use coal seams to sequester anthropogenic carbon dioxide. In South Africa there is an approximate dependence of 75% on coal as a source of energy.

3.1.1. Formation of Coal

Coal is form from residual plant material via a process called coalification. Thomas (2002) defines coalification as the alteration of vegetation to form peat, succeeded by the transformation of peat through lignite, subbituminous, bituminous, semi – anthracite to anthracite and meta-anthracite rank. The early stages of coal formation are characterised by Biological and Chemical degradation or organic material via a process called diagenesis. The onset of coalification is the formation of peat; a partially decomposed plant material (debris) formed under stagnant anoxic water but void of microscopic organism such as bacteria and fungi that can enhance decomposition. Most often these environments are poorly drained and over a long period of time the partially decomposed debris becomes peat. At the very early stages of peat formation, plant debris such as pores, twigs, branches and leaves settle at the bottom of stagnant swamps and are decayed aerobically by bacteria reducing their volume to 50% and giving off gases like carbondioxide, methane and water. Due to no aeration of the stagnant water, the bacterial quickly use up all the oxygen and aerobic decomposition stops. Decay is now catalysed by anaerobic bacteria and the process is accompanied by the production of acids and further matrix volume reduction. As acid levels rises to about 4.0, the anaerobic bacteria are killed and decomposition ceases. The

peat is now a dark brown, cheesy and gel like material which increases in quantity as bacteria activity continues in the upper columns.

This phase is gradually followed by a geochemical or metamorphic phase characterised by gradual or rapid increase in temperature which is dependent on the rate of deposition of overlying sediments and resultant burial. As the depth of burial and temperature increases, compaction increases and chemical reactions set in. These reactions result in the decrease of the Oxygen and hydrogen content mostly in the form of water with a corresponding increase in Carbon content and calorific value. During this process the peat loses its distinguishable plant remains while black macerals are produced. Progressive increased burial (temperature) is accompanied by correspondent increase in coal rank, physical and chemical processes.

The control of coalification is governed by three key parameters, temperature, time and pressure. The two main sources of temperature for coalification are igneous intrusions either from minor bodies or from deep seated intrusions and temperature from sediment burial. General increase in coal rank is dependent on the geothermal gradient and heat conductivity of the rock. High geothermal gradient cause the formation of high rank coals at shallow depths and vice versa. The effects of temperature is not independent of time, higher coal ranking is easily achieved with rapid heating rates in contact metamorphism than in slower heating rates from subsidence. In the same way, when sediments take longer time for burial implying longer cooking time a higher ranking is achieved than when subsidence is rapid. At the initial stages of coalification i.e during formation of peat to sub bituminous coal, the influence of pressure is at its greatest most especially in the reduction of porosity (Thomas, 2002) as well as in the expulsion of water.

3.1.2. Coal Rank

This refers to the degree of transformation of coal (figure 3.1). Coal rank is a function of the temperature regime, amount of cooking time and burial that a particular coal has gone through. It is also a function of constituent of the coal. Rank classification systems have been widely discussed by several writers and vary from region to region around the globe and are mostly dependent on its usage. One of the oldest classifications is by Seyler who centred his classification on the Carbon and Hydrogen proportion of the coal compared to

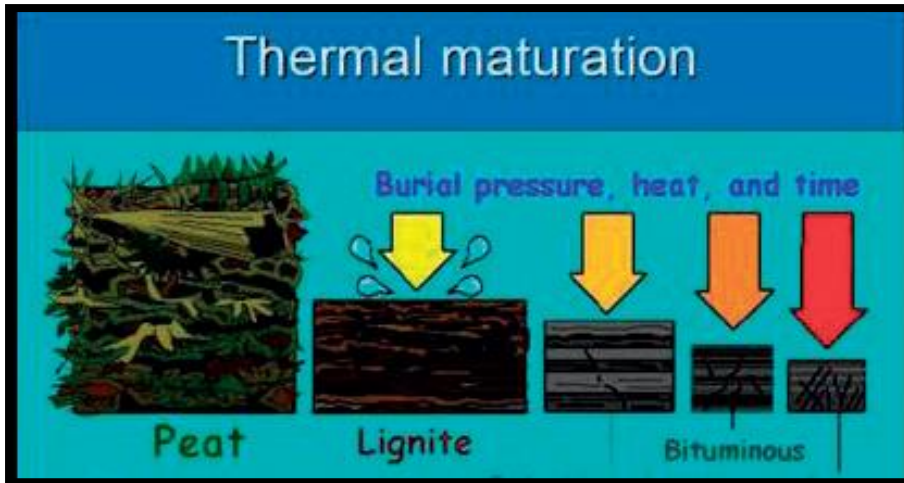


Figure 3.1: Coal rank depends on thermal maturity (Courtesy Kansas Geological Survey) in Crain, 2010

its dry mineral matter free basis. According to Seyler high rank coals have a high carbon and low hydrogen content with the reverse true for low rank coals. The American Society of Testing and Materials's (ASTM) classification is based on the fixed carbon content, calorific value and the cooking properties of the coal. The international Organisation for Standardization's ISO classification design for Europe to assist international trade makes use of the chemical and physical characteristics of Coal that are useful in the main market areas. Other classification systems include the Australian Standard Board and the Nation Coal

Table 3.1 ASTM Coal rank modified from ASTM D388-88, 1979

Class	Group	Abbreviation	Vitrinite
Anthracite	Meta Anthracite	ma	↑ Increase Vitrinite Reflectance and Rank
	Anthracite	an	
	Semianthracite	sa	
Bituminous	Low Volatile	lvb	
	Medium Volatile	mvb	
	High Volatile A	hvAb	
	High Volatile B	hvBb	
Subbituminous	High Volatile C	hvCb	
	Subbituminous A	subA	
	Subbituminous B	subB	
Lignite	Subbituminous c	subC	
	Lignite A	ligA	
Peat	Lignite B	ligB	

Board Classification of the United Kingdom which based their Classification on the chemical properties and the volatile/cooking properties of coal respectively. A more general and holistic characterisation utilises the vitrinite reflectance (VR) of the coal. VR is a property of coal that describes the amount of reflectance emitted by a polished coal surface. According to his classification coals with low VR i.e. dull coals are low in rank while those with high VR i.e. bright coals are higher in rank.

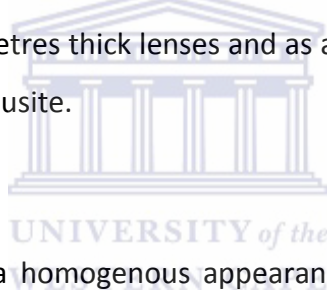
3.1.3. Coal Type or Lithotype

Ward (1984) defines coal petrology as the study of the origin, composition and technological behaviour of the different microscopic entities of coal while Coal Petrography is the systematic quantification of the microscopic proportion and characteristics of these materials which can be studied as macroscopic and microscopic components. It has already been established that coal is composed of decay and metamorphosed plant debris and since primarily trees form the bulk constituent in swamps, all coals in essence seem to be made up of similar fossil material. Physically coal is made up of three distinct components, moisture which may be surface or chemical bond, pure coal or maceral that forms the amount of organic substances and mineral matter which is made up of the inorganic components usually consisting of a series of primary and secondary minerals. Most often the amount of mineral matter is wrongly considered as the ash content which describe the residual material left after the combustion of coal. The amount and variation of the organic matter (microscopic) that makes up coal determines the physical appearance of the coal. This physical description of coal base on the mixture of microscopic components is term macroscopic description or coal type. When the coal is composed of different mixtures of microscopic plant remains, it is referred to as *Humic* but when made up of a limited mixture of plant debris it is referred to as *Sapropelic*.

3.1.3.1. Humic Coal

These are sometimes called banded coals because when examine with the naked eye they appear to be made up of distinct stratification consisting of layers of organic matter with different appearances. These coals are made up of assorted mixture of decay plant material. Stopes (1919) proposes a four recognisable distinction (lithotypes) for banded coal classification. These lithotypes are outline bellow.

- **Vitrain:** Name derived from the latin word Vitrum with means glass. It is a black, glass, brittle and vitreous substance that usually occurs as thin bands with close joints and break into angular fragments. It is mostly found in humic coals and contain the micro - lithotype Vitrite.
- **Clarain:** Its name is derived from the latin word Clarus which means bright. Lithotype is characterised by bright and silky lustred finely laminated coals. Common microlithotypes include Clarite, vitrite, durite, and fusite.
- **Durain:** The name comes from the latin word Durus which means hard. Lithotypes is characterised by grey to dark bands with dull or greasy lustre that breaks into rough fragments. Durain bands are usually thicker than 3-10mm and are less common in humic coals. Dominant micro-lithotype is Durite.
- **Fusain:** name comes from latin word Fusus that stands for spindle. Lithotype is characterised by soft black and friable material that easily break into fibrous powder. It occurs in several millimetres thick lenses and as a minor component of most coals. Main micro - lithotype is Fusite.



3.1.3.2. Sapropelic Coal

These coals are usually having a homogenous appearance limited variety of microscopic debris particularly high concentration multitudes of spores or algae. They are fine grained, dark in colour, have a dull greasy lustre, tough and often display conchoidal fracture. They often occur as faintly bedded to massive material banded with humic coals, most often forming roof material. There are two distinct Sapropelic macro-lithotypes, the *Boghead and Cannal coal*. Their fine nature makes it difficult to distinguish between the two of them in hand specimen. Intermediate forms are usually present, either Boghead – Cannal or Cannal Bog head Coal.

- **Cannal** coals are dark or dull homogenous material that is made up of mainly spores and fine organic mud deposited under water. They break with conchoidal fracture. Under the microscope they show micro-stratification.
- **Boghead** Coals on the other hand are composed of algae materials and may grade vertically or laterally into oil shales.

3.1.4. Coal Macerals

This section describes the organic elements that make up the coal framework. An examination of coal samples with the bare eye or under the microscope usually shows some stratification. Such stratification is derived from the variation of the plant material that makes up the coal. The type of organic material can only be identified and distinguished by examination of their microscopic components. Macerals are therefore micro-organic substances found in coal and can be compared to mineral components of inorganic rocks. The name maceral was first used by Stope in 1935. Later that year the Heerlen Congress adopted some of the maceral names that Stope used and the Stope – Heerlen classification of macerals was approved universally.

Table 3.2 Stopes – Heerlen Classification of Maceral Groups, Macerals and Submacerals of Hard Coal. After Stopes (1935) seen in Ward (1984).

Maceral Group	Maceral	Submaceral	
Vitrinite	Telinite		
	Collinite	Telocollinite	
		Gelocollinite	
		Desmocollinite	
		Corpocollinite	
Liptinite (Exinite)	Sporinite		
	Cutinite		
	Suberinite		
	Resinite		
	Alginite		
	Liptodetrinite		
	Fluorinite		
	Bituminite		
	Exudatinitite		
	Inertinite	Fusinite	
		Semifusinite	
		Macrinite	
Micrinite			
Sclerotinitite			
Inertodetrinitite			

This classification scheme utilises the physical appearance (morphology) and optical characteristics of macerals on a polished section under reflected light, their chemical

characteristics and their Botanical affinity to characterised coal into three broad groups. A detailed description and summary of each maceral and corresponding affiliate macerals from the various maceral groups can be found in the International Hand Book of Coal Petrography published by the International Committee of Coal Petrology (I.C.C.P. 1963, 1971). A coal sample may be made up of a single maceral type or group of two or more macerals. Such associations are term micro-lithotypes when studied under the microscope.

3.1.4.1. Vitrinite Group

The maceral Vitrinite originates from the roots stems and leafs of plants i.e. lignin and cellulose from plant cell wall as well as tannins that fill up cell lumen. It is considered the most predominant maceral group in most coals. It is moderately transparent and appears coloured in various shades of red orange and brown (Ward, 1984). According to Teichmuller (1989) the vitrinite group contains three morphological distinction; telinites (Telocollonite) from cell tissue, detritites (Desmocollinite) form tetritus material and gelinites or collinites (Gelocollinite) from gels.

When vitrinite occur as coalified products of plant stems, barks and large roots particularly in bands of 3-12mm and distinct cell structures such as the cell wall is visible it is called telinite but when the cell wall is nonvisible it is term telocolinite (Ward, 1984 and Teichmuller, 1989). If the degraded material resulted from tinier plant tissues such as grass and reeds as cell fragments or humic colloidal particles that usually occur as an attrital or detrital admixtures with other maceral and minerals the vitrinite is termed Desmocollinite. These particles are dark in reflected light and often have lost much of their structure. If during the decomposition lignin or cellulose tissue by fungi and bacterial is accompanied by the production of colloidal gel and the cell lumen of the material, the vitrinite is termed gelocollinite. Corpocollinites occur as circular, elliptical or rod-shaped bodies in isolation or as cell fillings (Ward, 1984).

3.1.4.2. Liptinite (Exenite)

These are diverse accumulation of small organic material derived from hydrogen-rich plant organs as well as from algal and bacterial substances with plant lipids, proteins, cellulose and other carbohydrates being the main sources of liptinite (Techmuller, 1989).They are

pale in colour when viewed in under transmitted light and dark in reflected light compared to their vitrinite equivalents. The stability of liptinites in their optical properties decrease with an increase in coal rank. They are relatively stable (low reflectance and high fluorescence) from peat to subbituminous coals. Higher ranking coals have increased reflectance and reduced fluorescence.

The sub-maceral nomenclature of the liptinite group as shown in Table 3.2 is generated from the small particles that make up each submaceral group. It is called sporinite when derived from the outer cell wall of pollen and spores. Alginite is representative of coalified algae; occur rarely in humic coal and more in sapropelic coal. Resinites is derived from resins, waxes, fats, and latexes. Cuticles from the surface of leaves and twigs make up the cutinite maceral. Suberin a waxy polymer in corky cells of plants make up the Suberinite.

3.1.4.3. Inertinite

Inertinite macerals are derived from same sources as those of vitrinite. They are only different in that inertinites are more oxidized than vitrinites during the very early stages of coalification. The group name inertinite was chosen because these macerals show relative inertness in technological processes such as coke manufacturing when compared to other macerals from different groups. High reflectance, higher carbon and lower hydrogen content compared to other macerals in coals of equivalent rank are characteristic of most inertinite macerals. Table 3.2 Show the various subgroups of the inertinite group. Since inertinite is derived from oxidized material they do not change much during the coalification process.

3.1.5. Micro-Lithotype

Teichmüller (1989) and Ward (1984) define micro - lithotype as the naturally occurring association of macerals as seen under the microscope. Consequently the nature of distribution of these macerals is key to micro-lithotype formation. Micro- lithotypes can be made up of a single maceral (monomaceral) or two macerals (bimaceral association) as well as all three macerals which forms a trimaceral association. A minimum bandwidth of 50 micrometres must be reached and each constituent that make up less than 5% of association must be disregarded before an association is classified as a micro-lithotype according to established convention such as I.C.C.P. (1971).

Table 3.3 Micro-lithotype Composition (McCabe, 1984)

Microlithotype	Composition
Vitrite	Vitrinite>95%
Liptite	Exinite> 95%
Inertite	Inertinite> 95%
Fusite	Inertite with no macrinite or micrinite
Clarite	Vitrinite and exinite> 95%
Durite	Exinite and Inertinite> 95%
Vitrinertite	Vitrinite and Inertinite> 95%
Trimacerite	Vitrinite. Exinite, inertinite, each > 5%

3.1.6. Moisture and Volatile Material in Coal

Coal moisture occurs in four different modes.

Surface Moisture: This is peripheral water that occurs as coatings or layers on the surface of coal particles. This moisture can be removed by low temperature air drying.

- **Hydroscopic Moisture:** This is moisture held in the capillaries of the coal substance (Ward, 1984)
- **Decomposition moisture:** This kind of water is assimilated in some of the coals organic substances.
- **Mineral moisture:** This is water incorporated in the crystal structure of clays and other minerals present in the coal.

Volatile matter in coal refers to all coal components but for moisture that are release at high temperature in the absence of air. This material comes from the organic matter in coal and a very minor part of it from the mineral matter. The amount of volatile material varies with different coal rank and types, the determination of the amount of volatile material is very necessary to set standards for various coal usages. For example, if the generation of electricity by stoker firing a volatile matter limit of 25-40% is (d.a.f) is required (Thomas, 2002)

3.1.7. Carbon and Hydrogen

They occur as complex hydrocarbons in the organic component of coal. Carbon may also be trapped in the molecular structure of carbonates while hydrogen may form part of the water in clay and hydrous minerals. They are both liberated as carbon dioxide and water after the coal has been heated. In some cases they occur as methane (CH₄) adsorbed chemically or physically on the coal surface.

3.1.8. Fixed Carbon

This is carbon found in coal after all volatile material has been given off. It is used as a measure of the amount of coke produced from a coal sample after carbonisation.

Other elements that commonly occur in coal include Nitrogen, sulphur, oxygen, Chlorine, Phosphorous. Sulphur occurs as organic sulphur, sulphides in minerals and sulphate minerals as hydrous ions and sulphur sulphates (Thomas, 2002). Both Nitrogen and Sulphur when present in coal poses problems with utilisation and pollution. Oxygen forms part of most of the organic, inorganic compounds as well as water in the coal while chlorine is present in very low proportions as inorganic salts. Chlorine contributes to atmospheric pollution in flue gas and causes corrosion in boilers.

3.1.9. Coal Distribution and Age

As earlier seen, coal is a product of the remains of decay plant debris. As a result when discussing the distribution of coal deposits around the world reference is to be made to their chronostratigraphic appearances or units. According to Thomas (2002), land plants first appeared in early Palaeozoic but withstanding the first coal deposits are registered to be of Devonian in age with the Carboniferous-Permian Periods forming the first substantial coal accumulations. He further established that during the entire geologic columns there are only three major episodes of coal accumulation. The high ranked, structurally deformed worldwide black coal reserves formed during the carboniferous and early Permian periods are the first significant occurrence. The second major episode occurred during the Jurassic-Cretaceous period present in Canada, the USA and the Commonwealth of Independent States CIS. The Tertiary Period marked the third major episode characterised by the deposition of most of the world's brown coal with thick seams that have undergone minimal structural deformation. These coals rank from Lignite to Anthracite.

The deposition and occurrence of coal worldwide as well as the kind of coal deposited could be linked to plate tectonics or paleo-plate movement. Plate tectonics describes the movement of blocks of the earth crust relatively to one another as a result of convection current upwelling from the asthenosphere. Today's positioning of continents or landmasses at different locations on the globe results from plate movements. A reconstruction of the shorelines of landmasses show strong evidence that millions of years ago all landmasses were once together; the Pangaea. As proposed by Du Toit (1937) the northern part of the Pangaea (Laurasia) started moving away from the Southern Pangaea (Gondwanaland) in the early Triassic time and continues lateral extension resulted in the formation of today's continents.

Before the onset of continental break up, during the Carboniferous, the Pangaea as a whole was located towards the south of the globe with the North Pangaea (area occupied by present day USA, CIS and Europe) equatorially located (Thomas, 2002). Such tropical equatorial climate gave rise to the formation of peat mires with floral such as *Lepidodendron* and *Sigillaria*. During this time Gondwanaland experience no coal deposition. Deposition only begin in Gondwanaland (present day South America, Southern Africa, India and Australia) during the early Permian time under cooler climatic conditions with peat mires characterised by *Glossopteris* flora (Thomas, 2002).

Though the cretaceous plate tectonics was dominated by the breakup of the Pangaea there are astonishingly very few coal deposits associated to rift basins or passive continental margins, rather most cretaceous coal deposits are located in the foreland basins created by thrusting and crustal loading (McCabe, 1984). As a result detailed chronostratigraphic delineation of coals has been difficult due to the non-marine nature of these deposits but for the carboniferous with a few marine regressive sequences enabling their differentiation into stratigraphic sections with the aid of intercalated mudstones. Consequently in establishing a stratigraphic framework for coal bearing sequences we need to combine both lithostratigraphic and chronostratigraphic study i.e detailed examination of the coals themselves or an examination of the sedimentary sequence in which these coals occur (Thomas, 2002).

3.2. Coal Bed Methane Resource

Methane (CH₄) is an saturated hydrocarbon with four hydrogen atoms and one carbon atom bonded covalently in every molecule. It is the most common natural gas and the first member of the alkane series. It is described by some writers as one of the most abundant organic compound on earth as such it is a very valuable source of fuel but controversially a toxic greenhouse gas. Under standard conditions i.e. room temperature and pressure it occurs as a colourless and odourless gas. It boils at a temperature of -161°C. It occurs naturally as geologic deposits in gas fields where by coal seam is adding as a major source. Methane is a product of fermentation of organic matter. In geologic formations at shallow depths it is formed from biological processes mainly by anaerobic decay of organic matter while at greater depth it is generated from diagenetic or catagenetic processes i.e. it is a by-product of coalification (Cervik, 1969). When compared to natural gas from conventional reservoir, CBM is cleaner (over 90% methane) containing small portions of other gases and can be introduced into commercial pipelines with little or no treatment (U.S. EPA, 2004).

Coal Bed Methane (CBM) previously referred to as Coal Mine Methane by miners is sometimes called coal seam gas (CSG). We can therefore define Coalbed Methane as Methane that resides within coal seams while Coal mine methane is methane that resides within coal seams and its surrounding strata but given off as a result of mining activities (U.S. EPA, 2008). CBM exploration and production activities are still in the very early stages in the world. In conventional oil and gas exploration, geologist focus on the five components of the petroleum system (source, reservoir, trap, migration and seal) which in most cases are spread around different rock units. The reservoirs are usually sandstones or carbonates, shale form the source rocks, very low permeability rocks form the seal while trapping may be structural, stratigraphic or a combination of the two. Consequently exploration and production activities require analysis of all the various rock units active in the entire petroleum system. Unlike conventional hydrocarbon systems the CBM petroleum system is concentrated on a single rock unit; the coal seam which acts as source, reservoir and trap. In this section we shall look at coal as a reservoir rock paying attention to important reservoir properties like porosity, permeability, cleat network, we shall briefly discuss coal trapping mechanism of sorption as well as recent global advances in the exploration and development of CBM.

3.2.1. Recent Trends

Countries like the United States of America, Canada, China, New Zealand and Australia have made some significant progress in exploration and production of CBM. CBM activities in South Africa are still in the very early stages with main focussed centred on exploration. Finding coal apparently is the first step toward the development of the resource but not all coals are suitable for CBM development. The coal needs to be characterised for its potential use, these attempts are numerous but mostly tilted toward mining and development of the resource for other uses. South Africa has vast coal deposits and its economy rely heavily on the development of this resource. According to Jeffrey (2005) 73% of South Africa's primary energy needs in the form of electricity, liquid fuels, cooking and heating are provided by its coal industry. The coals in South Africa are locked in 19 different coal fields with the latest total estimated reserve of 33.8 billion tons set by Mineral Bureau of Mines (Prevost, 2004). The characterisation of South African coals makes use of different criteria for different processes; such includes thicknesses, maceral content, rank, grade, moisture and a multiple of others. Characterisation geared towards methane mine degasification usually quantifies the amount of adsorbed gas, fracture bound gas, flow characteristics, fracture or cleat geometry. Such characterisations are also necessary for CBM production.

In the mid 1990's due to coal production South Africa was ranked in the top five CMM emitters in the world but when re-estimated in 2000 she ranked 11th (M2M, 2008). The amount of methane released from South Africa's coalmining industry decreased from 323 GB/a in 1990 to 317Gb/a in 1994 as estimated by the National Communication, however recent studies by University of Cape Town Energy Research Centre reports estimates of 72Gb/a (Lloyd et al., 2003). Despite these figures the percentage of operating mines in South Africa considered "gassy" is very low (M2M, 2008). This can be explained by the estimated 80% of methane loss during the coalification process particularly in the shallower fields (UNFCCC, 2000). According to Lloyd et al. (2003) 88 percent of methane released was directly from underground mines while the rest was from recently mined coals and surface mines. Although the figures of methane in South African coals particular in the deeper fields are high the methane to market International CMM Project currently identifies no CMM operation or Development recovery projects in South Africa (M2M Projects, 2008). CBM resource in South is estimated to be 0.14 – 0.28 trillion m³ (M2M, 2008). In the United States of America exploration activities to aid reduce methane emission began in 1989,

identifying coal mining as a significant global source (Schultk, 2003). Just like in South Africa surface mining in the United States accounts for the greater half of its coal production (67%), nevertheless surface mining constitutes only 16% of America’s methane emissions (USEPA, 2008). U.S. seconds China as world largest methane emitter with 133billion cubic feet (Bcf) liberated in underground mines in 2001(Schultk, 2003).

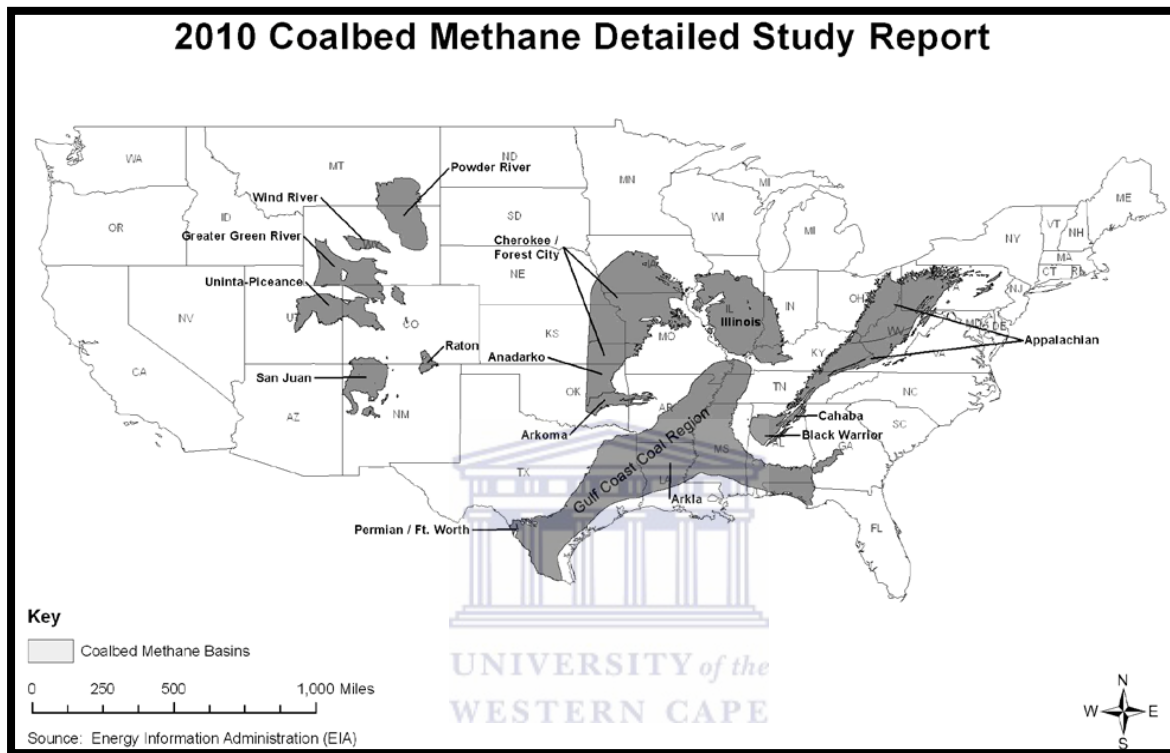


Figure 3.2: Locations of Currently Producing CBM Basins in USA. (U.S. EPA, 2010)

The earliest attempts of commercial CBM production was from the Mulky coal seam in south eastern Kansas in 1920 were vertical wells drilled for approximately 1000fts deep were thought to be producing from shaly formation not knowing the source was the Mulky coal seam (Stoeckinger, 1990). The driven force behind the development of CBM was the creation of a safe environment for mining. In 1954 Haliburton carried out an experimental project to fracture the first CBM well and by 2000, 3.7 Bcf/D of methane was produced from 13 986 wells in the United States of America (Principle and Practice CBM, 2007). Gathered from different sources, estimates for CBM resources in the U.S. is in the neighbourhood of 4 to 11 trillion cubic meters (Tm^3) (Kuuskra, 1992; Cairn Point Publishing, 1997; Schultz, 1998; Potential Gas Committee, 2001) ranking behind Canada, Russia, China and Australia.

Currently CBM is being produced in 15 basins in the United States (figure 3.2) (U.S. EPA, 2010a).

In 2008 CBM production from 12 of the 15 production basins in United States totalled 1,988 Bcf with highest production of 755 Bcf from the San Juan Basin followed by Power River Basin with 607 Bcf (U.S. EPA 2010a).

3.2.2. Coal Bed Methane Production

Methane in coal is stored in the coal fractures as free gas or absorbed in the coal matrix. Adsorption of methane onto the coal seam is facilitated by pressure from the water in the coal seam (U.S. EPA, 2010). As earlier seen in this section methane released from coal mines in both South Africa and America is approximately four times greater for deeper coal seams than in the shallower ones. It is also established that this is due to better maturity in the coals as a result of coalification. Proper burial condition is therefore required to trap methane in the coal seam or coal forming substance. The United States Environmental Protection agencies (2010) explains that coal gas content relies heavily on the Rank of the coal where the low rank coals (peat and lignite) contains small proportions of biogenic gas associated with high porosity and high water content while in the high rank coals, the heat which accompany their formation helps in the breakdown of complex organic matter. As a result higher rank coals (bituminous) contain high gas content, low water content and high porosity and are usually the target of CBM development. However anthracites which rank highest have low methane and water content accompanied by low porosity (ALL, 2002).

At great depths, underground and open cast mining is no longer possible. Poor structural geometries of the coal seam also make it not possible or costly to exploit the coal resources. Apparently Coal Bed Methane production becomes the only option in utilising this coal resource. Gas production of 10 to 15 million standard cubic feet per day is not uncommon for deep mines in U.S.A. (Thakur, 2003). During mining once a flow path is established the fractured held methane quickly escapes into the mine shaft while the matrix bound methane dissolves relatively slowly and approximately 50% of it is lost within the first day (Lloyd et al., 2003).

Table 3.4 Main Difference between conventional and Coalbed Methane Reservoir

Conventional Gas	CoalBed Reservoir
Gas flow to well bore by Darcy flow	Diffusion through micro-pores by Fick's Law. Gas flow to well bore by Darcy flow through natural fractures
Storage of gas in macro-pores.	Gas storage by adsorption on micro-pore Surface, free gas in fractures and absorbed gas in matrix
Reservoir different from source rock. Requires seals and traps for resource accumulation.	Reservoir and source rock are same. Requires burial and pressure for accumulation.
Pore size is usually macro: $1\ \mu$ to 1 mm (Levine, 1990).	Pore sizes are predominantly micro: 5\AA to 50\AA (Levine, 1990).
Gas Storage reliant on pore volume	Gas storage reliant on surface area of micro- and meso-pores. Gas is trapped by organic substance.

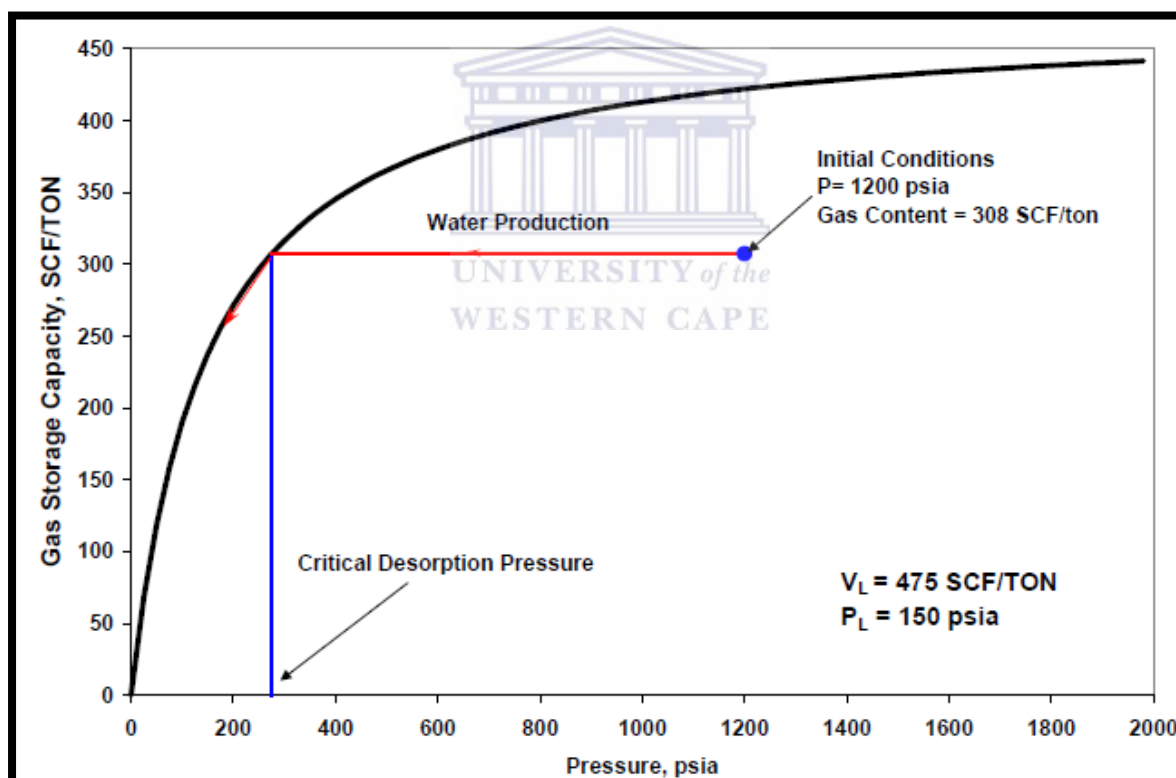


Figure 3.3: Typical Langmuir Isotherm (Aminian, 2007)

CBM production requires drilling into the coal formation. Once the formation is open to the borehole, water is produced from the coal seam of interest and the formation pressure drops releasing methane from the seam (Wheaton et al., 2006; U.S. DOE, 2006). Initially the well produces mainly water and once the pressure drops in the fractures network is significant i.e. at “critical Desorption pressure” gas desorbs from the matrix (Aminian, 2007).

According to Aminian this pressure is the pressure on the sorption Isotherm corresponding to the initial gas content as illustrated in figure 3.3. In most cases due to the low permeability of coals, hydraulic fracturing is needed for coal production.

3.2.4. Coal Petrophysical Parameters

3.2.4.1. Coal Fractures or Cleats

Fractures are present in all rock types but are highly visible and probably more important in sedimentary rocks particularly in coals and shale. Cleats, another name used for natural occurring fractures in coals accounts for a large amount of Coalbed gas reservoir porosity and permeability and literature on it covers more than a century (Laubach et al., 1998). In coals there are generally five different types of natural fractures present with at least two fracture sets oriented perpendicular to each other and the bedding surface (Dipak et al., 2004). Coals have the tendency of breaking along their natural fracture system. The perpendicular fracture system is made up of face cleats and Butt cleats. Face cleats are more dominant and often extend long horizontal distances cutting across different bedding surfaces while butt cleats are short poorly developed and often truncated by face cleat (Diamond et al., 1976). Face cleats are also known as master or main cleats while Butt cleats could be called board or cross cleats. Dipak et al., (2004) established the presence of tertiary cleats in coal reservoirs which may be micro in dimension or may be faults. Micro cleats differ from face and butt cleats in their direction and size and often terminated on the perpendicular cleats system. On the other hand fractures and faults usually cut across coal seams and non-coal beds. Figure 3.4 is an illustration of the relationship between face, butt and micro cleats.

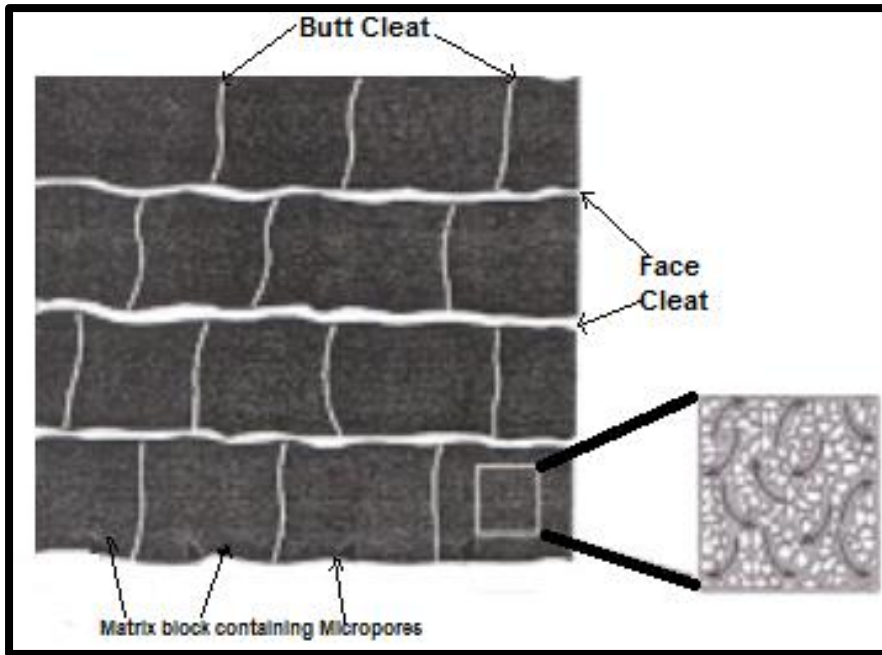


Figure 3.4: Relationship between different cleats in Coal (Dipak et al., 2004).

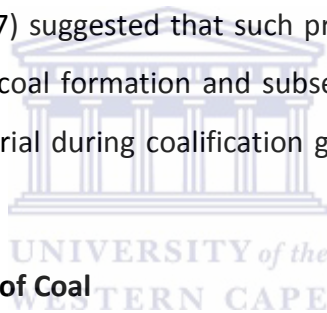
Dimensionally cleats are very close to each other. Their spacing varies from a few millimetres to ten centimetres (Dipak et al., 2004). Most cleats are generally centimetres in length and heights and typically have nearly indiscernible apertures (Laubach et al., 1998). Most studies on cleat width base their measurements on out crop studies and on microscopic examination of coal samples under non confining pressures. Gamson et al. (1993) estimated cleat widths under in situ conditions to range from 0.001 to 20mm. In most cases cleats are limited to individual coal beds particularly those with same maceral types, sub-vertical in horizontal beds and oriented at right angles to stratification even in tilted and folded units (Laubach et al., 1998).

3.2.4.1.1. Origin of Cleats

Controversies exist as to the origin of coal cleats. Some writers consider a tectonic origin (Kaiser, 1908; Sturtzer et al., 1940) while others consider a non-tectonic origin; some also consider a combination of both Tectonic and non-tectonic origin (Hofer, 1915; Moore, 1932). These broad controversial theories are a sum up of various generic questions to the origin of cleats. Are they a result of stresses caused by folding and faulting or result from contraction of coal during dewatering and chemical metamorphism? Do they results from

heat and elastic response to tectonic extension and uplifts or to increase pore pressure caused by the expulsion of water?

The tectonic origin of cleats was pioneered by Kaiser (1908) who postulated that since in England the strike of the cleat was parallel to the fissures formed in the region, then the cleat must have a tectonic origin. Hofer (1915) argued that cleats are fissures that originate from the contraction of carbonaceous material during progressive coalification of the original plant material. In latter studies by Ammosov et al (1963) the origin of cleat is anticipated to be a product of both nontectonic and tectonic processes where one type of cleat is endogenetic i.e. relies on the nature of the rock in which contraction takes place during cooling and recrystallisation while the other type exogenetic with fractures resulting from external forces during the last stages of development of the tectonic process. The nature and uniqueness of coal cleats is an indication that they are formed from a process common to all seams. Ting (1977) suggested that such processes involved the compaction and coalification of peat during coal formation and subsequent dehydration associated to shrinkage of carbonaceous material during coalification generating stress that permits the formation of fractures.



3.2.5. Porosity and Permeability of Coal

Porosity and permeability is a measure of the storage and flow capacity respectively of a material. The storage capacity of rocks is a function of the proportion of voids present within the rock. When these voids are connected they permit the flow of any resident fluid within them, making up the permeability of the rock. Consequently porosity and permeability are related to one another; nevertheless their relationship is not direct for all rock types. It is apparent that a permeable rock is a porous rock but it is not true that all porous rocks are permeable rocks. The pore and flow systems are different for different rock types.

3.2.5.1. Coal Porosity

One significant difference between coal seam reservoir and conventional petroleum reservoir is their ability to store gas significantly greater than their open pore volume. It is not uncommon to find a coal bed which can store 3 to 7 times the amount of methane per

cubic foot of reservoir rock than conventional sandstone at similar depth and temperature (Harpalani and Schraufnagel, 1990). The heterogenous and complicated nature of coal makes the gas storage process to be very complex. Gash (1991) describes coal as a dual porosity rock containing micropores (matrix or primary porosity) and macropores (fracture porosity). A bulk of the gas is stored in the microporous matrix which has a large internal surface area (Jun et al., 2009) and the storage capacity has been attributed to the coal organic matter composition and the thermal maturity of the rock (Clackson et al., 1999a) while the gas in place is highly dependent on the formation porosity, pressure, temperature and water saturation. Gary (1987) estimates that coal micropores contribute to 98% of coals porosity while the remaining 2% is provided by the macropores. However due to coal heterogeneity estimates that the porosity of the macropores of the cleat system ranges from 1 to 5% (Rudy et al., 2007). Porosity of coal is therefore highly related to gas adsorption. A wide surface area is therefore required for gas adsorption (Sagafi et al., 2007) which is provided by the micropores. One distinct importance of coal macro porosity or cleat porosity is that it provides room for water storage while the micro porosity provides room gas storage. Evaluation of cleat porosity aid in the determination of water saturation while evaluation of micro porosity helps in characterising the coal surface area thereby gas storage capacity.

3.2.5.1.1. Coal Pore Structure

An understanding of the nature of the pore structure is usually necessary to understand the heterogenous nature of coal and how it affects the gas content of the coal. The International Union of Pure and Applied Chemistry (1972) classify pores into macropores, mesopores, micro and sub-micropores according to their pore size. Accurate and concise evaluation of the dimension, size distribution and connectivity of microporous network of coals has been made difficult by the small dimension of micropores and the amorphous physical structure of many coals (Stasia A. et al., 1997). The micropores have a dimension ranging from 5 to 10Å while the macropores is made up of cleats varying from a few Å to microns (King, 1985). Coals contain an interconnected microporous network with both closed and interconnected pores, the slit-shaped pores have constricted openings that are of molecular dimensions (Mahajan, 1991) but the extend of closure or opening of the pores is still highly debatable (Marsh, 1987; Mahajan, 1991).

Within the coal microporous matrix gas is stored primarily by adsorption (Gary, 1987; Seidle et al., 1992). In coal, porosity variations result from, differences in maceral content, rank variation, variation due sorption induce strain. When gas is desorbed or adsorbed into coal, there is a correspondent decrease or increase in pore pressure and effect stress resulting in increase or decrease in porosity associated to shrinkage or swelling of the rock type. Increased coal rank is usually accompanied by decreased porosity. Rock compaction caused by overburden loading helps in decreasing the water content of rocks as well as their porosities.

3.2.5.2. Gas Adsorption in Coal

In this sub section we shall use the word adsorption to describe the various sorption processes involve during gas retention in coal seams. It is also necessary to define key words use when describing the sorption process.

- Adsorption: this is the process where a gas molecule (adsorbate) forms a layer on the coal surface (adsorbent).
- Absorption: In this case the adsorbate (gas molecule) penetrates the adsorbent (coal matrix).
- Chemisorption: In this process a bond is formed between the adsorbate and the adsorbent i.e. the gas molecule and the coal matrix.

Adsorption and Absorption are usually referred to as physical adsorption, meaning they are physical processes. Both Adsorption and Chemisorption are exothermic reaction i.e. the process result in the release of energy while the absorption process requires energy to be successful. Of these three processes adsorption i.e. the retention of gas on coal surface is the most dominant storage process in coal. Consequently the surface area required for retaining this gas is one of the most important physical parameter to be considered when estimating the quantity of gas stored in coal. A clear illustration of the enormous surface area in the micropores of the coal is that 1 lb of coal has a surface area of 55 football fields, or 1 billion sq ft per ton of coal and a good coalbed well in the San Juan or Warrior basin would hold two to three times more gas in a given reservoir volume than a sandstone reservoir of similar depth having 25% porosity and 30% water saturation (Kuuskraa and Brandenburg, 1989).

Apart from the surface area of interest the kind of adsorbate, the petrography and characteristic of the adsorbent are key parameters in determining adsorption potential. Coal adsorption potential is different for different kind of gases; different gases have different molecule structures. Adsorption is therefore dependent on more than one variable; coal type, moisture content, maceral composition, temperature and pressure of adsorption as well as the adsorbate. The following paragraphs will describe how the characteristics of coal affect its sorption potential.

3.2.5.2.1. Preferential Adsorption of carbon-dioxide to Methane

It has already been established that the adsorption potential of coal is not only dependent on the nature of the coal in question but also on the kind of adsorbate use. It is also clear that the adsorption process requires adequate surface area to act and that the micro-porosity of the medium is of great importance as well. Consequently the size of the molecular constituent of the adsorbate has a great role to play in the quantity of gas adsorbed. Singh (1968) and Garnier et al (2011) observed that 1.4 to 2 times more carbon dioxide than methane can be adsorbed in coal at 345 KPa (50 psi) pressure while more than 4 times Nitrogen than methane is adsorbed at similar pressures. Nevertheless at higher pressures these ratios may be low (Gunther, 1965).

An explanation for the difference in adsorption potential for different gases may be due to their differences in relative molecular sizes and the distribution of electrostatic forces. The molecular radius of methane is large than that of carbon dioxide; 0.289nm for carbon dioxide and 0.310nm for methane while the adsorption energy of carbon dioxide is much higher than of methane. This difference in adsorption energy and molecular diameter makes it easier for carbon dioxide with small molecular size and larger adsorption energy to easily permeate the micro porous coal matrix. Also more carbondioxide molecules can be trapped than methane. Gertenbach (2009) also suggested that another reason for preferential adsorption of carbon dioxide to methane in coals may be due the multilayer sorption of carbon dioxide in the large meso-pores as well as in the micro-pores while methane is predominantly adsorbed in the micro-porous matrix.

CO₂/CH₄ adsorption ratios are highly dependent on temperature and pressure. Adsorption ratios decrease with increase in pressure. It is yet not certain as to the effects of coal rank

on CO₂/CH₄ ratio. Staton et al. (2001) established a positive rank correlation while Mastalerz et al. (2004) saw no correlation on CO₂/CH₄ ratios.

3.2.5.2.2. Coal Type and Adsorption Capacity

Garnier et al. (2011) studied adsorption isotherms of selected coals with different maturity from different areas. In this study they established that high rank coals have higher adsorption potential for both CO₂ and CH₄ while lower rank coals have lower adsorption potential. However they also found out that coal rank dependent sorption potential is also subject to the composition, quantity and nature of ash present within the coal. Nevertheless a similar study by Dutta et al. (2011) on 14 Indian low volatile bituminous coals with VR ranging from 0.64% to 1.9% gave completely different trends where low ranked bituminous coals exhibited higher adsorption affinity than higher ranked coals. The sorption capacity showed a U-shaped with rank. The trend showed a decreasing capacity with rank followed by a more stable unchanging capacity and a subsequent increased capacity with rank.

3.2.5.2.3. Maceral Content and Adsorption Capacity

Dutta et al. (2011) established a relationship between sorption potential and maceral content. Within an iso-ranked system coals with higher vitrinite content showed higher capacity or affinity for methane while those with Higher Inertinite content have a negative impact on sorption capacity. However the effects on vitrinite content on gas adsorption is not clear as the experimental results throughout the world show some variation. Crosdale et al. (1998) reports that vitrinite-rich bright coals have significantly higher gas adsorption capacity than that of dull coal samples of same rank. He observed a U-shaped curve for adsorption capacity with vitrinite content and explained that the decrease in adsorption capacity in lower range of vitrinite content for high to low volatile bituminous coal can be attributed to plugging of the micropore system (Clarkson et al., 2000). Vitrinite is predominantly micro-porous while Inertinite is meso- to macro-porous implying that a surface with micro pores has a larger surface area than another with same size but contains meso to macro pores. The internal surface area is represented by the sum of electronically active surfaces and generally increases with increase coalification and is higher in vitrinite than in inertinite. It is observed that amongst all macerals telocollinite has the greatest

influence on sorption capacity (Clarkson et al., 2000). Adsorbed volumes are generally greater for bright and banded coals than for dull coals.

3.2.5.2.4. Mineral Matter and Gas Adsorption

The gas adsorption trend with mineral matter is not certain. Mineral matter adsorbs very limited amount of gas. Dutta et al. (2011) established an increased gas adsorption capacity with decrease inorganic matter. However Mastalerz's et al. (2004) studies of coals from Indiana show poor correlation between mineral matter and adsorption capacity. Such correlation is not strange but simple comes to strengthen the point on adsorption potential highly dependent on organic matter.

3.2.5.2.5. Ash Content and Gas Adsorption

The relationship between ash content and sorption capacity is similar to that of mineral matter. The presence of ash in coal significantly reduces the sorption capacity of coal, but there is no define trend established for all coals. Dutta et al. (2011) sorption experiments on Indian coals showed a reduction of sorption capacity by an average of 0.9ml/g for every 1% increase in ash content. A similar study by Levy et al. (1997) for Bowen Basin coals showed an average decrease in methane sorption capacity of 0.38cm³/g for every 1% increase in ash.

3.2.5.2.6. Grain Size and Gas Adsorption

Previously we say that there is a positive relationship between vitrinite content and adsorption capacity while a negative relationship exist between inertinite and adsorption capacity. Coal samples with larger grain size particles are characterised by higher vitrinite content and small proportions of macro porosity. However larger particle coals have the tendency of experiencing increased mineralisation. Increased mineralisation has a negative effect on gas adsorption. On the other hand increased vitrinite and low macro porosity have a positive contribution gas adsorption. This explains the why larger grain size coals have higher affinity for gas than smaller grained sized coals.

3.2.5.2.7. Physical Parameters Affecting Gas Adsorption Experiments: Temperature, moisture content and Grain size

3.2.5.2.7.1. Grain Size

Most sorption studies have been carried out on finely ground coal samples. This process does not usually represent in situ reservoir conditions. It is assumed that pore structures are destroyed during the process of grinding as well as some new pores are created. The grinding process also destroys the fracture network that forms the main transport system and contributes to part of the coals porosity. Consequently gas adsorption capacities and rates are altered.

The rapid adsorption process observed with increased grain size can be attributed to complex pore structure in the larger particles (Gertenbach, 2009) however there is an increased in diffusion rate with decreasing grain size explained by Nandi and Walker (1975) to result from the creation of new macro pores during grinding. Nevertheless Floretine et al. (2009) in related studies concluded that Contrary to general belief, the adsorption duration for a given gas appears not strongly affected by the coal particle size.

3.2.5.2.7.2. Temperature

Gas adsorption is an exothermic process i.e. the process releases energy. Consequently an inverse relationship exists between temperature and adsorption capacity. The higher the temperature the lesser the adsorbed gas and the higher the percentage of stored gas in free state for a particular pressure range realised in the laboratory (up to 50MPa) (Crosdale et al., 2008). Consequently a decrease in temperature favours adsorption while an increase in temperature favours desorption (Levy et al., 1997). However from thermodynamics the sorption capacity of a specific sample is similar for all temperatures at infinite gas pressures, assuming no change of the sample surface area over this temperature range (Busch and Gensterblum, 2011).

3.2.5.2.7.3. Moisture Content

The amount of moisture that coal seams hold is a function of its rank and composition. Just like other fluids present in coal. Water or moisture is either adsorbed or occur in Free state. Consequently sorption sites are scrambled upon by different fluids water inclusive. A decrease in methane adsorption capacity caused by the presence of moisture in was recorded by Coppens (1936).

Sorption capacity decreases with increasing moisture content until the equilibrium moisture content is reached (Busch and Gensterblum, 2011). Above this moisture content the gas sorption capacity remains constant but the effect of moisture is also dependent on the rank of the coal as high rank coals are less affected by moisture (Day et al., 2008c). The reason for this effect is that adsorption sites in particularly polar sites such as the hydroxyl group on coals are preferentially occupied by water than methane. Busch and Gensterblum (2011) pointed out that the fact that methane and other gases like carbondioxide continue to be adsorbed on moisture equilibrated coal proof that water and these two gases compete only for a portion of the sorption site. Figure 3.5 illustrates the relative proportion of sorption site occupied by the three fluids in the presence of the other.

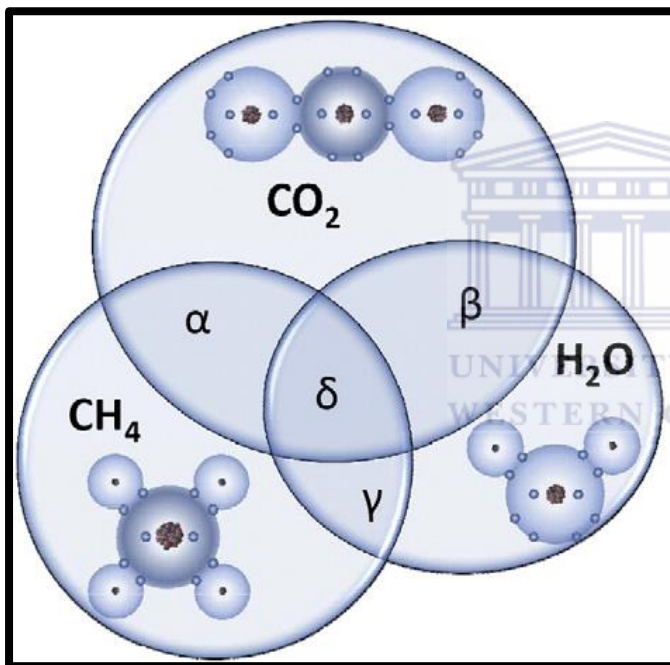


Figure 3.5: Sorption sites of each gas at one given fixed surface coverage (fixed P, T) and the intersection for multi-component sorption isotherms (Busch and Gensterblum, 2011).

3.2.5.3. Coal Permeability and Fluid Flow

Permeability defines the ability of a medium to allow fluid to flow through it. In conventional sandstone reservoirs where permeability is subjected to the porosity, fluid flow is reliant on how interconnected the pore spaces are. In conventional reservoir fluids flow according to Darcy's Law and mass movement is highly reliant on pressure gradient. The fluid flow system in coal is complex and not same as in conventional sandstone

reservoirs. A matrix diffusion system defined by Fick's law is added onto the normal Darcy flow to make up the flow system in coals (figure 3.6). The driving force in this case is the methane diffusion gradient set up across the micropores. Therefore in coals, diffusion occurs in the matrix while Darcy flow occurs in the cleat network. However flow in coals is found to be primarily via micro-fractures (Dabbous et al., 1974) by laminar flow obeying Darcy's Law. Effective and efficient methane production from coal seams highly depend on the permeability and it is the single most important factor that must be determine early enough in a the life cycle of the CBM play.

However methane is not the only fluid that resides in the voids of coal seams, it is sometimes associated with proportions of heavier hydrocarbons like ethane and propane, in most cases carbondioxide and always with water. If the permeability of a rock is independent of the type of the fluid at 100% saturation and relies only on the medium, it is referred to as **absolute permeability**. For CBM reservoir engineering, the coal permeability is often described by absolute methane permeability and/or absolute water permeability as they can be defined accordingly (Shen et al., 2011). Should the rock contain two or more fluids e.g. water and gas as in the case of coal, the permeability of each fluid independent of the other is regarded as the **effective permeability** of that fluid.

During methane production from coal there is simultaneous flow of methane and water within the cleat network. Suppose each constituent fluid *saturates* the rock to a particular degree then the permeability of the rock to any one of the fluids as a function to its fluid saturation and absolute permeability is considered as the *relative permeability* of the rock to that fluid. For example permeability of a coal with 50% water saturation is different from the permeability with 100% water saturation. Relative permeability to air and water for Arizona coals measured by Hapalani and Schraufnagel (1990) widely vary from less than 0.01md to 100md. Literature on relative permeability in coals is limited. The little attention received by relative permeability according to Paterson et al. (1992) can be attributed to the proprietary nature of the testing or the difficulty of obtaining useful results. According to Paterson et al. (1992) gas production in coal is proportional to the product of the absolute permeability and relative permeability of the gas. This varies from coal seam to coal seam and laterally across distinct coal units as a result of coal heterogeneity.

3.2.5.3.1. Gas Diffusion in Coal and Fick's Law

Diffusion is a mode of transport of most gases. The word diffusion stands for “Diffundere” in Latin which means to “spread out”. The process follows Fick's Law (as illustrated in the equation below) where particles move from a region of lower concentration to a region of higher concentration. In this case the diffusion flux is proportional to a minus concentration gradient.

$$D\delta/r^2\delta (r^2c/r) = \delta c/\delta t \dots\dots\dots (1)$$

Where,

C = gas concentration (kg/m³)

t = time (s)

D = effective diffusion coefficient

r = radial distance from centre of particle (m).

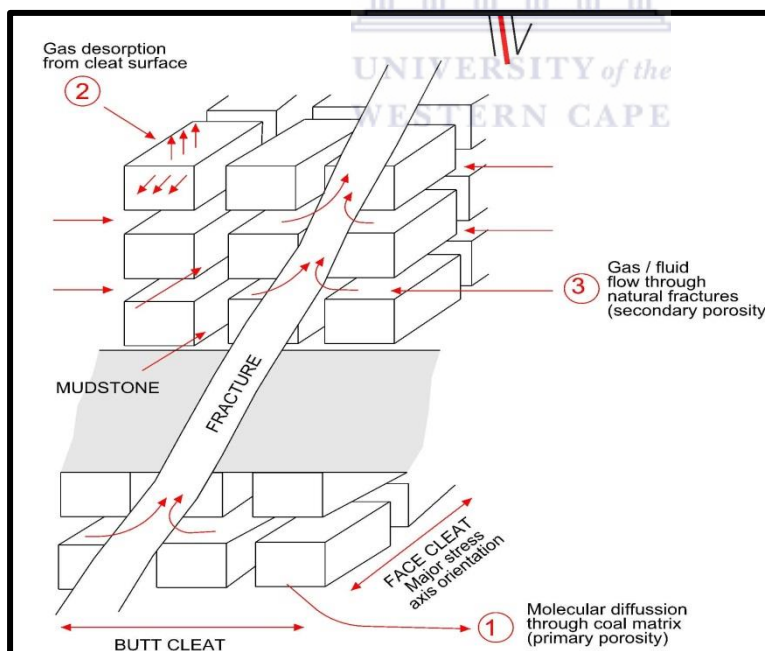


Figure 3.6: Different fluid flow systems in coal (modified after Fourie, 2000), sourced from Anglo Coal Data base.

In coals, gas molecules either diffuse into the coal matrix during gas adsorption process or out of the coal matrix during gas desorption process. Figure 3.6 shows gas diffusing out of

the matrix in the cleat network (2). The diffusion interface in this case is the coal micro pores or a network of capillaries that exist within the matrix block (Rudy et al., 2007). According to Collins (1989) gas diffusion via coal micro pores is either through one or a combination of the following processes.

Bulk Diffusion: This process is piloted by the presence of a concentration gradient and occurs within the gas phase. The process is facilitated by larger pore diameter, higher pressures and larger particle size.

Knudsen – type diffusional flow: This process occurs within the capillaries and is prevalent in capillaries with diameters smaller than the mean flow path for gas molecule. Molecules flow to regions of lower concentration. Knudsen flow requires lower pressure.

Surface Diffusion: In this type of flow the adsorbed gas moves along the micropore surface in some form of liquid.

3.2.5.3.2. Darcy Flow/Cleat Permeability

Upon gas diffusion via the micro-pores from the coal matrix into the cleat system during desorption, the gas flows linearly within the cleat network by Darcy flow. Fracture permeability accounts for almost all of coals permeability. In conventional reservoirs, the dimension of the pore throat is a permeability deterministic factor. Cleat aperture opening can be analogous to pore throats and along with cleat length they both also impact the cleat permeability of coal seams.

The fracture system in coals as seen earlier on is made up of the primary continues face cleats which lies orthogonally to the secondary discontinues butt cleats. Fluid flow in coal may be vertically (perpendicular to the bedding surface) or parallel to the bedding surface. It may also be in the butt or face cleat direction. Gash et al. (1992) conducted experiments to determine the effect of flow direction permeability. They discovered that permeability within the cleat network are predominantly in the face cleat direction and parallel to the bedding surface regardless of the confining and reservoir pressures. At 1000psig absolute permeability to water for these coals range from 1.7 to 0.6md in the face cleat direction and 1.0 to 0.3 in the butt cleat direction. However minor fractures which are not oriented in

either the face or butt cleat direction facilitate gas movement in that they aid in conducting gas from the matrix to the flow stream. Extreme face to butt cleat permeability ratios may range from 1:1 to 17:1 (McElhiney et al., 1989; Rogers et al., 2007).

3.2.5.3.2.1. Permeability and Rank Variation

The cleat network is most highly developed in low volatile bituminous coal (Rogers et al., 2007). In lower ranked coals most of the organic matter has not been broken down geothermally thereby the coal is still highly elastic and difficult to fracture. However as coals developed from low volatile bituminous rank to anthracite crosslinking under high pressures and very high temperatures of maximum burial may help seal those cleats (Levine, 1990; Rogers et al., 2007). Increased number of cleats per unit volume increases the permeability of coal seams. So it is expected that a permeability vs rank curve should have a U shape. A series of experiment conducted by Shen et al. (2011) to measure the effects of rank variation on relative permeability on some Chinese coals indicated that the selected coals show high reducible water of saturation with low relative permeability to water and gas under this condition. The result further showed that with increase in rank the irreducible water of saturation exhibit a U-shaped tendency whereas the methane permeability under irreducible water saturation increases with increase in rank.

3.2.5.3.2.2. Permeability and Organic matter Variation

The mineralisation of coal cleats and the kind of organic composition of the coal also determines the development of the fracture network in coal thereby affecting its permeability. Vitrinite rich coals display the best cleat and fracture development while mineralisation of cleats closes up flow pathways and hinder production of fluids from cleats (Paterson et al., 1992). However acid leaching of these coals increases its permeability for up to a magnitude of two. Contrary to this trend the methane permeability under irreducible water condition relates negatively with vitrinite content and positively with inertinite content (Shen et al., 2011).

3.2.5.3.2.3. Permeability and Pressure variation

Gas adsorption and desorption in coal seams are highly dependent on pressure. Gas desorption from coal matrix and diffusion into coal fractures is triggered by a pressure

difference (drop) between the matrix and the cleat network. Corresponding flow within the fracture system is initiated by a pressure gradient between the well bore and the cleat network. In coal bed methane production two pressure forces are in control. The confining pressure generated by the fluids in the pore spaces and the hydrostatic pressure or reservoir from overburden load. A decrease in the reservoir pressure results in a net increase in confining pressure (Gash et al., 1992). The confining pressure and permeability have an inverse relationship. An increase in confining pressure results to a decrease in the relative permeability to gas and water; however the flow to gas is less than the flow to water (Gash et al., 1992). Absolute water permeability for some San Juan coals perpendicular to the bedding surface dropped from 0.8-.04md at 450psig to 0.007mD at 1000psig.

3.2.5.3.2.4. Variations in Permeability due to Gas Sorption

One very important parameter to consider when measuring permeability of coal seams are the changes in permeability caused by adsorption and desorption of fluids. As seen earlier coal beds have the ability to adsorb large quantities of gas. These gases travel primarily through the fracture network by Darcy flow. So we can consider coal as a natural fracture reservoir. Unlike other non-fractured reservoirs the adsorbed or desorbed gas causes the coal matrix blocks to either swell or shrink thereby narrowing the fractures (reducing permeability) or widening the fracture (increasing the permeability of the seams). Coal permeabilities of sorbed gases such as CH₄ and CO₂ measured in the laboratory are known to be lower than permeabilities to non sorbing such as nitrogen (N₂) (Siriwardane et al., 2009) and may decrease by as much as five orders of magnitude for confining pressures increasing from 0.1 to 70 MPa (Huy et al., 2010). Of recent, many researchers have attempted to measure or model the degree to which sorption induced strain affects permeability. Such includes Harpalani et al., 1990; Robertson and Christiansen, 2005; Robertson, 2005; Wang et al., 2010, 2011; Liu et al., 2011.

According to Liu et al. (2011), at the onset of gas injection or adsorption the swelling is localized within the vicinity of the fracture compartment, but as adsorption continues the swelling zone is extended further into the matrix. This process is same for desorption. The relationship between the amount of adsorbed gas and swelling strain is not clear. Cui et al.

(2007), Robertson and Christiansen (2005) found the relationship between swelling strain and the amount of volume of gas sorbed to be linear. However Day et al. (2008) established that it is nonlinear. Under constant total stress, adsorbing gas permeability decreases with the increase of pore pressure due to coal swelling (Robertson, 2005; Wang et al., 2010, 2011). Yet this decrease in permeability is instantaneously reversed at certain pressure and is explained by Liu et al. (2011) by the fact that the matrix swell ultimately ceases at high pressure and the influence of effective stress takes over.

In some coal the swelling and shrinking show strong anisotropy with greater swelling in the direction perpendicular to bedding than in the parallel direction (Pan and Connell, 2011). Results presented by Lavine (1996) on two Illinois high volatile C bituminous coal samples showed that one coal sample swelled approximately 10% in the direction perpendicular to bedding than in the bedding direction while the other have equal magnitudes in both directions. Lower coal ranks turn to show stronger anisotropy than higher coal ranks (Day et al., 2008). Permeability calculated using the averaged (volumetric) swelling strain tends to overestimate that using the anisotropic swelling model (Pan and Connell, 2011).

3.4. Coal Porosity and Permeability Measurement

Most methods used for both conventional and unconventional reservoir evaluation are usually both laboratories based or field based experiments. In the laboratory based experiments rock samples from the formation of interest are harvested and simulation experiments are conducted in the laboratory. Field based experiments measure in situ reservoir properties. Parameters are evaluated on site. Most porosity evaluations are conducted in the laboratories.

3.4.1. Laboratory Based Simulation Experiments

In the oil and gas industry there are no generally adopted standards methods for laboratory measurements of porosity, permeability and water saturation for coal (API, 1998).

3.4.1.1. Porosity Measurements

Measurement of coal porosity makes use of coal cores or fresh samples derived from coal mines. Measurements require the preparation of samples suitable for the technique to be used. Part of the coal sample preparation in early times requires the drying of the samples for 24 hours in the oven at 80°C (Dabbous et al., 1974). This process relieves the sample of all its moisture content. Later works indicated that the process of drying alters the coal's structure and should not be used during measurements (Berkowitz, 1979). Due to coal's dual porosity nature, most measurement techniques used are modelled from conventional methods but adapted to accommodate coal's highly anisotropic nature and to measure different and specific porosity (micro or macro porosity).

The matrix porosity is usually higher than cleat porosity but most of the gas stored in coal is in the sorbed form in the matrix rather than as free form in the cleat. Therefore matrix porosity measurements are rarely carried out for coal samples (API, 1998). Should the matrix porosity be required, the Helium Boyle's Law technique can be used. In this process only helium can be used because the gas is not adsorbed by coal. In case any of the gas is adsorbed, erroneous porosity values may be derived.

The Miscible Drive technique, commonly used for conventional reservoirs is routinely used to measure cleat porosity. Another technique used to measure cleat porosity is the mobile water porosity technique determined during measurement of unsteady state relative permeability (Gash, 1991).

3.4.1.1.1. Miscible Drive Technique

The miscible Drive Technique utilises non-dried coal cores. In this technique the fluid saturating the core is displaced with a different fluid with different physical properties. Measurements are usually done under uniform confining pressure since cleat porosity is a function of confining pressure (API, 1989). Both the saturating fluid and the displacement fluid should be miscible (Meyer, 1982). If the tracer element such as sodium iodide is used, the technique is called "the miscible tracer technique". Supposed the tracer element is adsorbed onto the coal, erroneously high cleat porosity measurements may be recorded (Gash, 1991; Dabbous et al., 1974)

The coal cores are initially saturated with water. Before saturation the core with water Helium saturated with water vapour is injected into the core to remove mobile water in the core. The core is then evacuated to remove any free gas and the core is saturated at atmospheric pressure. Water is then injected at constant pressure with a constant back pressure from the bottom of the vertical hydrostatic core holder. A tracer element is then injected into the core until the concentration of the tracer in the effluent is same as that in the injector. Effluent volumes are monitored using electronic balance while tracer element concentration is monitored using electrical conductance and refractive index.

The tracer element is continually injected for long hours. The solution in the core is then displaced with distilled water in the same manner and the while monitoring the tracer element concentration and the effluent volume. The tracer element concentration and effluent volume is then used to calculate total displaced volume from which the system dead volume (core holder inlet and exit lines) are subtracted to calculate the cleat pore volume (Gash, 1989). The cleat pore volume is divided by the measured bulk volume of the core to calculate the cleat porosity.

This technique infers direct measurement of the reservoir rock. However, the technique is time consuming and requires pre-drilling, coring, core handling and core preservation. All these processes if not properly done will lead to erroneous results.

3.4.1.1.2. Multi Scale Imaging

This technique is new and mainly used by Digital core labs. Analysis involves characterising the heterogeneity and connectivity of pores and fractures, and distribution of minerals at the millimetre to micron scale as well as imaging and analysing the pore connectivity and mineral occurrences at the nano scale (Digital Core, 2012). With this analysis both micro and macro porosity of coal can be inferred. The cores are not simulated in this case.

This approach integrates 3D micro –CT (Computer Tomography) imaging with Scan Electron Microscopy (SEM) to characterised pores. Connected porosity regions are highlighted by supplementing imaging with functional fluids (figure 3.7 a and b). The porosity, mineral distribution and fracture network can be characterised and quantify at different scale from micro down to 2 μ m (Digital Core, 2012).

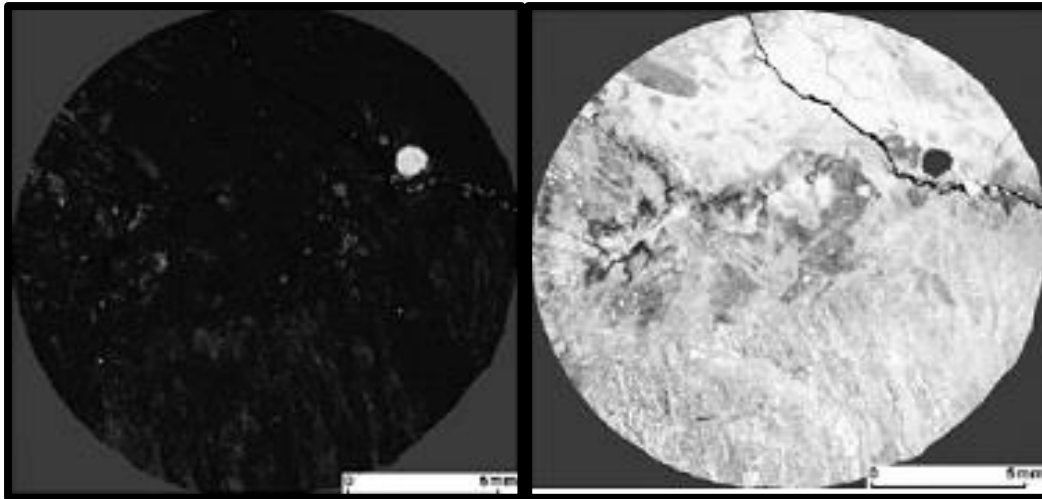


Figure 3.7a: Quantification of connected porosity in 3D, (left) Bituminous coal, (right) Connected porosity map (darker grey = higher porosity) (Digital Core, 2012)

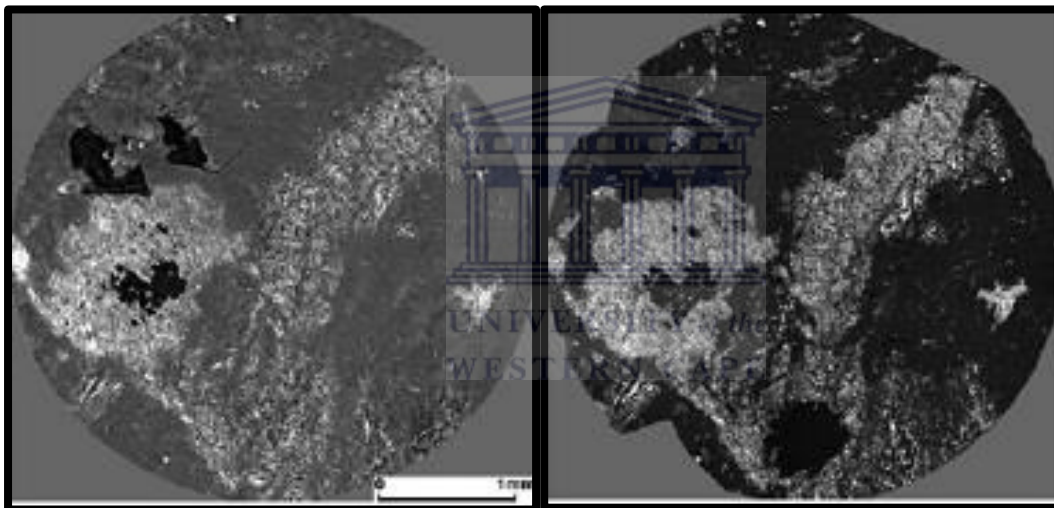


Figure 3.7b: Investigation of open and occluded porosity 3D, (top left) μ CT image, (top right) SEM image (Digital Core, 2012).

One great advantage of this technique is that it is a non-destructive technique i.e. rock samples are not altered during measure consequently no erroneous result may arise as a result of sample destruction. The techniques also characterise the rock at all scales. However this technique is very expensive.

3.4.1.1.3. Other porosity Measurement Technique

Other methods used to evaluate coal porosity include; gas adsorption Techniques, Mercury intrusion porosimetry (MIP), imaging (Scan electron microscopy and Transmission electron microscopy) and Nuclear magnetic Resonance (NMR). Procedures like MIP require injection

of mercury at high pressures which may change the porous structure of the sample (suuberg et al., 1995). Other high pressure effects include shielding of larger pores by smaller pores thereby reducing the amount of larger pores (Gane et al., 2004). Most of the microscopic imaging techniques only provide local pictures of the samples (Sing, 2004) while gas adsorption techniques also destroy the sample and only provides information on the micro- and meso-pores (Yao et al., 2006). NMR is also a non-destructive technique which is less time consuming but makes use of measurements with portable equipment.

3.4.1.2. Permeability Measurements

Rock permeability measurements involve the evaluation of the fluid conductivity of the rock. If a rock is homogenous, then the permeability of the rock is the same throughout the rock. Conversely most rocks especially coal is heterogonous and has varying permeability; permeability vary with direction and the rock heterogeneity. Coal permeability can be measured both in the laboratory and in the field. Just as in porosity measurements coal permeability measurements in the laboratory require analysis of core plugs. Since permeability of coal represents flow in the fracture medium, laboratory permeability measurements tend to be lower than those measured in the field since small cores may not sample large fractures (Schraufnagel et al., 1990; Rogers et al., 2007)

Hanby (1991) reports that laboratory derived permeability measurements can be as low as 10 times field measurements. Laboratory permeability errors may come from; low sample representation, core damage during extraction and difficulty in replicating formation stresses in the laboratory.

3.4.1.2.1. Laboratory Measurement of Permeability

Absolute permeability measurements in coal are carried out using the same measurement technique used for porosity evaluation above; the miscible drive technique. However the parameters considered when carrying out these measurements for permeability are different from those of porosity.

Relative permeability as seen earlier is the permeability of a fluid to the rock in the presence of another fluid at a particular saturation. Relative permeability is affected by the wettability of the rock. Since methane is readily adsorbed to the coal surface the coal matrix is

therefore methane wet compared to other fluids like water Nitrogen and Helium (Gash, 1991). This explains why most often helium rather than methane is used as the gas phase for relative permeability measurements. However the use of helium rather than methane may have an effect on the relative permeability since methane cause the coal to swell (Harpalani and Zhao, 1989) and consequently reduces the permeability which is not experienced with the use of Helium. Relative permeability measurements in the laboratory are either by the “Steady State Technique” or the Unsteady State Technique”.

3.4.1.2.1.1. Steady State Method

Steady state describes a scenario where the upstream (inlet) and downstream (outlet) pressure of the core holder and the flow rate all become invariant with time (API, 1989). At steady state mass flow rate is constant throughout the sample and does not change with time. The steady state method used to measure relative permeability to water of coal makes use of helium gas as the gas phase and water as the liquid phase. A tracer element is also introduced into the system to aid evaluate the saturation of water. Since coal is an adsorptive medium plus the low sensitivity of the technique due to lower porosity the concentration of the tracer element is increased (Gash, 1991). Both brine (saturated with tracer element) and gas are injected into the core simultaneously at constant rate for a long time until equilibrium is reached. The fluid saturation is calculated when equilibrium is reached.

3.4.1.2.1.1. Unsteady State Method

In the unsteady state simulation method contrary to the steady state method both gas and liquid states are not simultaneously pumped into the core. Here the core is initially saturated with water which is subsequently displaced by gas. As usual the technique needs to be modified for application in coal.

The gas is saturated with water vapour before injection. The mixture is pumped into the hydrostatic holder with the aid of a pump while the pressure of the injected fluid is regulated by a pressure regulator. Upon exit from the core holder the gas is separated by a separator. Automated data collection using mass flow meters to monitor total effluent (gas plus water) production after gas breakthrough and a gas water separator placed on an

electronic balance to monitor water production can be used to achieve accuracy (Gash, 1991).

When performing calculations the volume of the inlet and exit lines and distribution plates of the core holder (dead volume) is assumed to be water filled at the beginning of gas injection. Because of low porosity the dead volume is roughly equal to the volume of water produced from the coal core during gas injection (Gash, 1991). A piston-like displacement of water is assumed for the dead volume so that dead volume can be subtracted from water produced. Relative permeability can then be calculated using any model such as the Johnson, Bossler, and Naumann (Johnson, 1959). The system is considered 100% gas saturation when no more water is produced during the displacement process.

3.4.1.2.2. Field Permeability Measurements

Accurate measurements of permeability from core test is challenging since permeability relies on stress and cleat directions; laboratory derived permeability can be erroneous due to the difficulty in replicating stresses in the laboratory. Field permeability determination in both conventional and unconventional reservoirs has been established to give values of true fluid flow characteristic. Data derived from such method present true reservoir conditions of pressure, temperature and stresses. Similar to field methods historical matching production data are also routinely used for permeability determination. However in frontier regions with no production activity, this technique cannot be used. In CBM reservoirs permeability can be determine in the field by the use of one of the following pressure transient tests (Rogers et al., 2007).

- Slug Test.
- Drillstem test (DST).
- Pressure Build up test (PBU).
- Multi Well Interference test.
- Injection falloff tests (IFT).
 - Tank Test.
 - Below Fracture pressure injection falloff test (BFP-IFT).
 - Diagnostic fracture injection test (DFIT).

A detail description of these tests is presented in the book Coalbed Methane (Rogers et al., 2007). This thesis describes only one of the methods. Most of these methods are similar to those used in conventional reservoirs. In the injection test care is usually taken not to fracture the reservoir during fluid injection.

3.4.1.2.2.1. Multi - Well Interference Test

This test is conducted by monitoring responses in at least three wells while injecting or producing from another well. One aim of this test is to determine the heterogeneity of the reservoir and the degree of conductivity (Rogers et al., 2007). Absolute permeability in both face and butt cleat direction is derived from this test.

3.4.1.2.2.2. Pressure Build Up Test (PBU)

The pressure build up test provides us with permeability, skin and reservoir pressure. This test is conducted like in conventional reservoirs. This test is conducted for coal only in situations where there is sufficiently high reservoir pressure.

3.4.1.2.2.3. Drill Stem Test

Conducted in similar manner as conventional reservoir, in open hole. The four conventional reservoir stages are maintained. The pre flow period helps to clean the well while the first initial shut in period equilibrates the well from the pre-flow period. During the main flow period the formation flow characteristics are determined. The permeability and skin is determined during the final shut in period.

3.4.1.2.2.4. Slug Test

In this test a specific volume of fluid is instantaneously added (or withdrawn) from (into) a wellbore while measuring the pressure reaction as the fluid level returns to equilibrium condition (Rogers et al., 2007). The slug test also provides initial formation pressure and the skin factor provided the porosity – compressibility is known.

Just above the coal seam a hydrostatic water head is positioned in the wellbore. Pressures are kept below fracturing pressures. Water is pumped into the seam at a known hydrostatic head and the influx rate is measured. A pressure transducer is used for this purpose and is

positioned in the borehole just below the equilibrium water level. The time to conduct the test can derive from the influx rate. This time depends on the permeability of the formation and the hydraulic head, see mathematical illustration below (Schraufnagel, 1992).

$$t_s = 75.9\mu D_i^2 / kh$$

Where

t_s = time to perform slug test, hr

μ = viscosity of water test fluid, cp

D_i = inside diameter of casing, tubing, or open hole confining the test fluid, in.

k = formation permeability, md

h = height of coal seam tested, ft

3.4.1.2.2.5. Injection Falloff Tests

3.4.1.2.2.5.1. Tank Test

This test makes use of gravity drainage which occurs as a result of the difference between the reservoir pressure and the hydrostatic gradient. The reservoir pressure is expected to be lower. The gravity drainage creates an injection potential.

3.4.1.2.2.5.2. Below Fracture Pressure-Injection Falloff Test (BFP-IFT)

Has been widely used in the CBM industry for skin and permeability determination. Applicable in both under and over pressured reservoirs provided the fracture pressure is not surpassed. This method makes use of conventional falloff analysis. Shut-in falloff pressure data derived from this test are analysed to obtain pore pressure, permeability and skin. In low permeability coals very low injection rates are used to avoid fracturing and the shut in period has to be at least four times the injection period (Rogers et al., 2007).

3.4.1.2.2.5.3. Diagnostic Fracture Injection Test (DFIT)

This technique makes use of after-closure data to determine permeability and pore pressure. Technique can be applied regardless of fracture creation during injection since it

use late time data but any fracture created is taken into account. Technique makes use of small fluid volume and the test time is short.

Table 3.5 Summary of Main Advantages and Disadvantages of the Different Field Permeability Methods (modified from Rogers et al., 2007).

Method	Advantages	Disadvantage
DFT	<ul style="list-style-type: none"> -Short test duration -The test can be applied to both pre- and post-stimulated coals. - It can determine unique pore pressure and permeability values. -It is the only test of coals in which closure pressure and leak off type can be determined in conjunction with pore pressure and permeability <p>The test can analyse BFP-IFT data if it exceeded the fracture pressure.</p>	<ul style="list-style-type: none"> -It cannot obtain quantitative skin damage values, and -If pseudoradial flow was not observed during shut-in, the results may not be unique.
BFP-IFT	<p>Does not need relative permeability curves because of single-phase testing conditions.</p> <ul style="list-style-type: none"> • Can be applied to both pre- and post-stimulated coals. . 	<ul style="list-style-type: none"> • A breakdown is needed before the test because a poor connection between the wellbore and the reservoir can lead to erroneous results. • A non-stable reservoir pressure before the test can result in non-unique solutions. • The test is not applicable to very low-permeability coals because pumping below fracture pressures may not be possible.
Tank Test	<ul style="list-style-type: none"> • Is conducted under single-phase testing conditions and hence there is no need for relative permeability curves. • Can be applied to both pre- and post-stimulated coal seams. • Costs comparatively less. 	<ul style="list-style-type: none"> • A small breakdown treatment is required to establish good communication between the wellbore and the coal. • The radius of investigation is limited to the created water bank. • Because of the limitation above (bullet 2), a long injection period is required to create a sufficiently large water bank before the falloff data is affected by two-phase flow.

Slug Test	<ul style="list-style-type: none"> • Simple execution • Costs less. • Requires no flow rate control mechanism. • Requires relatively simple analysis. • Can be performed if the well is under-pressured. 	<ul style="list-style-type: none"> • Test duration could be excessively long for low-permeability coals. • Radius of investigation is relatively small. • Results may be incorrect if gas saturation is present.
Drill Stem		<ul style="list-style-type: none"> • Low safe of technique. • High cost. • Low radius of investigation.
PBU	<ul style="list-style-type: none"> • Drawdown/build-up are preferred for estimating reservoir properties in reservoirs with initial gas saturation. • The test can be applied in both pre- and post-fracture stimulated coals. 	<ul style="list-style-type: none"> • For wells with low deliverability, drawdown/build-up may not be feasible. • Because drawdown occurs, the probabilities are high for two-phase flow. • The test requires relative permeability curves to account for possible two-phase flow conditions.
MWI	<ul style="list-style-type: none"> • To understand the magnitude and orientation of the permeability in the butt and face cleat directions. • To understand the heterogeneity of the CBM reservoir. • To help determine well locations. • To help optimize the CBM well spacing. 	<ul style="list-style-type: none"> • It is very expensive to perform. • When two-phase reservoir conditions exist, only small saturation gradients should exist between wells (GRI, 1994)

3.5. Geophysical Wireline Logs

Most subsurface petroleum reservoirs description and characterisation are based on information derived from wire-line well logs. Although core characterisation is the basis for reservoir characterisation, not all wells, well sections or formations are cored during a drilling process. However wire-line are more universally available and can be used to characterised un-cored portions of the well. Application of geophysical Wire line well logs in reservoir characterisation has been going on for decades now in the oil and gas industry.

Well logs are products of survey operations consisting of one or more sets of digitized data or curves, which display an array of permanent record of one or more physical measurements as a function of depth in a well bore (Olajide, 2005). The wireline log is a graph and the data are continuous measurements of a log parameter against depth (Opuwari, 2010). Acquisition of well log data involves lowering a specially design tool

(sonde) into the well to record the response of the tool to the physical character of the formation. Data acquisition may be during drilling (logging while drilling-LWD) or after drilling. It may be in a cased hole or in an uncased hole depending on the parameter to be measured.

The logging device (sensor) housed in a sonde is lowered to the bottom of the well using a survey cable. Logging is conducted by pulling the tool upward during which time the tool makes continuous physical measurements of the formation through which it is raised.

Direct measurement of reservoir properties such as porosity, permeability, water saturation etc. is not possible with the use of well logs. Well log analysis are always integrated with laboratory core measurements or well test analysis. The logging tool measures physical characteristics of the reservoir that are related to reservoir properties. The derived geophysical properties are then computed with the use of different mathematical formulae to generate the parameter of interest.

Many properties of coals such as natural potential, conductivity, density, radioactivity and acoustic time can be measured directly (Hou, 2000). Logging data has been previously used in CBM gas content estimation, estimation of coal mechanical properties, petrophysical characterisation such as porosity and permeability, moisture content and evaluation of physical properties (Li et al., 2011; Fu et al., 2009a; Morin, 2005; Charbucinski et al., 2003; Hawkins et al., 1992 and Oyler et al., 2010)

3.5.1. Classification of Well Logs

- 1. Nuclear and Radioactive Logs:** Gamma Ray (GR), Density and Neutron.
- 2. Electrical Logs:** Spontaneous Potential (SP) and Resistivity.
- 3. Acoustic:** Sonic log.

Well logs can also be classified based on their usage. This shall not be discussed here.

3.5.2. Principles and Characteristics of Interested Wire-line Logs

3.5.2.1. Nuclear or Radioactive Logs

3.5.2.1.1. Natural Gamma Ray Log (GR)

Most rock especially sedimentary rocks contain some natural radioactivity (Baker Hughes, 2002). The natural radiation is due to the disintegration of natural radioactive elements within the subsurface. Typical natural radioactive elements in the subsurface include Potassium, Uranium and Thorium. The concentration of these radioactive materials varies amongst different rock types.

A radioactive sensor lowered into the borehole records the variation of intensity of natural formation radioactivity of different formation while being raised to the surface. The total GR measurement is representative of the sum of potassium, thorium and/or uranium present in the formation.

In a sedimentary succession the higher GR reading usually occur in front of a shale bed while the lower readings occur in front of other sediments. Most rock types have different radioactive signatures. This rock property makes it possible to use GR log to distinguish between different rock types. Clean sands has fairly low levels of <45 API and shales has high gamma reading > 75 API (Opuwari, 2010). GR log is routinely used for rock identification, determination of formation thickness, calculation of shale content, clay content and a good correlation tool.

In a composite log sheet the GR log is usually recorded in the first track with a scale of 0 to 150API. In interpretation displacements to the left is indicative of sandstone while deflections to the right is indicative of increasing shale content with maximum deflection to the right representing the shale baseline.

3.5.2.1.2. Density Log (RHOB).

The formation density log can be used for porosity determination, mineral identification, gas detection and determination of hydrocarbon density. Of all the log measurements used for porosity determination the density log is most important because it provides the bulk density value that is the density of the matrix and the fluid present which is most sensitive to effective formation porosity.

The tool measures the electron density of the formation. The tool is equipped with a radioactive source, say Cesium. The source generates gamma rays that penetrate into the formation. The gamma rays while in the formation collide with electrons losing energy and hence reducing the amount of GR detected at the Geiger counter receiver.

It is assumed that the electron density is equal to the bulk density and the number of GR counted can be directly related to the formation bulk density (Baker Hughes, 1992). Pore space in a rock reduces the bulk density of a formation. As a result the lower the GR count the higher the formation density and the lower the formation porosity. The reverse is true for high porosity rocks. Porosity can then be computed if the fluid density and the mineral density is known.

$$\text{Porosity}(\phi) = (\rho_{ma} - \rho_b) / (\rho_{ma} - \rho_f)$$

Where ρ_{ma} is the matrix density, ρ_b is the bulk density read from log, ρ_f is the fluid density.

However the density of small quantity of oil is not noticeable since the fluid density is close to oil density (Baker Hughes, 1992). Also Shale density will show up on log.

3.5.2.1.3. Neutron Log

The neutron log is another porosity log widely used in the oil and gas industry. It is also used as a tool to detect gas intervals particularly when compared with other logs. Neutrons are electrically neutral, have approximately same size as the hydrogen atom, less ionising but more penetrating. With neutron logging, neutrons generated from a source in the tool penetrate the formation. While in the formation if the neutrons collide with a hydrogen atom it loses half of its energy and after 20 of such collision the neutron is captured by some elements in the formation (Baker Hughes, 1992). Some detector measure the neutron count while others measure secondary GR count generated by the neutron during capture.

Neutron log therefore measures the amount of hydrogen in formation. Higher neutron count therefore represents low porosity while lower counts represent high porosity. There is little difference between oil and water so the neutron tool does not differentiate oil and water. Anomalous low porosity is indicative of gas presence. Shales on the other hand have

the ability to trap more water as a result porosities determined in shally formations may be inaccurate (Baker Hughes, 2002) and will show high porosity (Baker Hughes, 1992).

3.5.2.2. Electrical Logs

3.5.2.2.1. Self-Potential (SP)

The SP is a measure of the natural occurring direct current potentials in a bore hole as a function of depth (Baker Hughes, 1992). The SP log is used with resistivity data to separate permeable rocks from impermeable rocks. It can also be used to differentiate formations, in calculation of volume of shale.

The voltages are measured by down-hole electrode relative to ground surface. As the sonde move through the borehole relative records of small direct currents (millivolts) are registered. SP for shale varies very little with depth so shale will normally give constant reading providing a “shale baseline” for reference (Baker Hughes, 1992). The direction of the SP usually depends on the salinity of the drilling fluid and formation water. If the mud filtrate is saltier than the formation water the SP is positive and negative if the formation water is more saline than the mud filtrate. Maximum negative deflection to the left of the shale base line occurs in front of clean sandstone and represents the Static Self Potential (SSP).

For a self-potential to occur there must be a flow of ions between the mud and the formation water. Flow requires the formation to be permeable. If the formation is not permeable then no SP develops. It is consequently easy to differentiate between non permeable and permeable formation. The equation below illustrates the use of SP for shale volume calculation

$$V_{sh}(\%) = 1.0 - (PSP/SSP)$$

where:

Vsh = Volume of shale

PSP = Pseudo static SP (SP of a shaley formation)

SSP = Static SP

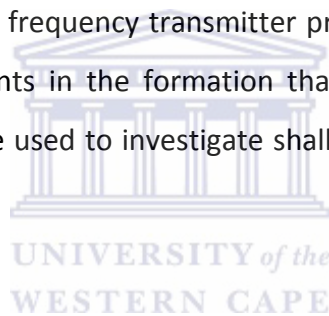
3.5.2.2.2. Electrical Resistivity Logs.

Electrical resistivity is the reciprocal of conductivity which defines the ability of a medium to permit the flow of current. The ability of a medium to hinder conduction of electricity defines resistivity. Resistivity is a function of the pore spaces and the fluid it contains. The type and amount of water in a formation determines the resistivity of the formation.

Resistivity logs are generally used to determination hydrocarbon saturation. The log is recorded on track two or three on the log sheet usually on a logarithmic scale with the ohm-meter as the unit.

Resistivity logs are grouped into three category; induction logs, laterologs and micro resistivity logs. Induction logs measure formation conductivity instead of resistivity. Induction tools use high frequency transmitter to measure the conductivity of the undisturbed formation. The high frequency transmitter produces alternating current which intend induces secondary currents in the formation that induces signals to the receiver current. Micro-resistivity logs are used to investigate shallow depths of penetration i.e. the invaded zone.

3.5.2.2.2.1. Dual Laterologs



Laterolog measurements use electrodes in the sonde. The source electrode is connected to a power source that lets current flow from the electrode through the borehole fluids into the formation and back into the receiver electrode. The electrode measures potential difference which is related to formation resistivity. The highest voltage drop is registered where higher resistivity occurs. The electrode spacing is very important in dual laterolog resistivity measurements. The distance between the source and the receiver electrodes determine the radius of investigation. If the investigation is close to the bore hole the tool records the resistivity of the flushed zone as is known as Shallow Laterolog Resistivity (SLL) while the Deep laterolog resistivity measures the resistivity of the uninvaded zone (DLL).

Dual laterogs can be used to measure over pressure zones, for fluid saturation determination and to measure the true resistivity of the formation. However the tool cannot be used in oil based mud and air fill holes.

Log measurement in thin beds is difficult but the resolution is better for laterologs than for induction logs.

3.5.2.2.3 Acoustic Log/Sonic Log

The sonic log records the time it takes for compressional waves to travel a given distance in the formation close to the borehole. The tool contains a transmitter and two receivers. Sound pulses are emitted from emitter; they travel through the formation and back into the receivers. The difference in arrival time from the two receivers is used to calculate the formation velocity. The log measurement records the interval travel which is the reciprocal of the velocity.

The sonic log can be used for porosity determination. The travel time depends on the kind of formation and how porous it is. The travel time is shorter in consolidated rocks and longer in less consolidated rocks. The travel time increases with an increase in porosity.

$$\text{Porosity } (\phi) = \frac{\Delta t_{\log} - \Delta t_{ma}}{(\Delta t_f - \Delta t_{ma})}$$

Where:

Δt_{\log} = Reading from sonic log in $\mu\text{s}/\text{ft}$

Δt_{ma} = Transit time of matrix material

Δt_f = About 189 s/ft (corresponding to a fluid velocity of about 5,300 ft/s)

Porosity values are increased if the sandstone contains shale since Δt readings are increased because Δt shale generally exceeds Δt sandstone (Baker Hughes, 1992). If the formation is hydrocarbon bearing the porosity is multiply by 0.7 for gas bearing zones and by 0.9 for oil bearing zones.

CHAPTER FOUR: ANALYSIS AND RESULTS

4.1. Wells Selection

Well selection was done on the following basis.

- Geologic and geographic position of the wells. The wells are selected from the deeper Eastern section of the basin separated from the shallower Western section by the Daarby Fault.
- Initially 16 wells were selected to form four profiles. Two profiles each on either side of the North-South trending river with one profile trending North-South and the other trending East West. However due to incomplete data set from all of the wells to complete the analyses the wells were reduced to 8 with only two profiles preserved to the East of the river.
- The “nine red” core holes as displayed on the map used for petrographic analysis are different for those used for geophysical wire-line log analysis (represented by black dots). However the petrography of the basin is virtually uniform.
- The wells used in the study are: WTB45, WTB48, WTB56, WTB58, WTB62, WTB65, WTB70 and WTB72 (see figure 4.1)

4.1.1. Zone Delineation

The initial stratigraphic zones classified by the South African Council of Stratigraphers are maintained. Within the wells, the interested strata are limited to coal horizons of the Ecca group. The coal seams intercepted by the wells delineated into eleven different zones. Seams belong to same zones are geometrically close to each other and have similar geological properties. Zones 11 to 5 are from the upper Ecca formation but considered as the Beaufort Seam One (BS1) coals by local geologist. Zones 4 to 1 are from the middle Ecca. Figure 4.2 illustrates the different zones.

Coals from zones 11 to 5 are generally bright coals while those from zones 4 to 1 are dull coals. However some bands of dull coals are seen alternating with the bright coals in zones 11 to 5 (figure 4.3).

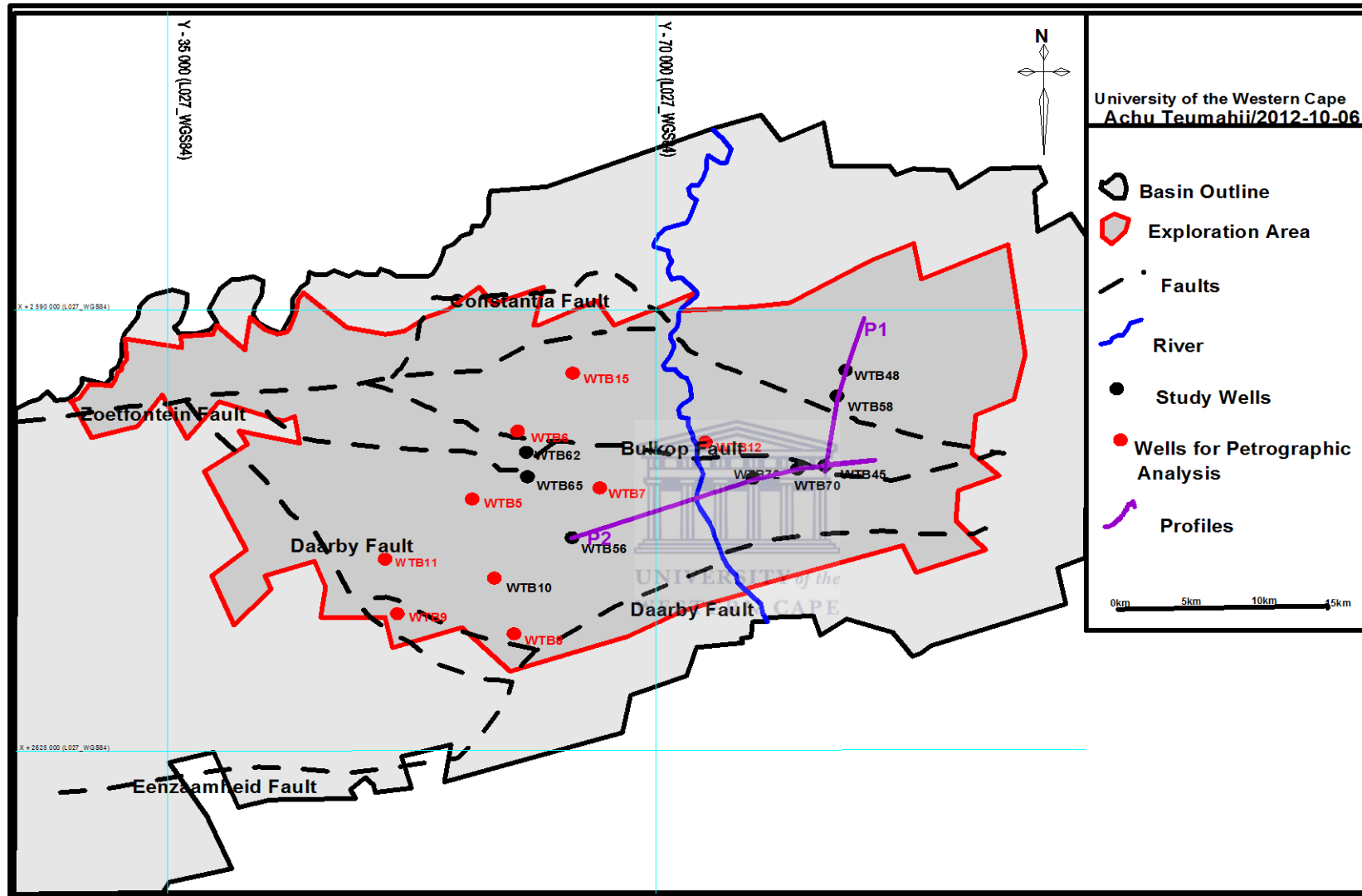


Figure 4.1: Well Location Map.

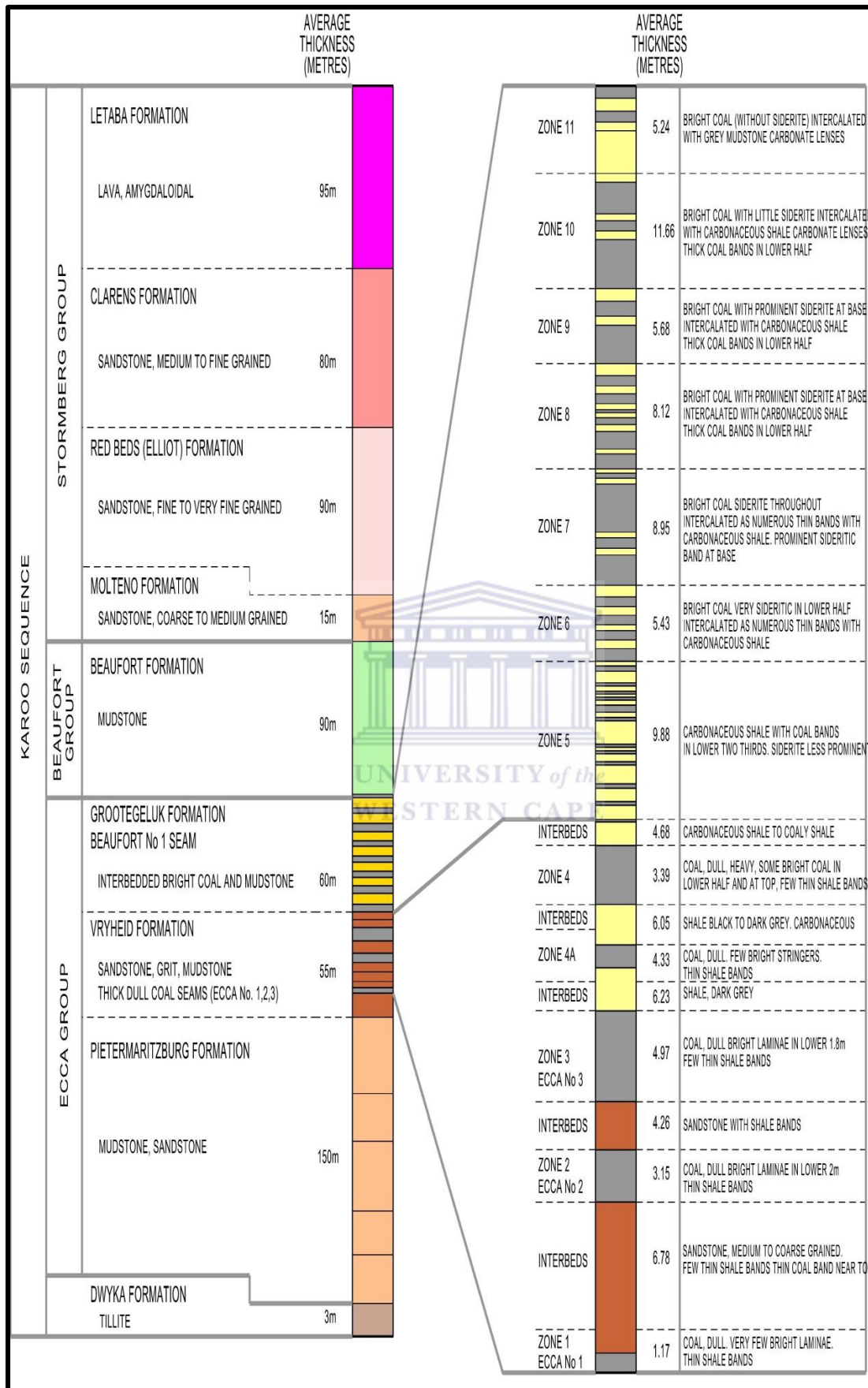


Figure 4.2: Coal zone delineation (Fourie, 2000) sourced from Anglo Coal data base.

4.2 Petrographic Maceral Analysis

Petrography is a division of petrology that focuses on the description of rocks. The description may range from megascopic to microscopic and may be limited to mineral content or texture. In this case the mineral content is the centre of the description. As previously stated a distinguishing character of coal is its high organic matter content which in most cases is the basis for petrographic studies on coal.

The results of the petrographic analysis for this study was supplied by Anglo operations limited consulting Geologists' Department of the Coal Division. Petrographic blocks were prepared in accordance to ISO Standard 7404-2, 1985 and the vitrinite random reflectance measurements (VR) were carried out in accordance with ISO Standard 7404-5, (1994). An additional group maceral analysis was carried out in accordance with ISO Standard 7404-3, (1994), while reactive inertinite maceral were identified according to Steyn and Smith for South African Coals.

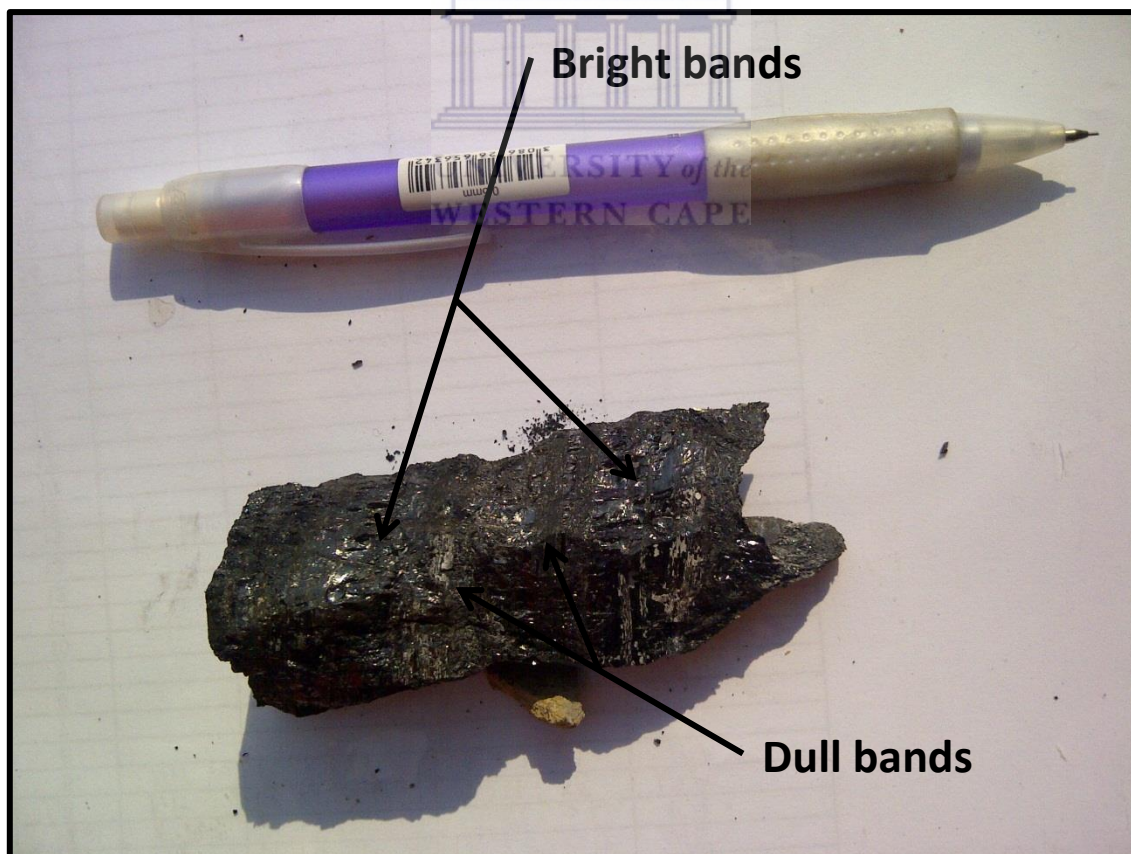


Figure 4.3: Banded coal from BS1; alternating bright and dull bands.

Due to the relative homogenous nature of the different maceral type throughout the basin, the analysis was conducted only for samples from a few wells drilled in the early exploration stages; WTB5, WTB6, WTB7, WTB8, WTB9, WTB10, WTB11, WTB12 and WTB15 as indicated in figure 4.1 above. They are then applied upon assumption on the wells used for this study. These wells are spatially spread throughout the basin and experimental results are almost same. The Standard deviations (see appendix 1) are very low giving their usage in this study justified.

A total of 48 samples were analysed (refer to appendix 1 and 2) from the 9 coreholes. Samples are representative of zones rather than depth. Each well is divided into 11 different zones on the bases of coal type groups. Zone 1 represents the deepest depth encountered while Zone 11 is shallowest depth. The shallowest sample analysed was derived from a depth of 175m in WTB65 while the deepest sample was from a depth of 521m in WTB09 from Zone 3.

4.2.1. Results of Petrographic Maceral Analysis

A summary of the results averaged for each zone from the various wells is presented in table 4.1 below. The table shows the average total Vitrinite, average total inertinite, average total Liptinite and average total vitrinite reflectance for each zone represented in percentages.

Table 4.1 Summary of Petrographic Maceral Analysis (% by volume mineral matter basis).

Zone	Total Vitrinite	Total Liptinite	Total Inertinite	VR (%) RD=1,80
11	83	4.3	5.7	0.65
10	73	4.5	9	0.66
9	78	3.5	4.5	0.66
8	74	4.5	10	0.69
7	78	6.5	7	0.72
6	77	4.5	8.5	0.67
5	63.2	5.9	22	0.72
4	52	5	34	0.75
3	15	3.5	74.3	0.84
2	27.5	4.5	59	0.77
1	6	3	80.7	0.75

Refer to appendix 1 for the results below.

The vitrinite content ranges from 0% to 71% while the Pseudovitrinite content ranges from 0% to 77%. Total Vitrinite content which is a sum of both vitrinite and pseudovitrinite spans from 2% to 88%.

The Sporinite, resinite and cutinite content together (S/R/C) ranges from 0% to 9% while the alginite content ranges from 0% to 2%. Liptinite content is generally low for all zones. Total liptinite percentage varies from 3 to 9.

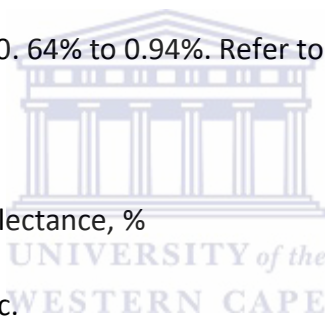
Total Inertinite content ranges from the neighbourhood of 3% to 92%. Nonetheless the total inertinite is a sum of Reactive semifusite (0-13)%, Inert semifusinite (1-22)%, Fusinite and Sclerotinite (0-4)%, Micrinite(0-3)%, Reactive inertoderinite (0-22)% and Inert inertoderinite (1-36)%.

Vitrinite reflectance ranges from 0.64% to 0.94%. Refer to appendix 2.

Where:

VR: Random Vitrinite Reflectance, %

RD: Relative density, g/cc.



4.3 Permeability Pressure Transient Well Test Analysis

The permeability pressure transient test for these wells was carried out by Advance Resources International (ARI), servicing for Anglo Coal. As seen earlier field permeability testing has been established in both conventional and unconventional industry as the most effective means of deriving reservoir permeability of the formation.

Injection falloff test permeability data was used to check the validity of the model estimated permeability.

The perm test employed by ARI made use of single phase testing with water to determine the absolute coal seam permeability. The test was carried out before any reduction in coal seam pressure to avoid a scenario where methane will desorb into and saturate the fracture network.

4.3.1. Equipment and Experimental Procedure

The experimental setup was composed of two units: the surface pump configuration for injection testing and a down-hole tool string for accurate pressure rating and pressure management.

The down-hole assembly was made up of two inflatable packers that are capable of Zonal isolation and surrounds and electronic memory pressure gauge. The tool is lowered into the formation with the aid of several hundred meters of 6 meter length 25mm outer diameter tube. Figure 4.4 shows the general setup of the down-hole tube. When the tool assembly is stationed at the required depth a 0.25inch outer diameter high pressure inflation hose is strapped to the tubing and the packers are inflated using air, water or hydraulic with a surface pressure of 870psig(60bars).

The surface pump arrangement consisted of a 2 642 or 1 321 gallons (10 000 or 5 000litres) water tank, a high and low pressure water pump. The water tank and pumps are connected directly to each other with the aid of a flow line. The pump to be used is based on the pre-determined flow rate.

Water from the pump passes through pressure releasing valves and a flow manifold. Characteristic features of the flow manifold includes: two needle valves for downstream injection pressure gauges; two turbines one high rate and the other low rate for flow meters.

Once the packer was in place and inflated the test procedure was commenced. The first process was to test the packer to be sure that at least one packer is set. The wellbore was given an hour to stabilize. The injection system was then pressure tested to a pressure exceeding the anticipated maximum.

The injection phase was performed at a constant rate so that the injection portion of the test could be analysed; however, analysis are carried out on falloff data and injection could still be carried out at constant pressure. A down-hole shut-in device is installed which isolates the wellbore and minimises wellbore storage effect. This is to ensure that fluid level does not fall below the surface during the shut in pressure since most coal reservoirs are under pressured.

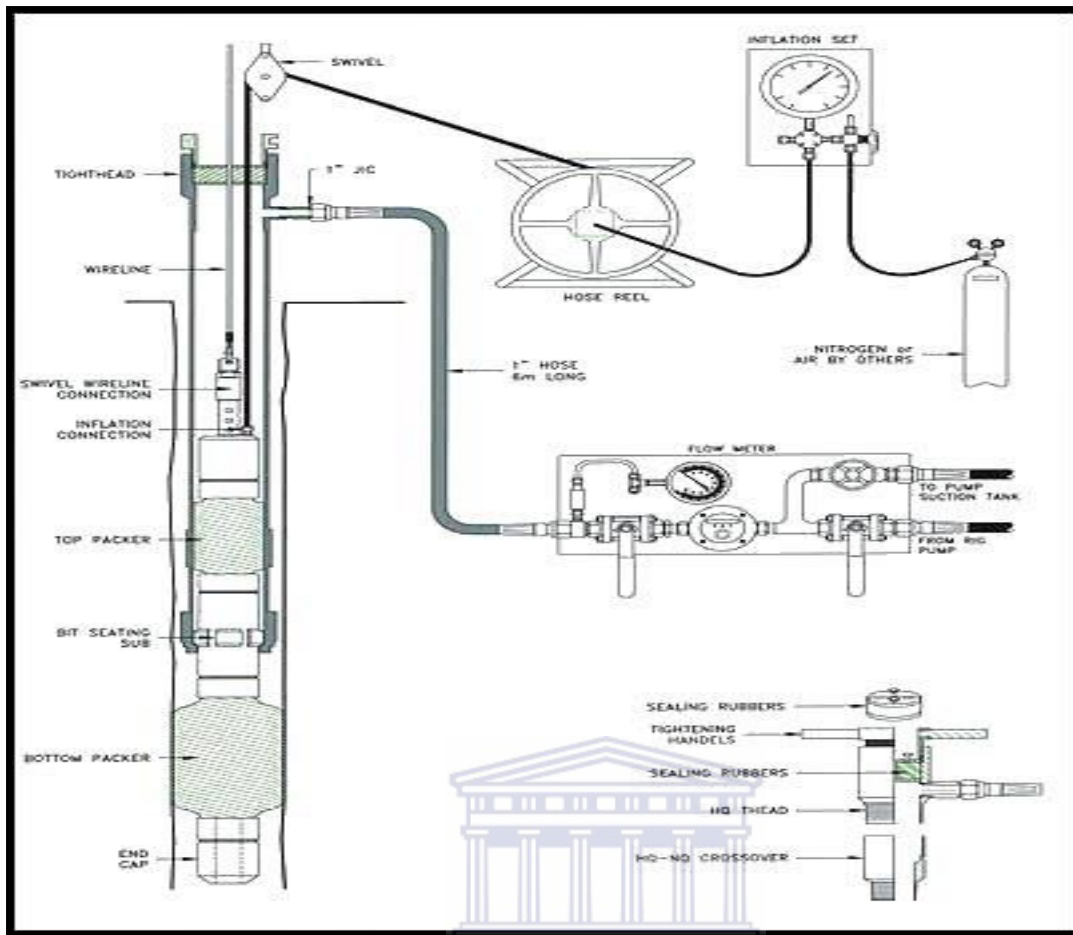


Figure 4.4: Experimental setup for pressure transient test (Cummins and Fredericks, 2006).

After pumping has commenced the pressure response was observed carefully for the first several minutes of injection while noting the rate of pressure gain. Rate adjustments were then made to bring the final injection pressure close to the final design pressure. At the end of injection, the well was shut in and the pressure falloff was monitored for about twenty hours. The core-holes were retested to verify the initial permeability results and to repeat unreliable test. Figure 4.5 is a typical example of analysed pressure data from WTB45 zone 10 and 11.

Some possible sources of data errors include parker leakage and reservoir damage.

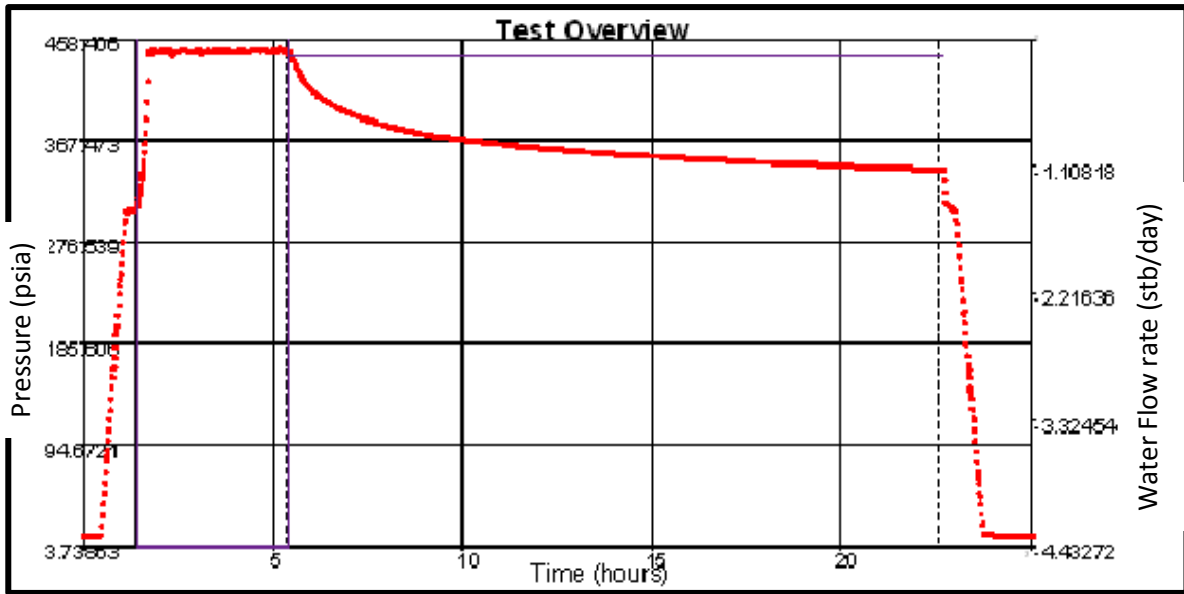


Figure 4.5: Analysed Pressure Data from Zone 10 and 11 WTB45 pressure transient test.

A summary of the results of the pressure transient test for the eight wells is presented on table 4.2 below.

Table 4.2 Pressure transient test Results summary.

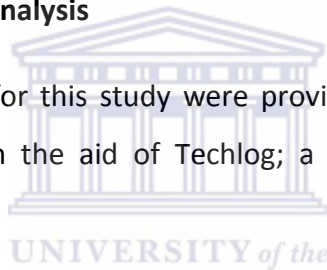
Well	Test Zone	Parker Interval	Net coal Thickness (m)	Formation Thickness (ft)	Permeability (md)	Skin	Closure Pressure (psia)
WTB 45	Upper	218-234.04	10.46	52.6	0.436	0.25	448.08
WTB 45	Middle	235-258.04	13.69	75.59	0.44	-2.7	524.93
WTB 45	Basal	262-286.4	13.52	80.05	0.436	-2.7	528.2
WTB48	Upper	288.66-304.83	8.88	53.05	1.2	1.9	634.88
WTB48	Middle	305.83-326	15.47	66.17	0.44	-2.7	647.33
WTB48	Basal	327-345.17	2.56	59.61	0.38	1.5	727.05
WTB56	Upper	270.68-292	20.07	69.94	0.42	0.36	567.58
WTB56	Middle	293.18-319	19.91	84.79	0.36	7.4	607.13
WTB56	Basal	319.9-338.23	10.54	60.14	0.03	0.5	676.23
WTB58	Upper	289.9-306.62	11.03	54.9	60.55	4.7	505.44
WTB58	Middle	307.80-330.52	14.79	74.5	2.59	-1.81	617.05
WTB58	Basal	331.65-351.37	11.02	64.7	142.2	50.6	642.94
WTB65	Upper	292.26-314.30		72.31	22.5	-1.6	598.98
WTB70	Upper	198.1-214.5	12.51	53.81	0.15	0.69	414.16

WTB70	Middle	214.50-236.90	12.17	73.49	0.09	-1.2	466.64
WTB70	Basal	236.20-260.60	8.92	80.05	0.18	4.5	510.13
WTB72	Upper	236.90-259.30		73.49	144.3	2.4	469.58
WTB72	Middle	260.6-285		80.05	0.17	-0.7	504.37
WTB72	Basal	286-302.40		53.81	0.7	2.5	548.47

ARI used a computer aided well test program PanSystem™ version 2.5 to perform all pressure transient test analysis. The permeability derived from pressure transient test for these wells ranged from 0.09md to 144.3md. Using arithmetic mean the average permeability of all wells is calculated to be 19.87md. Skin factor ranged from -2.7 to 50.6; lowest in basal and middle zone of WTB45 and the middle zone of WTB48 and highest in the basal zone of WTB58.

4.4. Geophysical Wire-Line Log Analysis

Raw digital wire-line logs used for this study were provided by Anglo Coal. The raw logs were plotted and analysed with the aid of Techlog; a specialized log analysis software designed by Schlumberger.



The down hole geophysical wire-line logs used for qualitative and quantitative analyses includes:

- Calliper logs (CALI),
- Gamma ray logs (GR),
- Density log (RHOB),
- Dual latero-resistivity log,
 - Deep Laterolog (LLD)
 - Shallow Laterolog (LLS)

Other data used includes composite paper log to check the correctness of the digital logs, well completion reports and Base map. The log signatures were first used for coal identification, then cementation index computation, porosity computation, fracture width computation and finally permeability computation.

A quantitative analytical approach was used to estimate the petrophysical properties from the digitized wireline logs. Different formulas were used for quantification.

In carrying out the analyses, the formulas used were not applicable to the entire log profile. The formulas were generated to satisfy coal zones. As such the reservoir zones were first identified; filtered out before running the analyses.

4.4.1 Coal Identification

A suite of geophysical wire-line logs were used for coal identification. Default maximum responses for coal are listed below;

- Maximum density for coal 2.0 g/cc
- Minimum Resistivity 10 Ohm.m

Coals contain very low radioactive substances; as such a radioactive detector in front of a coal formation registers very low radioactive counts. Gamma ray responses for coal are consequently very low sometimes even lower than for sandstone. However gamma ray logs can only be used for coal identification and reservoir delineation in conjunction with other logs. Same applies for resistivity; coals have a minimal resistivity of 10 Ohm.m and may sometimes rise as much as thousands of Ohm.m. As such resistivity logs are only used in collaboration with other logs.

The coals units were differentiated from the other rock types using a density cut off of 1.8 g/cc rather than 2.0 g/cc due to the intercalation of the coals and highly carbonaceous mudstones. Figure 4.6 show composite log plots for WTB45, WTB48, WTB56 and WTB58 with delineated coal zones while table 4.3 is a summary of coal thicknesses for each zone. Plots for WTB62, WTB65, WTB70 and WTB72 are displayed in appendix 3. Distinct zones are represented in track one. Track two carries the density log curve (red) and the black blocks are the coal units. The black curve in track three is the gamma ray log. The deep and shallow resistivity logs are recorded in track four. The deep log is blue and the shallow in black. The coal zones are aligned to low gamma ray signatures, high resistivity and low density as could be seen on the plots.

The coal thicknesses are as follows:

- 51.17m total coal thickness for WTB45. 37.15m for BS1 and 14.02m for Ecca.
- 27.08m total coal thickness for WTB48. 26.65m for BS1 and 0.27m for Ecca.
- 76.16m total coal thickness for WTB56. 56.52m for BS1 and 19.64m for Ecca.
- 50.3m total coal thickness for WTB58. 36.92m for BS1 and 13.38m for Ecca.
- 39.61m total coal thickness for WTB62. 29.51m for BS1 and 10.1m for Ecca.
- 68.24m total coal thickness for WTB65. 53.64m for BS1 and 14.6m for Ecca.
- 47.94m total coal thickness for WTB70. 33.6m for BS1 and 14.34m for Ecca.

Table 4.3 Coal Thickness derived from Density Logs

CBM Well- Zone	Depth (m)	Density Log (g/cm ³)	Zone Thickness (m)	Coal Thickness(m)
WTB45-11	218.00	1.62	2.5	1.35
WTB45-10	220.49	1.69	13.5	9.11
WTB45-9	234.00	1.64	5.5	2.31
WTB45-8	239.50	1.68	13.5	9.51
WTB45-7	252.50	1.69	5.8	1.87
WTB45-6	258.30	1.74	7.2	4.07
WTB45-5	270.75	1.73	14.8	8.93
WTB45-4	285.50	-	4.1	-
WTB45-3	289.55	1.64	7.4	4.07
WTB45-2	297.00	1.63	10.0	9.45
WTB45-1	307-312.10	1.78	5.1	0.5
WTB48-11	288.50	1.68	5.2	2.28
WTB48-10	293.70	1.73	11.5	6.5
WTB48-9	305.20	1.60	4.8	3.5
WTB48-8	310.00	1.65	9.5	8.57
WTB48-7	319.50	1.69	6.6	3.4
WTB48-6	326.15	1.70	6.1	2.4
WTB48-5	332.20	1.75	15.1	0.16
WTB48-4	347.30	-	28.2	-
WTB48-3	375.50	1.62	7.7	0.27
WTB48-2	383.20	-	7.1	-
WTB48-1	390.25- 395.80	-	5.6	-
WTB56-11	271.20	1.62	6.8	6.13
WTB56-10	278.00	1.66	14.5	13.94
WTB56-9	292.50	1.64	4.0	2.58
WTB56-8	296.50	1.70	14.8	11.22
WTB56-7	311.25	1.70	8.3	6.11
WTB56-6	319.50	1.67	10.5	9.19
WTB56-5	330.00	1.65	8.5	7.35
WTB56-4	338.50	1.75	11.5	3.17
WTB56-3	350.00	1.59	15.5	8.66

WTB56-2	365.50		1.69	14.0	5.37
	379.5-				
WTB56-1	382.50		1.52	3.0	2.44
WTB58-11	289.99		1.61	3.0	2.98
WTB58-10	292.99		1.69	13.6	8.13
WTB58-9	306.60		1.57	5.3	3.76
WTB58-8	311.95		1.63	8.5	3.62
WTB58-7	320.45		1.66	10.2	7.41
WTB58-6	330.60		1.69	4.2	0.25
WTB58-5	334.80		1.75	16.0	10.77
WTB58-4	350.80	-		19.9	-
WTB58-3	370.65		1.73	7.2	6.97
WTB58-2	377.85		1.67	6.7	6.06
	384.55-				
WTB58-1	391.56		1.67	7.1	0.35
WTB62-11	216.00		1.57	3.3	0.6
WTB62-10	219.35		1.65	17.1	13.36
WTB62-9	236.40		1.70	3.9	1.22
WTB62-8	240.35		1.71	8.8	5.4
WTB62-7	249.10		1.69	7.2	4.85
WTB62-6	256.30		1.66	13.7	2.04
WTB62-5	270.00		1.67	9.7	2.04
WTB62-4	279.70	-		30.0	-
WTB62-3	309.70	-		9.5	-
WTB62-2	319.20		1.69	9.5	8.89
	328.7-				
WTB62-1	336.10		1.59	7.4	1.21
WTB65-11	292.40		1.64	7.4	6.64
WTB65-10	299.75		1.63	14.8	13.39
WTB65-9	314.50		1.50	3.3	1.13
WTB65-8	317.80		1.65	11.3	7.94
WTB65-7	329.10		1.71	6.1	5.36
WTB65-6	335.25		1.66	16.6	14.99
WTB65-5	351.85		1.65	10.3	3.99
WTB65-4	362.10		1.69	13.7	-
WTB65-3	375.75		1.59	10.9	1.64
WTB65-2	386.60		1.68	2.1	11.61
	388.7-				
WTB65-1	396.90		1.54	8.2	2.35
WTB70-11	198		1.63	4.2	2.26
WTB70-10	202.15		1.71	13.1	10.25
WTB70-9	215.2		1.57	5.8	5.07
WTB70-8	220.95		1.66	8.5	3.6
WTB70-7	229.45		1.69	8.7	3.5
WTB70-6	238.1		1.76	10.8	2.71
WTB70-5	248.9		1.75	11.9	6.21
WTB70-4	260.75	-		4.9	-
WTB70-3	265.7		1.68	8.9	8.23

WTB70-2	274.6		1.62	8.4	6.11
WTB70-1	283-285.40	-		2.4	-
WTB72-11	237.82		1.78	5.1	
WTB72-10	242.9		1.79	17.2	
WTB72-9	260.14		1.79	6.7	
WTB72-8	266.85		1.80	7.8	
WTB72-7	274.61		1.80	11.1	
WTB72-6	285.7		1.79	6.5	
WTB72-5	292.2		1.80	9.6	
WTB72-4	301.75		1.80	12.8	
WTB72-3	314.5		1.80	10.1	
WTB72-2	324.55		1.80	9.1	
WTB72-1	336-340.15		1.79	4.1	



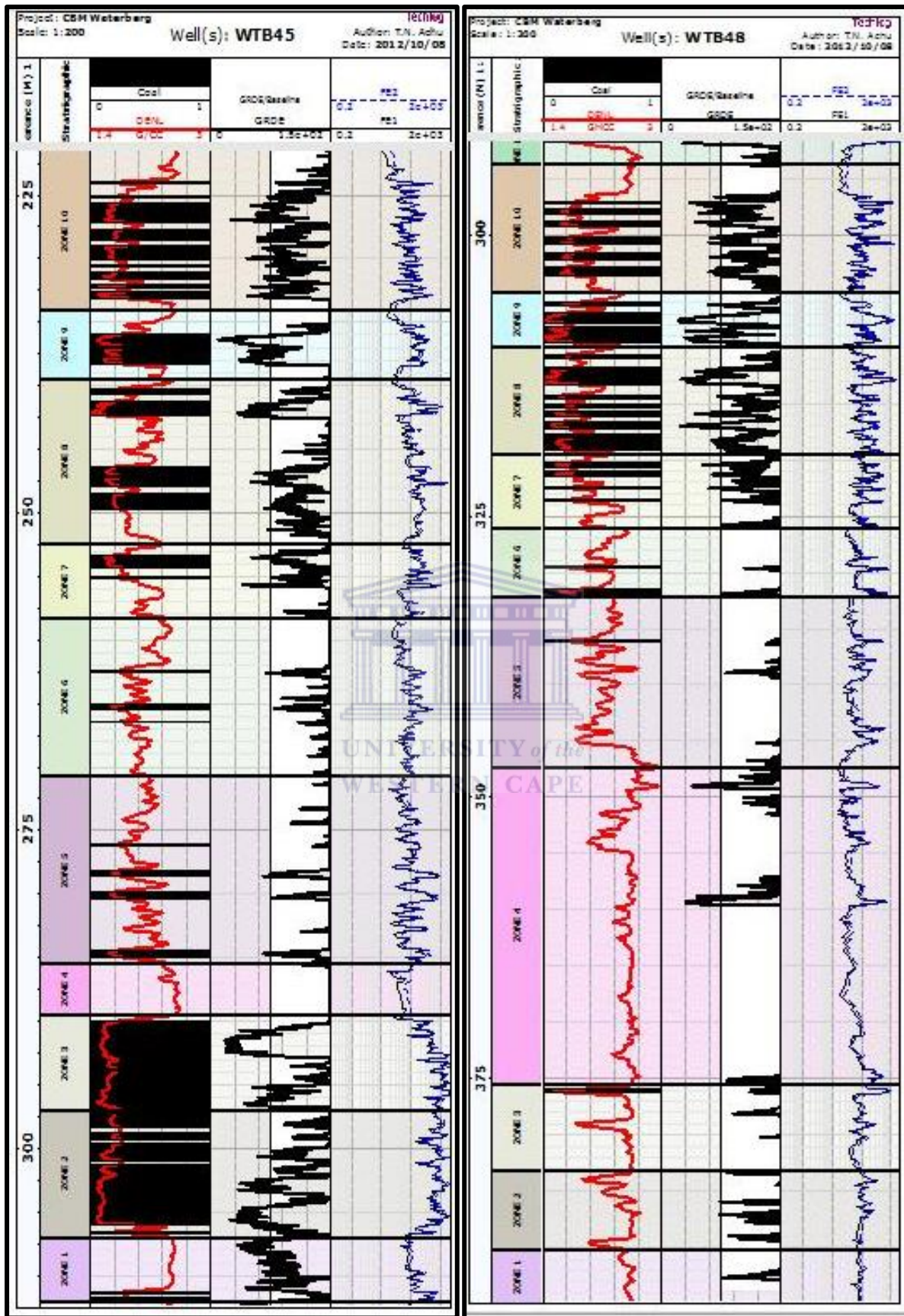


Figure 4.6: Composite Log plot for WTB45 (a) and WTB48 (b) indicating coal zones in black.

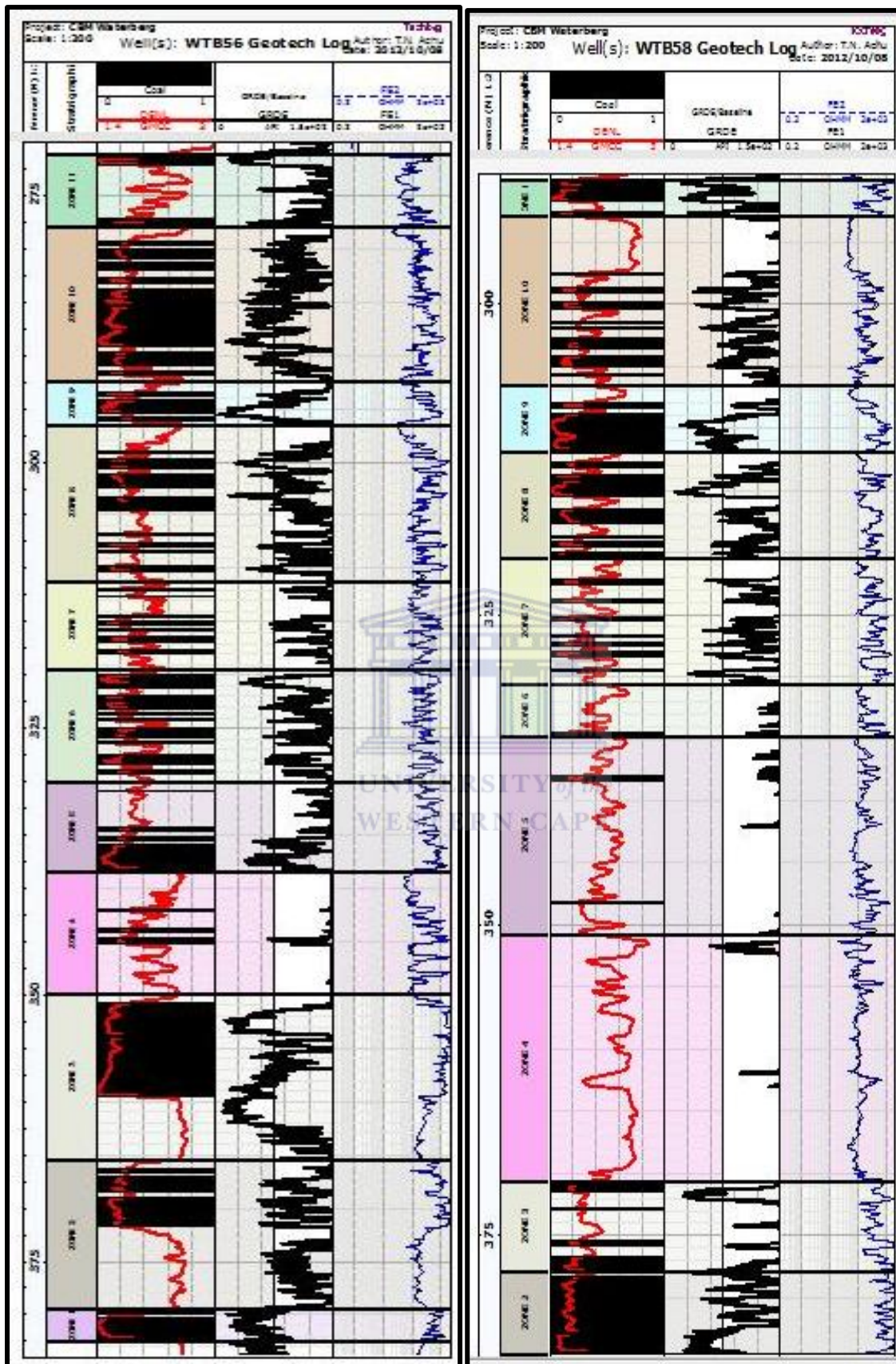


Figure 4.6: Composite Log plot for WTB56 (c) and WTB58 (d) indicating coal zones in black.

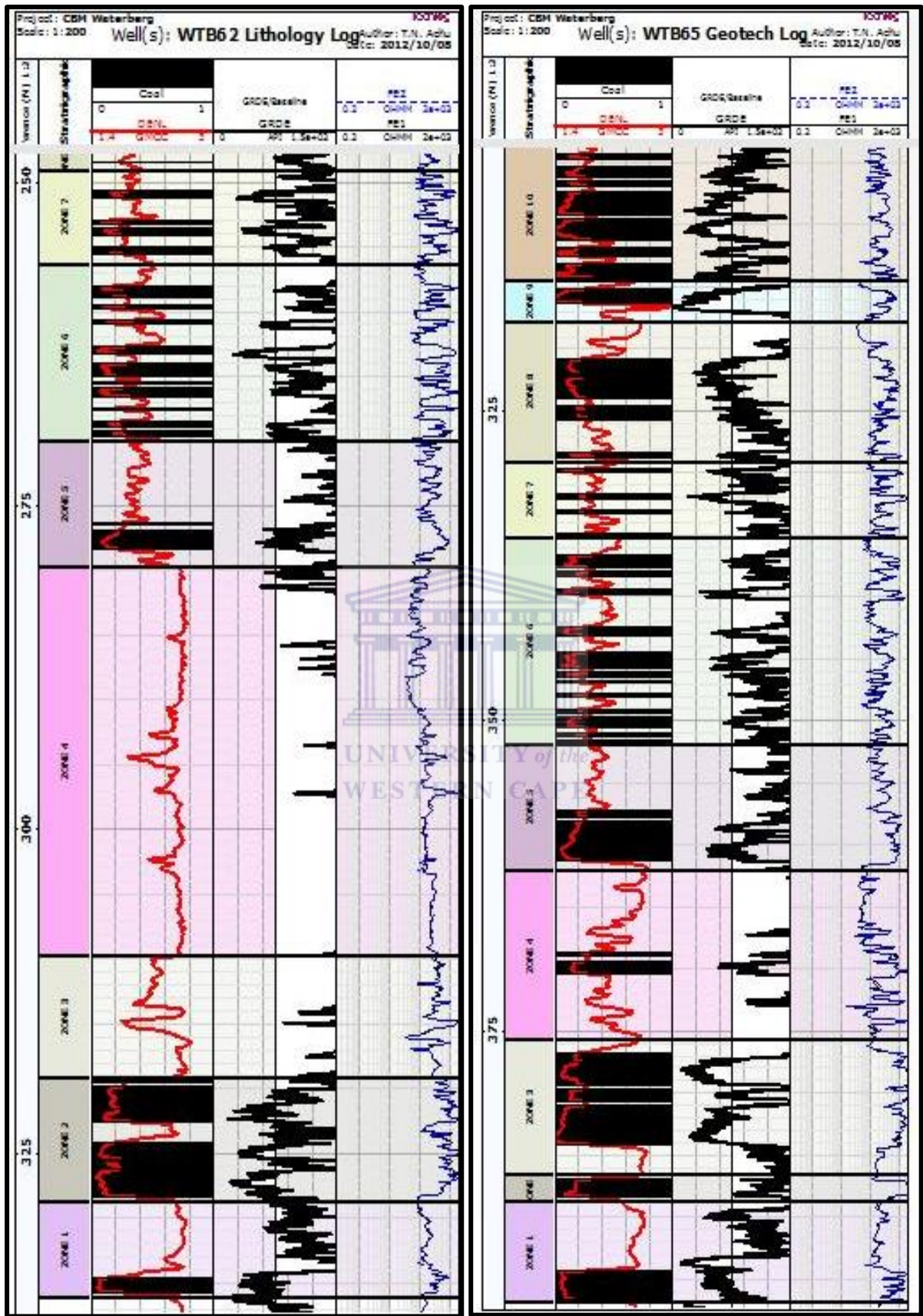


Figure 4.6: Composite Log plot for WTB62 (e) and WTB65 (f) indicating coal zones in black.

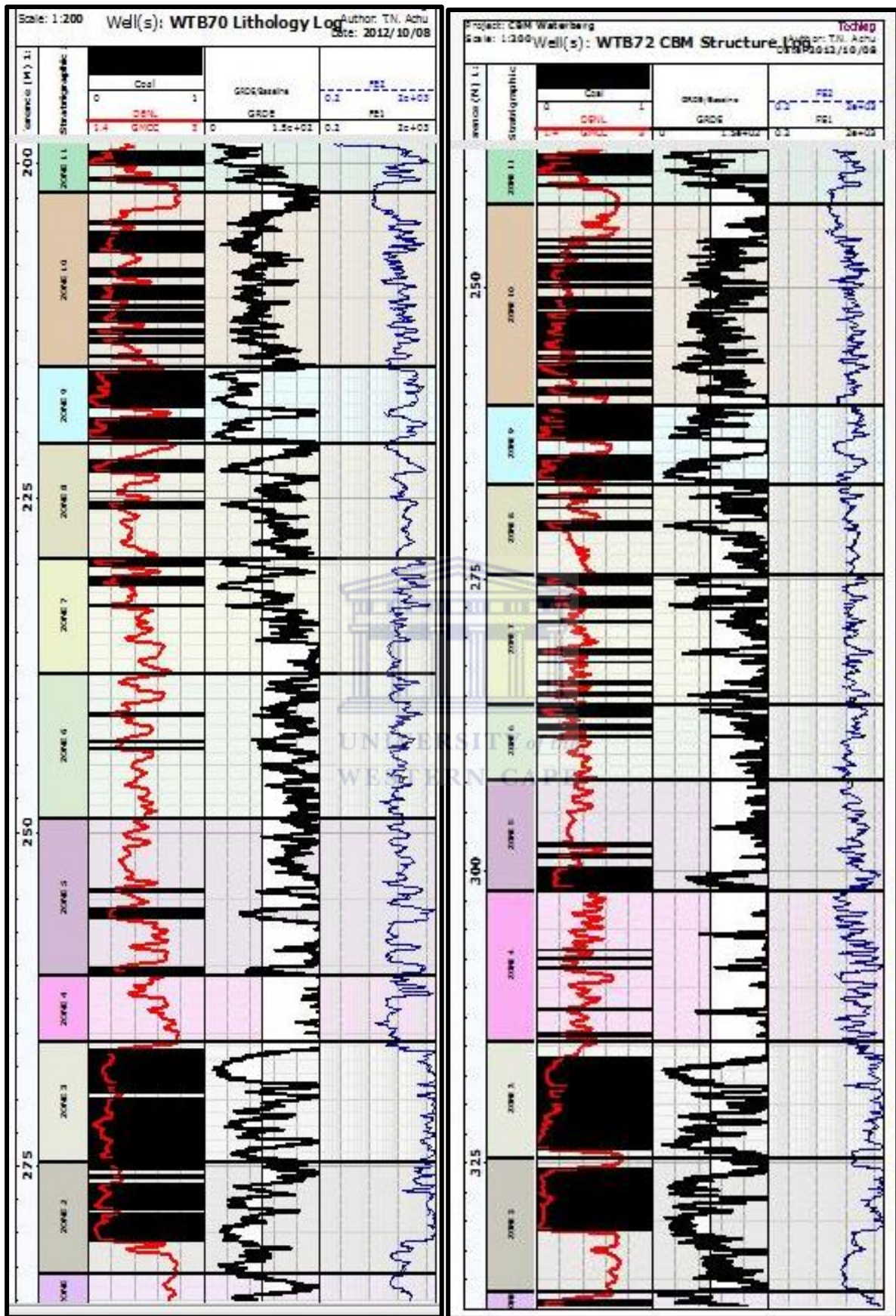


Figure 4.6: Composite Log plot for WTB70 (g) and WTB72 (h) indicating coal zones in black.

4.4.2. Fracture Permeability Estimation from Logging Data

Henry Darcy established in the mid 1850's that fluid flow (permeability) could be expressed by the equation:

$$k = \frac{Q}{A} \left[\frac{\mu}{dP/L} \right] \dots \dots \dots \text{Eq. 4.1}$$

Where,

K = permeability (darcy),

Q = flow per unit time (cm/s),

μ = viscosity of flow medium (cp),

A = cross section of rock (cm²),

L = length of rock (cm),

dP = pressure difference (drop).



This equation has been modified and applied in the oil and gas industry for almost a century to calculate the permeability of different reservoir rocks.

The permeability of reservoir rock however depends highly on the size of its pore openings, degree and size of its pore connectivity and the degree and type of cementing material between the rock grains. Coal unlike other conventional reservoir rocks is highly heterogeneous and composes of a dual pore system which includes the matrix pores and the natural fracture system.

It is the well-developed micro pores that form a bulk of coals porosity and offers an adsorptive for coal bed gases. The fracture network though provides a very small part of coal porosity; however provides a free passage way for fluids. In most cases it is made up of exogenous and endogenous face and butt cleats usually saturated with water. Coal permeability is therefore dependent on the width of the fracture network, degree of fracture connectivity (fracture length) and the degree of cementation and filling of fractures. Due to this heterogeneity nature of coal many models have been developed coal reservoirs.

4.4.2.1. Coal Permeability models

Reiss (1980) presents three ideal models for fracture coal reservoirs which include a collection of sheets (I), a bundle of matchsticks (II) and a collection of cubes (III). Model II and three are ideal for coal reservoirs with highly symmetric fractures. Coals with such fracture system are rare to find, only low ranked coals are closed to these models but are still very heterogeneous in their fracture distribution. The horizontal layering (considered as the y-axial cleats in model II and III) created in coal seams may be closed by overburden stress (Harpalani and Chen, 1997). Furthermore face cleats are much more continuous than butt cleats in coal and are most often the leading route for fluid flow (Li et al. 2011). For the above reasons the collection of sheet model (figure 4.7) was used in this study to represent the volatile bituminous C coals.

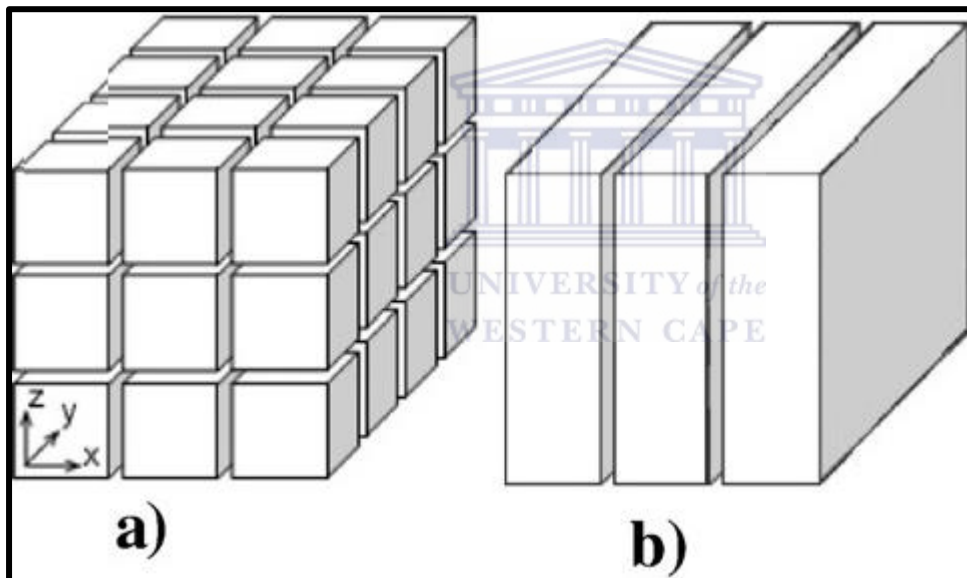


Figure 4.7: a) Collection of cubes, b) Collection of Sheets used for evaluating coal reservoir permeability (Wang et al. 2009)

The formula used for calculating coal reservoir fracture permeability for the collection of sheets model is given by (Hou, 2000):

$$k_f = 8.5 \times 10^{-4} w^2 \phi_f \dots \dots \dots \text{Eq. 4.2}$$

Where,

k_f = fracture permeability (md),

w = coal fracture width (μm),

ϕ_f = fracture porosity (%).

To compute for fracture permeability we had to derive the fracture porosity and the fracture width first.

4.4.3. Fracture Porosity estimation from logging data

The porosity of a medium could either be expressed as absolute or effective porosity. Absolute porosity as mentioned early refers to the ratio of total pore volume to the bulk volume whereas effective porosity is the fraction of the connected pores to the bulk volume. Since in coal the macro pores i.e. fractures are the only connecting pores as described by the above coal model, we can conveniently equate the fracture porosity to the effective porosity of coal.

In conventional reservoir evaluation rock porosity can be estimated from density, sonic and neutron logs. Density logging technique was used to obtain the value of the fracture porosity. The density tool measures the bulk density of the formation which is the density of the matrix plus that of the fluids occupying the pore spaces. However since fluid density is lower than matrix density; the more porous the formation the lesser its density.

The rock constituent contributes to bulk density as a percentage of its bulk volume calculated for limestone is expressed below. Limestone calibrations are used as standards in the oil industry since limestone show consistency and have little lithological variation.

$$\rho_b = \rho_{ma} + \rho_{sh} + \rho_f(\phi) \dots \dots \dots \text{Eq. 4.3}$$

Where

ρ_b = bulk density,

ρ_{ma} = density % percentage contributed by the rock matrix (g/cm³),

ρ_{sh} = density % consider by shale matrix in the rock,

ρ_f = density % contribution of the fluid -filled porosity,

ϕ = rock porosity.

The modified density porosity formula to calculate fracture porosity in coal is expressed as (Li et al., 2011):

$$\phi_f = \frac{(\rho_b - \rho_{ma}) \times (\rho_{ma} - \rho_{mf})}{(\rho_f - \rho_{ma}) \times [(\rho_{ma} - \rho_{mf}) + S_h \times (\rho_{mf} - \rho_h)]} \dots \dots \dots \text{eq. 4.4}$$

Where

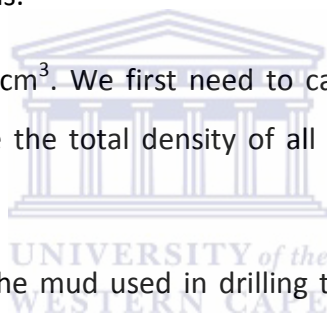
S_h = is the residual hydrocarbon saturation in coal,

ρ_{mf} = density of mud filtrate,

ρ_h = density of residual hydrocarbons,

ρ_f = total density of fluids.

All densities are expressed in g/cm^3 . We first need to calculate the residual hydrocarbon saturation in the coals, estimate the total density of all the fluids and the density of the residual hydrocarbon.



From well completion reports, the mud used in drilling these wells was pure water. Pure water has a density of 1 g/cm^3 .

4.4.3.1. Formation Water Analysis

The data for formation water analysis was supplied by Anglo Coal. Water pump out from five producing wells (Wells 1, 2, 3, 4, 5) in the basin was analysed for total dissolve solutes (TDS). The cations present includes: calcium, potassium, magnesium, sodium, aluminium, boron, barium, cadmium, cobalt, chromium, copper, iron, manganese, nickel, lead, strontium, zinc and ammonia.

Contained anions includes: bicarbonate, carbonate, fluoride, chloride, nitrate, sulphate, nitrite, sulphite, cyanide and silica. The detail TDS analysis is presented in Appendix 4 in mg/l . The average calculated TDS (anions + cations) for these wells expressed in mg/l was 7936.4 mg/l . This gave us the density of the formation water to be 1.0007 g/cm^3 . This was achieved by adding the density of the TDS with that of fresh water.

4.4.3.2. Gas and Coal Quality Analysis

The data for gas quality analysis from canister desorption test was supplied by Anglo Coal. Contained gases include methane (CH₄), Nitrogen (N₂) and Carbon dioxide (CO₂).

During coring coal cores were preserved in silver canisters; placed in temperature and pressure controlled boxes in order to preserve the initial reservoir state of the coal. In this state the gas trapped in the coal is assumed to remain adsorbed onto the organic material in the coal. During the desorption, the coal is degassed for ninety days during which the pressure of the canister is monitored and the quantity of desorbed gas estimated. The dissolved gas is separated into its various constituents and their respective volumes registered.

The degassed samples were first divided into half using a diamond saw. One half core sample was sent to the lab for residual gas determination while the other half was crushed to minus 7.5mm in order to liberate the inter-bedded coal and mudstone. After screening at 0.5mm, the 7.5 x 0.5mm fraction was subjected to float and sink separation at relative densities of 1.80 g/cm³. The result of the coal matrix was then used for petrographic analysis and calculation of matrix density. The matrix density was calculated by dividing the mass of the coal by its volume. The results; averaged for each zone per well is recorded on table 4.4.

The results of the average residual hydrocarbon saturation from all the wells calculated from gas quality data is also recorded on table 4.4. This was evaluated from the following equation:

$$S_h = \left(\frac{CH_{4\text{residual}}}{CH_{4\text{total}}} \right) \times 100 \dots \dots \dots \text{eq. 4.5}$$

Where S_h is the residual hydrocarbon saturation and

$$CH_{4\text{total}} = CH_{4\text{residual}} + CH_{4\text{desorbed}} \dots \dots \dots \text{eq. 4.6}$$

Appendix 5 contains raw data used to calculate the residual hydrocarbon saturation and matrix density.

Table 4.4 Grain matrix and Residual hydrocarbon saturation

Well	Zone	Matrix Density (g/cm ³)	Residual Hydrocarbon Saturation (%)
WTB45	10	1.62	40.37285454
WTB45	9	1.50	58.9105457
WTB45	8	1.66	55.21216831
WTB45	7	1.68	50.63018502
WTB45	3	1.52	43.57791545
WTB45	2	1.62	62.36947075
WTB45	1	1.79	75.84953061
WTB48	11	1.56	59.84064833
WTB48	10	1.63	46.22782879
WTB48	9	1.42	51.50013651
WTB48	8	1.46	50.84957347
WTB48	7	1.55	44.03651584
WTB48	6	1.55	45.17414619
WTB48	5	1.56	60.1707261
WTB48	3	1.79	71.76288832
WTB56	11	1.62	44.39731517
WTB56	10	1.62	43.35990213
WTB56	9	1.62	44.11191932
WTB56	8	1.62	39.68956885
WTB56	6	1.62	32.3129854
WTB56	4	1.62	45.76470239
WTB56	3	1.62	39.51021914
WTB56	2	1.62	51.08242037
WTB62	11	1.48	61.84340412
WTB62	10	1.53	50.41865554
WTB62	9	1.60	60.29206145
WTB62	8	1.51	48.51950832
WTB62	7	1.51	52.9659345
WTB62	6	1.55	54.65212903
WTB62	2	1.56	95.82701112
WTB62	1	1.60	96.9140738
WTB65	11	1.51	63.97850093
WTB65	10	1.51	59.32309358
WTB65	9	1.71	60.88318788
WTB65	8	1.585	66.67193804
WTB65	6	1.57	39.23911972

WTB65	5	1.6125	63.75246721
WTB65	4	1.58	64.23002054
WTB65	3	1.635	80.10252814
WTB65	2	1.56	71.68095062
WTB70	11	1.55	33.18529283
WTB70	10	1.52	37.51849896
WTB70	9	1.52	28.71509905
WTB70	7	1.60	55.19935957
WTB72	11	1.55	74.02800291
WTB72	10	1.53	49.22102663
WTB72	8	1.73	49.74323996
WTB72	7	1.56	39.18822847
WTB72	6	1.55	34.23297519

The calculated coal residual hydrocarbon saturation ranged from 28.72% in the shallower coal seams to 96.9% in the deeper coal seams. Residual hydrocarbon saturation averages at 54.01%.

The theoretical density of residual hydrocarbon (methane) was used as 0.668kg/m³ at normal temperature and pressure (NTP) while that for carbondioxide and nitrogen are 1.842kg/m³ and 1.165kg/m³ respectively. NTP is defined as air at 20°C and 1atm or 0 psia.

The total density of fluid (ρ_f) can thus be evaluated from the equation below.

$$\rho_f = \rho_{\text{methane}} + \rho_{\text{nitrogen}} + \rho_{\text{carbondioxide}} + \rho_{\text{water}} \dots \dots \dots \text{eqn.4.7}$$

Where:

- ρ_{methane} = density of methane,
- ρ_{nitrogen} = density of nitrogen,
- $\rho_{\text{carbondioxide}}$ = density of carbondioxide,
- ρ_{water} = density of formation water.

The results of the porosity calculated by inputting the above parameters in equation 4.4 are recorded on table 4.5.

Table 4.5 Density log derived fracture porosity

Well name – Zone	Depth (m)	Bulk Density from Logs (ρ_b) g/cm ³	Fracture porosity (ϕ_f) %
WTB45-10	220.49	1.69	0.008181985
WTB45-9	234.00	1.64	0.006921367
WTB45-8	239.50	1.68	0.001654156
WTB45-7	252.50	1.69	0.000610451
WTB45-3	289.55	1.64	0.008405546
WTB45-2	297.00	1.63	0.00083872
WTB45-1	307	1.78	0.000836236
WTB48-11	288.50	1.68	0.007170771
WTB48-10	293.70	1.73	0.010574424
WTB48-9	305.20	1.60	0.007250621
WTB48-8	310.00	1.65	0.009003163
WTB48-7	319.50	1.69	0.011238908
WTB48-6	326.15	1.70	0.011323633
WTB48-5	332.20	1.75	0.011511882
WTB48-3	375.50	1.62	0.02442
WTB56-11	271.20	1.62	0.00017045
WTB56-10	278.00	1.66	0.003710054
WTB56-9	292.50	1.64	0.00200492
WTB56-8	296.50	1.70	0.00912892
WTB56-6	319.50	1.67	0.006423754
WTB56-4	338.50	1.75	0.012731353
WTB56-3	350.00	1.59	0.003422371
WTB56-2	365.50	1.69	0.006180441
WTB62-11	216.00	1.57	0.003761905
WTB62-10	219.35	1.65	0.007938201
WTB62-9	236.40	1.70	0.006823643
WTB62-8	240.35	1.71	0.012280012
WTB62-7	249.10	1.69	0.010013057
WTB62-6	256.30	1.66	0.00669495
WTB62-2	319.20	1.69	0.004768143
WTB62-1	328.70	1.59	0.0004
WTB65-11	292.40	1.64	0.006130623
WTB65-10	299.75	1.63	0.006256052
WTB65-9	314.50	1.50	0.024044973
WTB65-8	317.80	1.65	0.003946782
WTB65-7	329.10	1.71	0.325482228
WTB65-6	335.25	1.66	0.00859046

WTB65-5	351.85		1.65	0.002644182
WTB65-4	362.10		1.69	0.00701861
WTB65-3	375.75		1.59	0.002753287
WTB65-2	386.60		1.68	0.006057112
WTB70-11	198		1.63	0.030133831
WTB70-10	202.15		1.71	0.026653518
WTB70-9	215.2		1.57	0.034824884
WTB70-7	229.45		1.69	0.006801
WTB72-11	237.82		1.78	0.013508402
WTB72-10	242.9		1.79	0.020316521
WTB72-8	266.85		1.80	0.01265
WTB72-7	274.61		1.80	0.020103234
WTB72-6	285.7		1.79	0.025517867

The fracture porosity values listed in column four in the table above. Calculated results estimated the coal reservoir fracture porosity to range from 0.00017% to 0.33 % (average 0.0156%) for all wells.

4.4.3.3 Fracture Width Estimation from Resistivity Logging Data

The method used to calculate the width of coal fractures in this thesis was developed by (Li et al, 2011). They modified the method previously adopted by Sibbit and Faivre (1985) to calculate the width of vertical fractures in ideal model I coal reservoirs with the use of Archie law and dual laterolog data.

Most sedimentary rock minerals are poor conductors. Consequently most of the current flow through the water in the pore spaces and not through the rock material. The nature of the contained pore water is thus of prime importance for resistivity determination. Pure water offers more resistance to the flow of current than water containing salts. However the conductivity of formation water is also dependent on pore geometry (in this case fracture geometry) which defines the width and length of the conducting medium. It was under these bases that Archie's equations were generated relating different parameters and summarized below:

$$F = \frac{R_o}{R_w} \dots \dots \dots \text{eqn. 4. 8}$$

$$F = \frac{A}{(\phi^m)} \dots \dots \dots \text{eqn. 4. 9}$$

$$RI = \frac{R_t}{R_o} \dots \dots \dots \text{eqn. 4.10}$$

$$S_w = \frac{1}{R_t} \times \frac{1}{N} = \left(F \times \frac{R_o}{R_t} \right) \times \frac{1}{N} \dots \dots \dots \text{eqn. 4. 11}$$

Where:

F = Formation factor,

A = 1 = Tortuosity factor

m = Cementation exponent,

n = Saturation exponent,

R_o = Resistivity of rock filled with water (ohm.m),

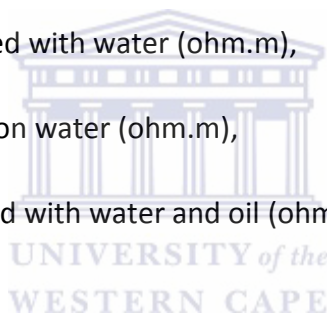
R_w = Resistivity of formation water (ohm.m),

R_t = Resistivity of rock filled with water and oil (ohm.m),

RI = Resistivity index,

S_w = water saturation (fractional),

φ = Porosity (fractional).



It was these formulas that were modified by Sibbit and Faivre (1985) and further modified by Li et al., (2011) to estimate coal fracture width. The following section shows some significant equations developed to calculate fracture width.

Equation 4.12 and 4.13 are the fracture porosity estimated from deep and shallow laterolog responses:

$$\phi_{fd} = \frac{(d_2 - r_w)w}{d_2^2 \pi - r_w^2 \pi} = \frac{W}{\pi(d_2 + r_w)} \dots \dots \dots \text{eqn4. 12}$$

$$\phi_{fs} = \frac{(d_1 - r_w)w}{d_1^2 \pi - r_w^2 \pi} = \frac{w}{\pi(d_1 + r_w)} \dots \dots \dots \text{eqn. 4. 13}$$

Equations (14) and (15) describe the characteristics of electro-conductivity in the deep and shallow laterolog detection zones.

$$\frac{1}{R_{LLD}} = \frac{\phi_{fd}^{mf} S_{wfd}^{nf}}{R_{zd}} \dots \dots \dots \text{eqn.4.14}$$

$$\frac{1}{R_{LLS}} = \frac{\phi_{fs}^{mf} S_{wfs}^{nf}}{R_{zs}} \dots \dots \dots \text{eqn.4.15}$$

Combining equation 4.14 and 4.15 to give equation 4.16 assuming that the fracture network around the borehole during drilling was invaded by drilling fluid while the coal matrix could not be invaded by drilling fluid (Li et al., 2011). Then the following is true $S_{wfs} = S_{wfd} = 1$, $R_{zd} = R_w$ and $R_{zs} = R_{mf}$.

$$\frac{1}{R_{LLS}} - \frac{1}{R_{LLD}} = \frac{\phi_{fs}^{mf}}{R_{mf}} - \frac{\phi_{fd}^{mf}}{R_w} \dots \dots \dots \text{eqn. 4. 16}$$

Combining equations (12) and (13), equation (16) can be transformed into:

$$\frac{1}{R_{LLS}} - \frac{1}{R_{LLD}} = \left(\frac{W}{\pi}\right)^{mf} \left[\frac{1}{R_{mf}(d_1 + r_w)^{mf}} - \frac{1}{R_w(d_2 + r_w)^{mf}} \right] \dots \dots \dots \text{eqn. 4. 17}$$

Equation (17) was used to obtain the fracture width but firstly the cementation index (m_f) was estimated. The parameters used in equations (12) to (17) are defined below.

Φ_{fd} = Fracture porosity obtain from deep laterolog,

Φ_{fs} = Fracture porosity obtain from shallow laterolog,

d_2 = Depth of investigation of deep resistivity (m),

d_1 = Depth of investigation of shallow resistivity (m),

r_w = Open hole radius (m),

W = Fracture width (μm),

R_{LLD} = Deep laterolog resistivity (ohm.m),

R_{LLS} = Shallow laterolog resistivity (ohm.m),

R_{mf} = Resistivity of mud filtrate (ohm.m),

R_w = Formation water resistivity (ohm.m)

m_f = Cementation exponent,

n_f = Saturation exponent,

S_{wfs} = Water saturation in shallow detection zone (fraction),

S_{wfd} = Water saturation in deep detection zone (fraction),

The hole radius was obtained from calliper log.

4.4.3.4 Cementation Exponent estimation from Logging Data

Methods of estimating cementation exponent in coal have not been fully reported. Investigations on cementation index have been previously focused on conventional gas reservoirs and carbonates reservoirs. The approaches were centred on (a) the use of Archie's law in experimental characteristics on rocks, (b) combining dual laterolog technique with Archie's law and the (c) establishment of relationship between cementation exponent and logging responses using regression analysis (Li et al, 2011).

The combination of dual laterolog technique and Archie's law was used to estimate the cementation index of coal reservoirs based on model I as applied by Li et al. (2011). Combining equation (8) and 9) two equations used to estimate cementation index based on relationship between the in situ resistivity from dual lateral logs and porosity are presented below.

$$\frac{R_{LLD}}{R_w} = \frac{1}{\phi_f^{m_f}} \dots \dots \dots 18$$

$$\frac{R_{LLS}}{R_{mf}} = \frac{1}{\phi_f^{m_f}} \dots \dots \dots 19$$

The fracture porosity calculated from density log in equation 4 was substituted in the above formulas to derive the cementation exponent (m_f). Two values for cementation exponent were derived from both deep and shallow resistivity and the average of both taken.

N.B Assumptions

The model was designed to be effective in situation where the deep laterolog resistivity is greater than the shallow laterolog resistivity. This is only possible if the resistivity of the mud filtrate is less than the resistivity of the formation water. However in this case fresh water mud was used in drilling with higher resistivity than that of the formation water. This resulted in the shallow resistivity surpassing the deep resistivity.

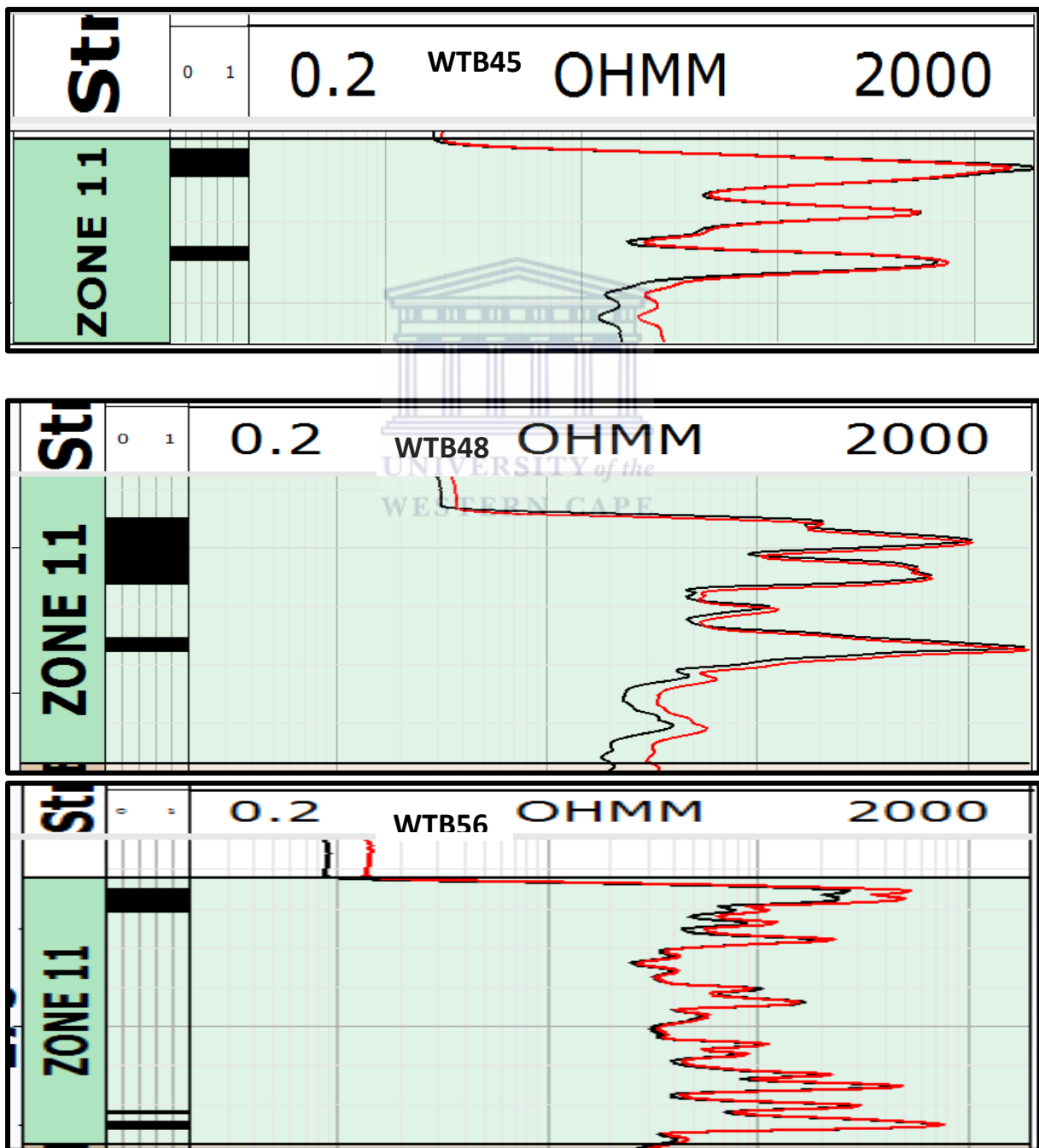
This however was not a limiting factor in the study as the model was designed to take into account the difference between shallow and deep resistivity. Resistivity is however a scalar quantity. We consequently had two options: (1) to consider the shallow resistivity in place of the deep resistivity and vice versa or (2) calculated the difference of their reciprocal which will give a negative value but then the absolute of this value is used since resistivity is a scalar quantity. Option one was used.

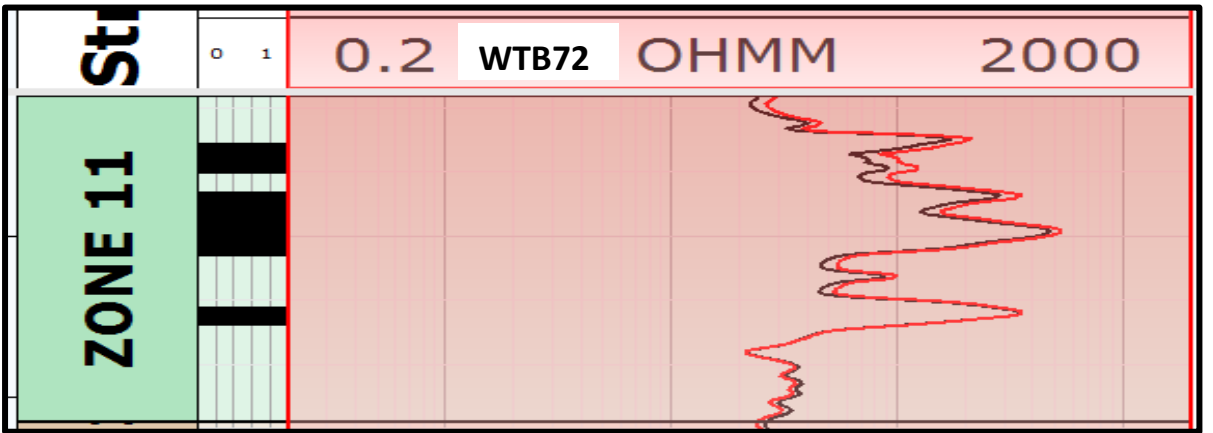
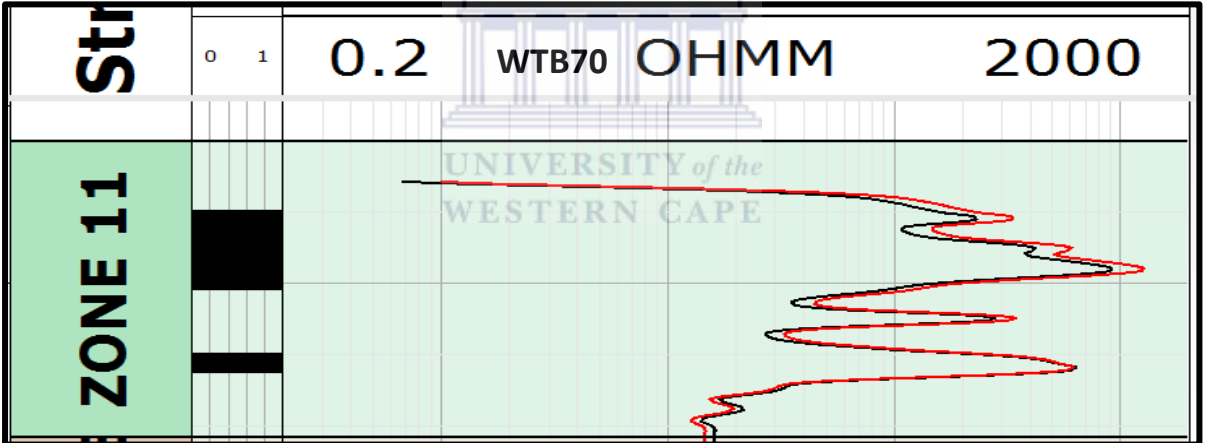
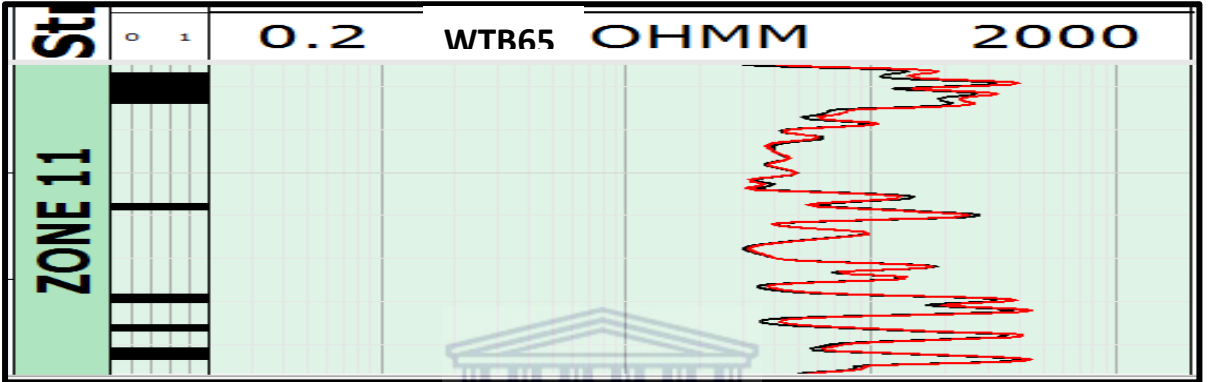
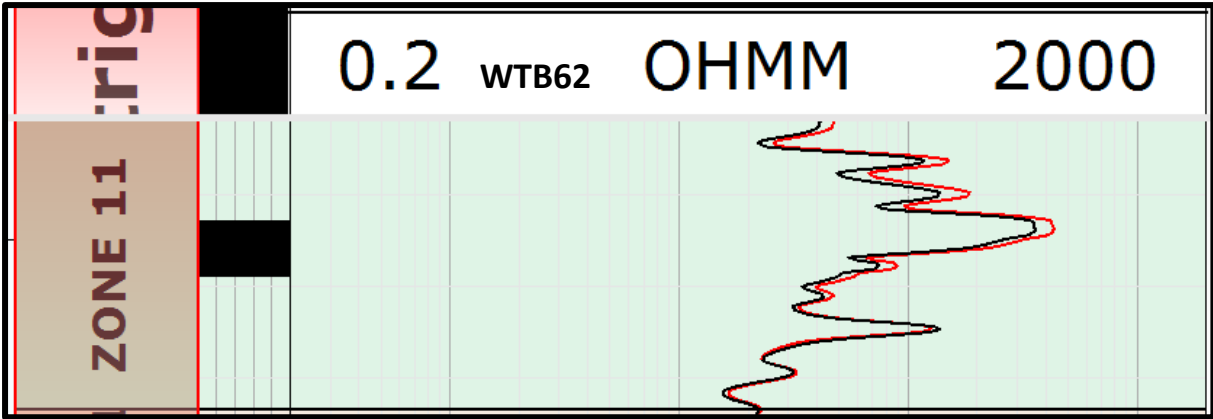
Supplied data also did not furnish us with the resistivity of the mud filtrate. Notwithstanding since the drilling fluid was pure water, no mud cake was created so only water infiltrated the formation and got mixed with the formation water in the flushed zone. However due to the closeness between drilling fluid resistivity and formation water resistivity as well as their depths of investigation, the resistivity of the mud filtrate was assumed as the resistivity of water. The resistivity of the mud filtrate used was $0.25\Omega.m$ and resistivity of formation water $0.2\Omega.m$

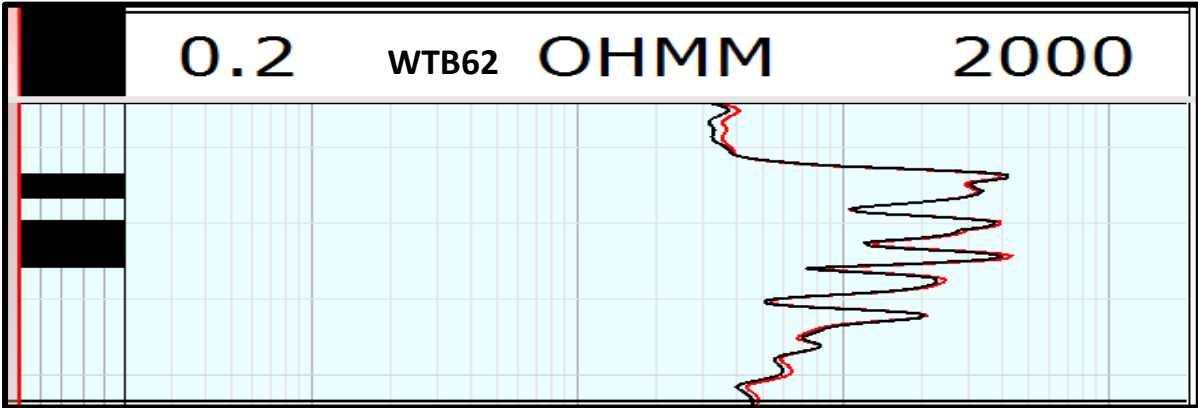
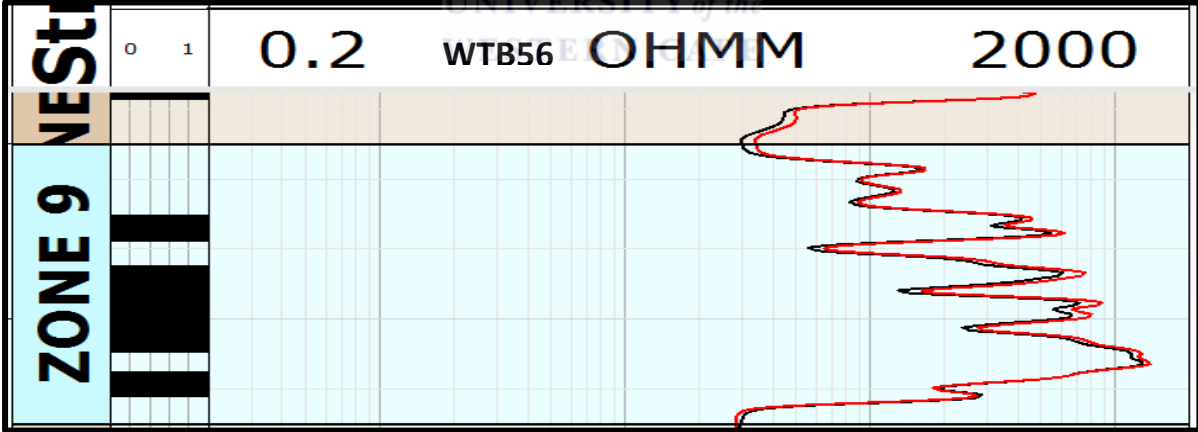
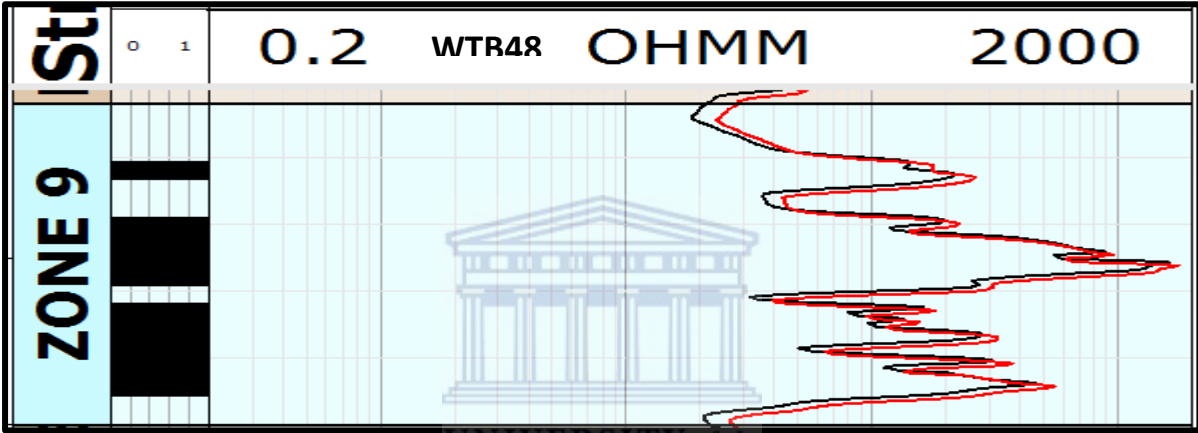
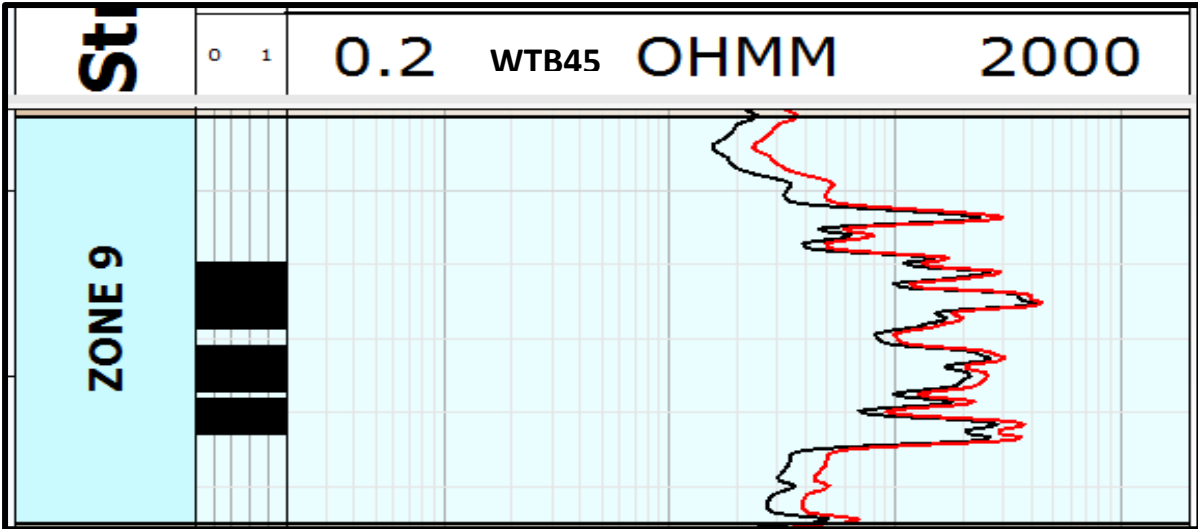
4.4.4. Results of Cementation Exponent, Fracture Width, Fracture porosity and Fracture Permeability Analysis

To apply the dual laterolog technique the intrusion of drilling fluids needs to be monitored during drilling. The technique cannot be applied where the shallow and deep resistivity log values are same. Figure 4.8 shows high dual laterog resistivity for coal seams than surrounding strata. The patterns observed for dual laterolog in Figure 4.8 are similar which ascertains the validity of the application of this technique.

The depth of investigation of the deep and shallow resistivity (d_2 and d_1) are 0.3m and 0.2m respectively while the hole radius is 0.052m. Due to low depths of investigation and small difference between both depths of investigation, the deep laterolog resistivity may have been affected by the drilling fluid and thus results in difference from the in place coal reservoir resistivity, this observation was also made by Li et al., 2011). The deep resistivity values may thus be slightly lower than the true formation resistivity. Deep resistivity logs are recorded in red while the shallow resistivity values are recorded in black for the figures 4.8.







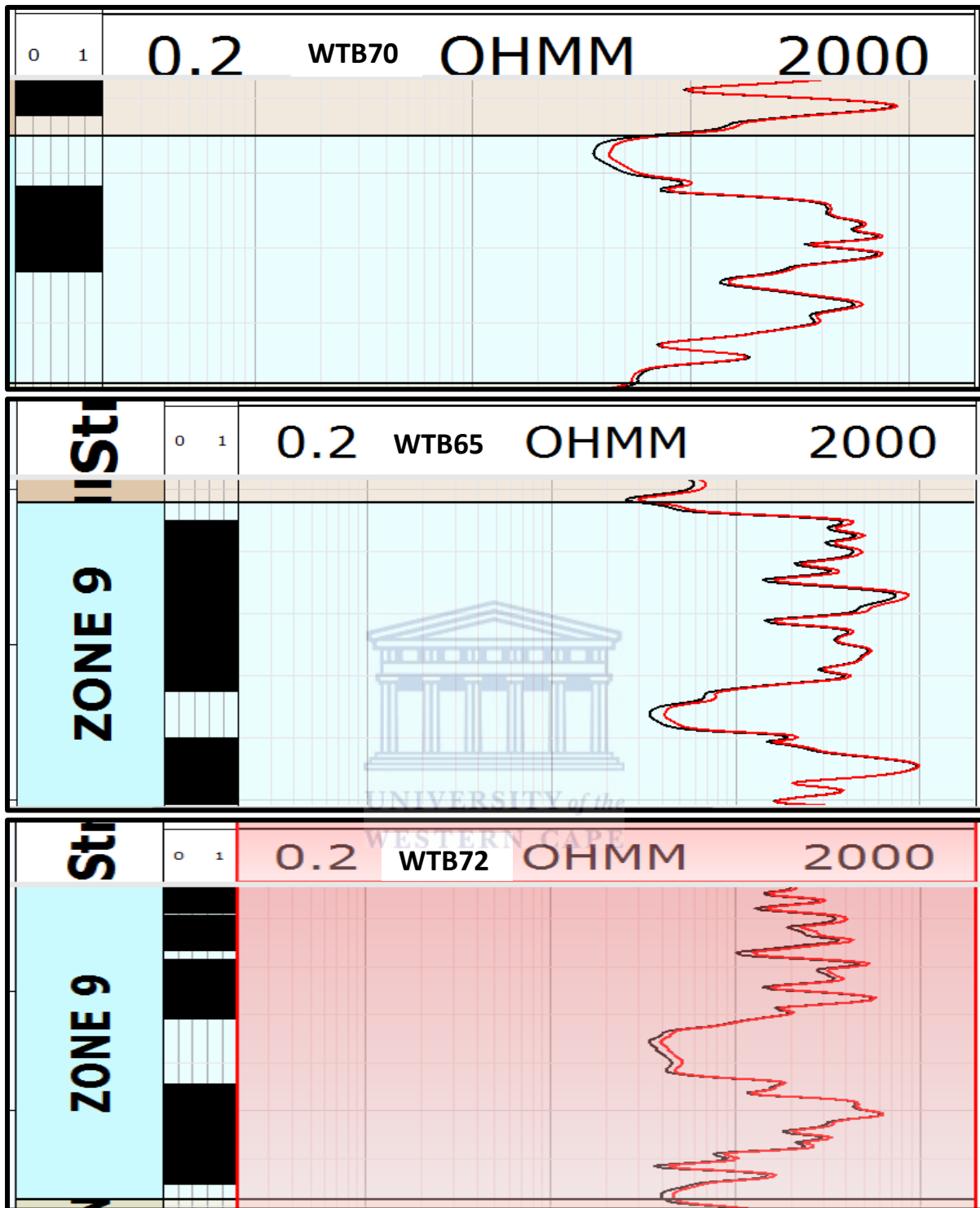


Figure 4.8: Dual Laterolog response of zone 11 and 9 for wells: WTB45, WTB48, WTB56, WTB62, WTB65, WTB70, and WTB72.

The results obtained by the above method are presented on table 4.6. The coal cementation index derived from logging data varies from 0.82 to 2.42. In the Beaufort Seam 1 coals a maximum cementation index of 2.04 was recorded against a minimum cementation of 0.82.

Average cementation index for this formation is 1.47. Higher cementation indices are recorded for the Ecca seams with an average of 1.58. Ecca coal seams records a maximum m_f of 2.42.

Calculated results reveal that the coal fracture width ranges from 0.68mm to 933.08mm in the Beaufort Seam 1 formation with an average of 214.18mm and from 8.42mm to 134.68mm with an average of 63.37mm in the Ecca seams.

Computed fracture permeabilities are higher in the BS1 coals than in the Ecca Coals. Fracture permeability from logging data average 0.025mD in the Ecca formation and 4.14mD in BS1. 0.0045mD and 6.05 mD were recorded for minimum and maximum permeabilities respectively for BS1 and in the Ecca 0.01 minimum permeability was recorded as against 0.1017 maximum permeability.

Table 4.6 Results obtained from geophysical Logging Data

CBM Well	Depth (m)	R_{LLS} ($\Omega.m$)	R_{LLD} ($\Omega.m$)	m_f	ϕ_f	w (mm)	K_f (md)
WTB45-10	220.49	122.9	150.6	1.33	0.0082	933.1	6.055
WTB45-9	234.00	194.8	234.0	1.38	0.0069	538.1	1.703
WTB45-8	239.50	288.2	339.7	1.13	0.0017	328.7	0.152
WTB45-7	252.50	172.1	209.2	0.91	0.0006	644.3	0.215
WTB45-6	258.30	14.9	282.2			445.8	
WTB45-5	270.75	302.4	392.8			475.8	
WTB45-3	289.55	846.3	980.5	1.74	0.0084	101.1	0.073
WTB45-2	297.00	790.8	921.0	1.16	0.0008	111.8	0.009
WTB45-1	307-312.10	673.5	787.9	1.14	0.0008	134.7	0.013
WTB48-11	288.50	529.7	505.8	1.57	0.0072	55.8	0.019
WTB48-10	293.70	278.9	281.7	1.57	0.0106	22.3	0.004
WTB48-9	305.20	329.0	369.8	1.49	0.0073	209.5	0.271
WTB48-8	310.00	280.7	310.4	1.53	0.0090	212.4	0.345
WTB48-7	319.50	229.7	233.9	1.55	0.0112	49.0	0.023
WTB48-6	326.15	330.4	304.3	1.62	0.0113	162.5	0.254
WTB48-5	332.20	351.1	366.2	1.65	0.0115	73.3	0.053
WTB48-3	375.50	754.3	825.8	2.20	0.0244	71.7	0.107
WTB56-11	271.20	248.1	328.1	0.82	0.0002	614.0	0.055
WTB56-10	278.00	344.8	390.1	1.32	0.0037	210.6	0.140

WTB56-9	292.50	459.9	527.3	1.24	0.0020	173.7	0.051
WTB56-8	296.50	626.2	726.7	1.71	0.0091	138.1	0.148
WTB56-7	311.25	490.5	553.8			145.6	
WTB56-6	319.50	469.8	499.9	1.52	0.0064	80.3	0.035
WTB56-5	330.00	769.8	825.8			55.1	
WTB56-4	338.50	1357.0	1501.5	2.01	0.0127	44.3	0.021
WTB56-3	350.00	1511.0	1611.7	1.56	0.0034	25.8	0.002
WTB56-2	365.50	1231.0	1385.0	1.71	0.0062	56.5	0.017
WTB62-11	216.00	229.9	189.7	1.23	0.0038	576.9	1.064
WTB62-10	219.35	297.7	268.8	1.48	0.0079	225.8	0.344
WTB62-9	236.40	293.7	285.1	1.44	0.0068	64.0	0.024
WTB62-8	240.35	552.9	462.3	1.76	0.0123	221.6	0.513
WTB62-7	249.10	1036.2	909.7	1.82	0.0100	83.8	0.060
WTB62-6	256.30	838.1	769.5	1.64	0.0067	66.4	0.025
WTB62-5	270.00	624.5	581.4			74.2	
WTB62-2	319.20	985.9	921.2	1.56	0.0048	44.6	0.008
WTB62-1	328.7- 336.10	912.0	825.5	1.06	0.0004	71.8	0.002
WTB65-11	292.40	169.2	199.2	1.32	0.0061	555.5	1.608
WTB65-10	299.75	296.8	319.1	1.42	0.0063	147.5	0.116
WTB65-9	314.50	438.2	462.3	2.04	0.0240	74.4	0.113
WTB65-8	317.80	470.7	523.5	1.39	0.0039	133.8	0.060
WTB65-7	329.10	517.7	579.4	2.42	0.3255	128.6	4.577
WTB65-6	335.25	393.0	417.1	1.58	0.0086	91.7	0.061
WTB65-5	351.85	671.7	733.8	1.36	0.0026	78.8	0.014
WTB65-4	362.10	750.2	841.2	1.65	0.0070	90.1	0.048
WTB65-3	375.75	1527.6	1633.5	1.50	0.0028	26.5	0.002
WTB65-2	386.60	1853.4	1938.9	1.77	0.0061	14.9	0.001
WTB65-1	388.7- 396.90	857.1	867.1			8.4	
WTB70-11	198	371.7	478.8	1.57	0.0301	3.0	0.970
WTB70-10	202.15	225.3	268.7	1.69	0.0267	2.7	2.689
WTB70-9	215.2	364.7	394.7	1.43	0.0348	3.5	0.079
WTB70-7	229.45	498.3	553.6	1.56	0.0068	0.7	0.091
WTB72-11	237.82	133.1	175.3	1.16	0.0135	3702.1	0.402
WTB72-10	242.9	282.0	305.8	1.50	0.0203	2462.1	0.855
WTB72-9	260.14	199.4	214.8				
WTB72-8	266.85	207.1	218.8	1.56	0.0127	2487.8	0.707
WTB72-7	274.61	368.9	403.6	1.46	0.0201	1960.4	133.108
WTB72-6	285.7	121.5	142.5	1.70	0.0255	1712.9	0.448

Injection fall off permeability data from six of the wells (WTB45, WTB48, WTB56, WTB58, WTB65, WTB70 and) for BS1 were selected to check the accuracy of the method. Their results are presented on table 4.2 above. However the permeability test was run for composite zones rather than single zones. In order to check the validity of this method the fracture permeability derived from logging data must be averaged for the composite zone represented by the injection fall off test permeability. The compared results are presented on Table 4.7 below.

Table 4.7 Comparison between Log and field derived permeabilities

Well	Test Zone	Parker Interval	Net coal Thickness (m)	Formation Thickness (ft)	Permeability (md)	Skin	Log Perm (mD)
WTB 45	Upper	218-234.04	10.46	52.6	0.436	0.25	6.055
WTB 45	Middle	235-258.04	13.69	75.59	0.44	-2.7	0.69
WTB48	Upper	288.66-304.83	8.88	53.05	1.2	1.9	0.012
WTB48	Middle	305.83-326	15.47	66.17	0.44	-2.7	0.21
WTB48	Basal	327-345.17	2.56	59.61	0.38	1.5	0.15
WTB56	Upper	270.68-292	20.07	69.94	0.42	0.36	0.1
WTB56	Middle	293.18-319	19.91	84.79	0.36	7.4	0.1
WTB56	Basal	319.9-338.23	10.54	60.14	0.03	0.5	0.04
WTB65	Upper	292.26-314.30		72.31	22.5	-1.6	1.3
WTB70	Upper	198.1-214.5	12.51	53.81	0.15	0.69	1.8
WTB70	Middle	214.50-236.90	12.17	73.49	0.09	-1.2	.08

CHAPTER 5: DISCUSSIONS AND INTERPRETATION

Amongst the most important coal reservoir parameters are coal burial depths, coal thickness, maceral composition, permeability and maturity of the source rock. These properties are sometimes interrelated and affect each other. To a certain extent the burial depth, maceral content, fracture network, the cementation index reflects the porosity and permeability of the coal seam.

This chapter shall focus on discussing the results presented in chapter four above. It shall focus on the calculated porosity and permeability and shall discuss how and to what degree to which they are affected by other parameters for this basin.

5.1 Burial Depth and coal Thickness

In Coalbed methane resource evaluation, the depth of burial of coal is of significant importance. Firstly suitable depths are required for coal maturity and thermogenic gas generation. Furthermore high pressures are the main trapping gas mechanism in CBM reservoirs. These pressures are hydrostatic resulting from the overburden sediments. The thicker the overburden sediments, the deeper the burial depth, the higher the pressure and the better the trap. An added importance of the depth parameter is its control over reservoir permeability by simply altering the fracture geometry.

In the same way, like every other reservoir; appreciable coal thickness is required for commercial gas accumulation. Production in CBM reservoir at some stage requires hydraulic fracking to create artificial flow path for the gas to flow from the formation to the borehole. Fracking can only be effective provided it is restricted to the coal seam. The coal seam consequently needs to be thick enough to avoid fracking of non-coal units above creating a pathway for gas to trickle out.

Figure 5.1 is an East – West cross section linking WTB56, WTB72, WTB70 and WTB45 while figure 5.2 is a North – South cross section joining wells WTB48, WTB58 and WTB45. From figure 5.1 the deepest coal seams in the study were penetrated by WTB56. The shallowest coal seam in WTB56 was recorded at a depth of 271m and the deepest seam at 382m. Contrary to WTB70 with shallowest record of 202m and deepest record of 285m. From this

we can see that the shallowest coal seam for WTB56 is almost at same depth as the deepest seam for WTB70.



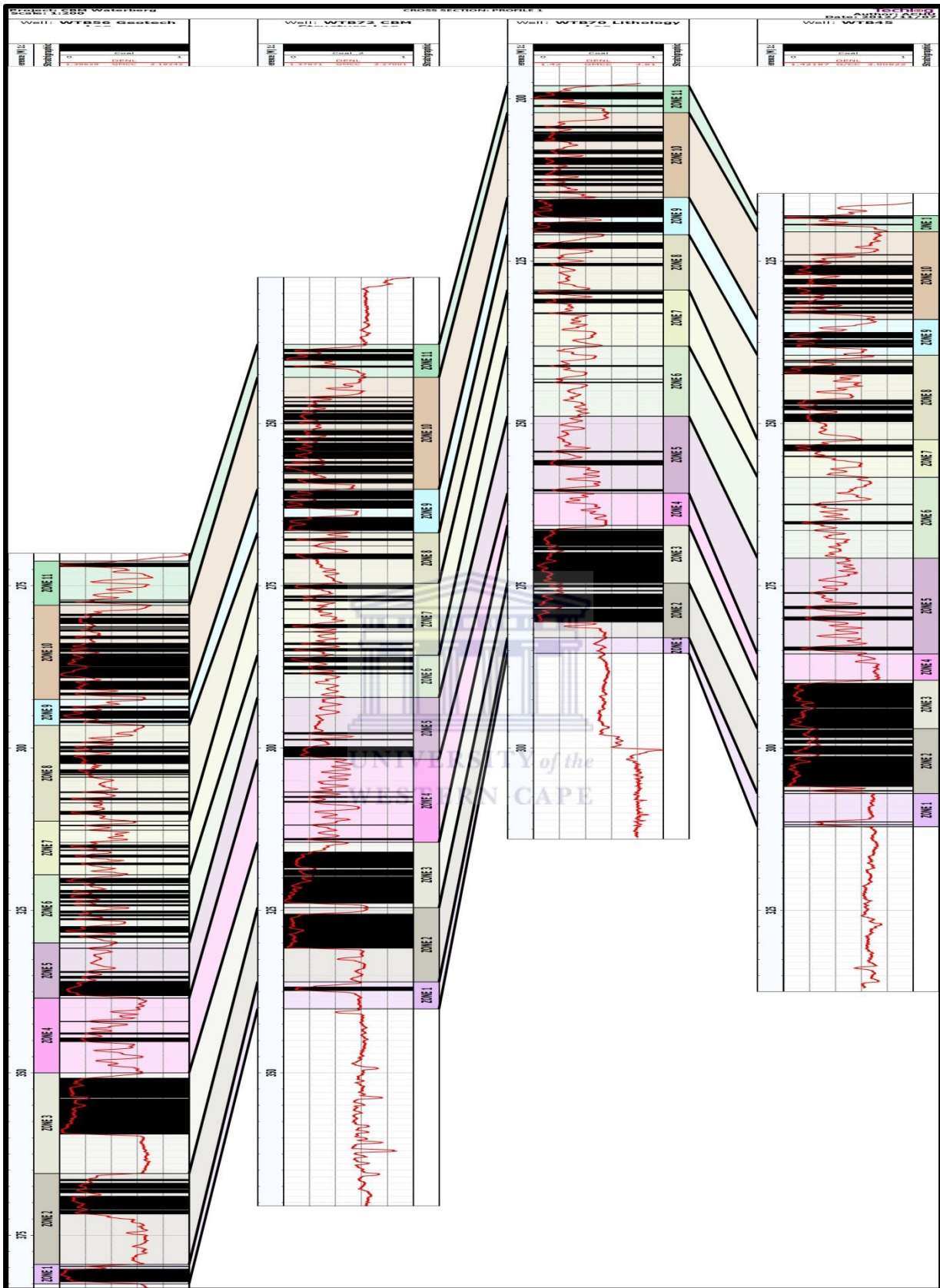


Figure 5.1: East – West cross section linking WTB56, WTB72, WTB70 and WTB45

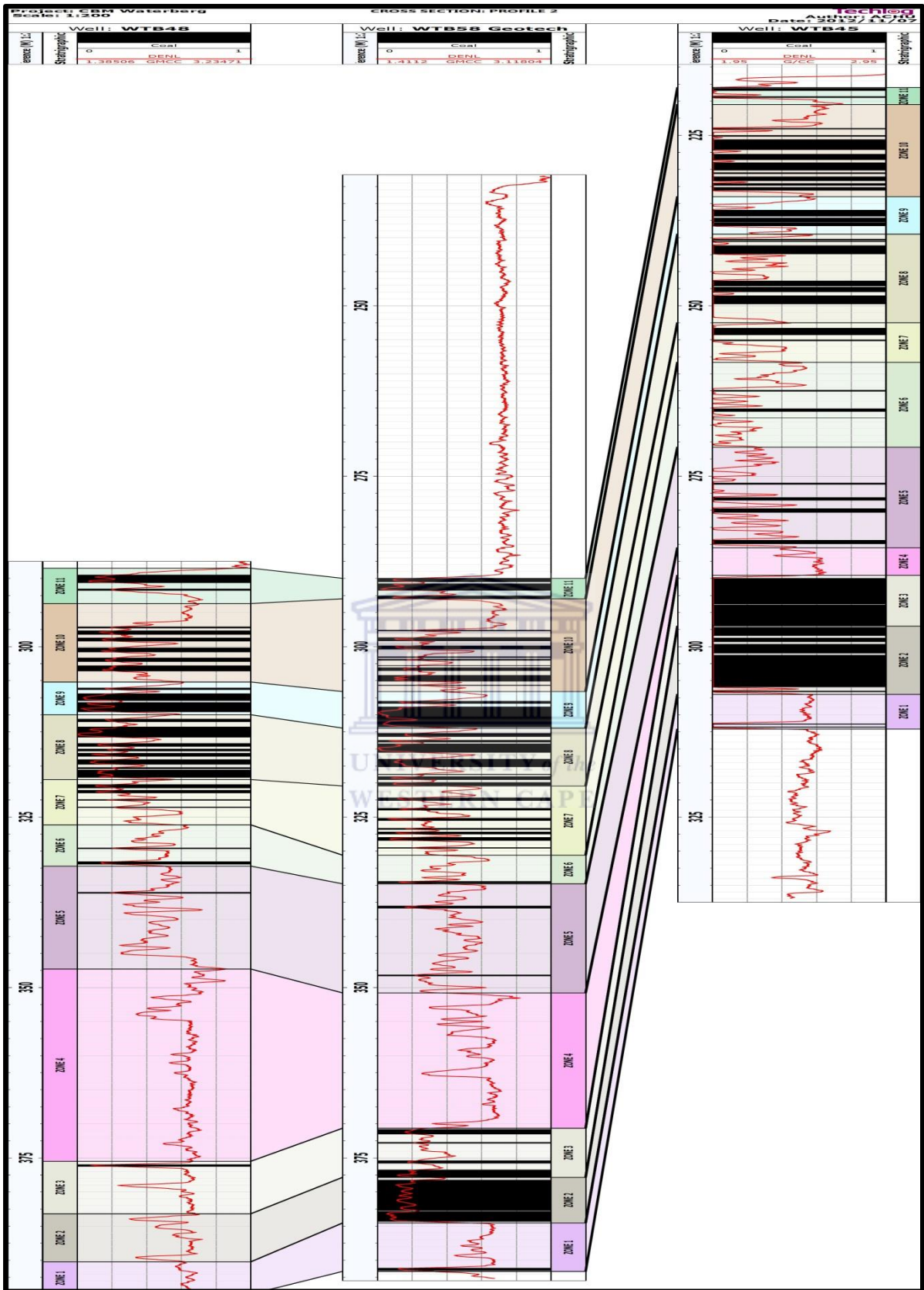


Figure 5.2: North – South cross section joining wells WTB48, WTB58 and WTB45

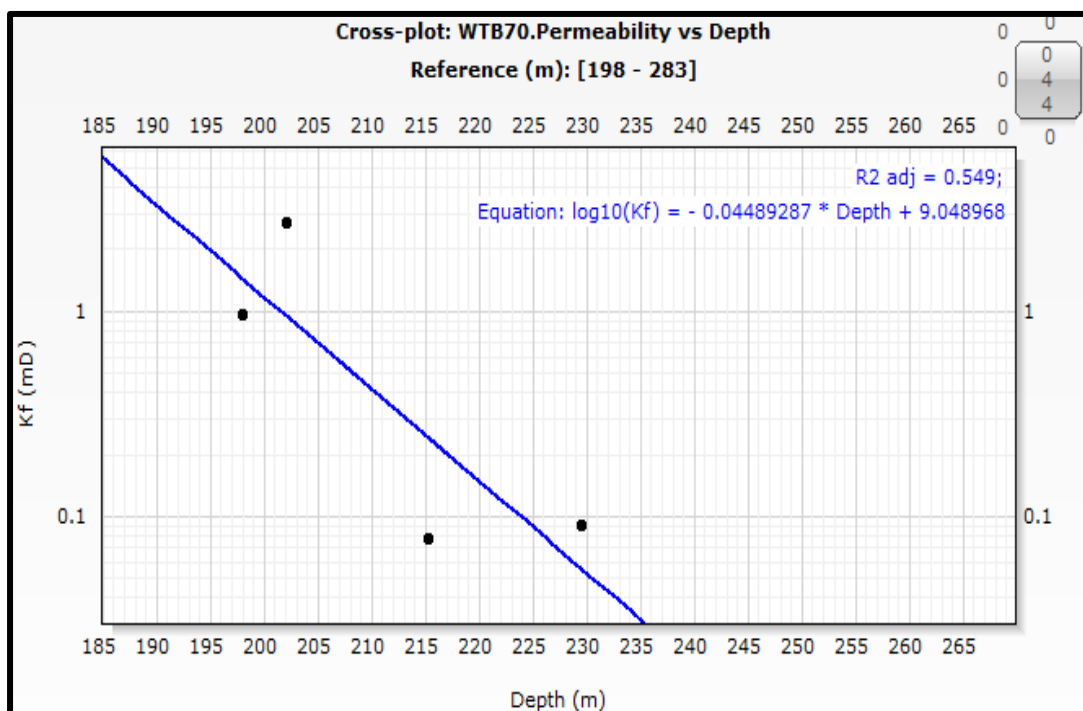
As we move westward the coal seams become shallower towards WTB 70. However WTB45 seams are found at deeper depths than WTB70. This is probably due to the down-throw movement of the rocks in WTB45 caused by Bulkop fault.

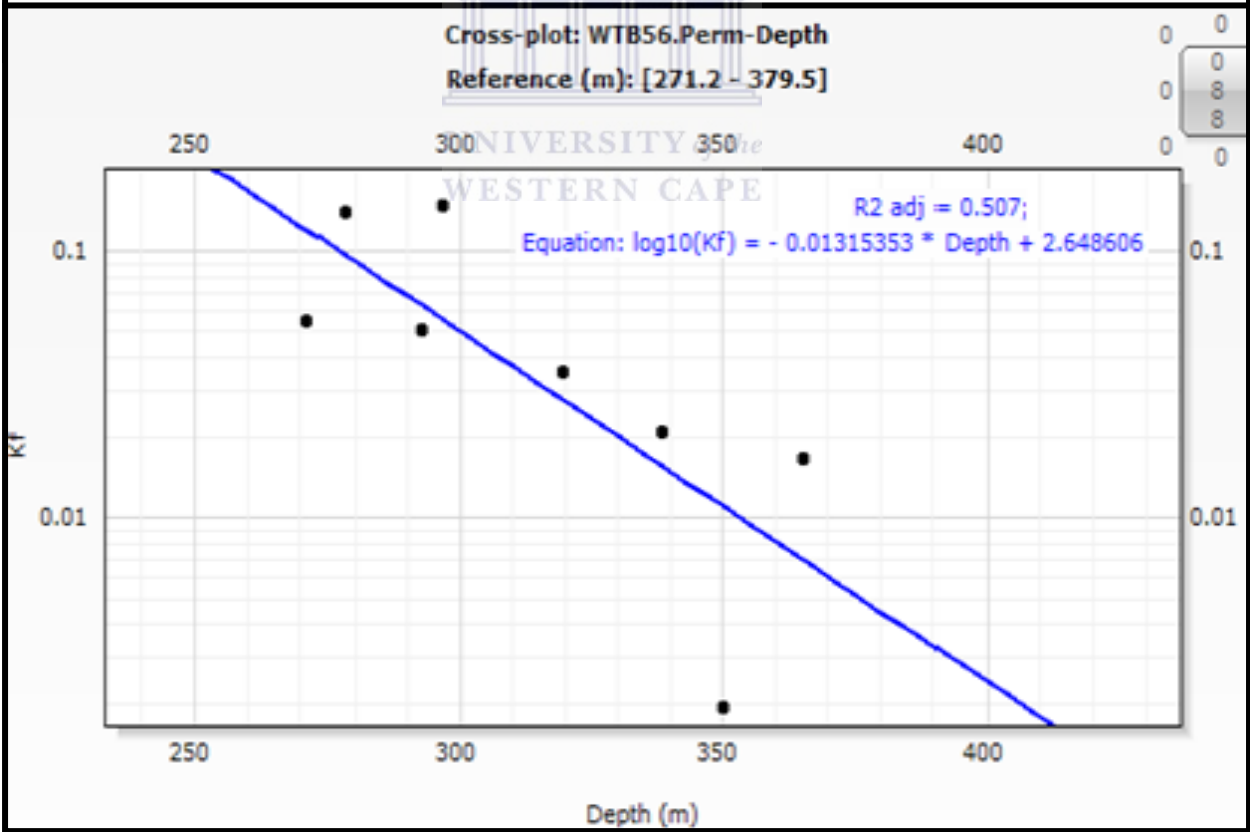
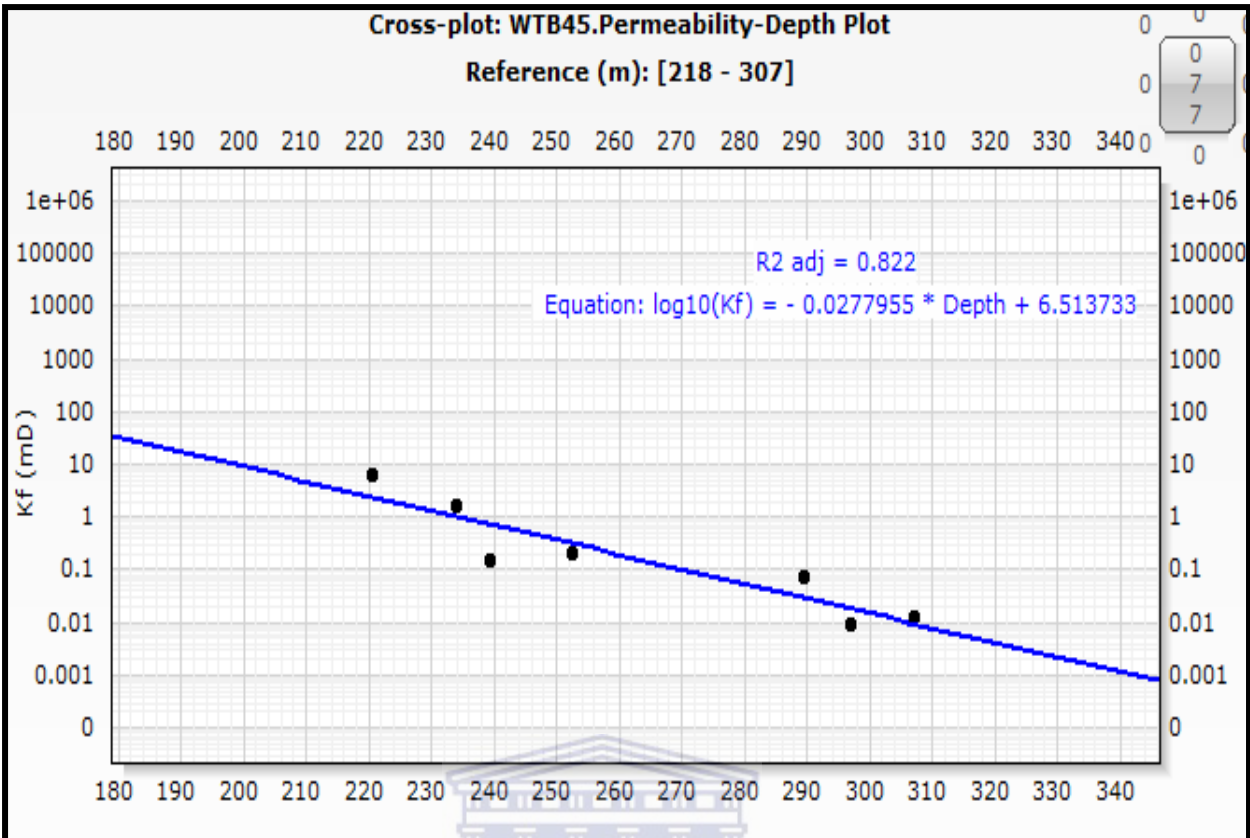
In figure 5.2, WTB48 and WTB58 were drilled in a different fault block and cut through deeper seams than in WTB45. WTB45 is separated from the other two by the western extension of the Constantia fault.

Confirming with literature distinct coal seams ranged from a few mm to more than 10m in thickness. The thickest coal seams are recorded in zone 3 for all wells. Zone 10 holds the thickest BS1 coal seams. Comparatively, the net BS1 coal thickness is approximately twice that of the net Ecca. The net thickness of the thickest coal was recorded in WTB56 (76.6m) while the shallowest net of 39.61m is recorded in WTB62.

From the study it is therefore evident that the depth of burial of the coal seams throughout the basin is controlled by the network of faults within the basin. However possible influence from bedrock geometry maybe an added control parameter. The study however does not give evidence to the varying seam thicknesses across the basin. This may be controlled by the nature of the bedrock topography as indicated in literature.

5.1.1 Depth controlled Permeability and Porosity





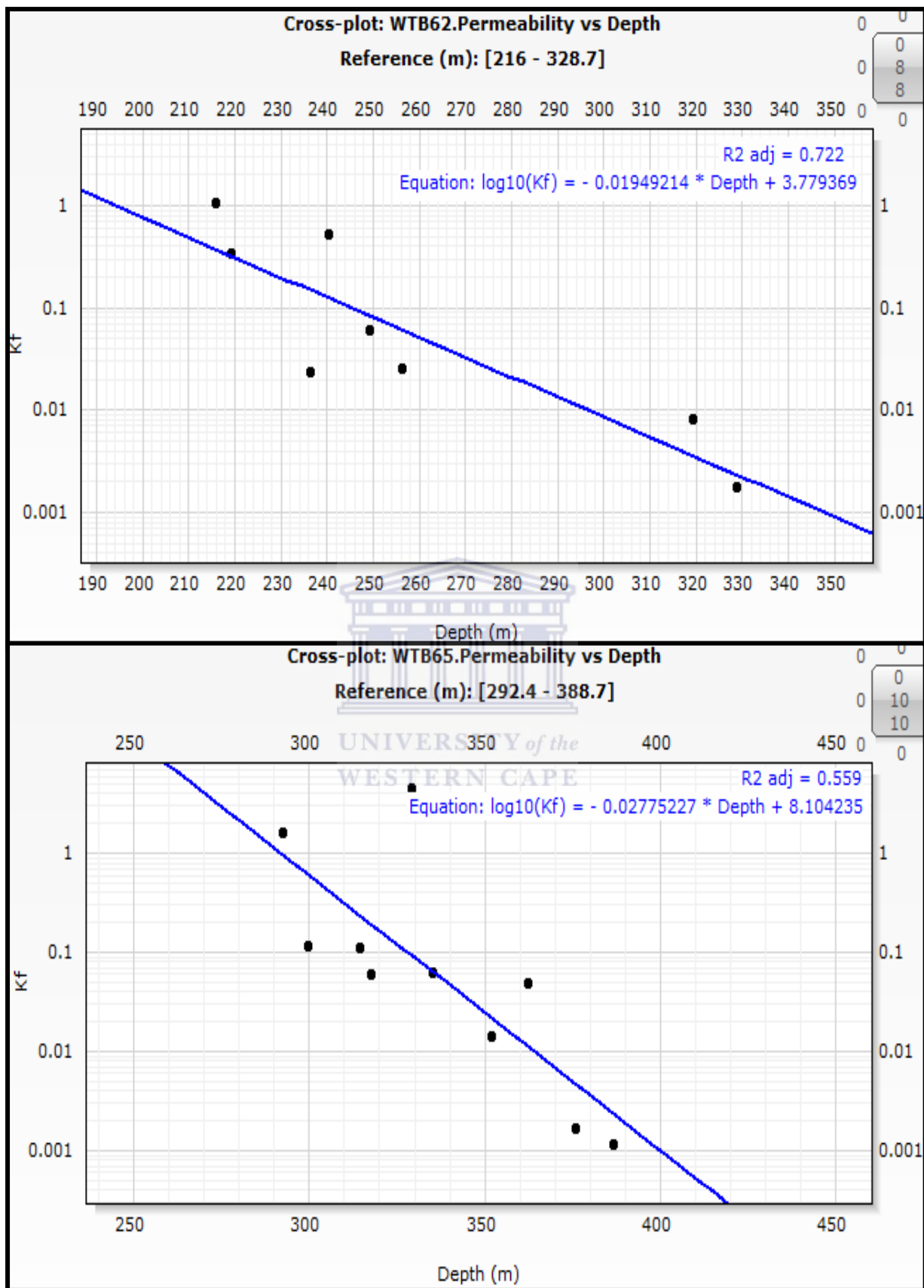
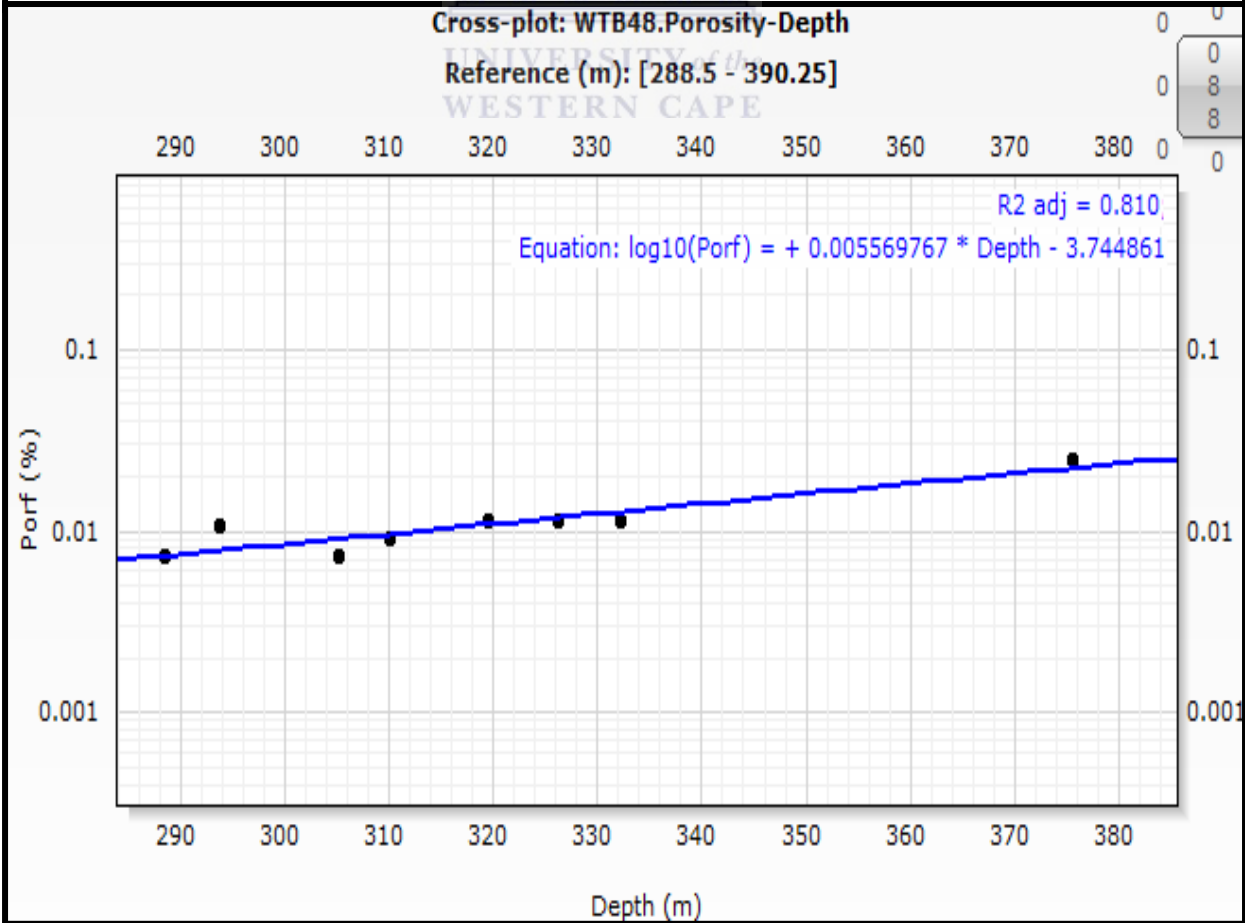
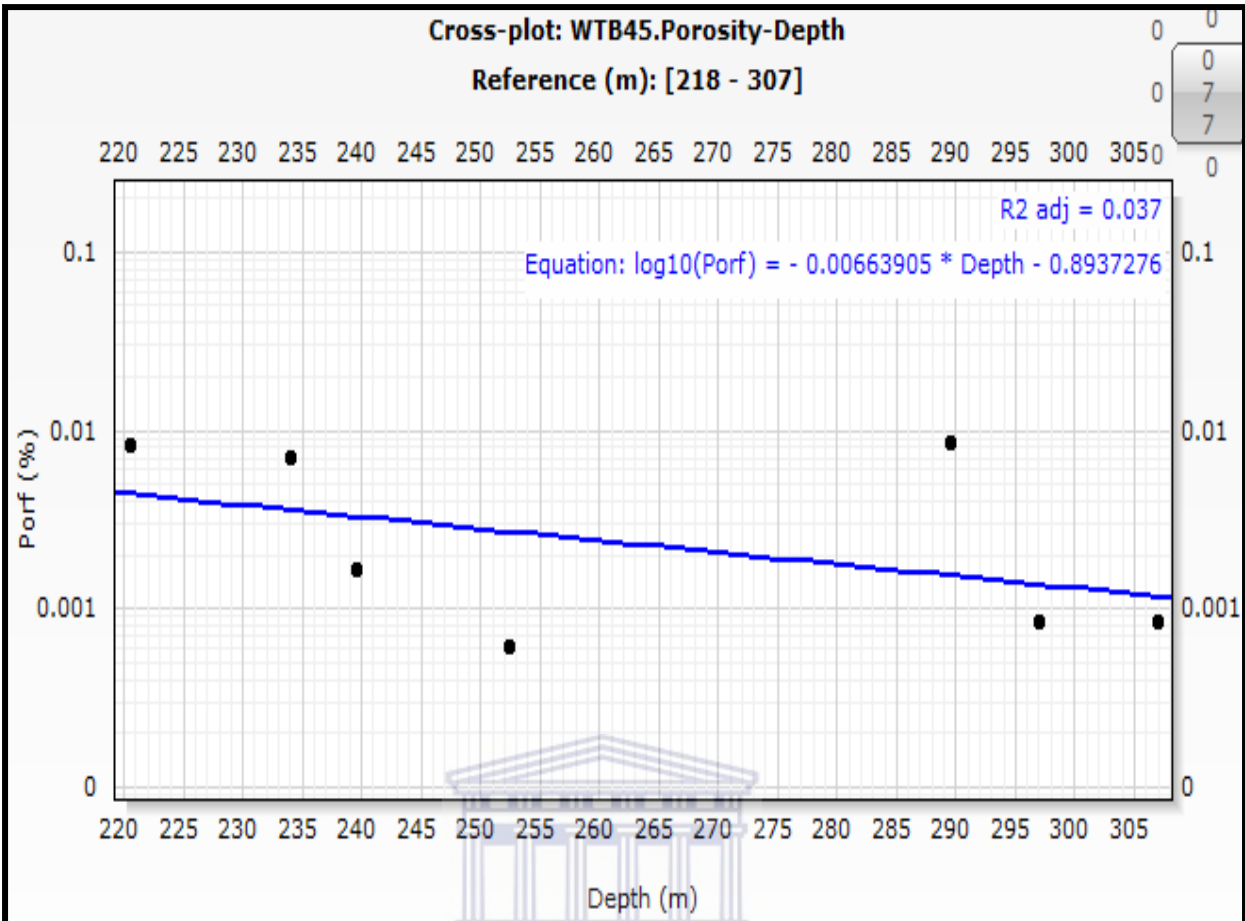
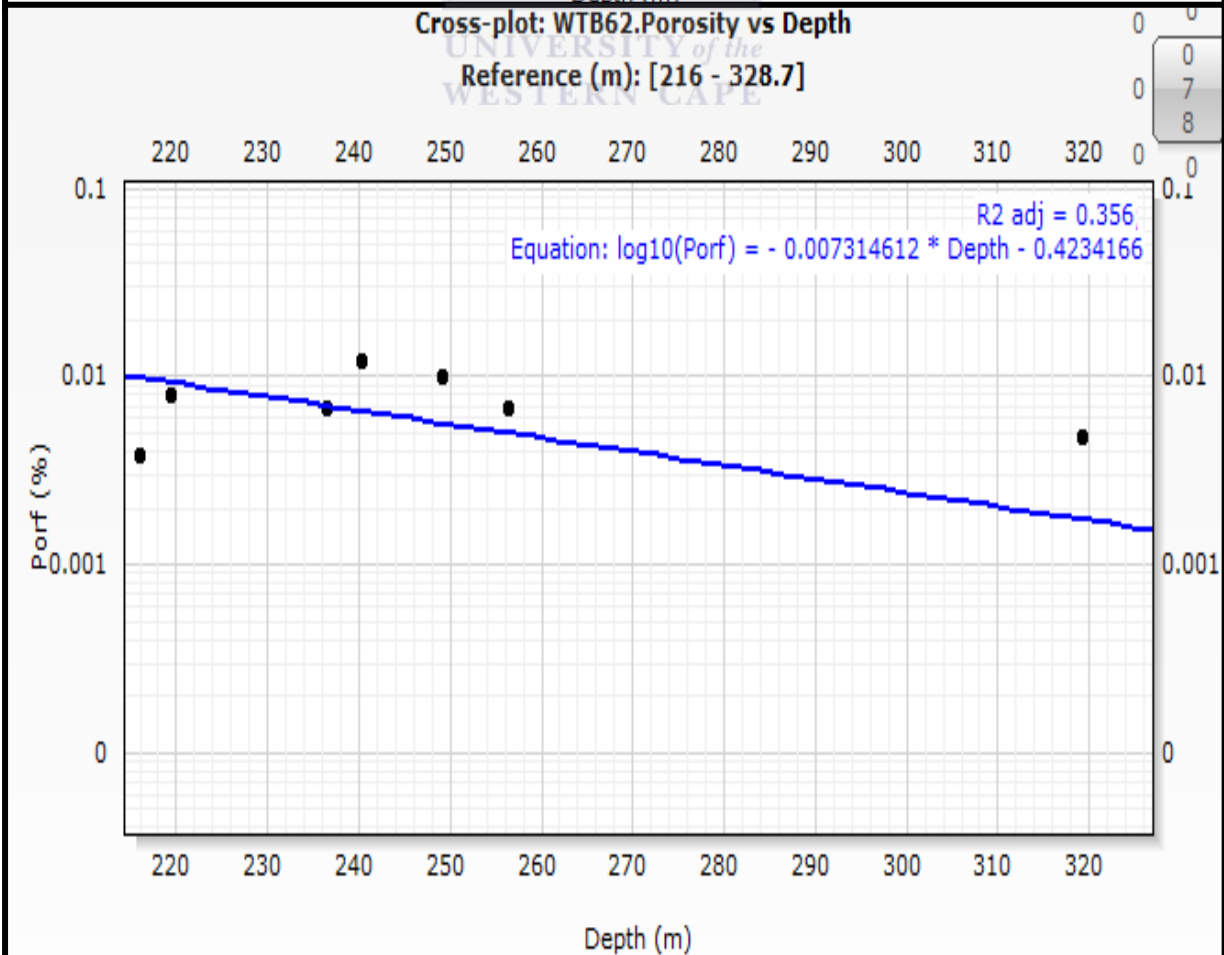
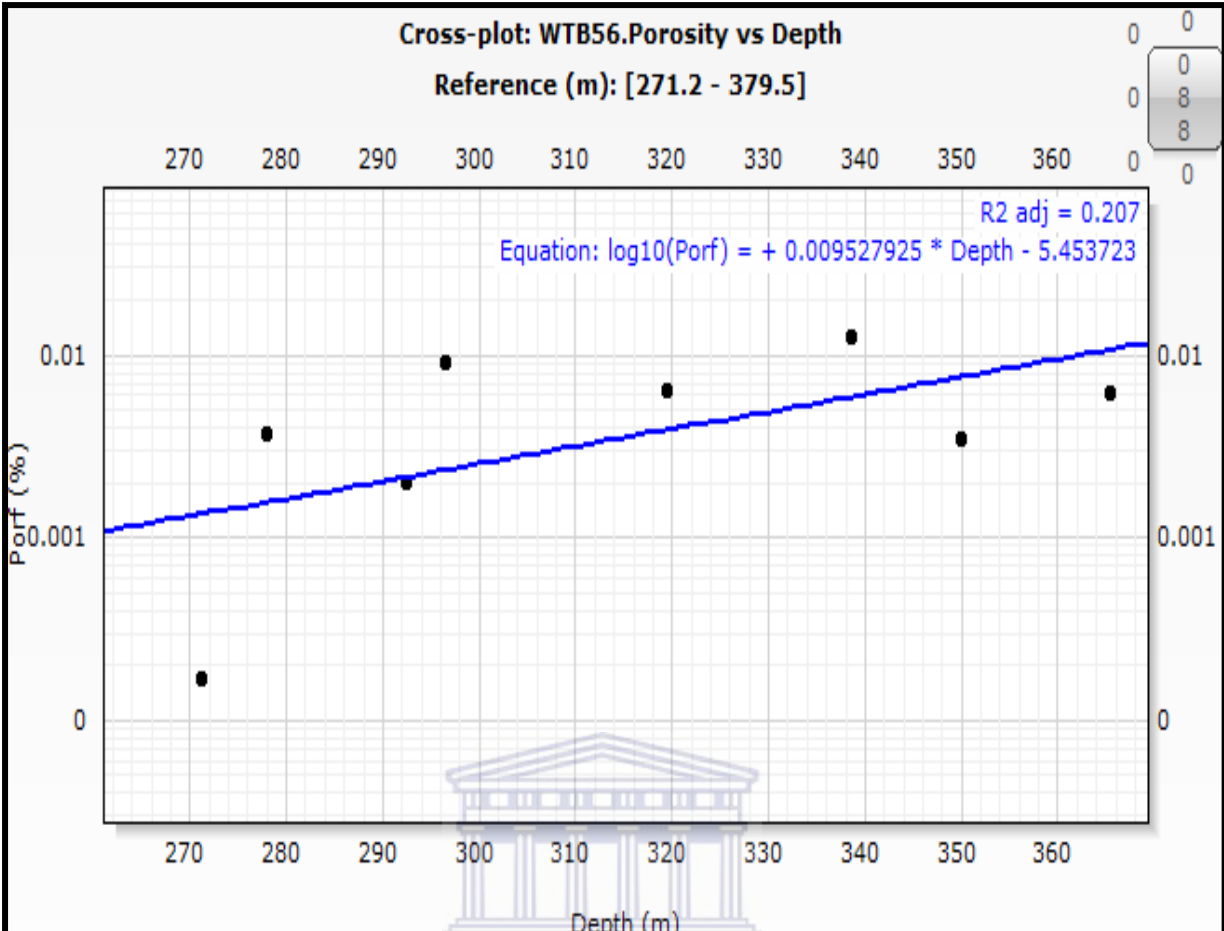


Figure 5.3: Permeability depth plots for WTB45, WTB56, WTB62, WTB65, and WTB70. Plots show negative correlation with depth.





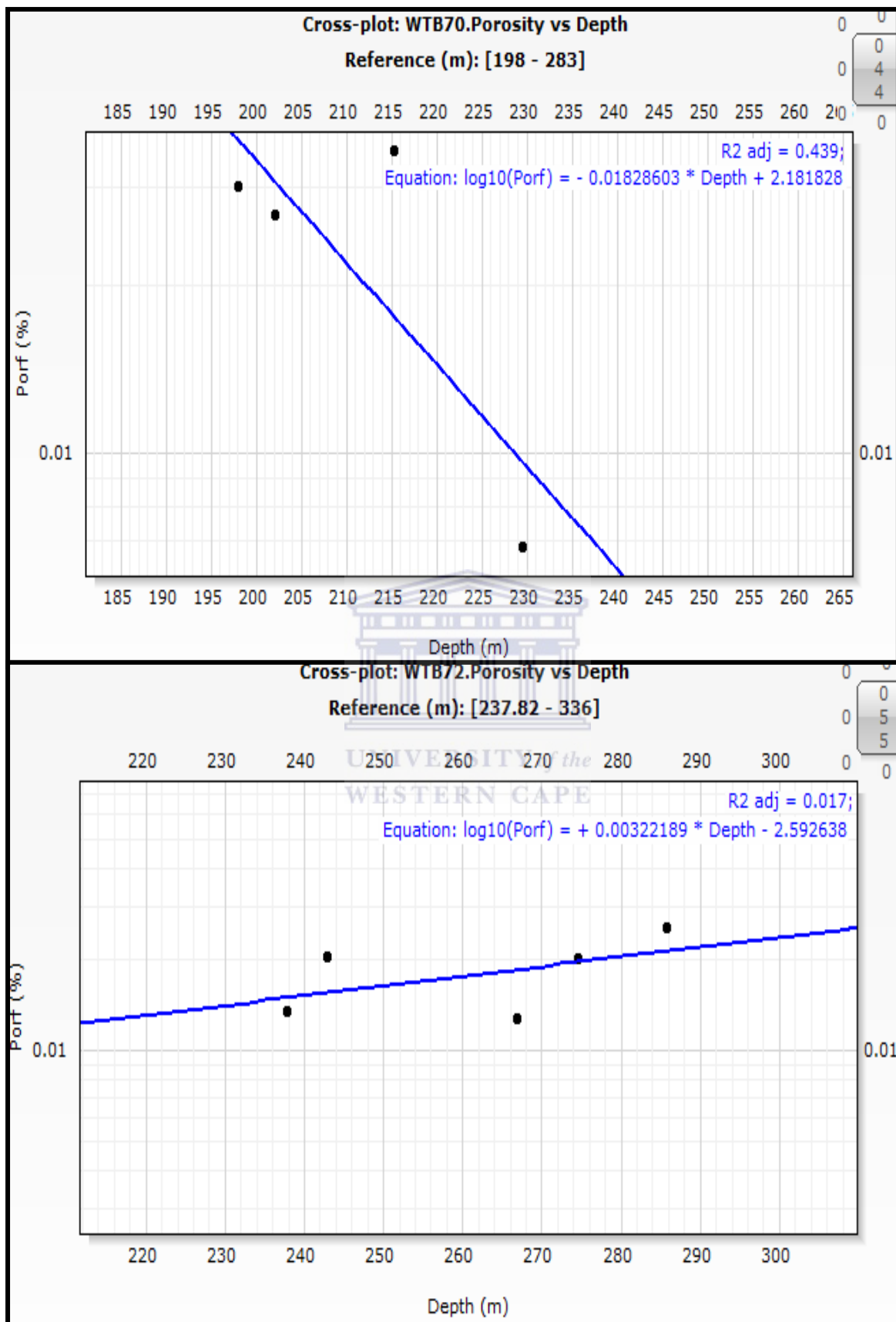


Figure 5.4: Porosity depth plot for WTB45, WTB48, WTB56, WTB62, WTB70, and WTB72.

The permeability vs depth plots are shown in Figure 5.3. According to these plots a strong correlation exists between permeability and depth. The plots (Figure 5.3) show a general decrease in permeability with increasing depth. This may result from an increase in crustal stress which aids in the closing up of fractures and thereby reducing the reservoir flow characteristics. However WTB48 and WTB72 show a gradual increase in permeability with increasing depths (Appendix 6). This behaviour is not unexpected in coal reservoirs as their heterogeneous nature makes them to have unsteady reservoir attitude. Coal fractures are less developed at shallow depths due to matrix stickiness from elastic organic material. As the organic material begins to break down, releasing some of the gas, coupled with overburden stress fractures turn to develop. In such situations we expect an increase in permeability with depth.

On the other hand injection falloff data indicates an overall decrease in permeability for the composite zones (upper, middle and basal BS1 coals) vs depth for WTB45 and WTB72. This data however does not represent the entire well since permeability tests were not run for zones 1 to 3. The data is consequently insufficient to draw reliable conclusions or to compare trends with Log data. Moreover, injection falloff tests were conducted for composite zones which included inter-layered mudstones whose properties were not taken into account when running the test.

On a basin scale log estimated permeability generally increases slightly from east to west. Permeability values show a marked increase when approaching faulted zones as could be seen in WTB45. Tectonic activities in some way may be a controlling factor. The general increase in permeability westward could be explained by the influence of magmatic bodies bounding the basin to the west. This may cause an increase in coal rank from magma heating resulting in increased fracture development.

The porosity depth plots for (figure 5.4) WTB45, WTB62 and WTB70 show a decrease in fracture porosity with depth while that for WTB48, WTB56 and WTB72 (figure 5.4) show increasing fracture porosity with depth. WTB65 (appendix 7) shows no distinct trend with porosity remaining almost the same across all depths.

The coal seams (i.e. between depths of 180m to 260m) of WTB45, WTB62 and WTB70 are located at shallower depths and show decreasing porosity with depth. At shallow depths;

progressing growing deeper newly created fractures easily close up due to increase gas generation and overburden pressure. The coal seams of the deeper wells (i.e. depths from 260 to 380) of WTB48, WTB56 and WTB72 display increasing fracture porosity with depths. Fractures are more developed in higher ranked coals than lower ranked coals. The porosity depth plot for WTB65 shows constant permeability with increasing depth (appendix 7). So we expect to have higher porosity with increasing depth. It is consequently evident that multiple factors contribute to porosity variation in coal. Inclusive are burial depth, organic content, gas generation and pressure variations.

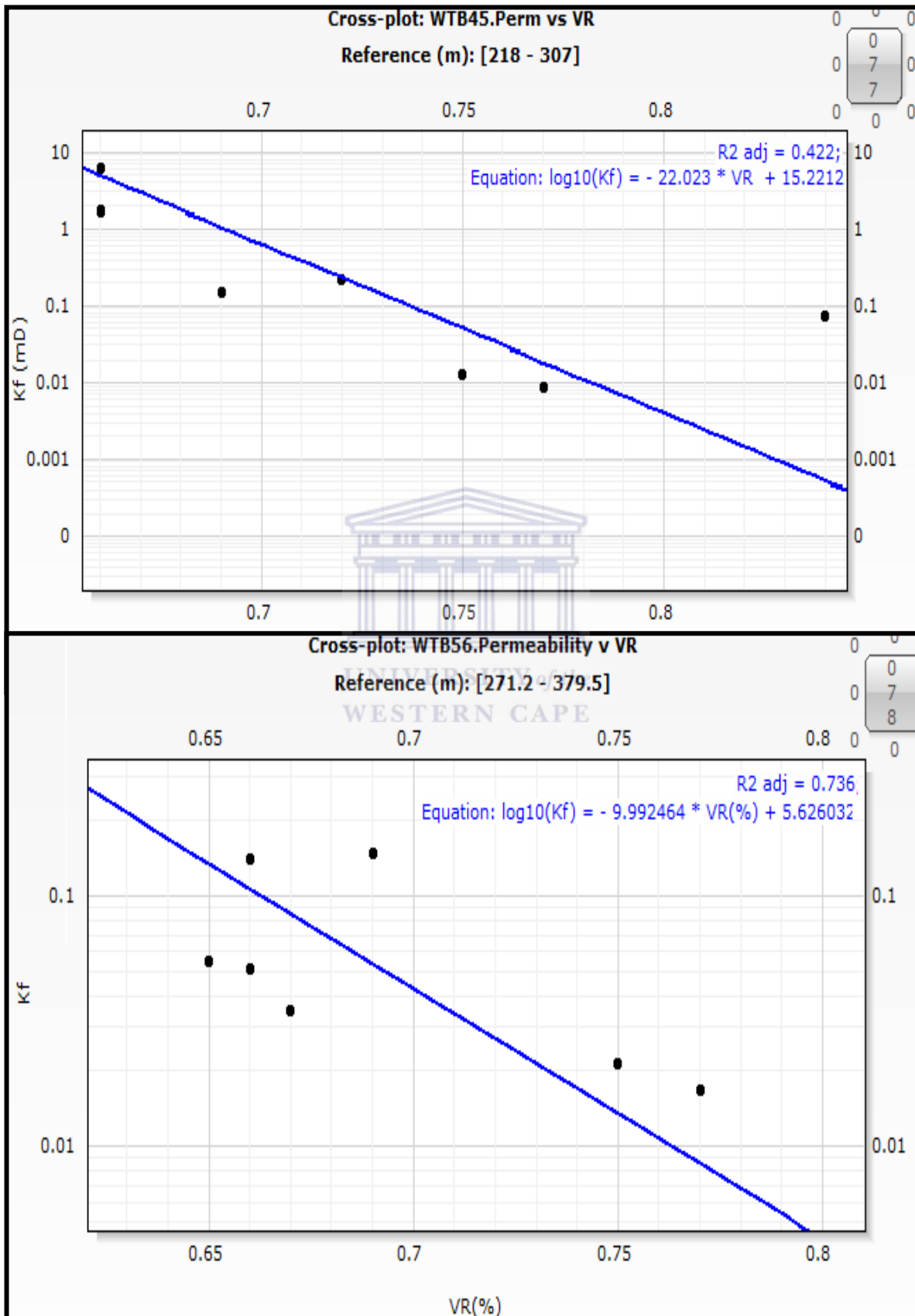
5.2 Maceral Content and Vitrinite reflectance controlled Permeability

The plots of vitrinite content, liptinite content, inertinite content and vitrinite reflectance vs depth (zones) are displayed in appendix 8. All three plots but for liptinite show very strong correlation with depths. While the vitrinite content decrease with depth the inertinite content increases with depth. Liptinite concentrations remain fairly stable. The environment of deposition of the different coal seams would explain the variation in organic material type. As expected the vitrinite content is higher in BS1 than Ecca seams while inertinite content is higher in Ecca seams than BS1. The vitrinite reflectance also increases with depth. This is due to increase maturity of the coals from burial geothermal influence.

Figure 5.5 displays permeability vs vitrinite reflectance (VR) cross plots for WTB45, WTB56, WTB62, WTB65, and WTB70. The plots display a decrease in permeability with a corresponding increase in vitrinite reflectance. Increased coal maturity or coalification is caused by increase in temperature. The change in temperature accompanying sediment burial is a prime cause of organic matter transformation. VR thus reflects the temperatures through which sediments have gone through and their depths of burial. As seen earlier cleats are most developed in low volatile bituminous coals (M2M, 2008).

However Lavine (1999) suggested that as the coal matures from low volatile bituminous to higher ranks, crosslinking under low pressures and high temperature may cause cleats to close up. This may be same for these coals. The difference is that average maximum recorded vitrinite reflectance for these coals are 0.84% (Appendix 2) placing the coal as bituminous coals. However the volatile content for these coals ranges from 39% in the shallower zones to 17% in the deeper zones which probably may stand as an explanation for

the variations of permeability. The plots for WTB48 and WTB72 (appendix 9) show no define pattern.



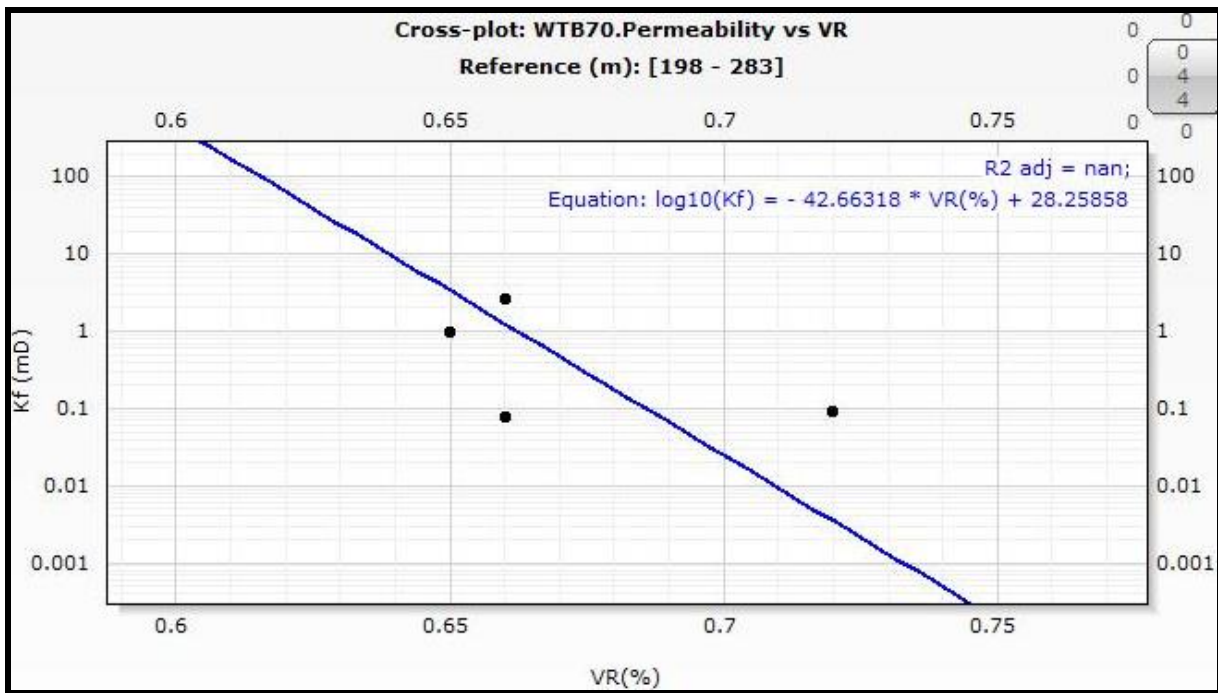
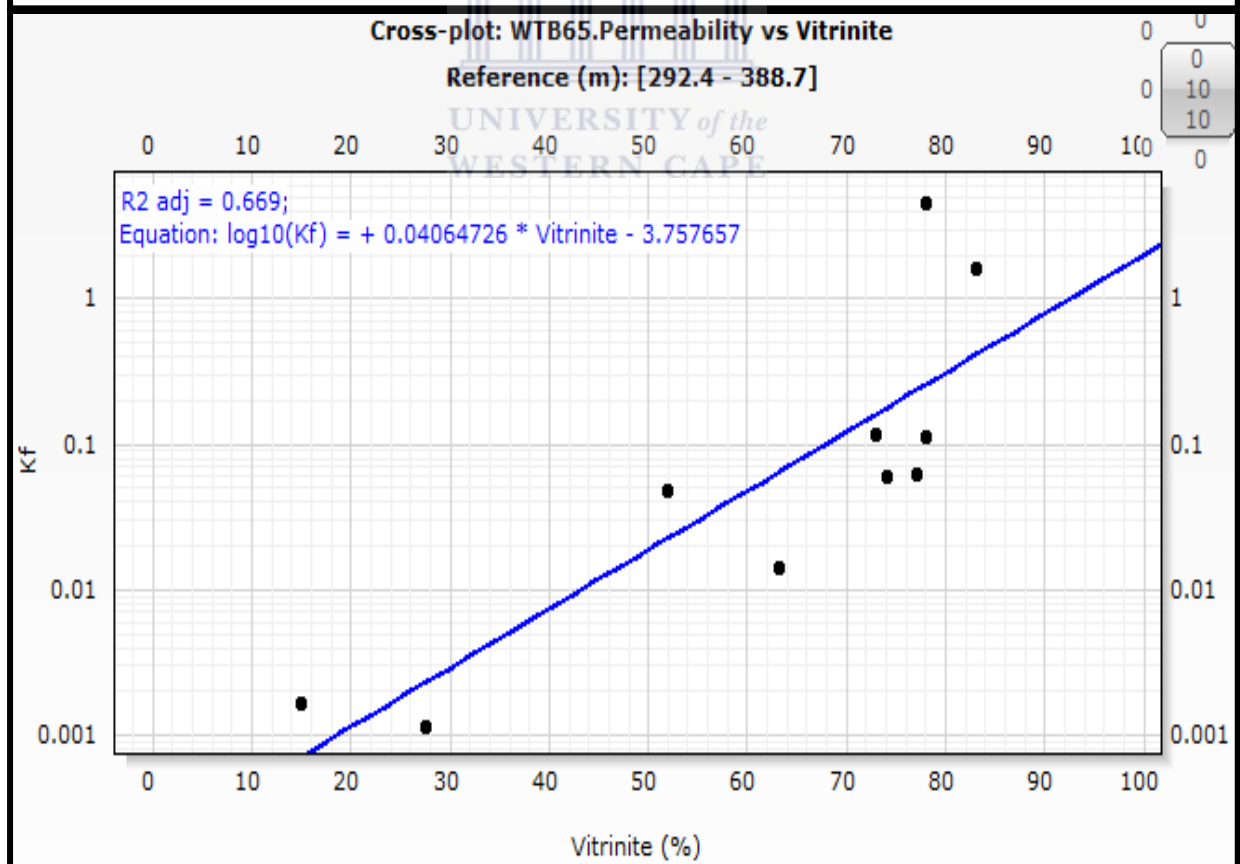
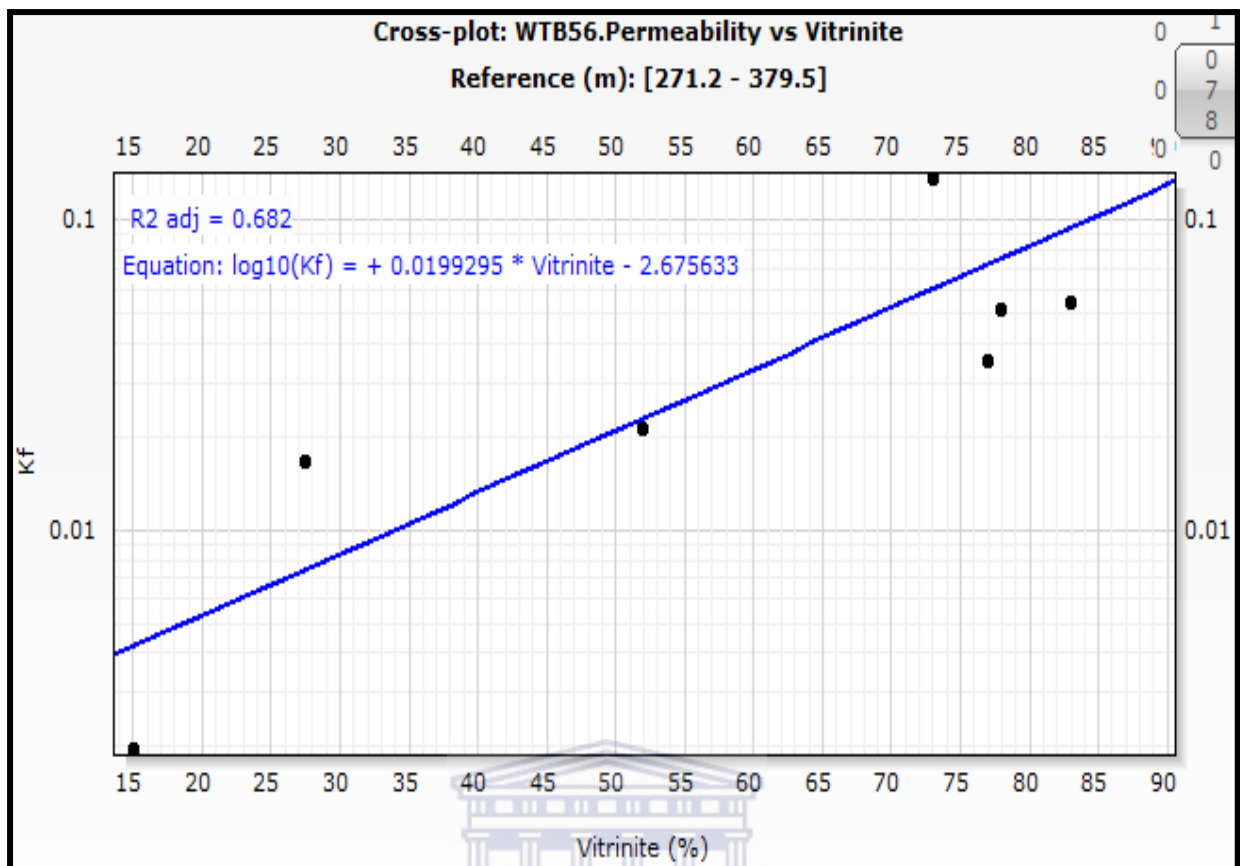


Figure 5.5: Permeability vs Vitrinite Reflectance cross plots for WTB45, WTB56, WTB62, WTB65 and WTB70.

Patterson et al. (1992) stated that vitrinite rich coals show best cleat development. As such the vitrinite content vs permeability cross plots in figure 5.6 displays increasing trends of permeability with vitrinite content while decreasing trends are displayed by the permeability and inertinite cross plots in figure 5.7.

Vitrinite is derived from woody plants. This maceral type produces a lot of gas when organic material is geothermally broken down. The breakdown of vitrinite releasing gas aids in releasing the inelastic properties of coal making it possible to fracture. Inertinite coals are formed from same maceral types like vitrinite coals but have been previously oxidized. Consequently coalification process alters inertinite coals very little. Irregular plots could be observed for permeability vs vitrinite content cross plots for WTB48, WTB70 and 72 (appendix 10) as well as for permeability inertinite cross plots for WTB48, WTB62, WTB70 and WTB72 (appendix 11).



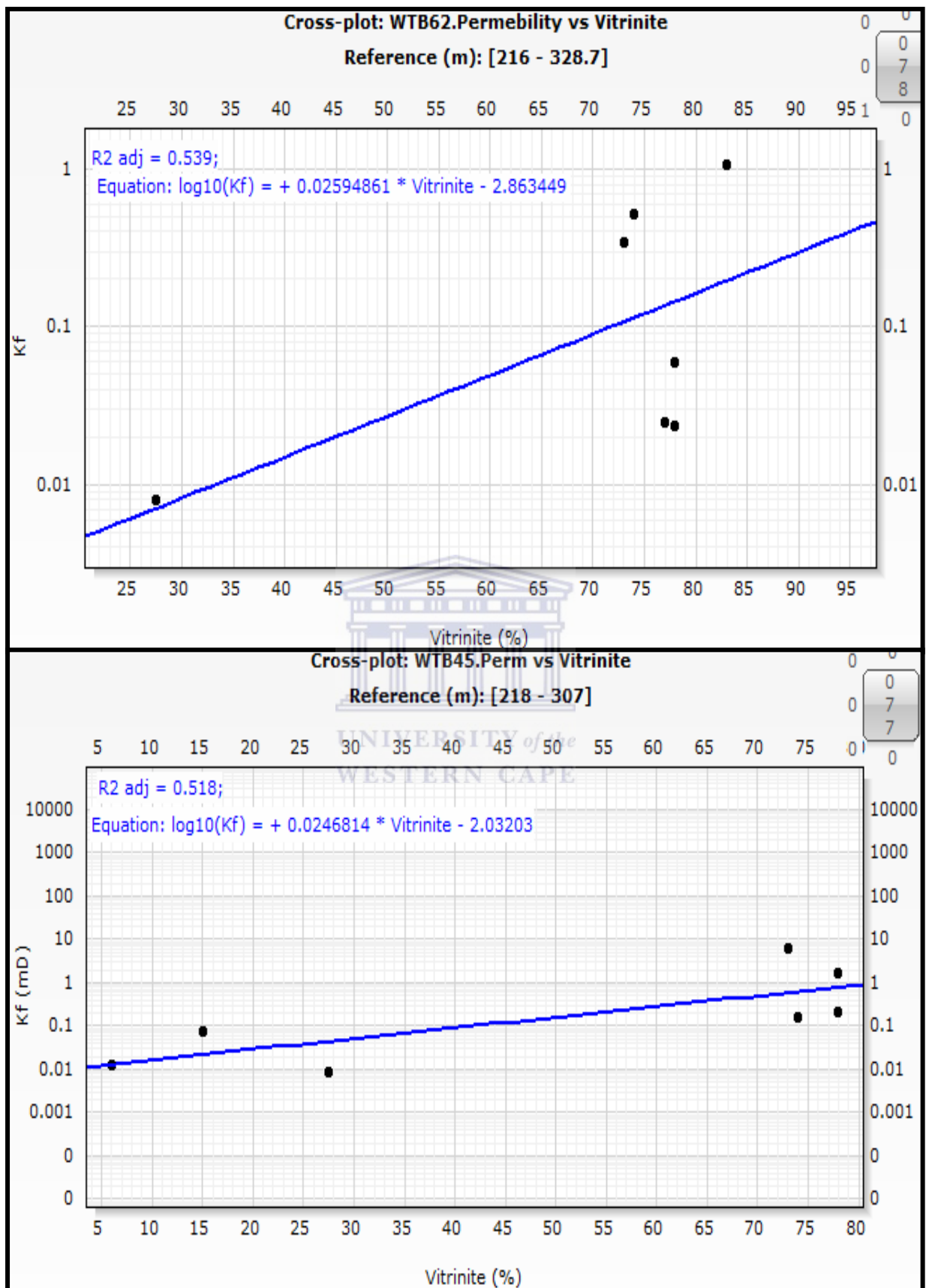
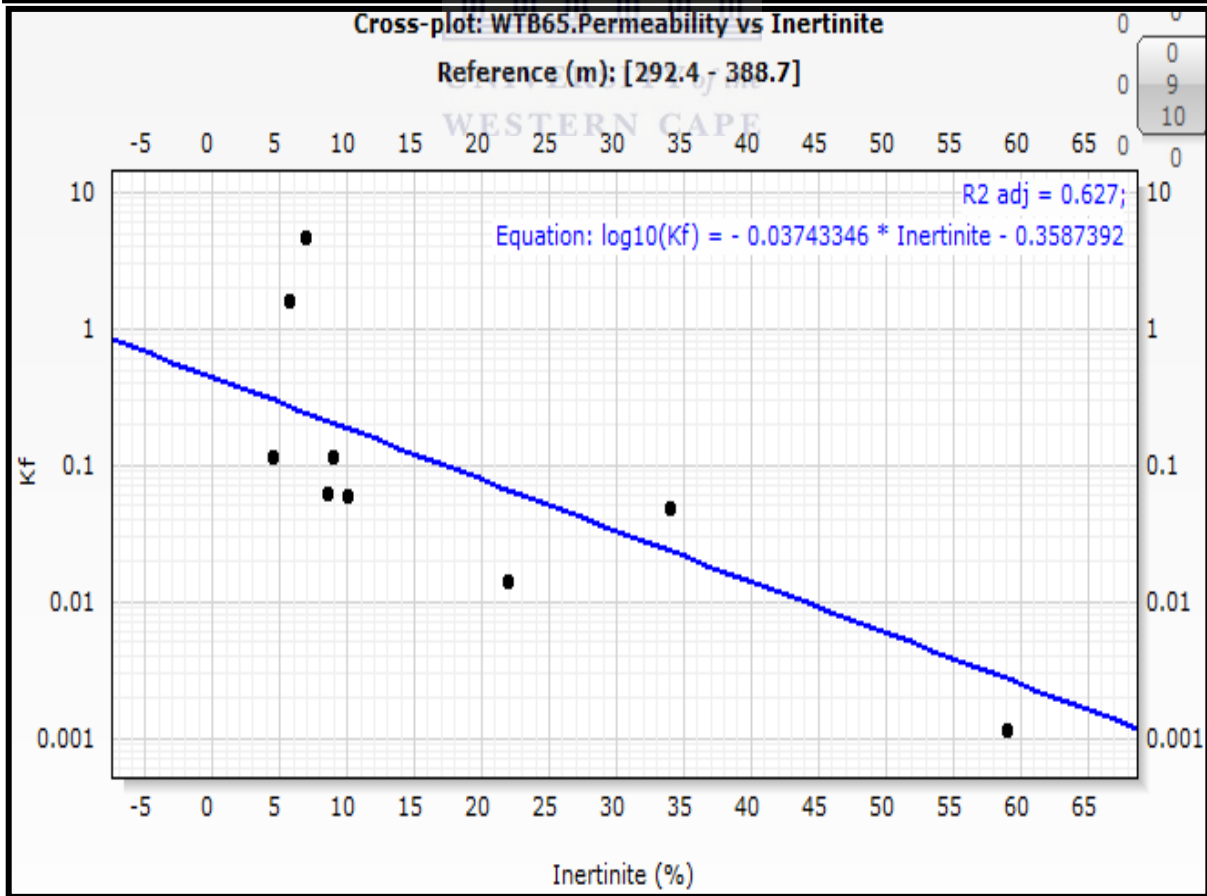
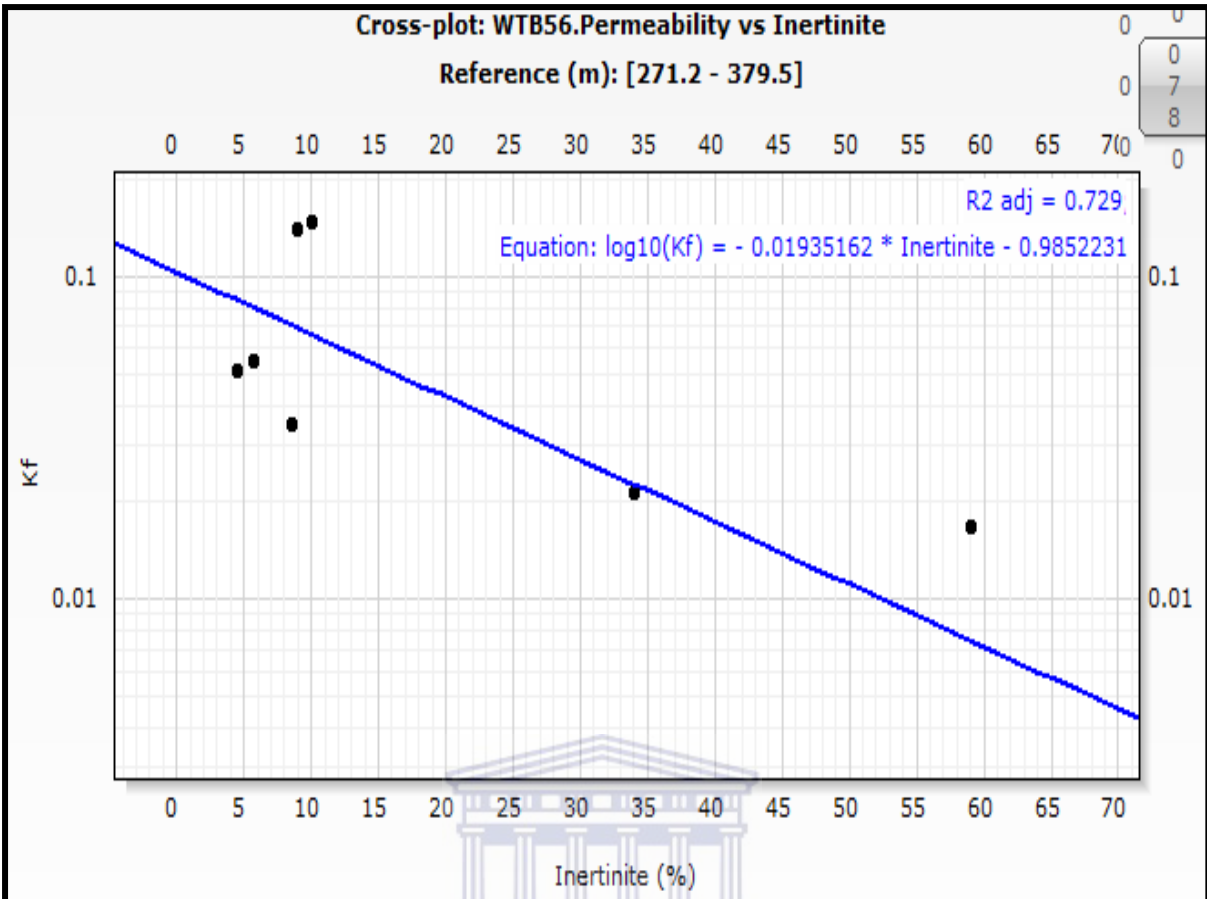


Figure 5.6: Permeability vs vitrinite content cross plots WTB45, WTB62, WTB56 and WTB65. Plots show positive correlation.



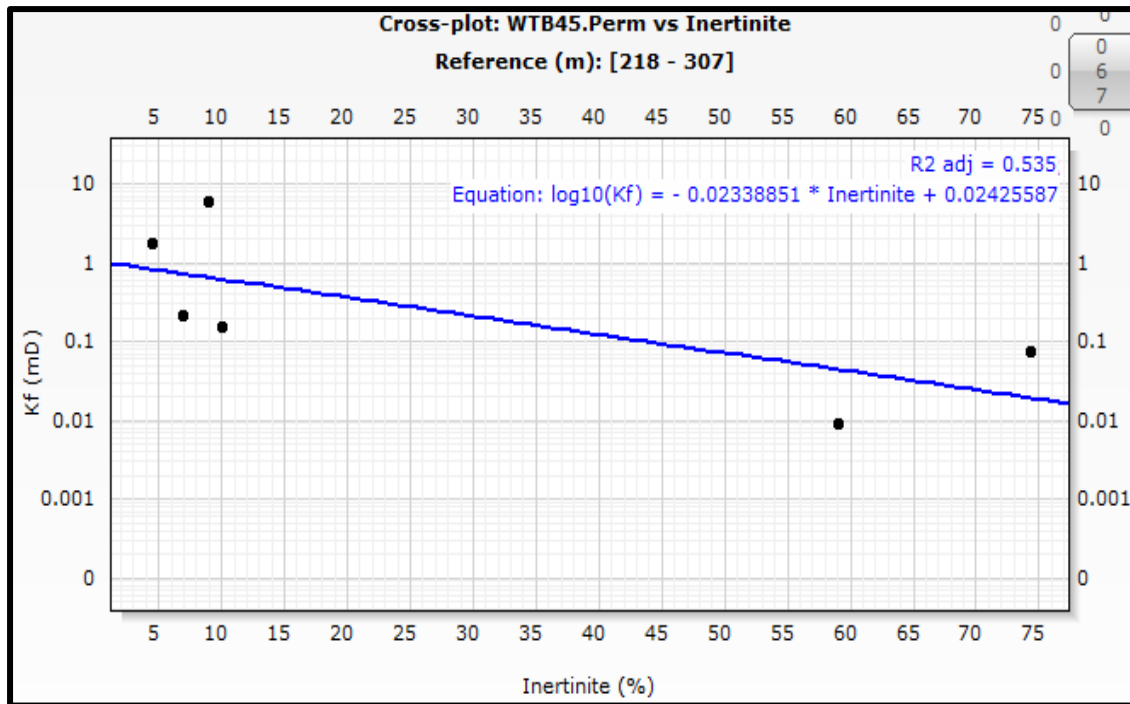


Figure 5.7: Permeability vs Inertinite content cross plots for WTB45, WT56 and WTB65. Plots show negative correlation for these wells.

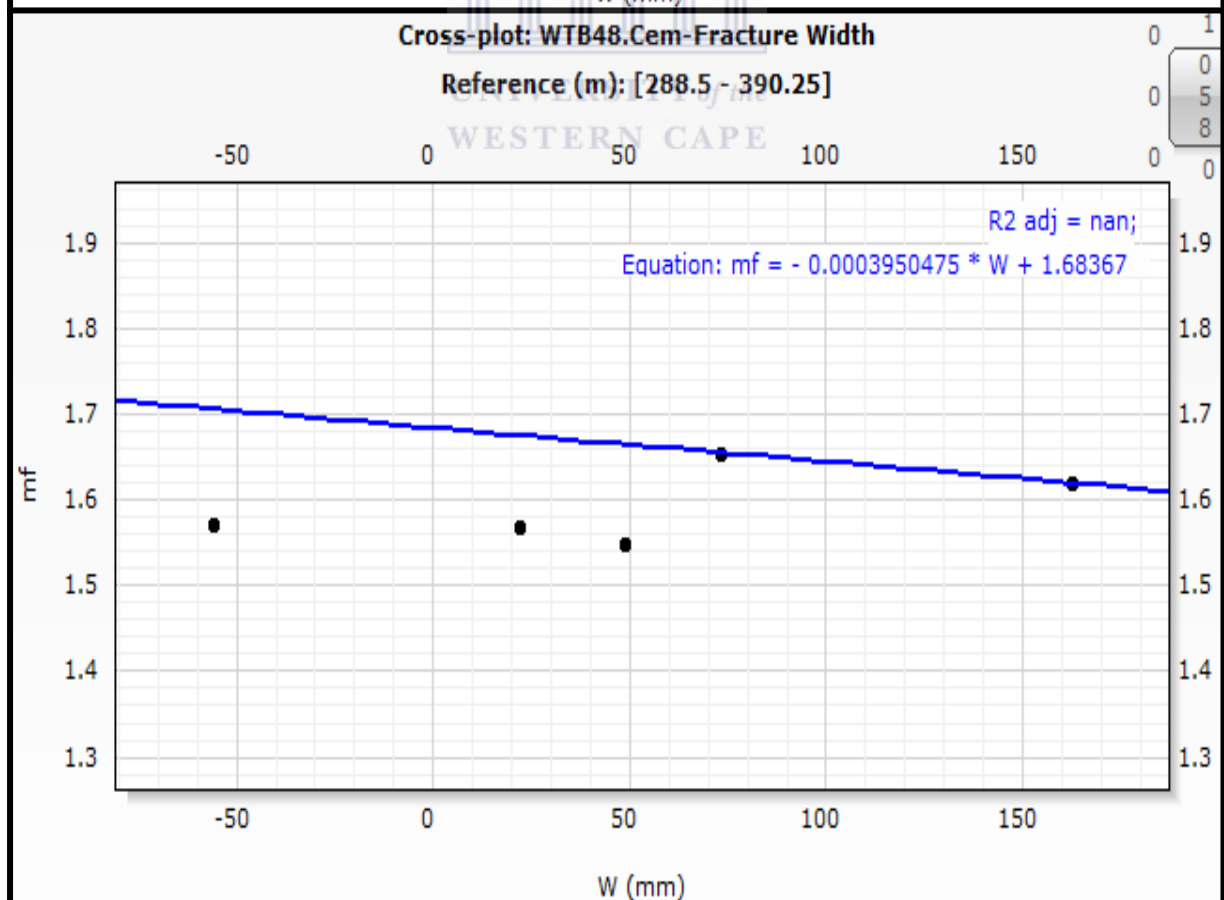
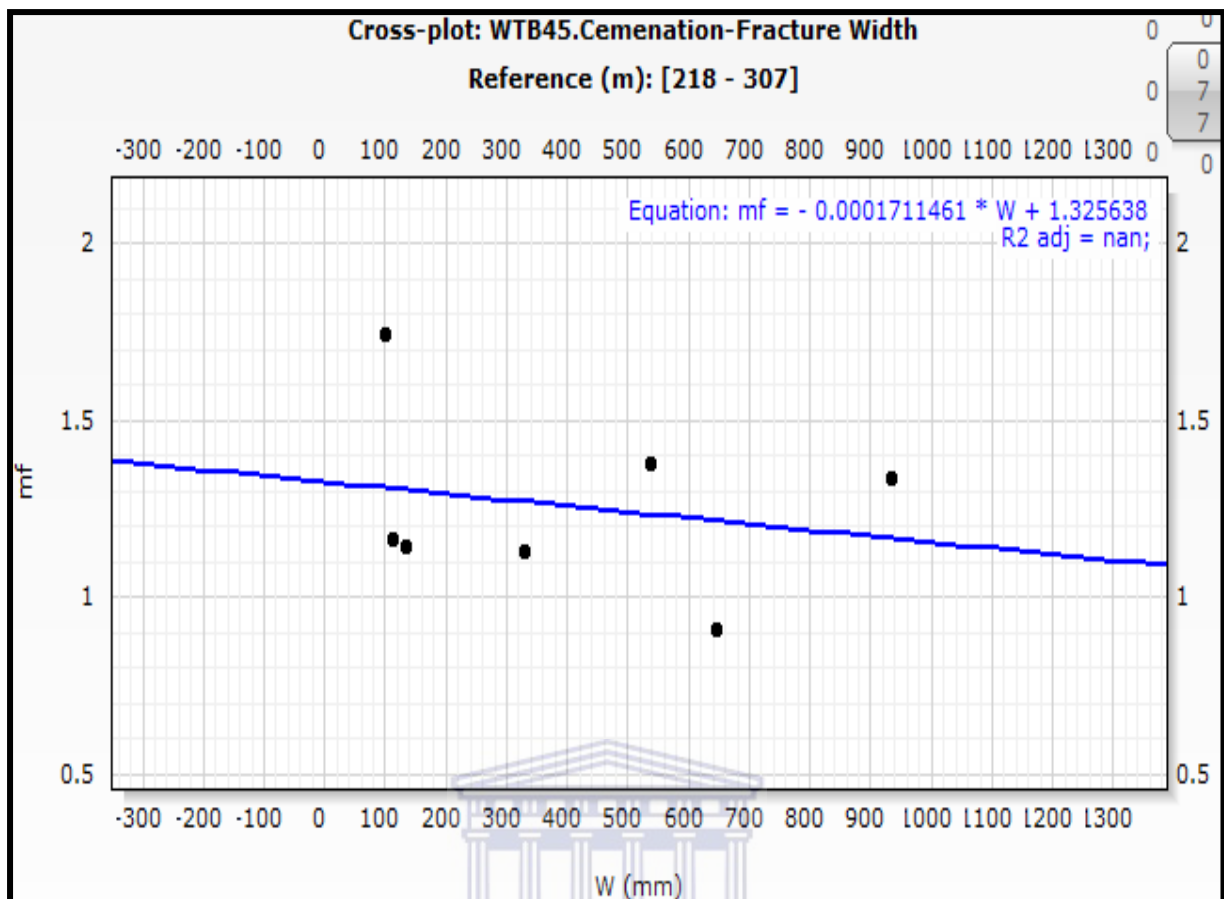
5.3 Reservoir Porosity and permeability - Fracture width and Cementation Variation

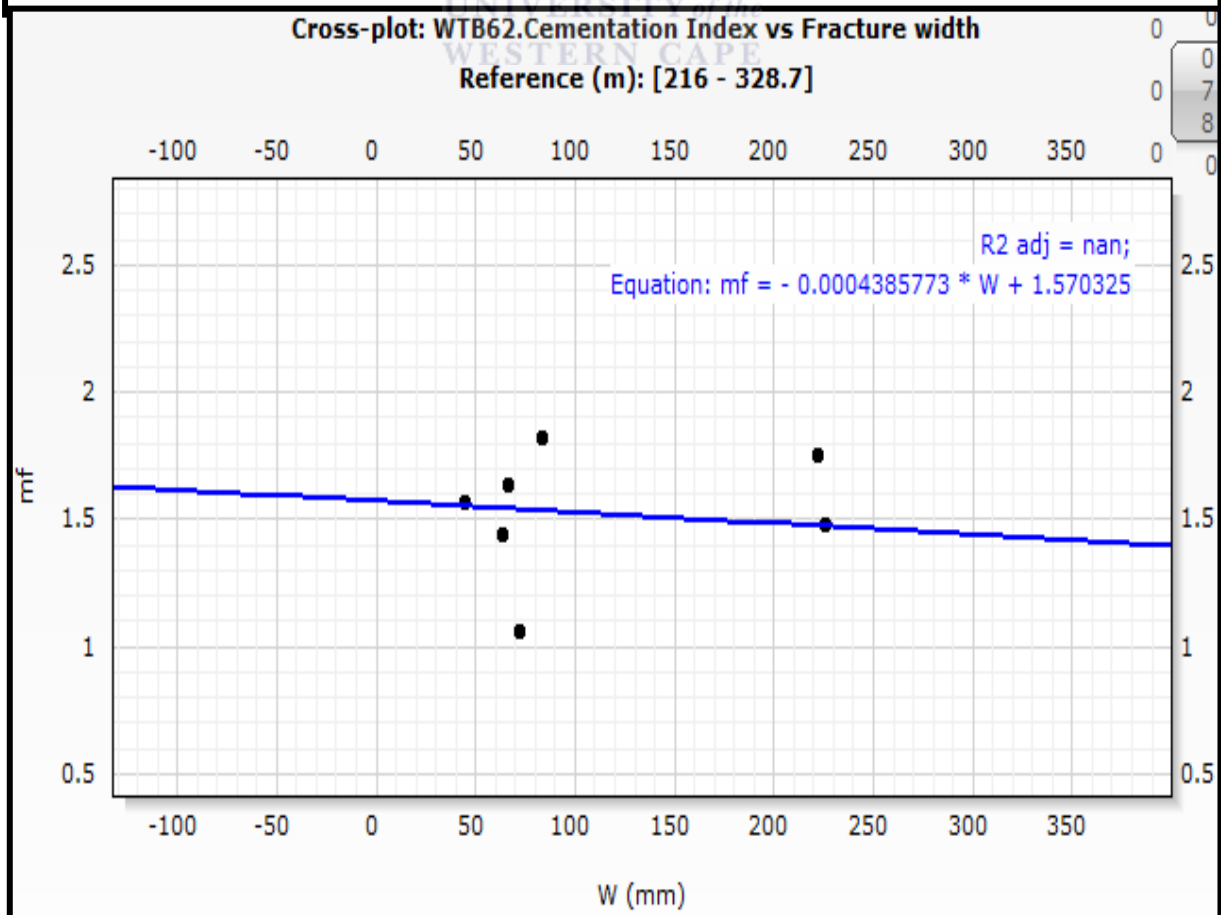
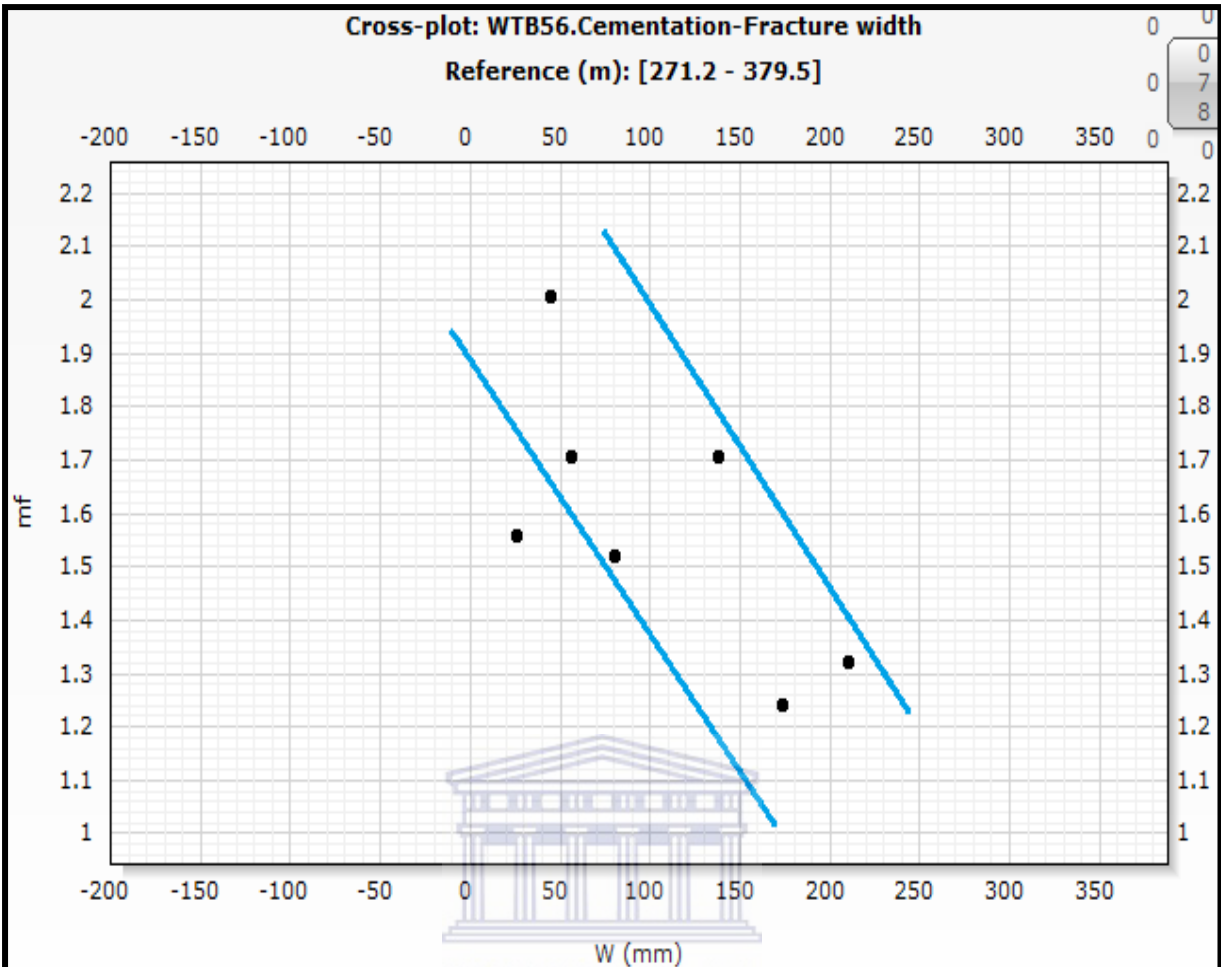
With finding based on the model used, coal reservoir permeability and porosity are influenced by the fracture width and to a degree the fracture network is mirrored by the cementation index of the coals.

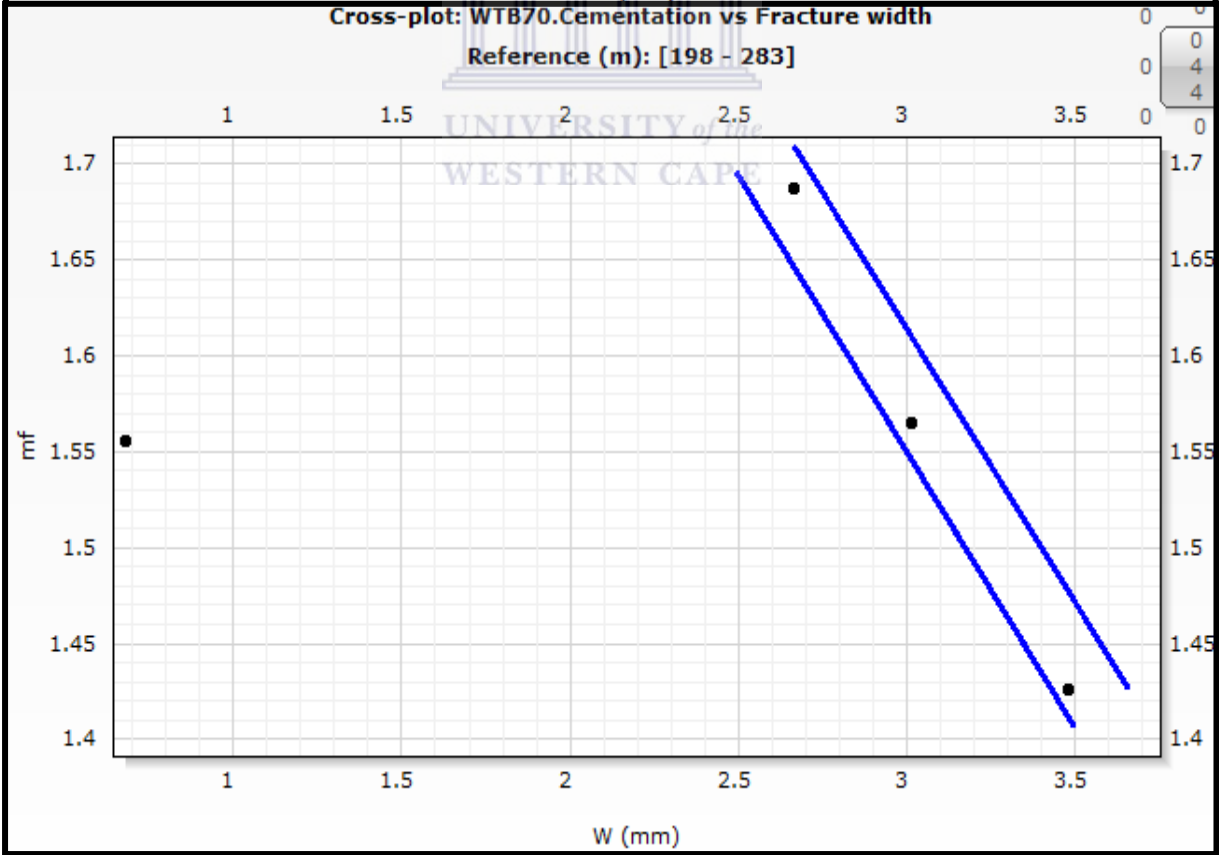
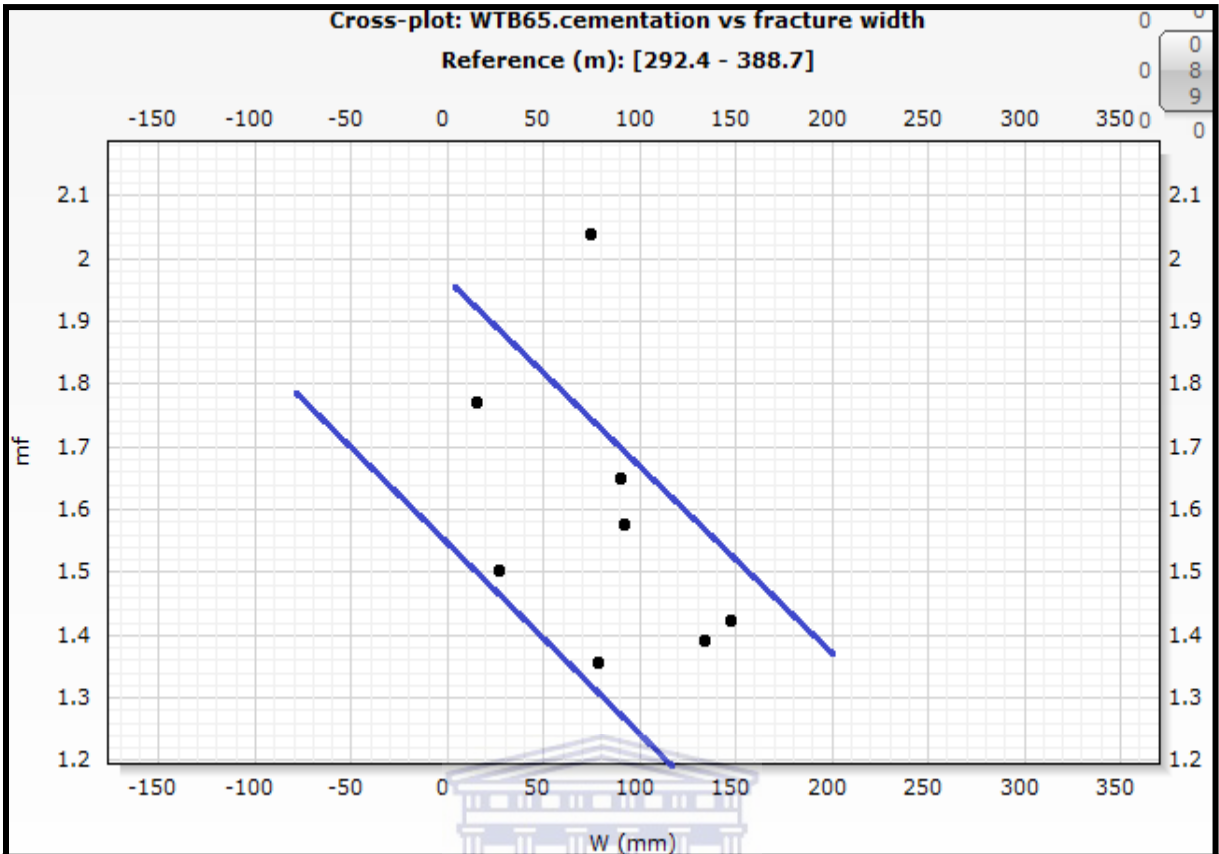
5.3.1 Cementation index vs fracture width variation

In conventional sandstone reservoirs the cementation index reflects the degree of compaction of the reservoir rock. In this case it is also a reflection of the pore configuration. Furthermore it models how much the pore network influences the resistivity since the rock itself is non-conductive. Higher cementation indices depict higher compaction while lower indices define non compacted rocks.

However since macro pores in coal are represented by fractures, the higher the cementation index the higher the compaction, resulting in reduced fracture width. Therefore the lower the cementation indexes the higher the fracture width.







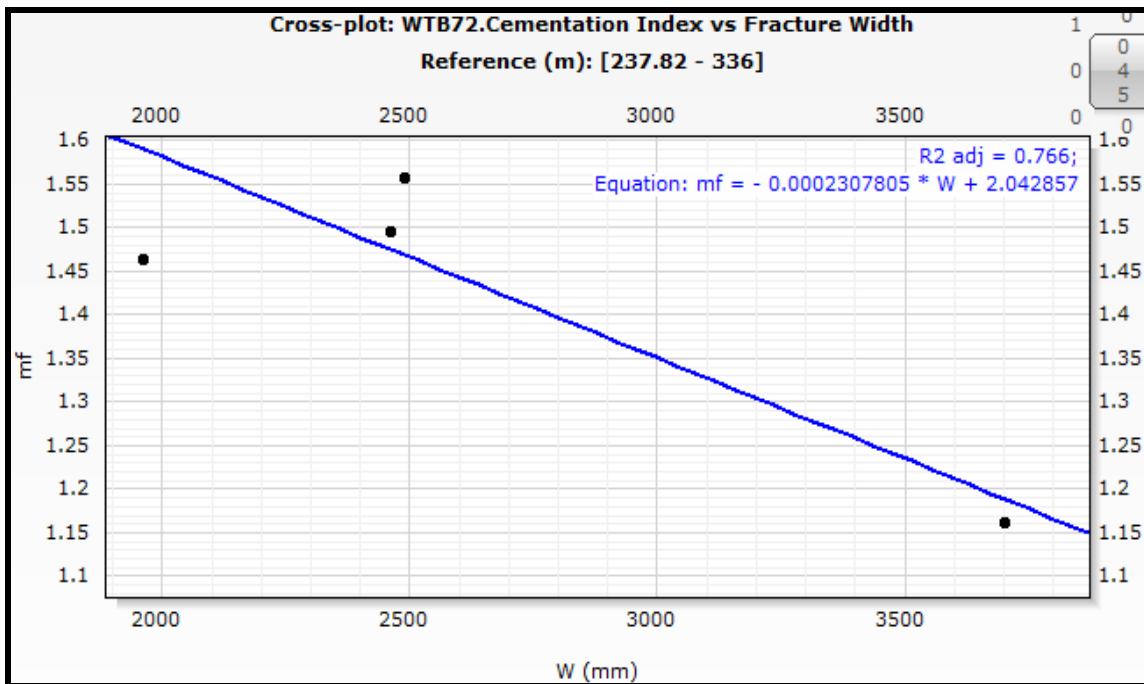
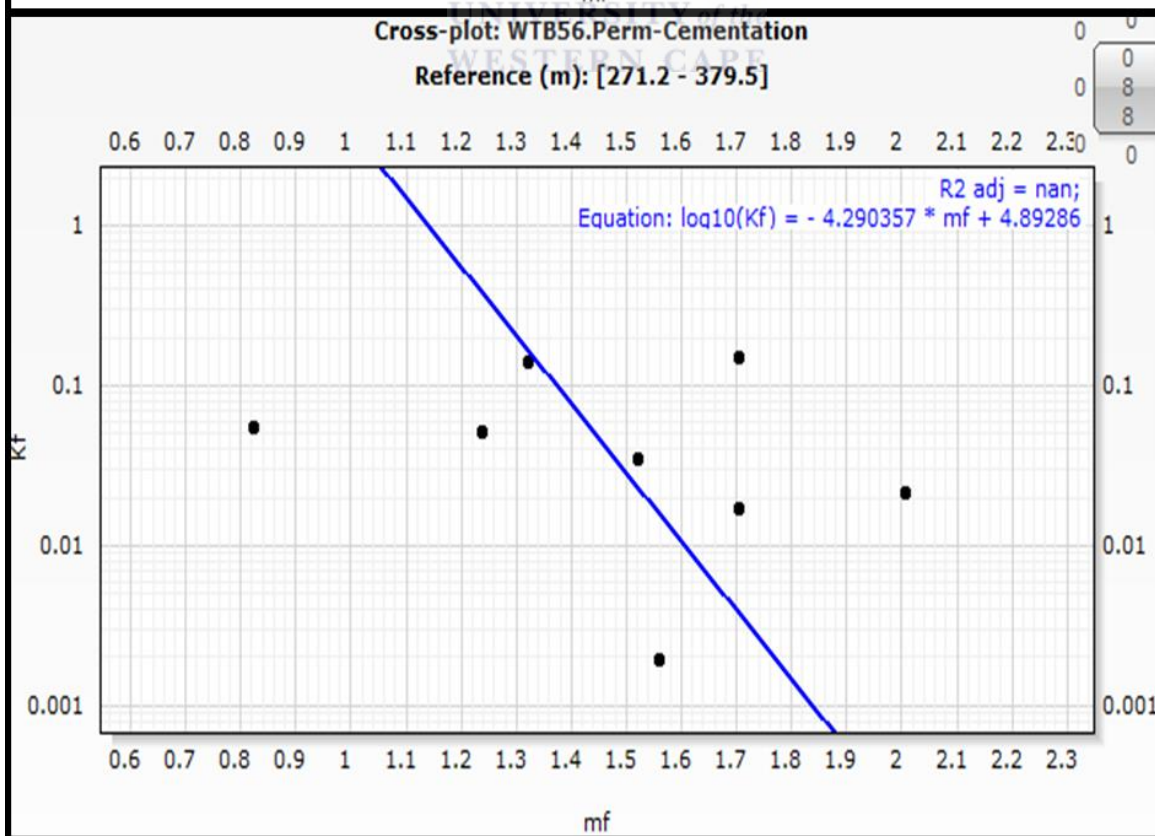
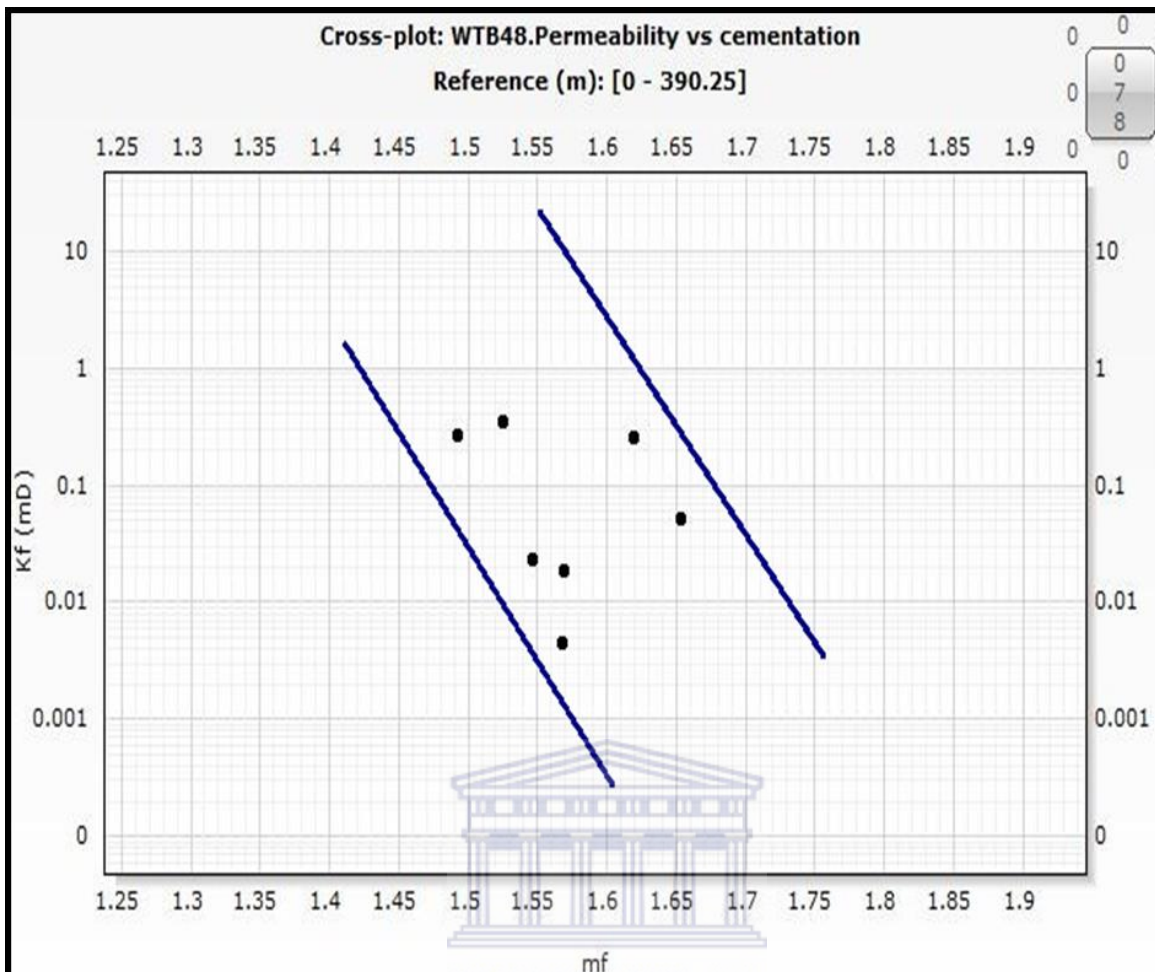


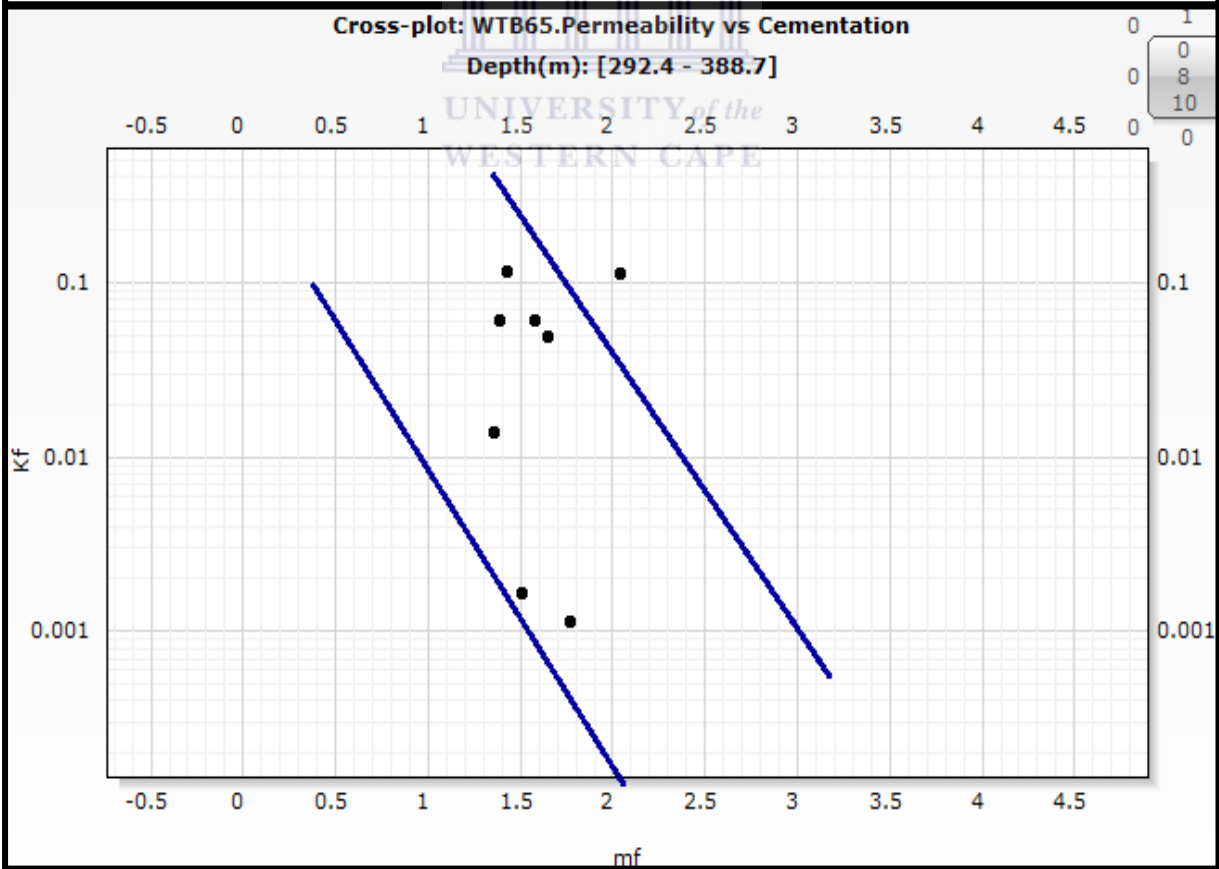
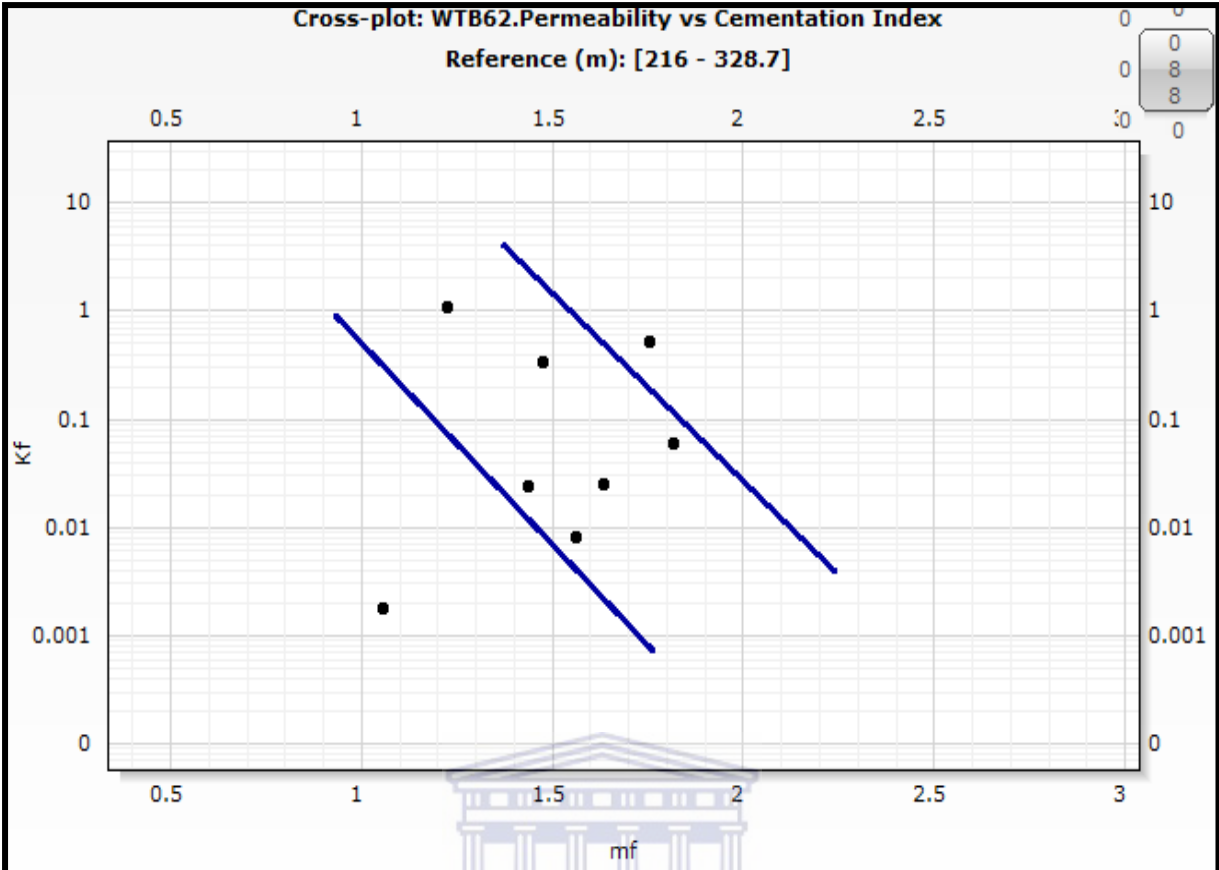
Figure 5.8: Cementation index vs Fracture width cross plots for WTB45, WTB48, WTB56, WTB62, WTB65, WTB70 and WTB72. All show decreasing cementation indices with fracture width.

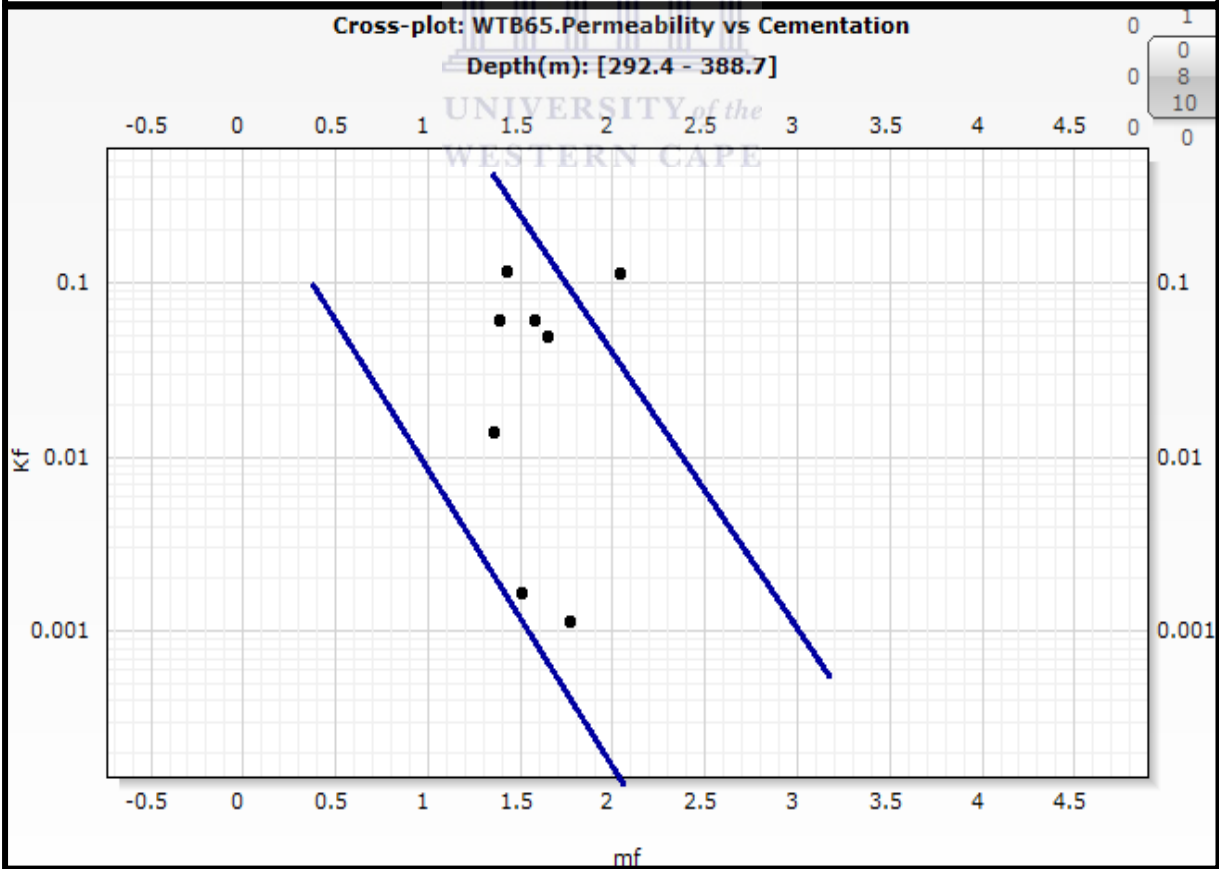
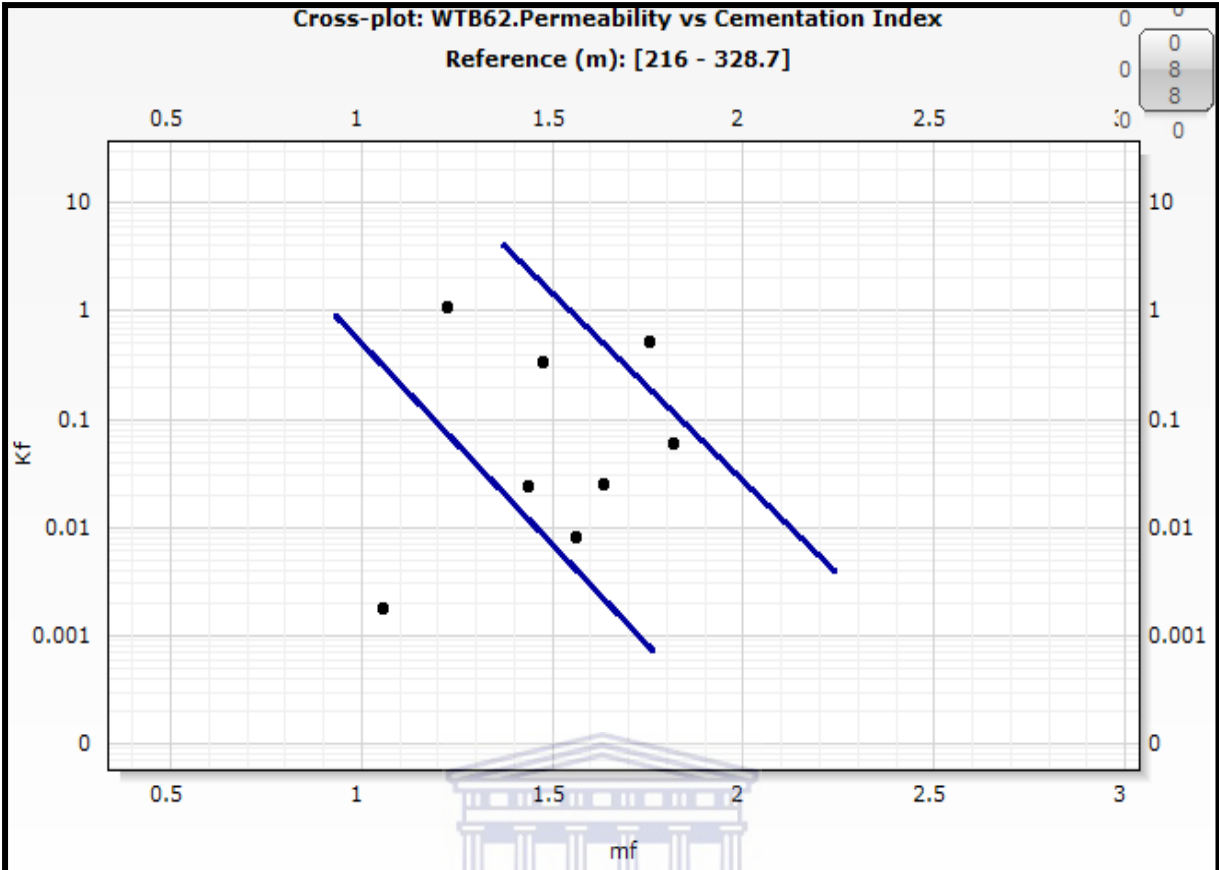
Figure 5.8 shows a gradual decrease in the cementation index of the coal accompanied by corresponding increase in fracture width. There is however a decreasing trend between the cementation index and fracture width plots. According to Li et al., (2011) the cementation property of coal is a representation of the fill degree of fracture network with minerals. Fluid flow is hindered by high cementation.

5.3.2. Permeability - Cementation Index Variation

Figure 5.9 contains plots drawn for permeability vs cementation index for WTB48, WTB56, WTB62, WTB65, and WTB72. The plots show decreasing permeability with increasing cementation index. Low cementation index facilitates intrusion of drilling fluid into the fracture network while high cementation index hinders the intrusion of drilling fluid into the fracture network thereby reducing the permeability. Figure 5.8 above already established a negative correlation between cementation index and fracture width. Relating cementation index, fracture width and permeability. Increased cementation index will lead to decrease fracture width (caused by over burden pressure or filled fracture) resulting in an overall reduction in permeability.







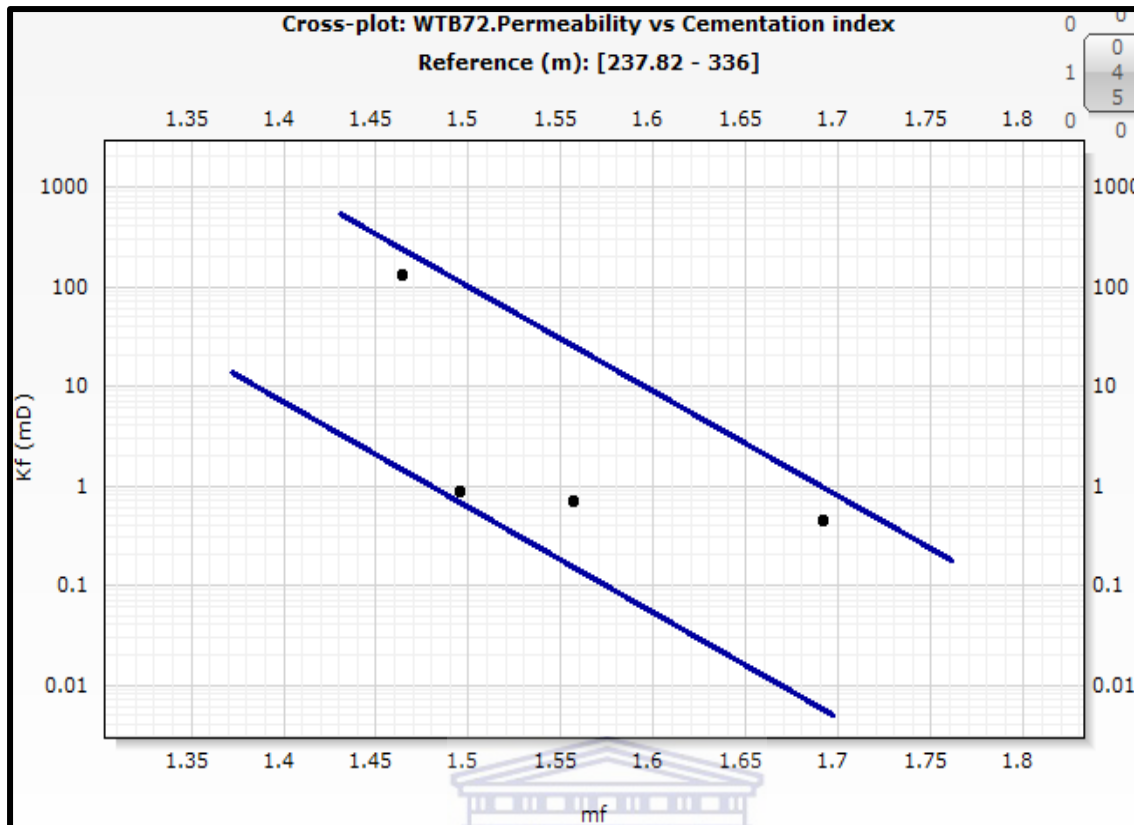


Figure 5.9: Permeability vs cementation index variation for WTB48, WTB56, WTB62, WTB65, and WTB72. Decreasing permeability with increasing cementation index.

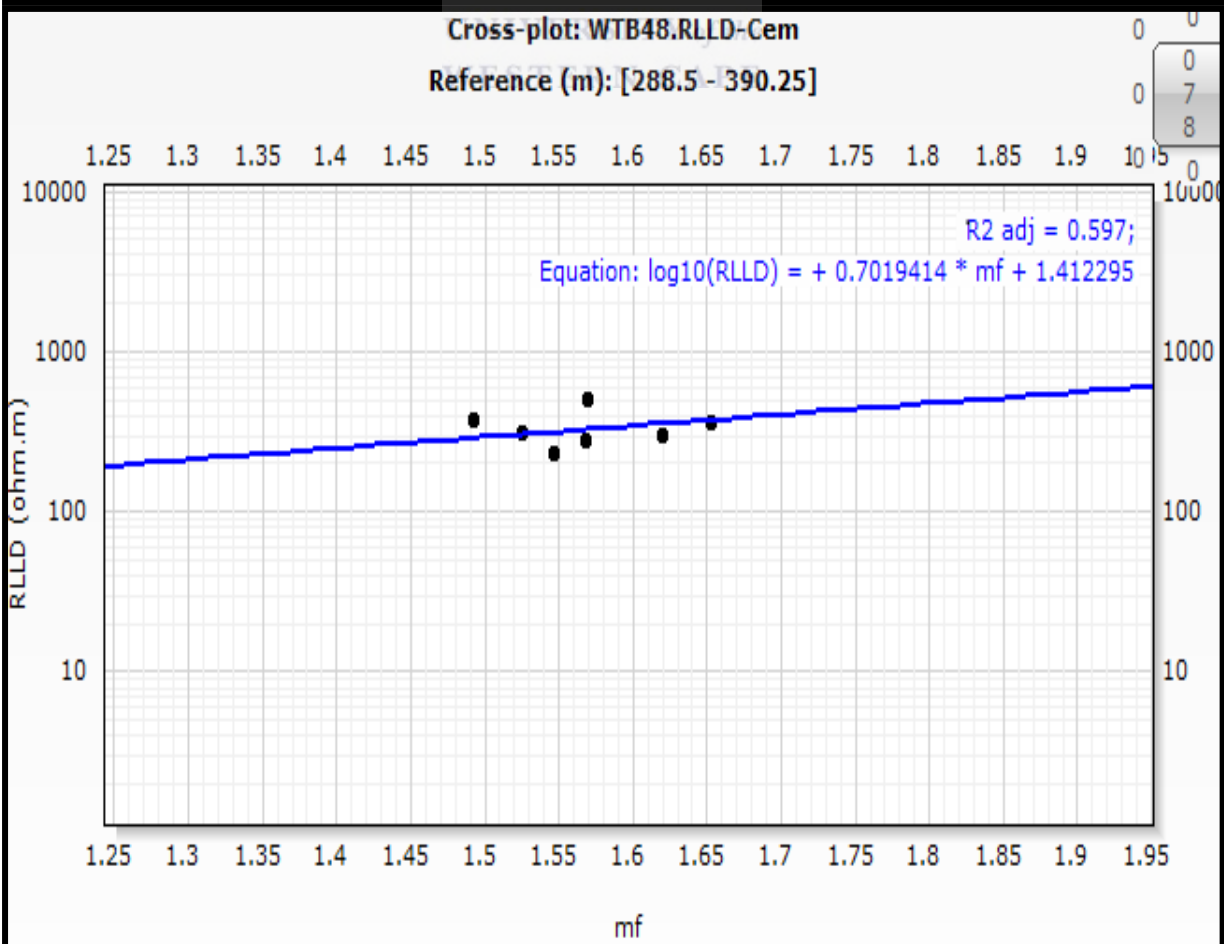
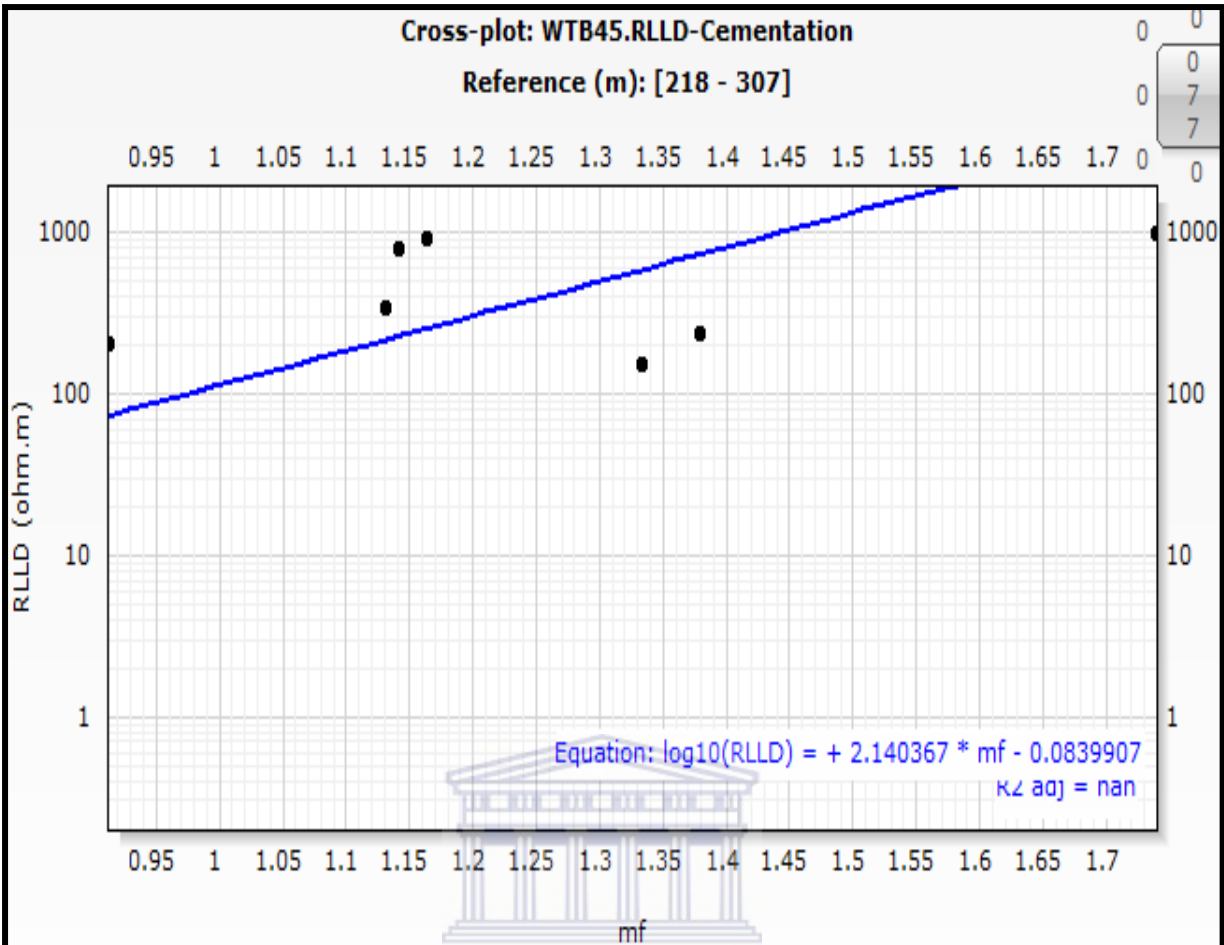
However for shallower coal seams like those penetrated by WTB45 and WTB70; the permeability increases with increasing cementation index (appendix 12). It is however expected that though the cementation index increases, the coal seams are shallow enough to represent the diagenetic phase whereby progressive increase in depth results in the creation of more fractures which will increase its permeability. Fracture geometries are however not described by fracture width alone. Fracture lengths and connectivity could also be a governing factor which was not considered in this study.

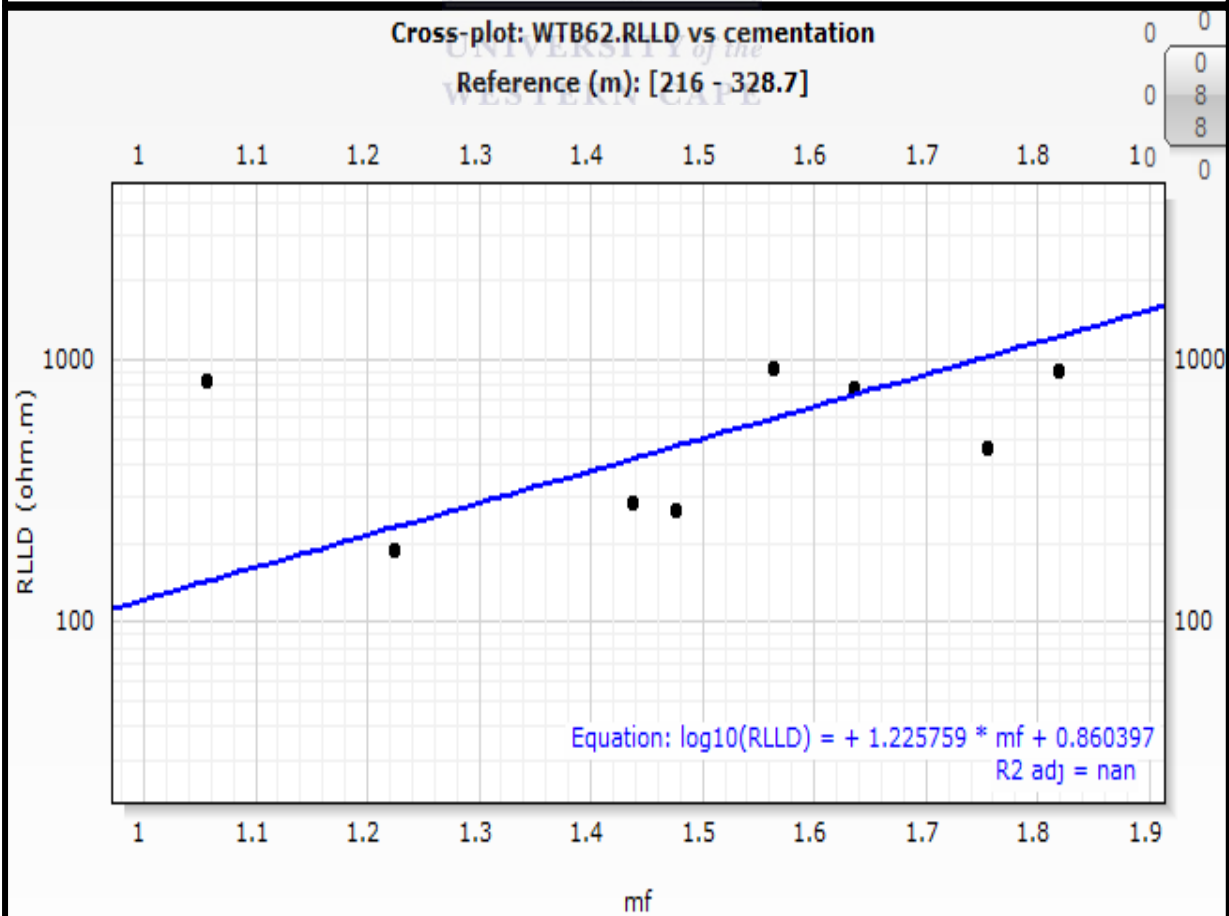
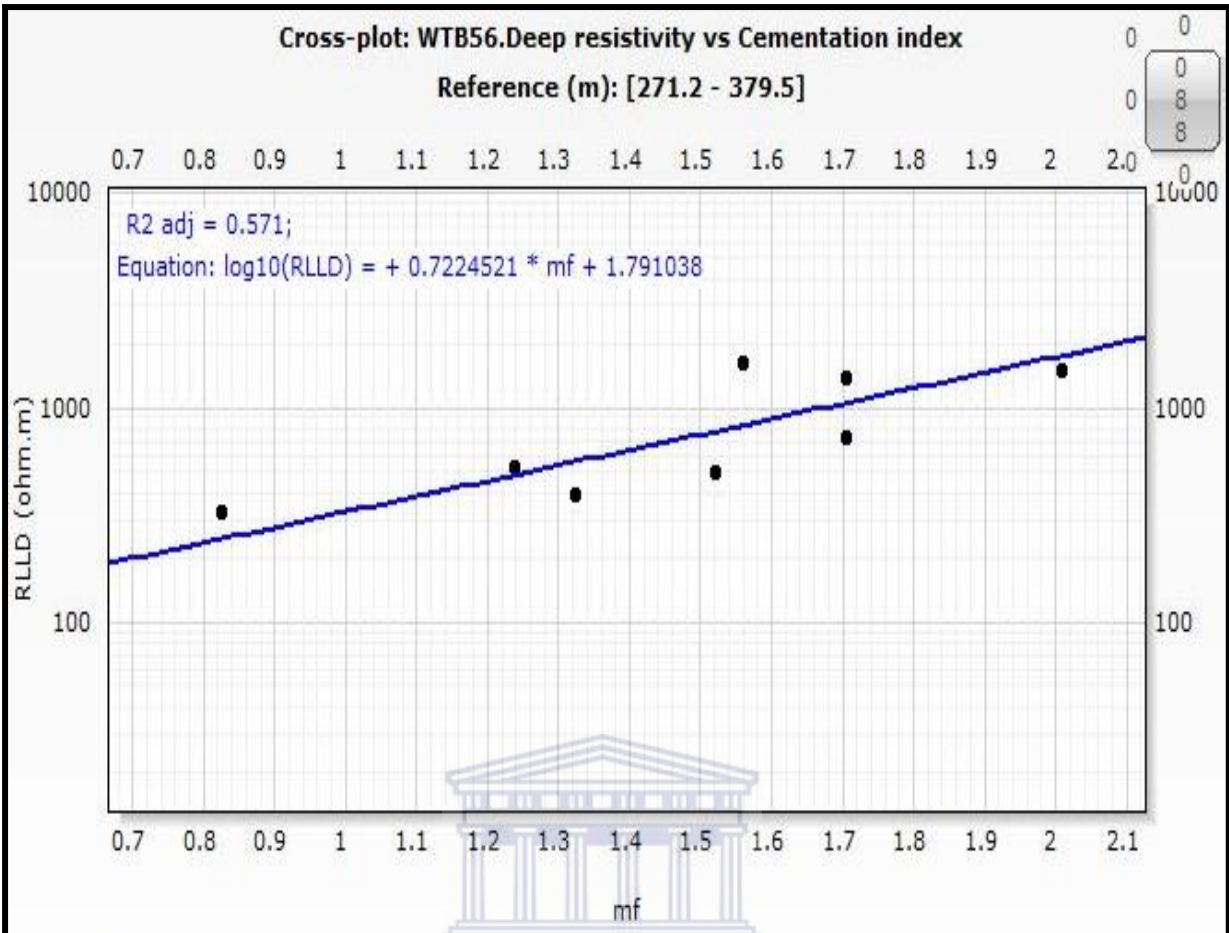
5.3.3 Permeability - resistivity relationship

Generally, as previously seen, most rock materials are poor conductors of electricity. Formation conductivity is therefore highly reliant on the fluids that fill the pore spaces. Consequently the more the Formation Water the higher the electrical conductivity (lower the resistivity). In the same way the greater the ionic concentration of the formation water the lesser its resistivity.

The averaged zonal resistivity values recorded for all the wells in table 4.6 are very high. Coals unlike other rocks contain high organic material and organic matter is highly resistive to the flow of electricity. This explains the high resistivity expressed by these coals. For all wells the shallow and deep laterolog resistivity increases down the well. The cementation index vs fracture width variation discussed above show that increasing cementation index is accompanied by decreasing fracture width with depth. A decrease of fracture width implies a decrease in moisture content. This results in a net decrease in conductive ions. Consequently the values of the deep and shallow laterolog resistivity will increase with increasing cementation index (figure 10 and 11) and depth. Very high resistivity values are recorded for the lower zones 4, 3, 2 of WTB 56 and zones 3 and 2 of WTB 65. Recorded depths for these zones ranged from 339m to 385m. These zones are marked by higher cementation indices i.e. lower moisture content than same zones for other wells. Undefined trends for deep and shallow resistivity variation with cementation index are experienced for WTB72.







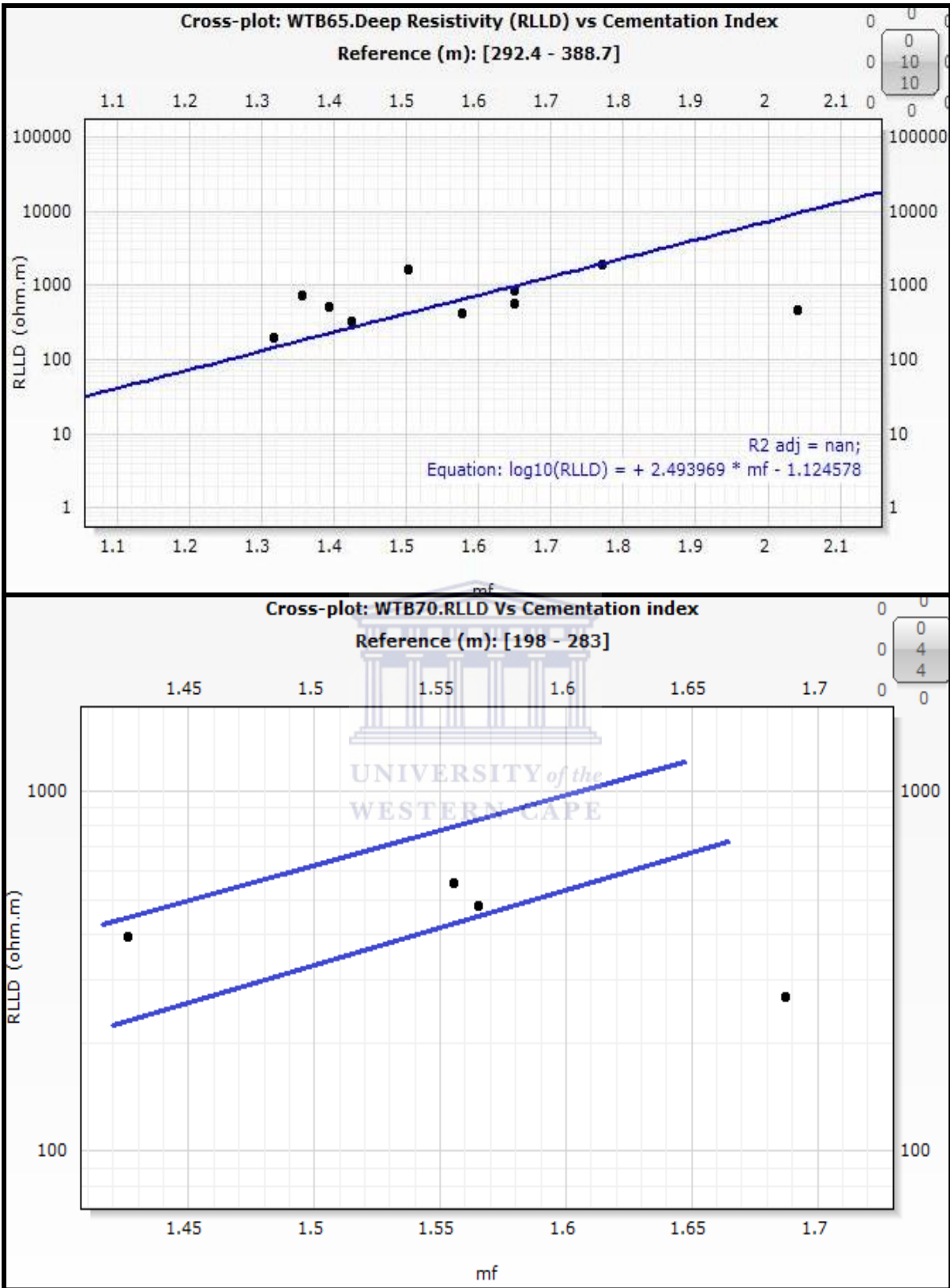
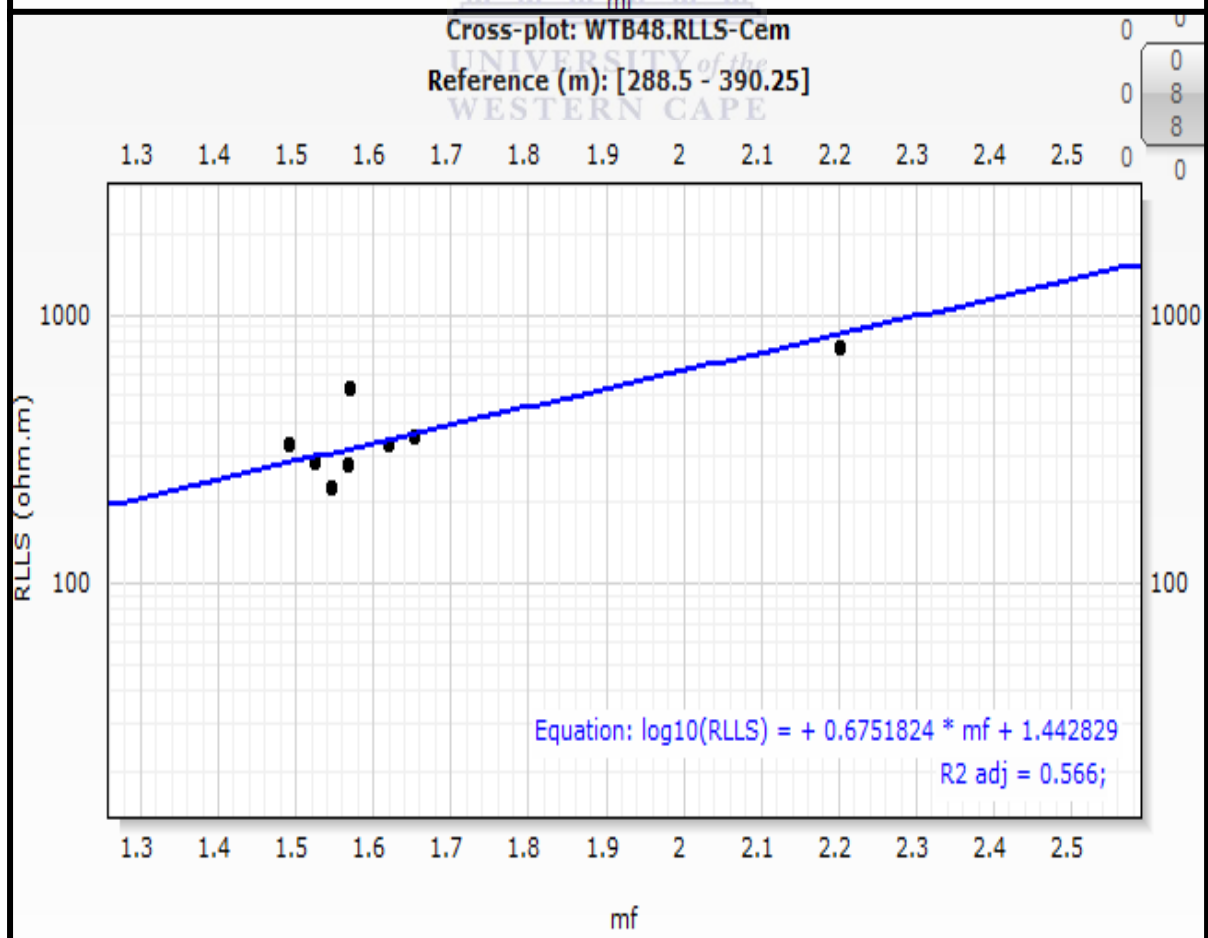
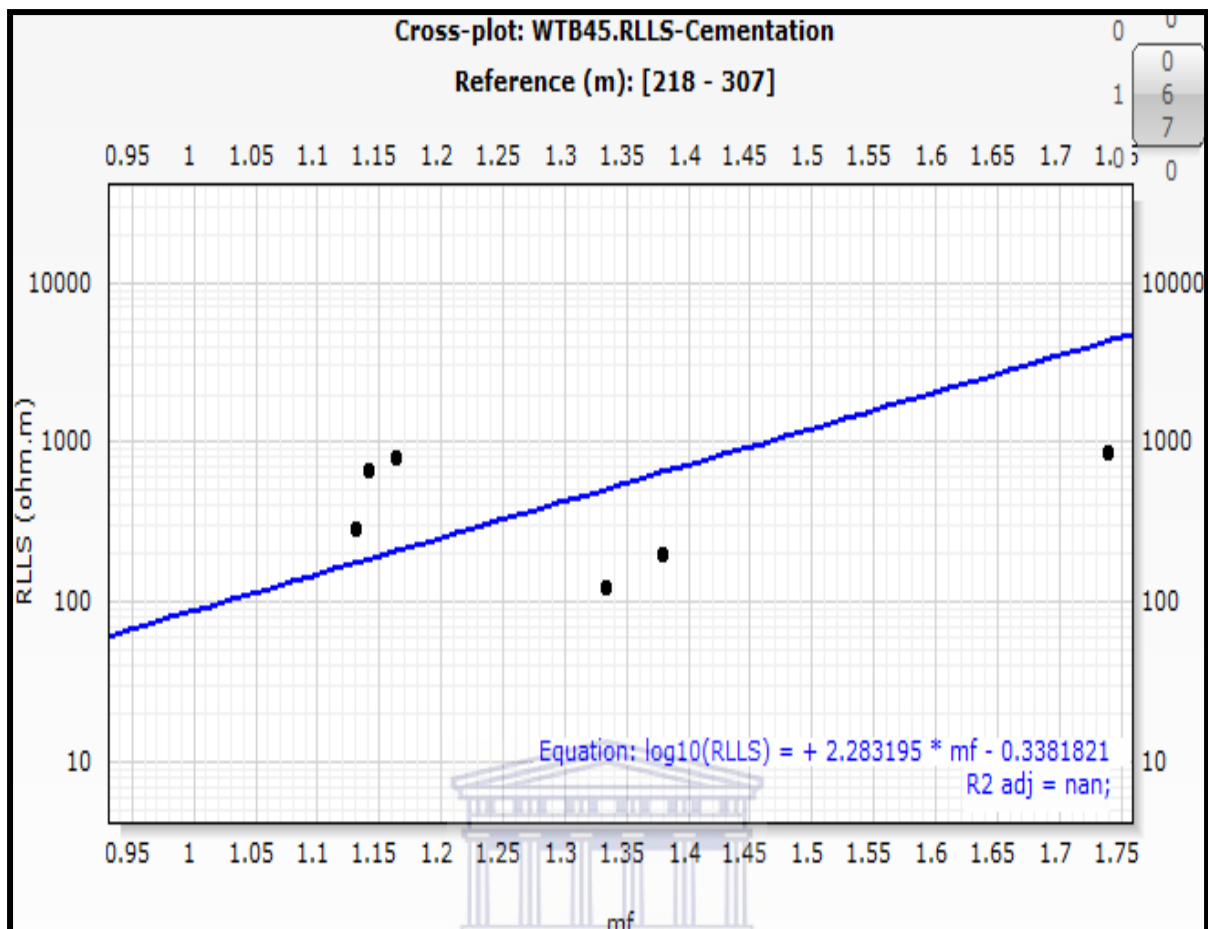
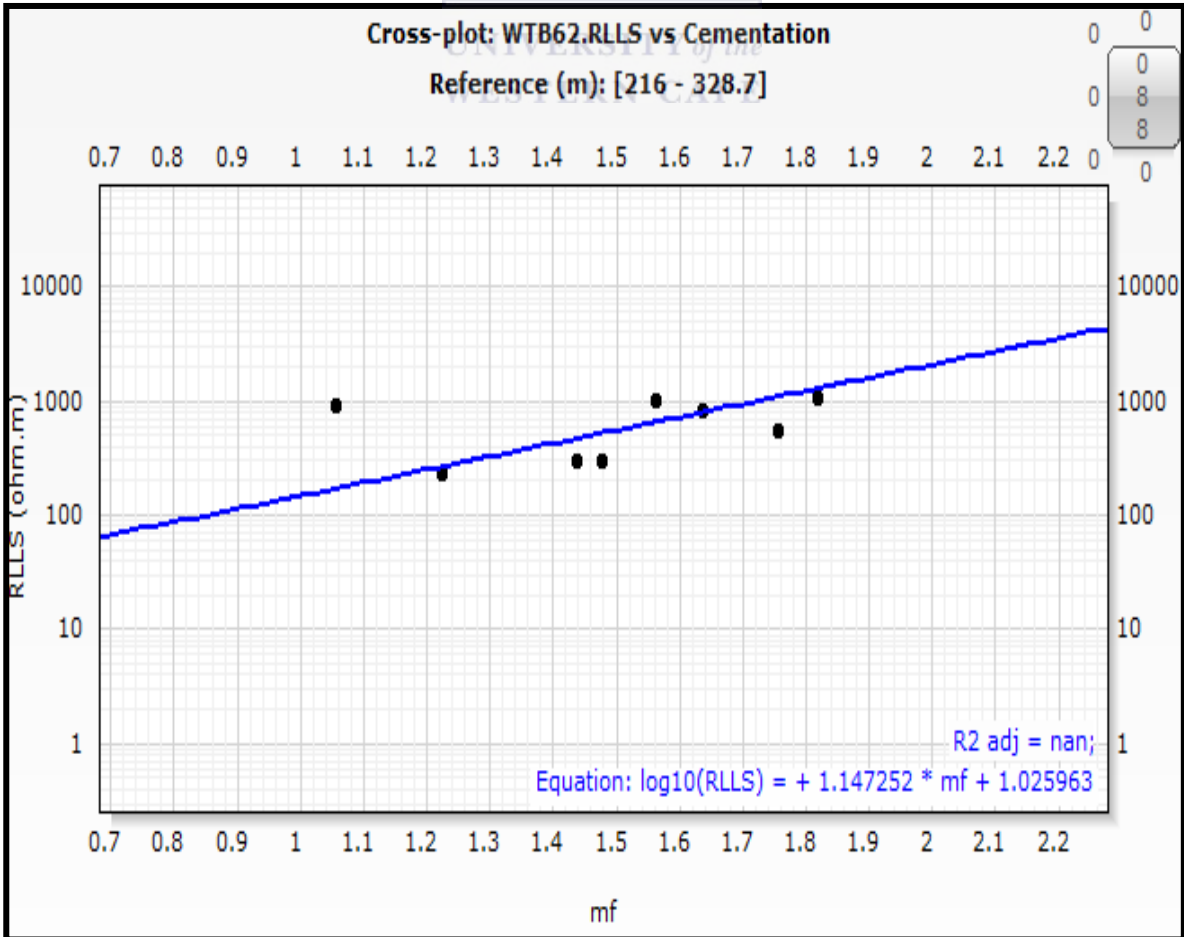
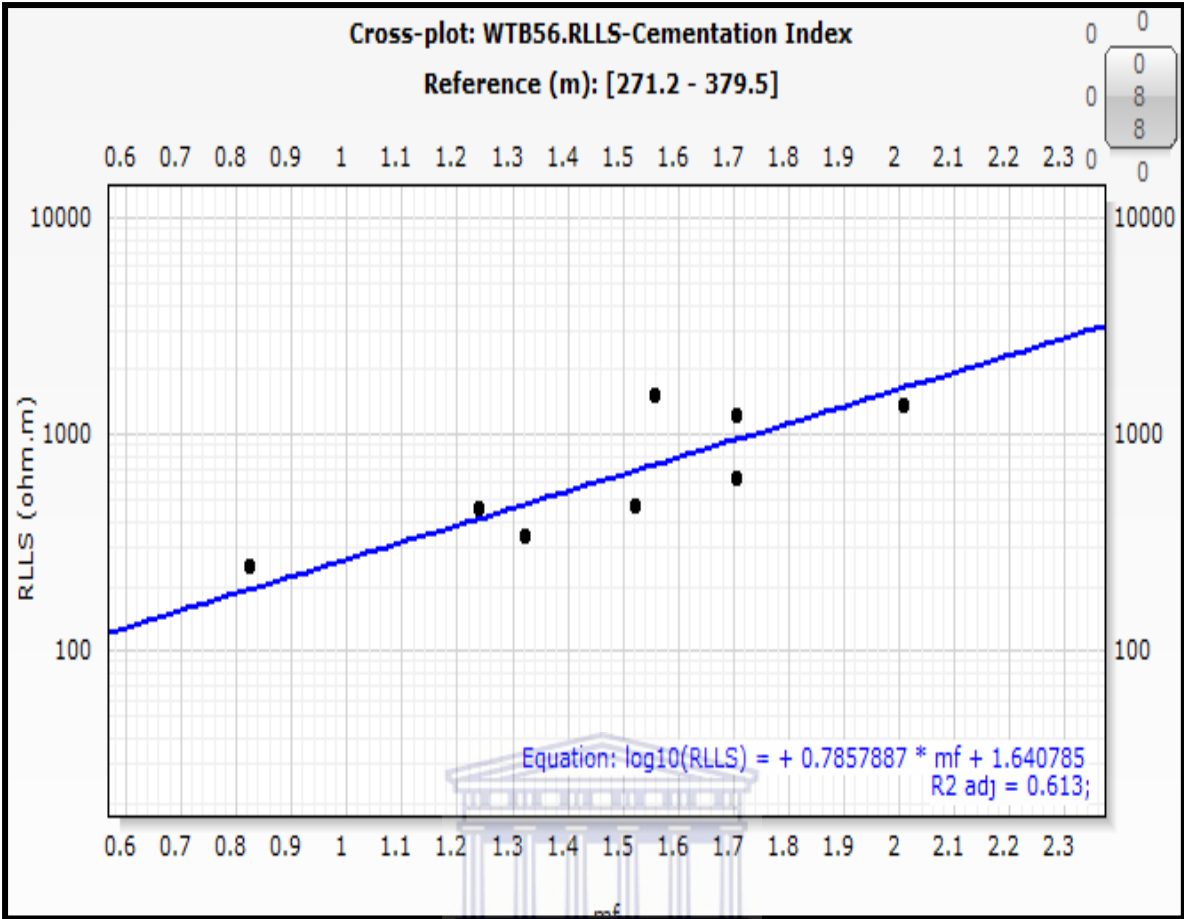


Figure: 5.10: Deep resistivity vs cementation index plots for WTB45, WTB48, WTB56, WTB62, WTB65 and WTB70. Shows positive correlation between deep laterolog resistivity and cementation index.





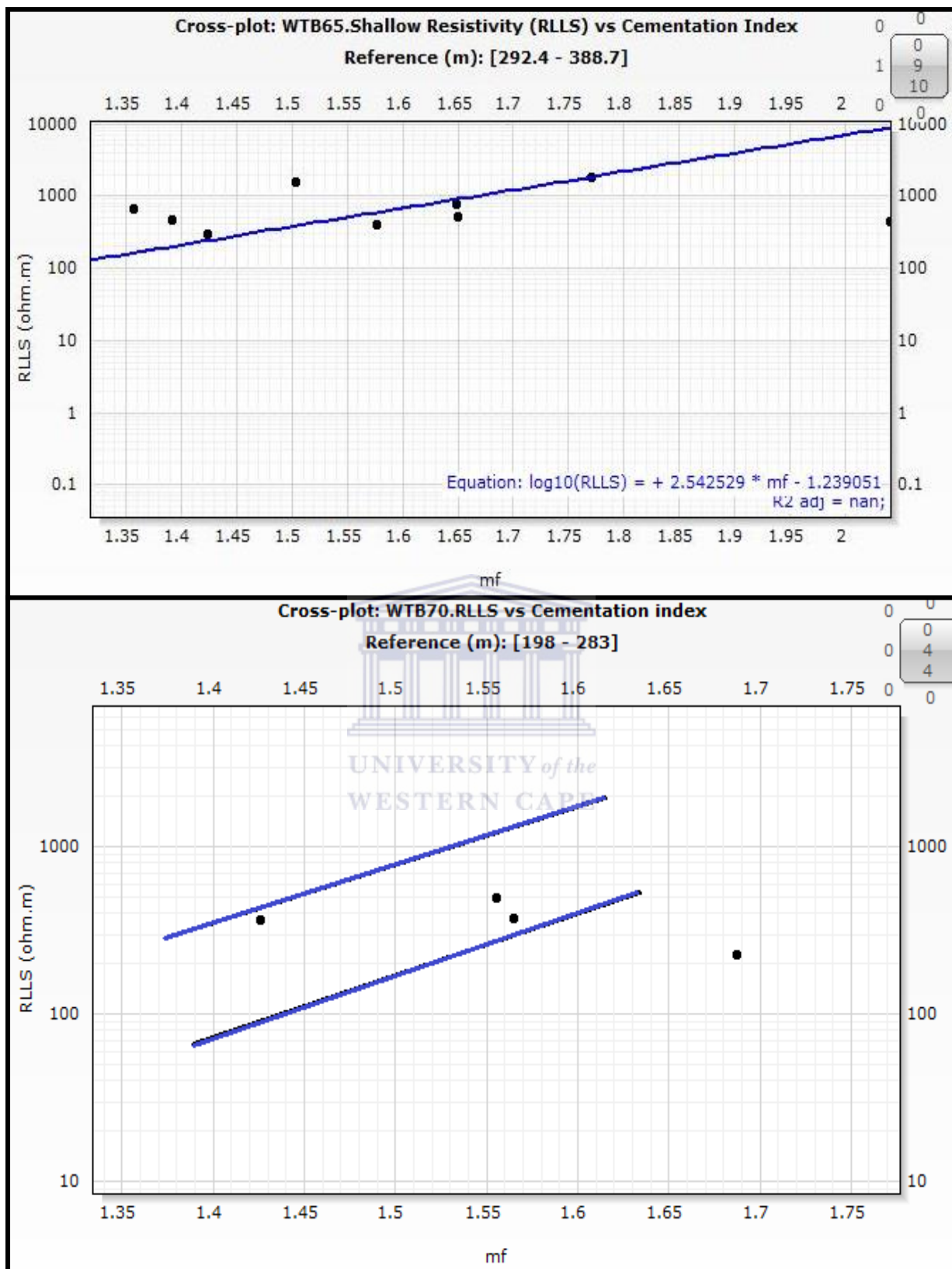


Figure 5.11: Shallow resistivity vs cementation index plots for WTB45, WTB48, WTB56, WTB62, WTB65 and WTB70. Show positive correlation between deep laterolog resistivity and cementation index.

5.3.4 Comparison of Log and Field derived Permeabilities

The values of log calculated permeability and those from injection falloff tests are displayed on table 4.7. The results shows that field derived fractured permeabilities are slightly higher than the model derived permeabilities. However both permeabilities show similar trends with depth. They both decrease with the depth of burial. The reason for the slight difference in permeability between the calculated permeability and that from field test can be explained by four reasons:

- The model did not take into account the influence of coal anisotropy. Coal anisotropy defines the non-uniform properties of coal. This includes anisotropy in electrical conductivity. The method depended highly on the electrical properties of the rock to calculate its permeability. However the electrical conductivity of rocks including coal varies when applied horizontal or parallel to bedding surface. The coal seams on their own are also not uniform in their texture and composition. This as well will impact on calculated values. The model did not take into account stress variations.
- The depth of investigation of the shallow resistivity is 0.2m while that of deep resistivity is 0.3m. Their difference, 0.1m is consequently very small. The idea is for the deep resistivity to record the true resistivity of the formation. However with such low difference, it is possible to be dealing with the invaded zone.
- During the drilling process fresh water without any additive was used as drilling mud. The formation brine itself is fresh with some dissolve solutes. However the quantity of dissolved solutes in formation water is very small raising the conductivity slightly greater than that of the formation water. As a results the conductivity of both fluids (i.e. formation water and drilling fluid) are very close to each. High precision is consequently required when analysing these results.

CHAPTER 6: CONCLUSION

In this study the fracture porosity and permeability of the Beaufort Seam 1 (Upper Ecca) and the middle Ecca seams were extensively studied within the limit of the data provided. Geophysical wire-line logging data was used to compute the fracture cementation index and fracture width of the coals from which the fracture porosity and permeability were calculated from various modified Archie and Darcy equations for “A Collection of Sheet Coal Reservoir model”. Comparison was made with previously conducted injection falloff test data to ascertain the accuracy of the method. From this the following conclusions were made.

- The study area is located within the deeper section of the Waterberg basin. The depth of investigation of the shallowest coal seam in the study area ranges from 198m to 292.4m while that of the deepest coal seams penetrated by the wells ranges from 274.6m to 396.9m. These depths are deeper than other coal basin in neighbouring basins particularly mineable units.
- Two cross sections linking the study wells was drawn: one South West – East orientation and the other North – South orientation in the east of the basin. From this it was deduced that the depth of burial of the coal seams was structurally controlled by the many faults that cut across the basin. The deepest coal seams are located in the centre of the basin bounded by the Zoetfontein Fault to the North, the Daarby Fault to the West and South and the Bulkop to the North East.
- Density logging data can be used in conjunction with gamma ray to delineate coal reservoirs. A density cut off of 1.8g/cc was employed. Net coal thickness for all eight wells ranges from 39.61m to 76.16m while individual coal seams ranged from a few mm to tens of meters. The study did not provide evidence as to why the coal seam thickness varies vastly.
- Density logging data can be used to evaluate coal reservoir fracture porosity. The porosity BS1 coals and Lower Ecca coal seams were evaluated with the aid of density logging data from eight study wells. From the results coal fracture porosity ranges from 0.0002% to 0.33% with an average of 0.02%.

- Geophysical Logging technique was successfully applied in the evaluation of coal reservoir permeability of the Waterberg Basin, South Africa using “a collection of sheets coal reservoir model”. Model calculated permeability is higher for BS1 coals than Ecca Coals. Calculated permeability ranges from 0.0045mD to 6.05mD. Calculated results are lower than those derived from Injection fall off test. Coal anisotropy was established as the main reason for variation between log estimated and field derived permeabilities. On a basinal scale the permeability was found to increase slightly from West to East.
- Results recorded low cementation indices ranging from 0.82 to 2.42. The cementation index reflects the degree of fracture closure or the degree of fracture infill with minerals which influences the coal permeability. The fracture permeability decreases with increasing cementation index and increases with increasing fracture width.
- For these coals the fracture porosity also decreases with increasing cementation index for the deeper coal seams and increases with increasing cementation index for shallower seams.
- The values of deep and shallow laterolog resistivity increases with increasing cementation index due to reduced amounts of conducting fluids as coal fractures closed up.
- Comparing the calculated fracture permeability with maceral content: there is an increase in coal seam fracture permeability with increasing vitrinite content and a decrease in permeability with increasing inertinite content. Liptinite content was very low and almost homogenous throughout the basin consequently permeability remained indifferent with liptinite content.
- It was also established that as the coal become more mature i.e. increase vitrinite reflectance the permeability reduces.
- In general coal fracture porosity and permeability show decreasing trends with increase in measured depth.

REFERENCES

- ALL, (2002): Handbook on Best Management Practices and Mitigation Strategies for Coal Bed Methane in the Montana Portion of the Powder River Basin. Prepared for: U.S. Department of Energy, National Petroleum Technology Office, National Energy Technology Laboratory. Tulsa, OK. EPA-HQ-OW-2008-0517, DCN 05254.
- Aminian, K., (2007): Coalbed Methane-Fundamental Concepts. Petroleum & Natural Gas Engineering Department West Virginia University, 8-15.
Url:Universityhttp://karl.nrcce.wvu.edu/regional/CoalbedMethane_Aminian_Paper_1.pdf. Accessed on the 10 June 2012.
- Ammosov, I. I. and Eremin, I. V., (1963): Fracturing i n Coal. Israel Program for Science. Transl., 112pp. API, (1998): Recommended Practice for Core Analysis. In: Recommended Practice 40, 2ndEdition. American Petroleum Institute.
- Arnott, D., and Williams, C., (2007): Mmamabula Project, South – Eastern Botswana. National Instrument 43 -101 Technical Report, Project number J912. CIC Energy Corp, Snowden Consultants.
- API RP 40, (1998): Recommended Practice for Core Analysis, American Petroleum Institute. Url: www.energistics.org/RP40/rp40.pdf, accessed on 24 Jan., 2013.
- ASTM D388-88, "Standard Classification of Coals by Rank," Annual Book ofASTM Standards (April, 1979), Part 26.
- Baker Hughes Inteq, (1992): Advanced Wireline & MWD Procedures Manual. Technical Publication paper, number: 80459H Rev. A, procedure manual.
- Baker Hughes, (2002): Introduction to Wire-line Log Analysis. Baker Atlas.
- Baker, O.B., (1983): A proposed Geotectonic model for the Soutpanberg Group within the Limpopo Mobile Belt, South Africa. Special publication of the Geological Society of South Africa, 8, p. 181-190.
- Berkowitz, N., (1979): An Introduction to Coal Technology, Academic Press, New York.
- Bordy, E.M., Knoll, F. and Bumby, A. (2010): New data on the palaeontology and sedimentology of the Lower Jurassic Lisbon Formation (Karoo Supergroup), Ellisras Basin, South Africa. Neues Jahrbuch für Geologie und Paläontologie Abh., DOI: 10.1127/0077-7749/2010/0091; Stuttgart. p. 1-11.
- Brandl, G., (1986): The Geology of the Ellisras Area. Exploration Sheet 2326, Geological Survey of South Africa, Pretoria, 49pp.
- Bumby, A. J., and Van Der Merwe, R., (2004): The Limpopo Belt of Southern Africa: Neoproterozoic to Palaeoproterozoic Orogen. In: P. G. Eriksson, W. Altermann, D. R. Nelson, W.

U. Mueller and O. Catuneanu (editors): The Precambrian Earth: Tempos and Events. Elsevier publication, Amsterdam, pp 201-223.

Bumby, A.J., (2000): The geology of the Blouberg Formation, Waterberg and Soutpansberg groups in the Area of the Blouberg mountain, Northern Province, South Africa. Unpublished PHD Geology Thesis, University of Pretoria.

Busch, A., Gensterblum, Y., (2011): CBM and CO₂-ECBM related sorption processes in coal: A review. International Journal of Coal Geology, vol. 87, pp 49–71.

Cadle, A. B., (1979): Depositional models from the middle Ecca and their influence on coal from the eastern Transvaal. Geological Society of South Africa 18th Congress Abstract, vol.1, pp77-78.

Cadle, A. B., (1982): Control on Coal Distribution. In: Cadle, A.B. (ed) Coal Exploration, economics and assessment. University of Witwatersrand, pp20-30.

Cadle, A.B., Cairncross, B., Christie, A.D.M., and Roberts, D.L., (1993): The Karoo basin of South Africa: type basin for the coal-bearing deposits of southern Africa. International Journal of Coal Geology, vol23, pp117–157.

Cairncross, B.C., (1979): Depositional frame work and control of coal distribution and quality, Van Dijks Drift area, northern Karoo Basin. Unpublished MSc Thesis, University of Natal, Pietermaritzburg, South Africa.

Cairncross, B.C., (1980): Anatomising river deposits: palaeo-environmental control on coal quality and distribution, northern Karoo Basin. In: Cadle, A.B. (ED) Karoo Basin Symposium, Geological society of South Africa, Special Issue, pp301-331.

Cairncross, B., (1989): Paleodepositional environments and sedimentary controls of the post glacial Permian coals, Karoo Basin, South Africa. International Journal of Coal Geology, vol.12, pp365-380.

Cairncross, B., (1990): Tectono-sedimentary settings and controls of the Karoo Basin Permian coals, South Africa. International Journal of Coal Geology, Vol.16, pp175–178.

Cairncross, B., (2001): An overview of the Permian (Karoo) coal deposits of southern Africa. African Earth Sciences, vol. 33, pp529–562.

Cairncross, B., and Langford, R.,(1991): Permian coal deposits of Africa, South of the Sahara; a geological overview. Conference on South Africa coal resources. Geological Society of South Africa. Witbank, 6-9 November 1991. Abstract.

Canadell, J.G., Le Quéré, C., Raupach, M.R., (2007): Contributions to accelerating atmospheric CO₂ growth from economic activity, carbon intensity, and efficiency of natural sinks. Proc Natl Acad Sci USA 2007; 104: 18866–70.

Catuneanu, O., (2004a): Basement control on flexural profiles and the distribution of foreland facies: the Dwyka Group of the Karoo Basin, South Africa. *South African Journal of Geology*, vol.32, issue 6, p. 517–520.

Cervik J., (1969): Behaviour of coal-gas reservoirs. US Bureau of mines Technical Progress Report number 10; Methane Control Program.

Charbucinski, J., and Nichols, W., (2003): Application of spectrometric nuclear boreholelogging for reserves estimation and mine planning at Callide coalfields open-cutmine. *Applied Energy*, vol. 74, pp313–322.

Clarkson, C. R., and Bustin, R.M., (1999a): The effect of pore Structure and pressure upon the transport of properties of coal. Isotherms and pore volume distributions. *Fuel*, vol. 78, pp1333-1344.

Clarkson, C.R., and Bustin, R.M., (2000): Binary Gas Adsorption /Desorption Isotherms: Effect of moisture and coal composition upon carbon dioxide selectivity over methane. *International Journal of Coal Geology*, vol. 42, pp241-271.

Collins, R.E., (1989): New theories for Gas Adsorption and Transport in Coal, Proc., International Coalbed Methane Symposium, Tuscaloosa, Alabama, April 1989, pp425-431.

Coppens, L., 1936. *Ann. Mines Belg.*, vol. 37, p173.

Crain, E. R., (2010): Coal. In: *Unicorns in the Garden of Good and Evil*, part 2. URL: www.spec2000.net/freepubs/2010-4UnconvGAS.pdf, accessed on 23rd January 2013.

Crosdale, P.J., Beamish, B.B., Valix, M., (1998): Coalbed methane sorption related to coal composition. *International Journal Coal Geology*, vol. 35, pp147–158.

Crosdale, P.J., Moore, T.A., and Mares, T.E., (2008): Influence of moisture content and temperature on methane adsorption isotherm analysis for coals from a low-rank, biogenically sourced gas reservoir. *International Journal of Coal Geology*, vol. 76, issue 1–2, pp166–174.

Cui, X., Bustin, R.M., and Chikatamarla, L., (2007): Adsorption-induced coal swelling and stress: Implications for methane production and acid gas sequestration into coalseams. *Journal of Geophysical Research*, vol. 112, B10202.

Cummins, T. and Fredericks, L., (2006): Development of In-House Coal Seam Permeability Testing Capabilities, in Aziz, N (ed), *Coal 2006: Coal Operators' Conference*, University of Wollongong & the Australasian Institute of Mining and Metallurgy, pp220-230.

Dabbous, M. k., Reznik, A.A., Tabor, J.J., and Fulten, P.F., (1974): The permeability of coal to gas and water. *SPE Journal*, vol. 14, issue 6, pp556-572.

Daniel, V. N., Ronald, J. P., Mark, S.S., Paul C. P. and Jonathan, P. M.,(2008): Structural Characterisation of Vitrinite-rich and Inertinite-rich Permian aged South African bituminous Coals. *International Journal of Coal Geology*, vol76, pp290-300.

Daniel, V.N., Gareth, D.M., and Jonathan, P.M., (2010): Petrographic and reflectance analysis of solvent-swelling and solvent-extracted South African Vitrinite-rich and Inertinite –rich coals. *International Journal of Coal Geology*, vol81, pp45-52.

Day, S., Fry, R., and Sakurovs, R., (2008): Swelling of Australian coals in supercritical CO₂. *International Journal of Coal Geology*, vol. 74, pp 41–52.

Day, S., Sakurovs, R., and Weir, S., (2008c): Supercritical gas sorption on moist coals. *International Journal of Coal Geology*, vol. 74, issue 3–4, pp203–214.

De Jager, F.S.J., (1983): Coal reserves of the Republic of South Africa – an evaluation at the end of 1982. *Geological Survey South Africa Bulletin* vol. 74, 20p.

De Jager, F.S.J., (1986): Coal Occurrences in the Central, North Western, Northern and Eastern Transvaal, 2047–2055. In: Anhaeusser, C.R. and Maske, S. (eds.), *Mineral Deposits of Southern Africa*. Geological Society of South Africa, 1315 pp.

De Jager, F. S. J., (1976): Steenkool. In: *Delfstowwe van die Republiek van Suid Afrika*, Vyfde druk. Geologiese Opname, Dept. van Mynwese Straatsdrukker, Pretoria, pp383-390.

De Wit, M. J, Van Reenen, D.D., Roering, C., (1992): Geologic Observations across a tectonic metamorphic Boundary in the Babangu Area, Giyani (Sutherland) Greenstone Belt, South Africa. *Precambrian Research*, vol. 55, pp111-122.

Diamond, W. P., McCulloch, C. M., and Bench, B. M., (1976): Use of Surface Joint and Photolinear Data for Predicting Subsurface Coal Cleat Orientation. *Bureau of Mines Report of Investigations 8120*, Pittsburgh, 1976.

Digital Core, (2012): Coal Bed Methane reservoirs in The New Dimension of Core Analysis. Digital Core Laboratories.

Dipak, M., Tewari, D.C., and Rautela, M. S., (2004): Analysis of Micro-fractures in Coal for Coal Bed Methane Exploitation in Jharia Coal Field. 5th Conference & Exposition on Petroleum Geophysics, Hyderabad-2004, India, pp904-909.

Dreyer, J.C., (2006): An overview of the geology of the Waterberg Coalfield, implications for future exploitation. Presented at the Fossil Fuel Foundation of South Africa Conference: The Waterberg Coalfield 2006 and beyond – quo vadis? Lephalale (previously Ellisras), 22 – 23 August 2006.

Du Toit, A. L., (1937): *Our Wondering Continent*, Oliver and Boyd.

Du Toit, A.L., (1954): *The Geology of South Africa*, third ed. Oliver and Boyd, Edinburgh, 611p.

Dutta, P., Bhowmik, S., and Das, S., (2011): Methane and carbon dioxide sorption on a set of coals from India. *International Journal of Coal Geology*, vol. 85, pp 289-299.

Emese, M., Bordy, G., Knoll, M. F., and Bumby, A., (2010): New data on the palaeontology and sedimentology of the Lower Jurassic Lisbon Formation (Karoo Supergroup), Ellisras Basin, South Africa. *N. Jb. Geol. Paläont. Abh.*, vol. 258, issue2, pp145–155.

Falcon, R.M.S., (1973): Palynology of the Lower Karoo Succession in the Middle Zambesi Basin. In: *Palaeontology of Rhodesia*. *Rhod. Geol. Surv. Bull.*, vol. 70, pp43-71.

Falcon, R.M.S., (1975b): Application of Palynology in in sub-dividing the coal –bearing formations of the Karoo Sequence in South Africa. *South Africa Journal of Science*, vol. 7 pp336-344.

Falcon, R.M.S., (1978b): Coal in South Africa, Part 3 – Summary and proposals – the fundamental approach to the characterisation and rationalisation of South Africa’s Coal. *Mineral Science and Engineering*, vol10, issue 2, pp130-153.

Falcon, R.M.S., (1986): A brief review of the origin, formation and distribution of coal in Southern Africa. In: Anhausser, C.R., Maske, S. (Eds.), *Mineral Deposits of Southern Africa*. Geological Society of South Africa, vol. 2, pp1979–1998.

Falcon, R.M.S., (1989): Macro and Micro factors affecting coal seams quality and distribution in the Southern Africa with particular reference to the No. 2 seam, Witbank coalfield, South Africa. In: P.C. Lyons and B. Alperns (Editors) *Peat and Origin: Origin, Facies and Depositional Models*. *International Journal of Coal Geology*, vol12 pp681-731.

Falcon, R.M.S., Pinheiro, H.J., and Shepherd, P., (1984): The Palynostratigraphy of the major coal seams in the Witbank Basin with Lithostratigraphic, Chrostratigraphic, and Palaeoclimatic implications. In: M.J. Lemos de Sousa (editor), *Symposium on Gondwana Coals*, Lisbon. *Proc. And Papers, Com. Serv. Geol. Purtugal*, vol 70 issue 2, pp215-243.

Faure, K., Armstrong, R.A., Harris, C., and Willis, J.P., (1996): Provenance of mudstones in the Karoo Supergroup of the Ellisras Basin, South Africa: geochemical evidences. *Journal of African Earth Sciences*, vol.23, issue 2, 189–204.

Faure, K., Wills, J.P. and Dreyer, J.C., (1996): The Grootegeluk Formation in the Waterberg Coalfield, South Africa: Facies, Palaeoenvironment and thermal history – evidence from the organic clastic material. *International Journal of Coal Geology*, vol. 29, p. 147 – 186.

Floretine, R., Aziz, N., Black, D., and Nghiem, I., (2009): Sorption Characteristics of Coal, Particle Size, Gas type and Time. *University of Wollongong Research Online: Coal Operators’ Conference*, Wollongong, Australia, 2009.

Fourie, C. J. S., and Henry, G., (2009): New airborne geophysical data from the Waterberg Coalfield - South Africa's major future energy source (PositionIT July 2009) www.csir.co.za/nre/mineral_resources/pdfs/CPO-0024.pdf (2009) (PDF file Date accessed 08 November 2012).

Fourie, C.J.S., Henry, G., and Maré, L.P., (2009): Structure of the Karoo-age Ellisras Basin in Limpopo Province, South Africa, in the light of new airborne geophysical data. 11th SAGA Biennial Conference and Exhibition, Swaziland, 16-18 September 2009, pp 27-32.

Fourie, C.J.S. and Stettler, R.H., (2011): New Gravity Data for the Waterberg Coalfield, Coaltech Research Association Annual Colloquium. Url: http://www.coaltech.co.za/Annual_Colloquium/Colloquim%202011/New%20Gravity%20Data%20for%20the%20Waterberg%20Coalfield%20by%20Dr.%20C.J.S.%20Fourie%20&%20R.H.%20Stettler.pdf, accessed on 24th of January, 2013.

Fu, X.H., Qin, Y., and Wang, G.G.X., (2009a): Evaluation of coal structure and permeability with the aid of geophysical logging technology. Fuel, vol. 88, pp2278–2285.

Fu, X.H., Qin, Y., Wang, and G.G.X., (2009b): Evaluation of gas content of coal bedmethane reservoirs with the aid of geophysical logging technology. Fuel, vol. 88, pp2269–2277.

Gamson, P.D., Beamish, B.B., Johnson, D. P., (1993): Coal microstructure and micro-permeability and their effects of natural gas recovery. Fuel, vol.72, pp87-99.

Gane, P.A.C., Ridgway, C.J., Lehtinen, E., Valiullin, R., Furo, I., and Schoelkopf, J., (2004): Comparison of NMR cryoporometry, mercury intrusion porosimetry, and DSC thermoporosimetry in characterizing pore size distributions of compressed finely ground calcium carbonate structures. Industrial Engineering Chemical Research, vol. 43, pp7920-7927.

Garnier, C., Fingueneisel, G., Zimny, T., Pokryszka, Z., Lafortune, S., Défossez, P. D. C. and Gaucher, E.C. (2011): Selection of coals of different maturities for CO₂ Storage by modelling of CH₄ and CO₂ adsorption isotherms. International Journal of Coal Geology, vol. 87, pp80-86.

Gash B.W., (1991): Measurement of Rock Properties in Coal for Coalbed Methane Production. SPE 22909. SPE Annual Technical Conference and Exhibition, 6-9 October 1991, Dallas, Texas.

Gash, B. W., (1991): Measurement of Rock Properties in coal for Coalbed Methane Production. 6th Annual Technical Conference and Exhibition of the Society of Petroleum Engineers, Dallas October. SPE publication, SPE 22909.

Gash, B.W., Volz, R. F., Potter, G., Corgan, J.M., (1992): The Effects of Cleat Orientation and Confining Pressure on Cleat Porosity, Permeability and Relative Permeability in Coal. SCA Conference paper number 9224, Oklahoma.

Gertenbach, R. M.,(2009): Methane and Carbon dioxide Sorption Studies on South African Coals. M. Sc. Thesis, University of Stellenbosch.

Gray, I. (1987): Reservoir engineering in coal seams: Part 1-The physical process of gas storage and movement in coal seams. SPE Reservoir Engineering, vol. 2, issue 1, pp28-34.

GRI, (1994): A Guide to CBM Reservoir Engineering, GRI-94/0397, Published by the Gas Research Institute, Chicago, Illinois.

Gunther, J., (1965): Study of the gas coal relationship. Rev. Ind. Min., Vol. 47 p10.

Hagelskamp, H.H.B., and Snyman, C.P., 1988. On the origin of low reflecting inertinites in coals from the Highveld coalfield, South Africa. Fuel, vol. 67, pp307– 313.

Hanby, K.P., (1991): The use of production profiles for CBM Valuation. Proc., CBM symposium, Tuscaloosa, Alabama, May 1991, pp443-452.

Harpalani, S. and Zhao, X., (1989): An effect of gas desorption on coal Permeability. Presented at 1989 CBM symposium, Tuscaloosa, Al, April 1989. Pp57 -64

Harpalani, S., and Schraufnagel, A., (1990): Measurement of parameters impacting methane recovery from coal seams. International Journal of Mining and Geological Engineering vol. 8, p369-384.

Haughton, S.H., (1963): Stratigraphic History of Africa, South of the Kalahari. Published by Oliver and Boyd. 201p.

Hawkins, J.M., Schraufnagel, R.A., and Olszewski, A.J., (1992): Estimating Coalbed Gas Content and Sorption Isotherm Using Well Log Data. SPE 24905.

Hobday, D. K., (1987): Gondwana coal basins of Australia and South Africa: Tectonic Setting, Depositional System and Resources. In: Coal and Coal – bearing Strata: Recent advances, Geology. Scott, A. C. (editor). Geological Society Special Publication No 2, pp219- 233.

Hobday, D.K., (1973): Middle Ecca Deltaic Deposits in the Muden-Tugela Ferry area of Natal. Geological Society of South Africa Transactions, vol. 76, pp309-318.

Hofer, H., (1915): Schwundspalten (Schlechten, Lassen). [Shrinkage cracks (cleats, separations)]. Mitt. Geol. Ges. Wien, vol. 7, issues 1 and 2.

Hopkins, C.W. et al., (1998): Pitfalls of Injection/Falloff Testing in CBM Reservoirs. SPE paper 39772 presented at the 1998 SPE Permian Basin Oil and Gas Recovery Conference, Midland, Texas, 25-27 March.

Hou, J.S., (2000): Logging Evaluation Technologies and Its Applications for Coalbed Methane Reservoirs. Metallurgical Industry Press, Beijing.

Huy, P.Q., Sasaki, K., Sugai, Y., Ichikawa, S., and (2010): Carbon dioxide gas permeability of coal core samples and estimation of fracture aperture width. *International Journal of Coal Geology*, vol. 83, pp1–10.

I.C.C.P., (1963): *International handbook of coal petrography - part 1-2*, 2nd Edition. Paris, Centre national de la recherche scientifique.

I.C.C.P., (1971): *International handbook of coal petrography – Supplement to 2nd Edition*. Paris, Centre national de la recherche scientifique, 494pp.

ISO Standard 7404-5, (1994): *Methods for the petrographic analysis of bituminous coal and anthracite -- Part 5: Method of determining microscopically the reflectance of vitrinite*. Url: www.iso.org/iso/catalogue_detail.htm?csnumber=14131

ISO Standard 7404-3, (1994): *Methods for the petrographic analysis of bituminous coal and anthracite -- Part 3: Method of determining maceral group composition*. Url: http://www.iso.org/iso/home/store/catalogue_ics/catalogue_detail_ics.htm?csnumber=14129&ICS1=1&ICS2=40&ICS3=73

I.U.P.A.C., (1972): *Manuals of Symbols and terminology of physical, chemical quantities and Units*. London, Butterworth.

Jeffrey, L. S., (2005): Characterization of the Coal Resources of South Africa. *Journal of the South African Institute of Mining and Metallurgy*, Vol. 105, issue 6, Pp 95-102.

Jeffrey, L.S., (2005b): Challenges associated with the further Development of the Waterberg Coalfield. *Journal of the South African Institute of mining and Metallurgy*, vol. 106, pp453 – 458.

Johnson, E.F., Bossler, D.P., and Naumann, V.O., (1959): Calculation of relative Permeability from Displacement Experiment. *Trans. AIME*, vol. 216, p370-372.

Johnson, M. R, Anhaeusser, C. R., and Thomas, R. J., (2006a): *The geology of South Africa*. Geological Society of South Africa, Johannesburg, and Council of Geoscience, Pretoria, 691p.

Jun, Y., Akkutlu, I. Y., Karacan, C. O. and Clarkson, C. R., (2009): Gas Sorption and transport in coals; A poroelastic medium approach. *International Journal of Coal Geology*, vol. 77, issue 1, pp137-144.

Kaiser, E., (1908): Erlxuterungenzur Gecl. Karte von Preussen. (Explanation of the geological map of Prussia). Blatt Bruhe, p44.

King, G.R., (1985): Numerical simulation of the simultaneous flow of methane and water through dual porosity coal seams during the degasification process, Ph.D. Thesis, Pennsylvania State University.

Krystyna, J. K., (2003): Fluorescing macerals in South African Coals. *International Journal of Coal Geology*, vol. 54, pp79-94.

Kuuskra, V.A., Boyer II, C. M., Kelefant, J.A., (1992): Hunt for Quality Basins Goes Abroad. *Oil & Gas Journal*, vol. 90, issue 40, pp49-54.

Kuuskraa, V.A., and Brandenburg, C.F., (1989): Coalbed Methane Sparks a New Energy Industry, *Oil & Gas Journal*, vol. 87, issue 41, p49.

Thomas, L., (2002): *Coal Geology*. Wiley.

Laubach, S.E., Marrett, R. A., Olson, J. E., and Scott A. R. (1998): Characteristics and Origins of Cleat: A review. *International Journal of Coal Geology*, vol. 35, pp175 - 207.

Le Black Smith, G., (1979): High constructive Deltaic Sedimentation and Coal Accumulation, Witbank Basin. *Geological Society of South Africa 18th Congress Abstract*, vol. 2, pp88-89.

Le Black Smith, G., (1980): Genetic Stratigraphy and Paleo-environmental controls on coal distribution in Witbank Basin Coalfield. Unpublished PHD thesis, University of Witwatersrands South Africa.

Letete, T., Guma, M., and Marquard, A., (2009): Information on climate change in South Africa: greenhouse gas emissions and mitigation options. Energy Research Center, University of Cape Town.

Levine, J.R., (1990): Coal Petrology with Applications to CBM R & D. short course presented at Tuscaloosa, Alabama, 13 September 1990.

Levy, J.H., Day, S.J., Killingley, J.S., (1997): Methane capacity of Bowen Basin coals related to Coal Properties. *Fuel*, vol. 76, issue 9, pp813-819.

Li, J., Liu, D., Yao, Y., Cai, Y, and Qiu, Y., (2011): Evaluation of the reservoir permeability of anthracite coals by geophysical logging data. *International Journal of Coal Geology*, vol. 87, pp121–127.

Liu, J., Wang, J., Chen, Z., Wang, S., Elsworth, D., and Jiang, Y., (2011): Impact of transition from local swelling to macro swelling on the evolution of coal permeability. *International Journal of Coal Geology*, vol. 88, pp 31-40.

Lloyd, P., and Alan, C., (2003): Methane Release from South African Coal Mines. Report of a Coaltech 2020–funded study conducted at ERC, University of Cape Town and Itasca Africa (Pty), Ltd.

M2M Projects (2008): Methane to Markets International Coal Mine Methane Projects Database, Methane to Markets, accessed July 2012.

[Http://www2.ergweb.com/cmm/index.aspx](http://www2.ergweb.com/cmm/index.aspx)

M2M, (2008): Summary of the coal Industry, South Africa: CMM Global Overview. www.mathanetomarkets.org/resources/coalmines/docs/overview_ch27.pdf.

MacRae, C. S. (1988): Palynostratigraphic correlation between the lower Karoo sequence of the Waterberg and Pafuri Coal-bearing Basins & the Hammanskraal plant macrofossil locality, Republic of South Africa. – Geological Survey of South Africa Memoirs, 75: 1-217.

Mahajan, O. P., (1991): CO₂ surface area of coals: The 25 years paradox. Carbon, vol. 29, issue 6, pp735-742.

Marsh, H., (1987): Adsorption Method to study micro-porosity in coals and Carbons - a critique. Carbon, vol. 25, issue 1, pp49-58.

Mastalerz, M., Gluskoter, H., and Rupp, J., (2004): Carbon dioxide and Methane sorption in high volatile bituminous coals from Indiana USA. International Journal of Coal Geology, vol. 60, pp43-55.

McElhiney, J.E., Koenig, R.A., and Schraufnagel, R.A. (1989): Evaluation of CBM Reserves Involves Different Techniques, *Oil & Gas Journal*, vol. 87, issue 44, pp 63-72.

McCabe, P. J., and Parrish, J. T. (1992): Tectonic and climatic controls on the distribution and quality of Cretaceous coals. Controls on the Distribution and Quality of Cretaceous Coals: Geological Society of America, Special Paper, vol. 267, pp1-15.

Meyers, R.A., (1982), editor: Coal Structure, Academic Press, New York, 1982.

Monika, J. F., and Krystyna, K.J.K., (2003): Relationship between petrographic and geochemical characterisation of selected South African Coals. International Journal of Coal Geology, vol54, pp95-114.

Moore, E. S., (1932): Coal, its Properties, Analysis, Classification, Geology, Extraction, Uses, and Distribution. John Wiley & Sons, Inc., New York, 1932, 462 pp.

Morin, R.H., (2005): Hydrologic properties of coal beds in the Powder River Basin, Montana I. Geophysical log analysis. Journal of Hydrology, vol. 308, pp227–241.

Mtikulu, M. N., (2009): A provisional Basinal Study of the Waterberg-Karoo, SA. Unpublished Master Thesis, University of Pretoria.

Nandi, S.P., Walker Jr., P. L., (1975): Activated diffusion of methane from coals at elevated pressure. Fuel, vol. 54, pp81-86.

Olajide, O., (2005): The petrophysical analysis and evaluation of hydrocarbon potential of sandstone units in the Bredasdorp Central Basin. Unpublished MSc. Thesis. University of Western Cape.

Opuwari, M., (2010): Petrophysical evaluation of the Albian age gas bearing Sandstone reservoirs of the o-m field, orange Basin, South Africa. Unpublished PHD thesis. University of Western Cape.

Oxburgh, L., (2010): Carbon Capture and Storage – building a low carbon economy. URL: www.ccsassociation.org/index.php/download_file/view/165/76/, accessed July 10, 2012.

Oyler, D.C., Mark, C., and Molinda, G.M., (2010): In situ estimation of rock strength using logging. *International Journal of Coal Geology*, vol. 83, pp484–490.

Pan, Z., and Connel, L.D., (2011): Modelling of anisotropic coal swelling and its impact on permeability behaviour for primary and enhanced coalbed methane recovery. *International Journal of Coal Geology*, vol. 85, pp257–267.

Paterson, L., Meaney, K., and Smyth M., (1992): Measurements of relative permeability, absolute permeability and fracture geometry in coal. *Coal Bed Methane Symposium*, Townsville, November 1992.

Pinheiro, H.J., Pretorius, C.C., Boshoff, H., and Du Cann, V., (1998): Analysis of product samples of producing South African Collieries, Bulletin No 112, Material Science and Technology CSIR, Pretoria, pp1 –43.

Plumstead, E. P., (1957): *Coal in Southern Africa*. Witwatersrand University Press, Johannesburg, 24p.

Plumstead, E. P., (1966): The story of South Africa's Coal. *Optima*, vol.16, issue 12, pp387-402.

Potential Gas Committee., (2001): Potential supply of natural gas in the United States (December 31, 2000): Golden. Colorado, Colorado School of Mines, Potential Gas Committee Report, pp346.

Prevost, X.M., (2004): South African reserves and the Minerals Act. *Coaltrans South Africa*, 1–2 March, 2004, Cape Town. 6p.

Robertson, E.P., (2005): Modelling permeability in coal using sorption-induced strain data. SPE Annual Technical Conference and Exhibition. Society of Petroleum Engineers, Dallas, Texas.

Rogers, E. R., (2007): *Coalbed Methane: Principles & Practice*. Prentice Hall Petroleum Engineering Series.

Reichle D., Houghton J., Kane B., Ekmann J., Benson S., Clarke J., Dahlman R., Hendry G., Herzog H., Hunter-Cevera J., Jacobs G., Judkins R., Ogden J., Palmisano A., Socolow R., Stringer J., Surles T., Wolsky A., Woodward N., York M., (1999): *Carbon Sequestration*

Research and Development, U.S. Department of Energy Report DOE/SC/FE-1. Available at www.ornl.gov/carbon_sequestration/

Reiss, L.H., (1980): The Reservoir Engineering Aspects of Fractured Formations. Gulf Publishing Company, Houston, pp. 67–77.

Robertson, E.P., and Christiansen, R.L., (2005): Measurement of sorption induced strain, Paper 0532, Proceedings of the 2005 International Coalbed Methane Symposium. Tuscaloosa, AL.

Rubidge, B.S., (2005): Reuniting lost continents–fossil reptiles from the ancient Karoo and their wanderlust. South African Journal Geology, vol. 108, p. 135–172.

Rudy, E.R., Mukukumarappan, R., Gary, R., and Muller, M., (2007): CoalBed Methane: Principle and Practice, Perry, J.H. (editor). Oktibheha publishing Co.

Saggerson, E.P., (1991): Distribution of Coal Rank in South Africa. Conference on South Africa's Coal Resources. Geological Society of South Africa, Witbank, 6-9 November, 1991. Abstract.

Saghafi, A., Faiz, M. and Roberts, D., (2007): CO₂ storage and gas diffusivity properties of coals from Sydney Basin, Australia. International Journal of Coal Geology, vol.70, pp240-254.

Schraufnagel, R.A., (1992): CBM Short course Overview, of GRI Research at the Rock Creek Site, Black Warrior Basin, GRI Short Course, Birmingham, Alabama (October 21, 1992).

Schraufnagel, R.A., McBane, R.A., and Kruuskraa, V.A., (1990): CBM Development Faces Technology Gaps. Oil and Gas Journal, vol. 88, issue 6, pp 48-54.

Schroeder, K., Ozdemir, E., Morsi, B., (2001): Sequestration of Carbon Dioxide in Coal Seams. In Proceedings of the First National Conference on Carbon Sequestration, NETL Publication DOE/NETL-2001/1144: May 14. pp 1-10.

Schultz K. H., (2003): Evolution of US Markets for Coal Mine Methane. Climate Mitigation Works Limited and C.C.

Schultz, K.H., (1998): Coalbed Methane Projects: An American and Global Perspective: Identifying Technologies, Markets and Finance Sources for Coal Mine Methane, SMI Conference – Investment Opportunities in Coalbed Methane Programs, U.S. Environmental Protection Agency, Washington, D.C., October 1998.

Seidle, J. P. (2002): Lessons Learned, Lessons Lost-Review of Selected Coalbed Methane Pilots.

Seidle, J., Jeansonne, M., and Erickson, D., (1992): Application of matchstick geometry to stress dependent permeability in coals. In: Proceedings of the SPE rocky mountain regional meeting, Casper, Wyoming, 15–21 May 1992.

Seipker, E. H., (1986): Genetiese Stratigrafie en Sedimentologie van opeenvolging Karoo in die westelike en noordelike deel van watergsteenkoolveld. Unpublished M. Sc Thesis, University of Pretoria.

Shen, J., Qin, Y., Wang, G. X., Fu, X., Wei, C., and Lei, B., (2011): Relative permeabilities of gas and water for different rank coals. *International Journal of Coal Geology*, vol. 86, issue 2, pp266-275.

Sibbit, A.M., Faivre, O., (1985): The dual laterolog response in fractured rocks. SPWLA 26th Annual Logging Symposium Dallas, Texas.

Sing, K.S.W., (2004): Characterisation of porous material: past, present and Future. *Coll Surf A*, vol. 241, pp 3-7.

Singh, A., (1968): Desorption studies of gases from coal. M.Sc. thesis, University of Alberta.

Siriwardane, H., Haljasmaa, I., McLendon, R., Irdi, G., Soong, Y., and Bromhal, G., (2009): Influence of carbon dioxide on coal permeability determined by pressure transient methods. *International Journal of Coal Geology*, vol. 77, pp109–118.

Snyman, C. P., (1998): Coal. In: Wilson, M. G. C. and Anhaeusser, C. R. (Eds). *The Mineral resources of South Africa*. Sixth Ed. Council for Geoscience, Pretoria, pp 136-205.

Snyman, C.P., Barclay, J., (1989): The coalification of South African coal. *International Journal of Coal Geology*, vol. 13, p. 375-390.

Snyman, C.P., and Botha, W.J., (1993): Coal In South Africa: *Journal of African Earth Sciences*, Vol. 16, Issue ½, pp171-180.

South African Committee of Stratigrapher, (1980): *Stratigraphy of South Africa, part I*. Compiled by L.E. Kent. Lithostratigraphy of the Republic of South Africa, S.W. A./ Namibia and the Republics of Bophuthatswan, Transkei and Venda. Handbook Geological Survey of South Africa, Vol. 8, 690p.

Stach, E., Mackowsky, M., Teichmuller, T., Taylor, G.H., Chandra, D., and Teichmuller, R., (1982): *Stach's Textbook of coal Petrology*. Gebr. Borntraeger, Berlin, 535pp.

Stasia, A.A., Hatcher, P.G., Radovicz, L.R., and Benesi, A., (1997): Investigation of the porous structure of coal using ¹²⁹Xe NMR with selective pre-saturation and saturation transfer. Accessed in June 2012, URL: http://web.anl.gov/PCS/acsfuel/preprint%20archive/Files/42_1_SAN%20FRANCISCO_04-97_0294.pdf.

Staton, R., Flores R., Warwick, P. D., Gluskoter, H., and Sticker, G.D., (2001): Coal Bed Sequestration of Carbondioxide. In first national Conference on Carbon Sequestration, US Department of Energy, Washington D.C.

Stoeckinger, W.T., (1990): Kansas Coalbed Methane Comes on Stream. Oil & Gas Journal, vol. 88, issue 23, pp88-90.

Stopes, M.C., (1919): On the Petrology of Banded Bituminous Coals. Fuel, vol. 14, pp4-13.

Stutzer, O., and Noe, A. C., (1940): Geology of Coal. The University of Chicago Press, Chicago, Ill., 461pp.

Suuberg, E.M., Deevi, S.C., and Yun, Y., (1995): Elastic behaviours of coals studied by mercury porosimetry. Fuel, vol. 74, pp1522- 1530.

Teichmuller, M., (1989): The genesis of coal from the view point of coal petrologist. In: P.C. Lyons and B. Alperns (Editors), Peat and Coal: Origin, Facies, and Depositional Models. International Journal Coal Geology, vol.12, pp1-87.

Thakur, P. C., (2003): Optimum Methane Drainage In Gassy Coal Mines. In: 2003 SME Annual Meeting and Exhibit February 24 – 26, Cincinnati, OH . 120pp

Ting, F.T.C., (1997): Origin and spacing of cleats in coal beds. J. Pressure vessel Technol.

Turner, B. R., Whateley. M. K. G., (1983): Structural and sedimentological controls of coal deposition in the Nongoma graben, northern Zululand, South Africa. In: Collinson, J. D. and Lewrn, J., (Eds.), Modern and ancient fluvial systems. Special Publication, International Association of Sedimentologists, Blackwell Sci. Publ., Keele, Staffs., U.K., 457—471Trans. ASME 99, 624-626.

U.S. DOE, (2006): Future Supply and Emerging Resources—Coalbed Natural Gas. Available online at: http://www.netl.doe.gov/technologies/oil-gas/FutureSupply/CoalBedNG/CoalBed_NG.html. Date accessed: July 12, 2006. EPA-HQ-OW-2004-0032, DCN 03480.

U.S. EPA, (2008): U.S. Surface Coal Mine Methane Recovery Project Opportunities, draft Report; EPA430-R-08-001. Coal Bed Methane Outreach Program. Accessed on 12/06/2012.http://www.epa.gov/cmop/docs/cmm_recovery_opps_surface.pdf.

U.S. EPA, (2004): Evaluation of Impacts to Underground Sources of Drinking Water by Hydraulic Fracturing of Coalbed Methane Reservoirs, EPA 816-R-04-003.

U.S. EPA., (2008): U.S. Surface Coal Mine Methane Recovery Project Opportunities, draft Report; EPA430-R-08-001. Coal Bed Methane Outreach Program, accessed June 2012 http://www.epa.gov/cmop/docs/cmm_recovery_opps_surface.pdf.

U.S. EPA, (2010): Coalbed Methane Extraction: Detailed Study Report EPA-820-R-10-022, Pennsylvania, December 2010.

U.S. EPA, (2010a): Screener Survey Database (CBI). EPA-HQ-2008-0517, DCN 07363.

UNFCCC, (2000): South Africa “Initial National Communication to UN Framework Convention on the Climate,” October 2000, p.77. <http://unfccc.int/resource/docs/natc/zafnc01.pdf>.

Van Vuuren, C.J., and Cole D. I., (1979): The Stratigraphy and Depositional environment of the Ecca group in the northern part of the Karoo Basin. Geological Society of South Africa Special publication, vol. 6, pp103-111.

Wagner, N.J., and Tlotleng, M.T., (2012): Distribution of selected trace elements in density fractionated Waterberg Coals from South Africa. International Journal of Coal Geology, vol. 94, pp225–237.

Walker, S., (2000): Major coalfields of the world. IEA Coal Research, London, 131 pp.

Wang, G.X., Massarotto, P., Rudolph, V., (2009): An improved permeability model of coal for coalbed methane recovery and CO₂ geosequestration. Int J. Coal Geology 77, 127–136.

Wang, G.X., Wei, X.R., Wang, K., Massarotto, P., and Rudolph, V., (2010): Sorption-induced swelling/ shrinkage and permeability of coal under stressed adsorption/desorption conditions. International Journal of Coal Geology, vol. 83, issue 1, pp46–54.

Wang, S., Elsworth, D., Liu, J., (2011): Permeability evolution in fractured coal; the roles of fracture geometry and water-content. International Journal of Coal Geology, vol. 87, pp13–25.

Ward, C., (1984): Coal Geology and Technology, Blackburn Scientific publication, 1984, 74p.

Wheaton, J., Donato, T., Reddish, S., and Hammer, L., (2006): 2005 Annual Coalbed Methane Regional Ground-water Monitoring Report: Northern Portion of the Powder River Basin. Open-File Report 538. Montana Bureau of Mines and Geology. DCN 03474.

Winter, M.F.W., (1985): Lower Permian palaeoenvironments of the northern Highveld Coalfield and their relationship to the characteristics of coal seams. Ph.D. thesis, University of Witwatersrand, Johannesburg, 254p.

Yao, Y., Liu, D., Huang, W., Tang, D., and Tang, S., (2006): Research on the pore fractures system properties of coalbed methane reservoirs and recovery of coalbed methane in Huainan and Huaibei coal fields. Journal China Coal Society, vol.31, issue2, pp164-

APPENDICES

Appendix 1: Results of Vitrinite Reflectance Analysis

Well	Sample	Zone	Vit (%)	Random Vitrinite% (RoV)	Standard Deviation	Standard Error of Mean
5	25	11	81	0.64	0.047	0.005
5	30	10	74	0.67	0.045	0.005
5	31	7	75	0.73	0.051	0.005
5	41	4	52	0.73	0.044	0.004
5	43	2	31	0.79	0.07	0.007
5	45	1	5	0.83	0.059	0.006
6	4	11	85	0.63	0.005	0.005
6	7	10	68	0.62	0.046	0.005
6	12	8	68	0.72	0.053	0.005
6	16	5	75	0.72	0.056	0.006
6	19	5	54	0.76	0.057	0.006
6	24	2	24	0.75	0.052	0.005
7	88	11	85	0.64	0.005	0.053
7	90	10	77	0.68	0.006	0.062
7	96	8	76	0.7	0.007	0.072
7	99	5	73	0.71	0.006	0.062
7	102	3	34	0.78	0.008	0.078
8	46	11	74	0.64	0.005	0.053
8	51	10	82	0.64	0.005	0.049
8	54	8	78	0.64	0.005	0.048
8	58	5	69	0.68	0.007	0.066
8	68	3	15	0.78	0.011	0.114
8	69	1	12	0.69	0.017	0.123
8	69s	1	2	0.73	0.009	0.089
9	73	11	88	0.7	0.006	0.062
9	72	8	67	0.66	0.005	0.053
9	78	6	78	0.66	0.007	0.067
9	80	4	52	0.76	0.007	0.074
9	84	3	9	0.84	0.009	0.088
10	105	10	62	0.66	0.006	0.055
10	113	9	82	0.66	0.005	0.051
10	116	8	76	0.67	0.005	0.05
10	6	5	68	0.67	0.006	0.059
10	10	3	3	0.95	0.017	0.122
11	15	11	85	0.66	0.004	0.045
11	20	9	74	0.66	0.005	0.047
11	23	8	66	0.74	0.006	0.061
11	28	5	66	0.74	0.006	0.064
12	2	10	68	0.64	0.005	0.045

12	5	8	85	0.69	0.005	0.051
12	10	7	81	0.71	0.007	0.069
12	13	5	38	0.75	0.006	0.061
15	64	10	76	0.68	0.007	0.68
15	66	10	77	0.66	0.006	0.66
15	69	8	76	0.69	0.006	0.69
15	72	6	76	0.68	0.007	0.68

Where,

VR %: random Vitrinite Reflectance,

RD: Relative density,

VIT: Vitrinite,

PV: Pseudovitrinite,

TV: Total vitrinite,

S/R/C: Sporinite/resinite/cutinite,

ALG: Alginite,

TL: Total Liptinite (Exinite),

RSF: Reactive semifusinite,

ISF: Inert Semifusinite,

F/SCL: Fusinite/Scerotinite,

MIC: Micrinite,

RINT: Reactive Inertoderinite,

lint: Inert inertoderinite,

TI: Total inertinite,

React: Reactive macerals = VIT + TL + RSF + RINT



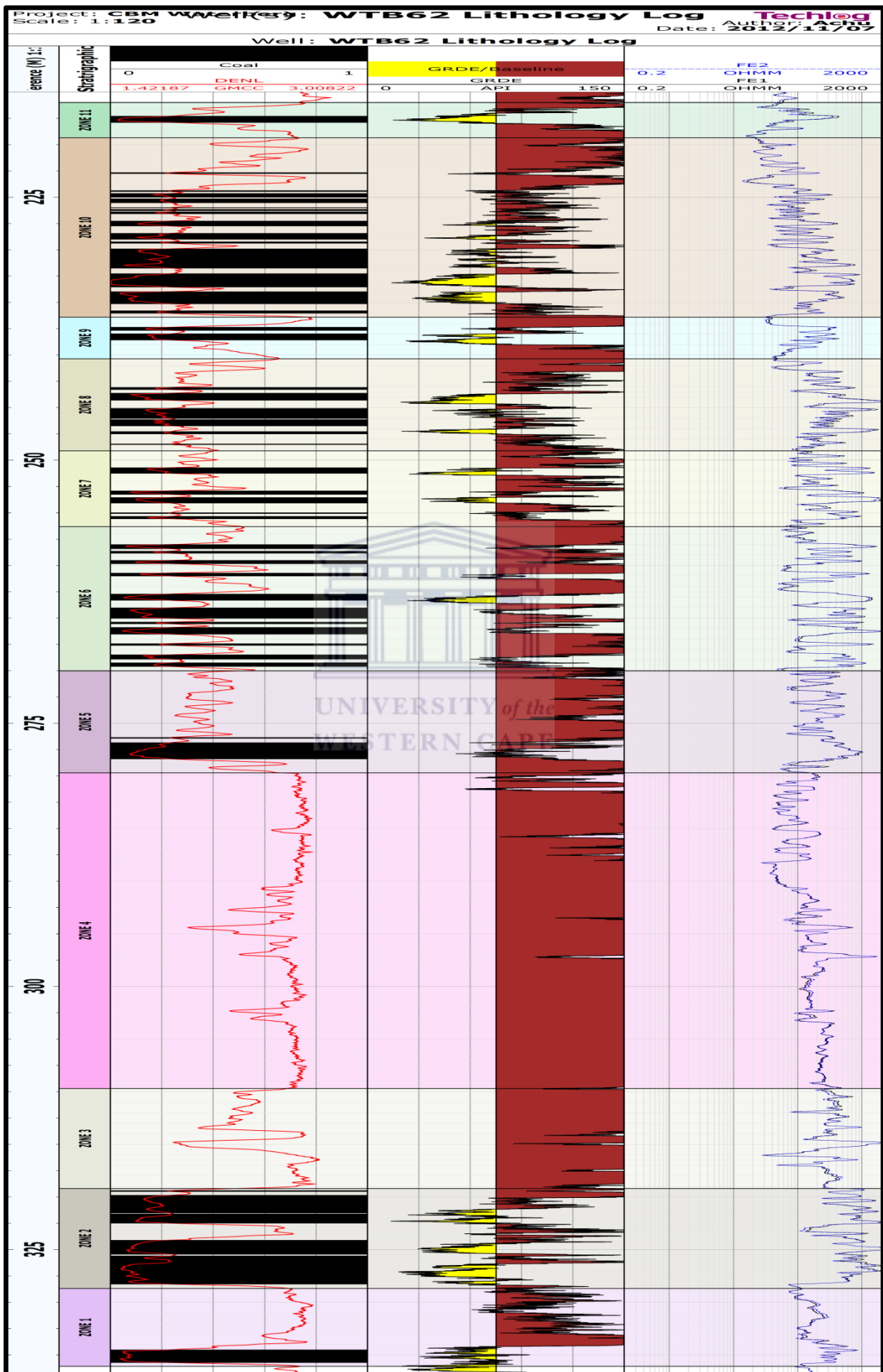
Appendix 2: Results of Petrographic Maceral Analysis

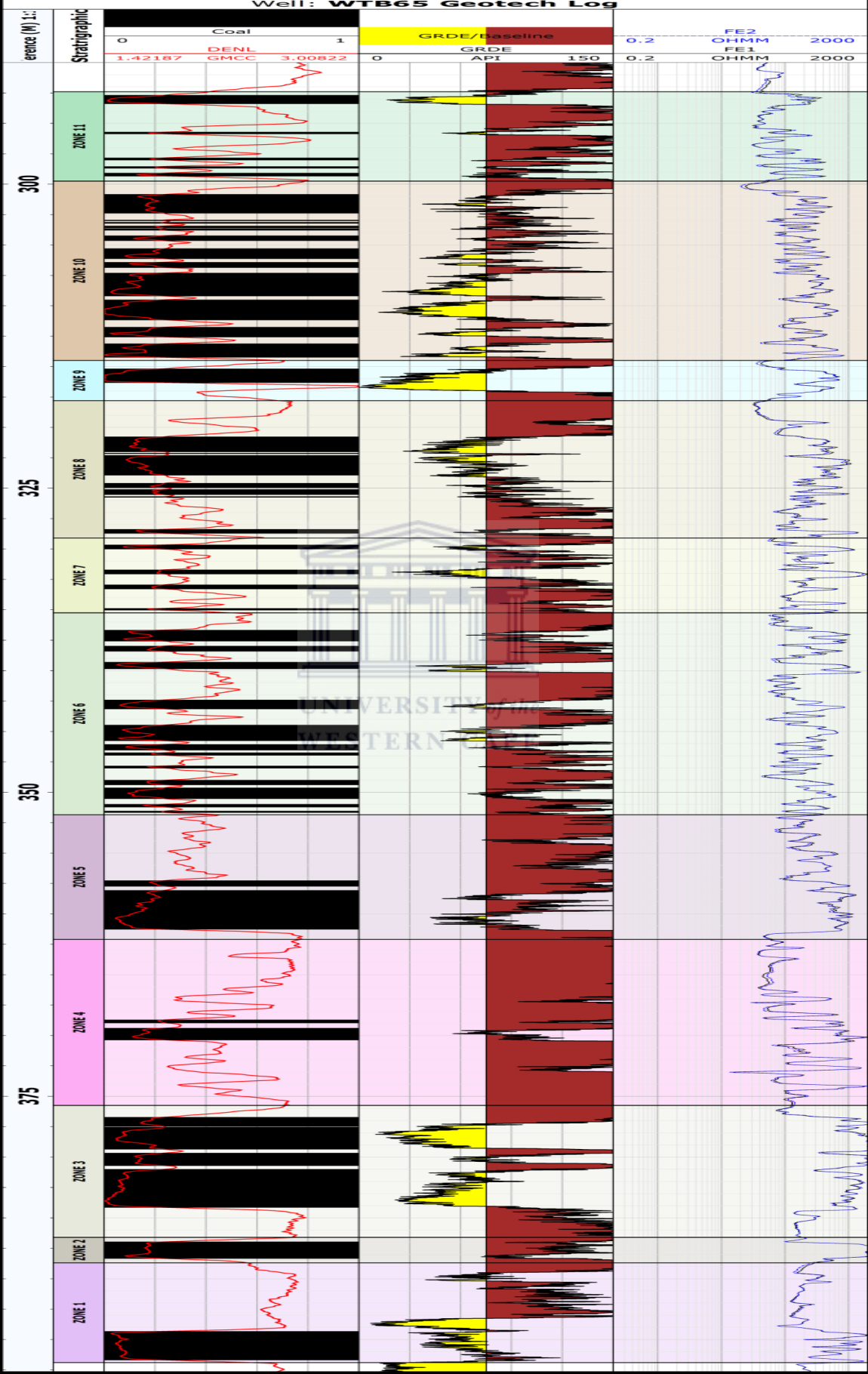
Sample	Zone	VIT	PV	TV	TL	%			React	Min- rals	Pyrite	RoVran% RD=1.80
						RSF	ISF	TI				
25	11	68	13	81	6	1	3	7	88	6	0	0.64
30	10	59	15	74	5	1	4	10	80	11	0	0.67
31	7	51	24	75	5	1	2	7	82	13	0	0.73
41	4	46	6	52	5	6	11	34	66	9	0	0.73
43	2	24	7	31	3	12	21	61	54	5	0	0.79
45	1	5	0	5	3	10	15	82	33	9	1	0.83
4	11	68	17	85	4	1	2	4	90	5	2	0.63
7	10	57	11	68	4	3	4	12	75	14	2	0.62
12	8	52	16	68	3	3	6	17	75	12	0	0.72
16	5	67	8	75	5	2	7	14	83	6	0	0.72
19	5	51	3	54	5	5	12	34	67	7	0	0.76
24	2	21	3	24	6	7	15	57	49	12	1	0.75
88	11	66	19	85	5	0	1	3	90	5	2	0.64
90	10	56	21	77	3	2	3	8	82	12	0	0.68
96	8	58	18	76	4	2	4	9	82	11	0	0.7
99	5	71	2	73	5	2	7	17	80	5	0	0.71
102	3	29	5	34	4	11	19	55	58	7	0	0.78
46	11	60	14	74	4	1	2	6	79	11	5	0.64
51	10	61	21	82	3	0	2	5	85	8	2	0.64
54	8	65	13	78	5	1	1	4	84	9	4	0.64
58	5	65	4	69	6	2	5	16	78	8	1	0.68
68	3	14	1	15	4	12	22	92	53	11	1	0.78
69	1	11	1	12	4	13	15	75	45	9	0	0.69
69s	1	0	2	2	2	13	14	85	39	11	0	0.73
73	11	11	77	88	4	1	4	7	93	12	0	0.7
72	8	63	4	67	4	3	5	13	75	16	0	0.66
78	6	72	6	78	3	2	3	12	83	7	0	0.66
80	4	49	3	52	5	5	14	34	65	9	0	0.76
84	3	9	0	9	3	11	18	77	41	10	1	0.84
105	10	51	10	61	4	1	6	15	67	20	0	0.66
113	9	70	12	82	4	1	1	4	87	10	0	0.66
116	8	68	8	76	4	0	2	7	81	13	0	0.67
6	5	63	5	68	6	3	8	20	77	6	0	0.67
10	3	3	0	3	3	7	10	73	31	21	0	0.95
15	11	70	15	85	3	1	2	7	90	5	0	0.66
20	9	65	9	74	3	0	2	5	78	18	0	0.66
23	8	53	13	66	4	2	4	16	73	14	0	0.74
28	5	54	12	66	5	3	5	17	76	12	0	0.74
2	10	58	10	68	6	2	3	11	77	15	0	0.64
5	8	70	15	85	6	0	2	4	91	5	0	0.69
10	7	73	8	81	8	1	2	7	90	4	0	0.71

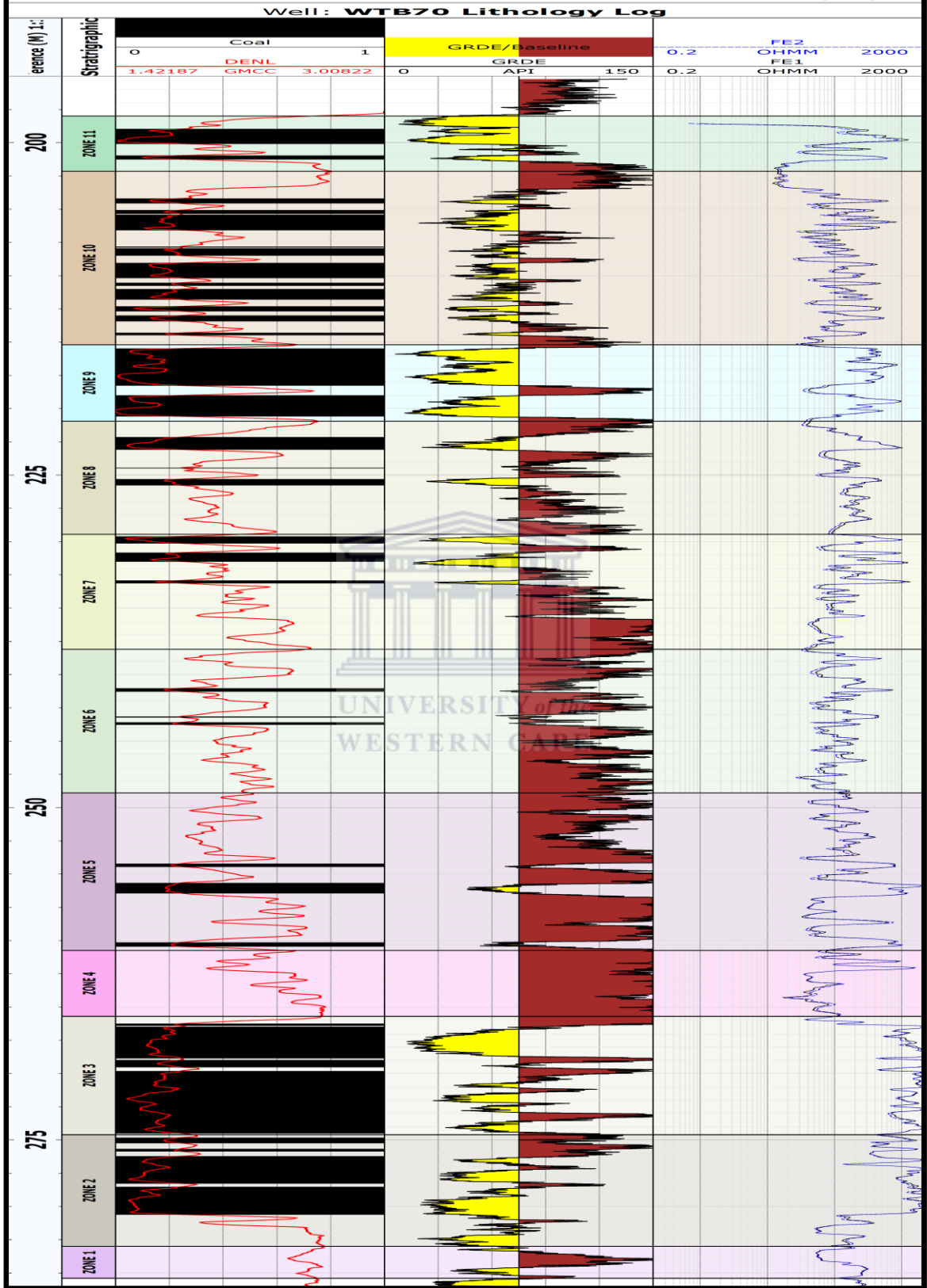
13	5	37	1	38	9	4	9	36	57	16	0	0.75
64	10	63	13	76	5	0	2	4	81	15	0	0.68
66	10	60	17	77	6	1	2	7	84	10	0	0.66
69	8	61	15	76	6	1	3	10	84	17	0	0.69
72	6	61	15	76	6	0	2	5	82	12	1	0.68

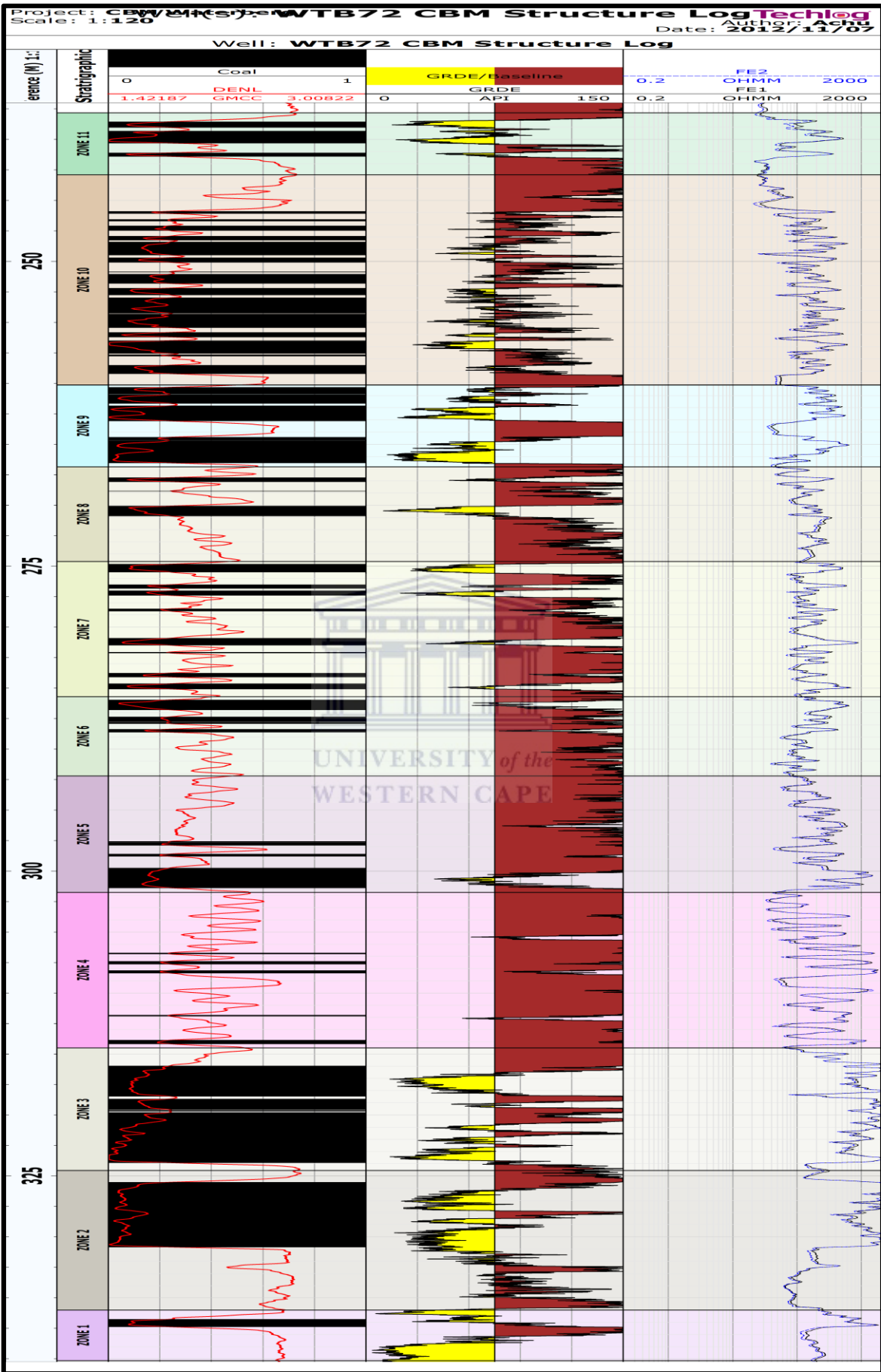


Appendix 3: Composite Log plots for WTB62, WTB65, WTB70 and WTB72.









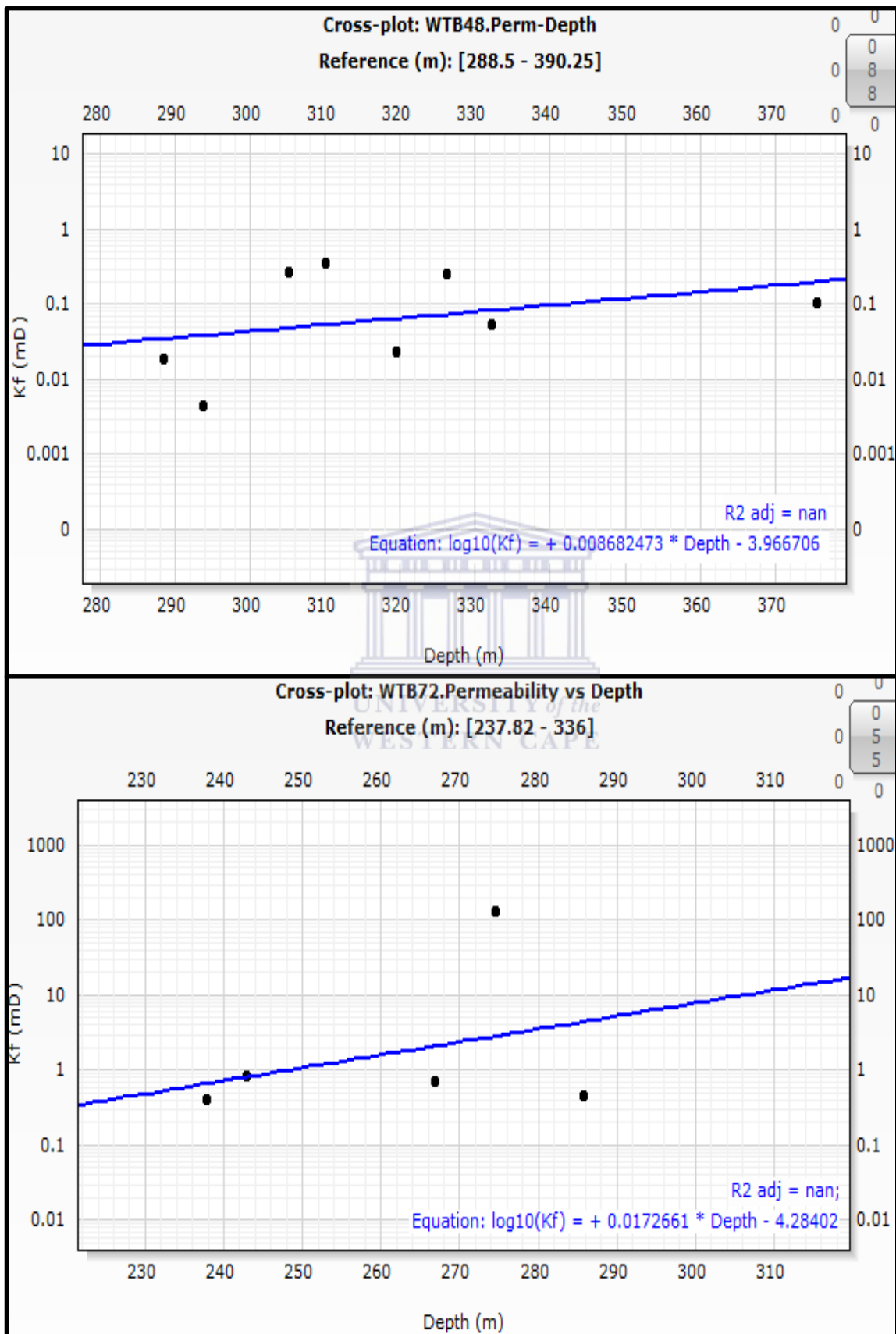
Appendix 4: Water Analysis

WATERBERG CBM 5-SPOT			Well 1		Well 2		Well 3		Well 4		Well 5		Combined		Standard Deviation
Description	Symbol	Mole Mass (g/mole)	mg/l	meq/l	mg/l	meq/l	mg/l	meq/l	mg/l	meq/l	mg/l	meq/l	mg/l	meq/l	
CATIONS															
Calcium	Ca ²⁺	40.08	27.49	1.3720	20.00	0.9980	21.27	1.0615	20.66	1.0312	20.96	1.0459	22.08	1.1017	2.74
Potassium	K ⁺	39.102	14.22	0.3636	14.43	0.3690	13.69	0.3500	14.11	0.3609	12.47	0.3188	13.78	0.3525	0.70
Magnesium	Mg ²⁺	24.312	11.96	0.9837	13.61	1.1196	13.09	1.0771	11.99	0.9866	11.70	0.9625	12.47	1.0259	0.74
Sodium	Na ⁺	22.9898	1918.58	83.4535	2043.27	88.8771	2313.14	100.6158	2278.39	99.1045	1899.97	82.6439	2090.7	90.9390	174.9
Aluminium	Al ³⁺	26.9815	0.15	0.0164	0.06	0.0072	0.06	0.0072	0.08	0.0091	0.06	0.0068	0.084	0.0093	0.032
Boron	B ³⁺	10.811		0.0000		0.0000		0.0000		0.0000		0.0000		0.0000	
Barium	Ba ²⁺	137.34	1.86	0.0271	1.35	0.0196	1.15	0.0168	1.03	0.0149	1.19	0.0173	1.31	0.0191	0.29
Cadmium	Cd ²⁺	112.4		0.0000		0.0000		0.0000		0.0000		0.0000		0.0000	
Cobalt	Co ²⁺	58.9332		0.0000		0.0000		0.0000		0.0000		0.0000		0.0000	
Chromium	Cr ³⁺	51.996		0.0000		0.0000		0.0000		0.0000		0.0000		0.0000	
Copper	Cu ²⁺	63.54		0.0000		0.0000		0.0000		0.0000		0.0000		0.0000	
Total Iron	Fe ²⁺ + Fe ³⁺	55.847	0.73	0.0392	0.80	0.0431	1.05	0.0566	0.90	0.0483	0.71	0.0384	0.84	0.0451	0.13
Manganese	Mn ²⁺	54.938	0.05	0.0019	0.03	0.0012	0.03	0.0011	0.03	0.0011	0.03	0.0011	0.04	0.0013	0.01
Nickel	Ni ²⁺	58.71		0.0000		0.0000		0.0000		0.0000		0.0000		0.0000	
Lead	Pb ²⁺	207.19	0.12	0.0011	0.09	0.0008	0.09	0.0009	0.08	0.0008	0.07	0.0006	0.09	0.0009	0.02
Strontium	Sr ²⁺	87.62	0.40	0.0091	0.31	0.0071	0.31	0.0072	0.43	0.0098	0.24	0.0055	0.34	0.0077	0.07
Zinc	Zn ²⁺	65.37		0.0000		0.0000		0.0000		0.0000		0.0000		0.0000	
Ammonia	NH ₃ - N	14.0067		0.0000		0.0000		0.0000		0.0000		0.0000		0.0000	
ANIONS															
Bicarbonate	HCO ₃ ⁻	61.016	4784.79	78.4186	5460.10	89.4864	6061.79	99.3476	5876.36	96.3085	4860.23	79.6551	5408.7	88.6432	517.3
Carbonate	CO ₃ ²⁻	60.0081	8.76	0.2918	9.58	0.3194	8.01	0.2669	8.55	0.2849	7.68	0.2561	8.52	0.2838	0.66
Fluoride	F ⁻	18.9984	3.22	0.1693	3.53	0.1860	4.18	0.2199	4.81	0.2531	3.46	0.1819	3.84	0.2020	0.58
Chloride	Cl ⁻	35.453	368.47	10.3933	349.23	9.8506	352.24	9.9354	351.93	9.9266	363.83	10.2624	357.1	10.0737	7.6
Nitrate	NO ₃ ⁻ - N	14.0067	0.36	0.0256	0.11	0.0079	0.12	0.0084	0.14	0.0102	0.11	0.0076	0.17	0.0119	0.10
Sulphate	SO ₄ ²⁻	96.06	7.11	0.1479	5.04	0.1050	5.47	0.1139	6.27	0.1306	5.00	0.1041	5.78	0.1203	0.81
Phosphate	PO ₄ ³⁻ - P	30.974	0.23	0.0226	0.49	0.0478	0.53	0.0514	0.53	0.0515	0.41	0.0392	0.44	0.0425	0.11
Nitrite	NO ₂ ⁻ - N	14.0067		0.0000		0.0000		0.0000		0.0000		0.0000		0.0000	
Sulphur	S ²⁻	32.064		0.0000		0.0000		0.0000		0.0000		0.0000		0.0000	
Cyanide	CN ⁻	26.018		0.0000		0.0000		0.0000		0.0000		0.0000		0.0000	
Silica	SiO ₃ ²⁻ - Si	28.086	7.39	0.5265	11.35	0.8084	10.01	0.7125	10.82	0.7703	11.39	0.8114	10.19	0.7258	1.49
OTHER															
Conductivity	Cond.	µS/cm	7039.47		7836.00		8514.83		8378.93		7116.33		7777		615
Chemical Oxygen Demand	C.O.D	mg/l	14.42		16.90		17.75		21.04		14.34		16.9		2.5
pH	pH	-	7.39		7.73		7.54		7.60		7.53		7.56		0.11
Suspended Solids	S.S.	mg/l	16.95		20.28		27.00		26.48		23.34		22.8		3.8
Total Alkalinity	Alk Total	mg/l CaCO ₃	4555.11		5073.37		5535.28		5374.93		4452.90		4998.3		431.2
Total Dissolved Solids @ 180 °C	DS @ 180 °C	mg/l	4646.58		5341.23		5846.72		5814.36		4782.10		5286.2		501.9
Total Hardness	TH	mg/l CaCO ₃	122.42		106.93		107.82		103.93		102.76		108.8		7.1
Turbidity	Turb.	NTU	2.26		4.46		8.25		6.15		4.77		5.2		2.0
STATISTICS															
Sum of cations	Σ(Cations)		86.2676	meq/l	91.4429	meq/l	103.1942	meq/l	101.5672	meq/l	85.0408	meq/l	93.5025	meq/l	7.6
Sum of anions	Σ(Anions)		89.9955	meq/l	100.8114	meq/l	110.6560	meq/l	107.7357	meq/l	91.3178	meq/l	100.1033	meq/l	8.4
Difference	= [Σ(Cations)-Σ(Anions)]		-2.11	%	-4.87	%	-3.49	%	-2.95	%	-3.56	%	-3.41	%	0.9
Measured TDS	TDS @ 180 °C	mg/l	4646.6	mg/l	5341.2	mg/l	5846.7	mg/l	5814.4	mg/l	4782.1	mg/l	5286.2	mg/l	501.9
Calculated TDS	[Σ(Cations)+Σ(Anions)]	mg/l	7155.9	mg/l	7933.4	mg/l	8806.2	mg/l	8587.1	mg/l	7199.5	mg/l	7936.4	mg/l	683.0
Measured TDS/Calculated TDS			0.649		0.673		0.664		0.677		0.664		0.666		0.010
Measured TDS/Conductivity			0.660		0.682		0.687		0.694		0.672		0.680		0.012
Calculated TDS/Conductivity			1.017		1.012		1.034		1.025		1.012		1.020		0.009

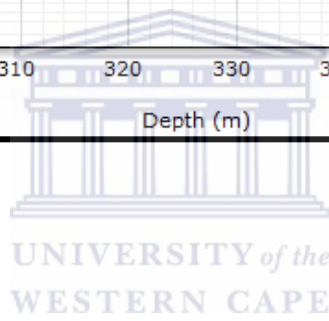
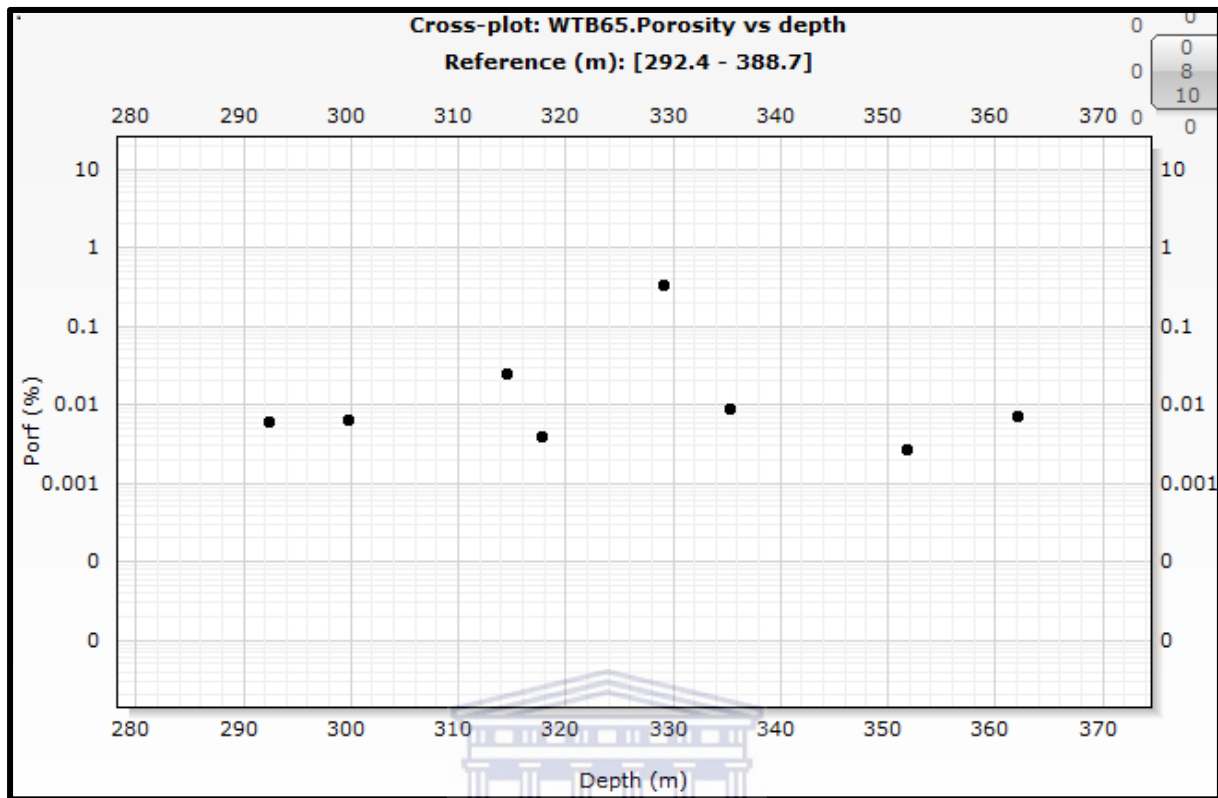
Appendix 5: Gas and Coal Quality Data

Column Description n:	Borehole	Seam	Number of Samples	Zone	From (m)	To (m)	Can Desorbed Gas (scf/t)	Lost Gas (scf/t)	Total Can Desorb Gas (scf/t)	N2 % norm Desorbed	CH4% norm Desorbed	CO2% norm Desorbed	Residual Gas (scf/t)	N2% norm Residual	CH4% norm Residual	CO2% norm Residual	CH4% norm	CO2% norm	N2% norm	SUM	SUM desorbed gas norm	Raw RD
1092	WTB62		1	11	217.63	218.2	38.46	0.98	39.44	2.33	70.92	26.74	84.23	28.56	53.83	17.62	55.13	18.31	26.56	100.00	100.00	1.48
1093	WTB62		1	10	230.74	231.27	57.35	2.99	60.34	1.68	76.77	21.55	47.52	27.51	47.00	25.49	51.18	24.94	23.88	100.00	100.00	1.70
1094	WTB62		3	10	233.02	233.59	58.59	2.92	61.51	1.98	76.56	21.45	149.48	19.44	56.14	24.43	57.42	24.24	18.34	100.00	100.00	1.40
1095	WTB62		1	10	234.17	235.48	67.05	3.04	70.09	1.80	75.71	22.49	85.47	20.93	55.12	23.95	57.41	23.79	18.80	100.00	100.00	1.49
1096	WTB62		4	9	238.3	238.85	40.14	1.09	41.23	2.06	74.06	23.89	83.28	18.25	55.67	26.08	56.99	25.92	17.08	100.00	100.00	1.60
1097	WTB62		3	8	240.97	242.91	65.59	2.20	67.78	1.71	71.17	27.11	73.42	17.22	55.61	27.17	57.51	27.16	15.32	100.00	100.00	1.50
1098	WTB62		2	8	243.29	244.54	59.73	2.11	61.84	1.86	72.69	25.45	83.57	15.68	56.35	27.97	63.30	26.90	9.80	100.00	100.00	1.51
1099	WTB62		2	7	250.9	251.64	51.59	2.00	53.59	1.91	70.74	27.35	84.72	20.04	50.39	29.57	52.31	29.36	18.33	100.00	100.00	1.51
1100	WTB62		1	6	258.03	261.09	53.48	0.69	54.17	2.57	70.41	27.01	84.09	17.98	49.88	32.14	51.93	31.63	16.44	100.00	100.00	1.51
1101	WTB62		1	6	265.92	266.45	45.18	0.55	45.73				78.60	11.28	54.35	34.37				0.00	0.00	1.59
1102	WTB62		1	3	315.41	315.93	1.26	0.05	1.31	54.96	28.87	16.16	18.35	45.86	9.10	45.04	10.02	43.70	46.28	100.00	100.00	1.66
1103	WTB62		1	2	320.81	321.33	2.48	0.05	2.53	32.13	19.49	19.57	25.32	37.76	22.26	39.98	22.03	38.28	37.30	97.61	71.19	1.63
1104	WTB62		1	2	321.54	322.09	2.58	0.13	2.72	51.80	15.55	32.65	27.62	28.01	28.27	43.72	27.39	42.95	29.66	100.00	100.00	1.60
1105	WTB62		1	2	325.47	326	2.55	0.06	2.61	49.31	19.59	31.10	30.71	5.09	66.69	28.21	63.96	28.38	7.66	100.00	100.00	1.46
1106	WTB62		1	1	335.88	336.45	2.65	0.11	2.76	63.84	10.20	25.96	14.97	22.68	59.10	18.22	53.66	19.08	27.26	100.00	100.00	1.60
1261	WTB70	BS1	2	11	199.82	200.81	35.72	1.47	37.19	5.34	78.92	15.74	17.47	2.56	83.46	13.98	80.37	15.18	4.45	100.00	100.00	1.55
1262	WTB70	BS1	3	10	204.19	206.92	57.59	3.04	60.62	3.90	73.15	22.95	16.32	0.38	75.83	23.79	73.72	23.13	3.15	100.00	100.00	1.47
1263	WTB70	BS1	3	9 and 10	213.52	215.88	42.92	2.61	45.54	1.67	73.61	24.73	42.69	0.39	82.71	16.90	78.01	20.94	1.05	100.00	100.00	1.57
1264	WTB70	BS1	2	9	217.56	218.18	79.32	22.33	101.66	3.87	71.56	24.57	16.68	0.68	82.38	16.94	72.41	23.97	3.62	100.00	100.00	1.51
1265	WTB70	BS1	2	9	219.73	220.58	62.42	2.92	65.34	1.71	71.55	26.74	17.27	12.96	77.00	10.05	72.69	23.25	4.06	100.00	100.00	1.49
1266	WTB70	BS1	1	7	231.61	232.18	45.72	2.50	48.22	1.50	73.87	24.63	56.55	2.15	77.61	20.24	75.89	22.26	1.85	100.00	100.00	1.60
1267	WTB70	ES3	1	3	268.63	269.18	2.68	0.37	3.05	-	-	-	2.56	-	-	-	-	-	-	0.00	0.00	1.51
1268	WTB70	ES2	2	2	275.26	276.66	0.95	0.21	1.17	-	-	-	10.62	65.65	6.69	27.65	6.69	27.65	65.65	100.00	0.00	1.63
1269	WTB70	ES2	2	2	277.61	278.76	1.63	0.08	1.70	-	-	-	14.23	80.55	8.52	10.93	8.52	10.93	80.55	100.00	0.00	1.52
1270	WTB70	ES2	2	2	280.67	281.81	0.40	0.04	0.44	-	-	-	19.56	46.49	31.79	21.72	31.79	21.72	46.49	100.00	0.00	1.46
1284	WTB72	BS1	2	11	238.72	239.61	8.58	0.35	8.93	7.80	82.99	9.21	24.79	6.06	85.21	8.72	84.62	8.85	6.52	100.00	100.00	1.55
1285	WTB72	BS1	3	10	249.15	250.15	21.80	0.86	22.66	8.06	85.95	5.99	22.61	4.96	89.59	5.45	87.77	5.72	6.51	100.00	100.00	1.55
1286	WTB72	BS1	2	10	255.96	257.07	26.87	1.07	27.94	5.29	88.66	6.05	37.78	0.52	93.04	6.44	91.18	6.27	2.55	100.00	100.00	1.51
1287	WTB72	BS1	3	8	270.03	270.77	21.78	1.11	22.89	4.34	89.67	6.00	21.79	0.79	91.29	7.92	90.46	6.94	2.61	100.00	100.00	1.73
1288	WTB72	BS1	1	7	280.67	281.24	21.39	0.93	22.32	6.10	86.14	7.77	30.53	1.74	91.32	6.94	89.13	7.29	3.58	100.00	100.00	1.57
1289	WTB72	BS1	3	6 and 7	284.5	286.20	28.41	1.39	29.80	5.46	86.37	8.17	18.06	0.76	91.81	7.43	88.42	7.89	3.68	100.00	100.00	1.55
1290	WTB72	BS1	1	5	300.34	300.91	46.85	2.45	49.30	1.29	85.01	13.70	23.97	0.75	91.03	8.22	86.98	11.90	1.12	100.00	100.00	1.68
1291	WTB72	ES3	1	3	316.1	316.67	0.40	0.01	0.42	-	-	-	1.33	-	-	-	-	-	-	0.00	0.00	1.72
1292	WTB72	ES3	1	3	318.71	319.28	0.56	0.04	0.60	-	-	-	6.59	86.83	1.21	11.96	1.21	11.96	86.83	100.00	0.00	1.70
1293	WTB72	ES2	1	2	325.66	326.23	0.56	0.02	0.59	-	-	-	2.54	-	-	-	-	-	-	0.00	0.00	1.56
1294	WTB72	ES2	1	2	327.28	327.83	1.18	0.13	1.31	-	-	-	1.24	-	-	-	-	-	-	0.00	0.00	1.53
1015	WTB56	BS1	3	11 and 10	276.75	279.73	53.61	1.27	54.88	10.32	51.49	38.20	60.98	23.22	37.00	25.50	43.79	31.45	17.17	92.41	100.00	
1016	WTB56	BS1	3	10	280.18	282.20	58.60	2.25	60.85	3.78	56.70	39.51	62.03	20.68	46.86	32.46	51.74	35.95	12.31	100.00	100.00	
1017	WTB56	BS1	2	10	282.95	285.22	74.90	2.57	77.47	2.03	59.51	38.46	53.86	27.66	42.20	30.13	52.41	35.05	12.54	100.00	100.00	
1018	WTB56	BS1	2	10	287.15	288.69	27.34	2.22	29.56				35.20	29.89	44.01	26.10				0.00	0.00	
1019	WTB56	BS1	3	10	288.69	289.99	73.91	2.04	75.95	1.62	54.17	44.22	84.09	21.01	44.06	34.93	48.86	39.34	11.81	100.00	100.00	
1020	WTB56	BS1	2	9	293.54	294.64	70.24	2.52	72.76	1.65	58.06	40.28	60.04	23.26	41.39	35.35	50.53	38.05	11.42	100.00	100.00	
1021	WTB56	BS1	1	9	295.02	295.58	59.41	1.49	60.90	3.02	51.67	45.31	75.49	19.70	44.04	36.26	47.45	40.30	12.25	100.00	100.00	
1022	WTB56	BS1	3	8	298.30	300.40	55.45	3.25	58.70	2.51	51.67	45.82	55.89	27.52	38.02	34.46	45.02	40.28	14.70	100.00	100.00	
1023	WTB56	BS1	4	8	303.78	305.56	51.93	1.67	53.60	1.72	55.90	42.38	58.66	23.60	37.45	38.94	46.26	40.58	13.15	100.00	100.00	
1024	WTB56	BS1	3	8	306.49	307.80	58.93	1.91	60.84	1.61	55.90	42.48	73.85	23.58	38.09	38.32	46.14	40.20	13.66	100.00	100.00	
1025	WTB56	BS1	1	8	309.46	310.04	63.77	2.71	66.49	2.07	54.10	43.83	36.14	24.12	39.24	36.64	48.87	41.30	9.83	100.00	100.00	
1026	WTB56	BS1	3	6	324.76	326.14	82.28	1.95	84.23	1.11	51.41	47.48	41.52	29.14	34.58	36.28	45.85	43.78	10.36	100.00	100.00	
1027	WTB56	BS1	3	6	327.51	328.56	63.73	1.57	65.30	1.03	45.86	53.11	56.99	22.06	39.41	38.53	42.85	46.32	10.83	100.00	100.00	
1028	WTB56	BS1	1	6	332.78	333.32	32.45	0.43	32.88	1.19	46.18	52.63	20.14	35.18	31.29	33.54	40.52	45.38	14.10	100.00	100.00	
1029	WTB56	TR	3	4	345.89	347.83	16.73	0.12	16.86	1.92	46.53	51.55	25.05	38.08	26.43	35.49	34.51	41.95	23.54	100.00	100.00	
1030	WTB56	ES3	2	3	350.24	351.34	44.49	0.81	45.30	1.93	49.03	49.04	42.37	46.05	21.14	32.81	35.55	41.19	23.26	100.00	100.00	
1031	WTB56	ES3	1	3	353.75	354.32	35.04	0.38	35.42	2.36	48.67	48.97	17.93	41.77	28.34	29.89	41.83	42.56	15.61	100.00	100.00	
1032	WTB56	ES3	1	3	353.18	353.75	41.42	0.27	41.69	1.71	39.50	58.79	37.55	7.20	46.00	46.80	42.58	53.11	4.31	100.00	100.00	
1033	WTB56	ES3	1	3	354.36	354.94	44.21	0.62	44.82	1.62	39.84	58.53	43.83	19.62	41.00	39.38	40.42	49.06	10.52	100.00	100.00	
1034	WTB56	ES2	1	2	367.75	368.32	16.69	0.48	17.16	3.41	49.04	47.55	17.69	19.57	39.79	40.64	44.34	44.04	11.61	100.00	100.00	
1035	WTB56	ES2	1	2	369.99	370.54	18.99	0.72	19.71	5.50												

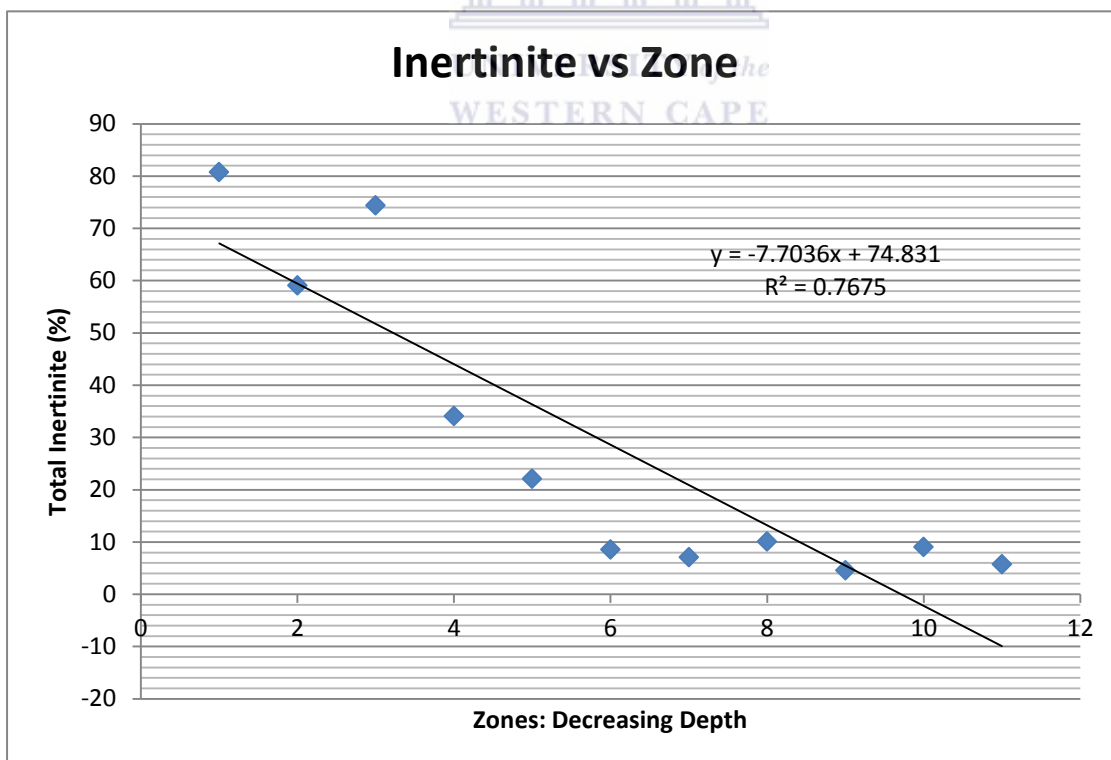
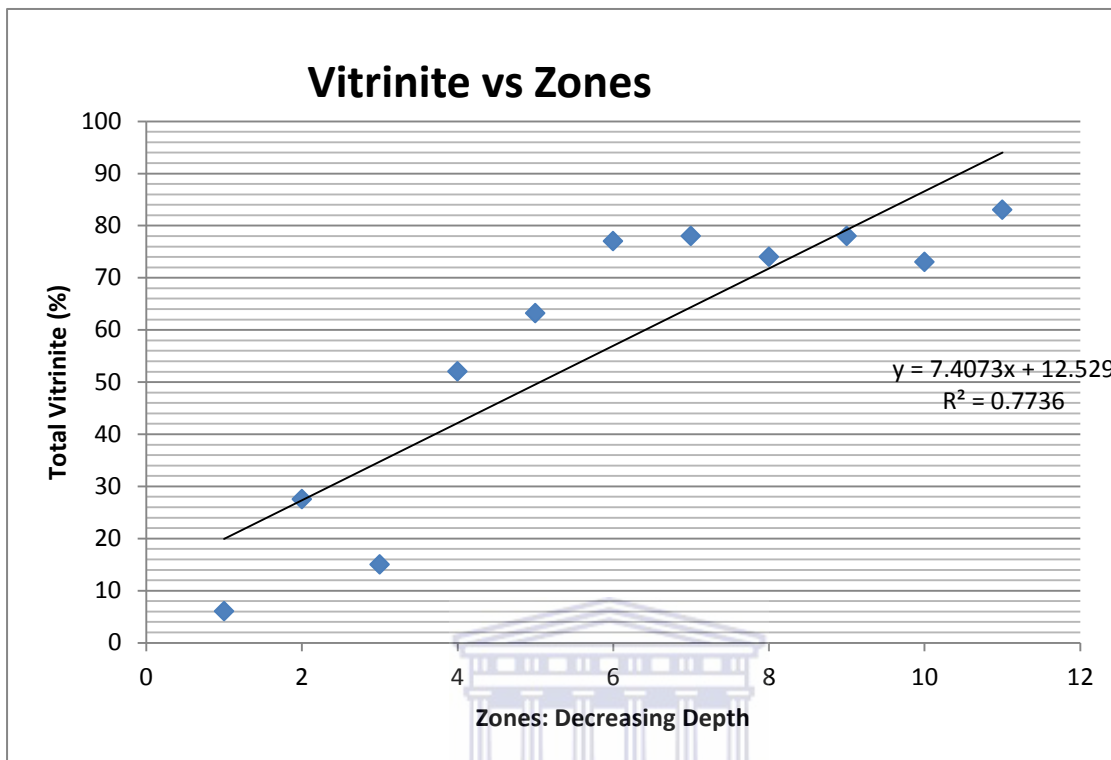
Appendix 6: Permeability vs Depth plots for WTB48 and 72

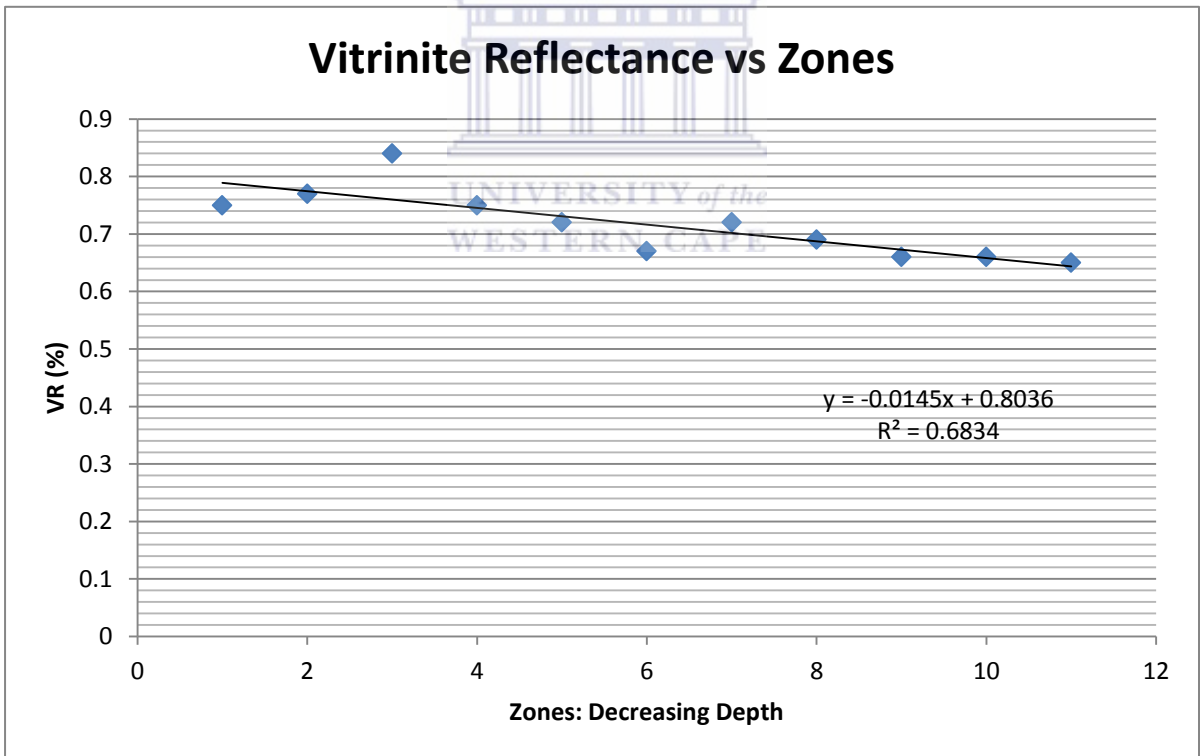
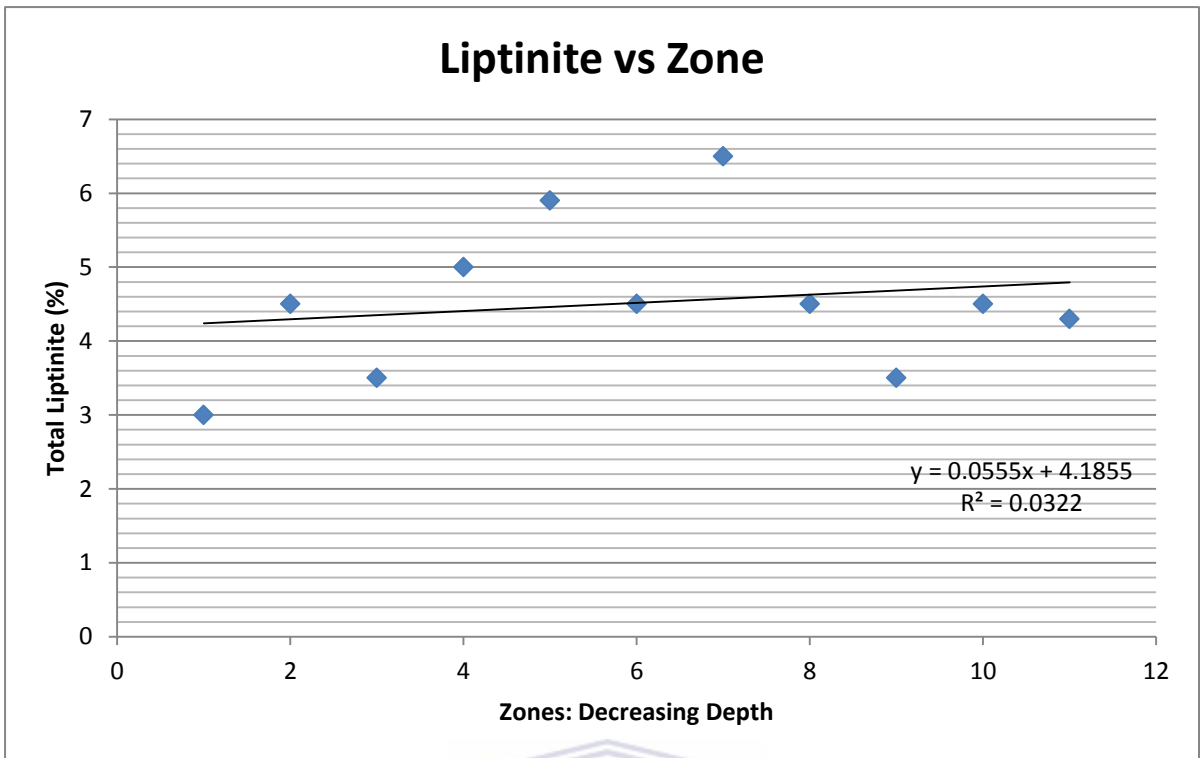


Appendix 7: Porosity Depth Plots for WTB56.

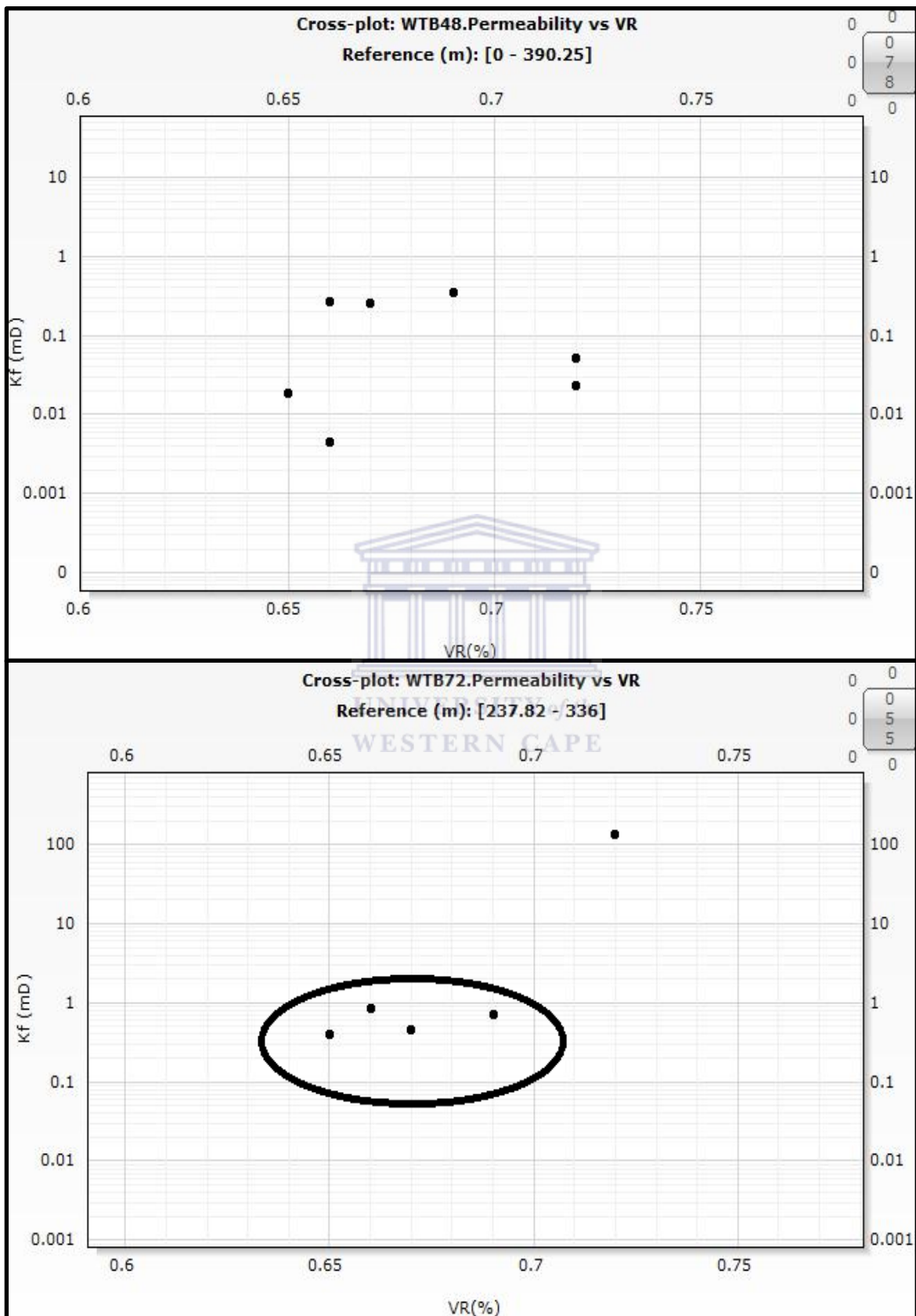


Appendix 8: Cross Plots of Vitrinite content, Liptinite content, Inertinite content and Vitrinite Reflectance vs Depth (zones)

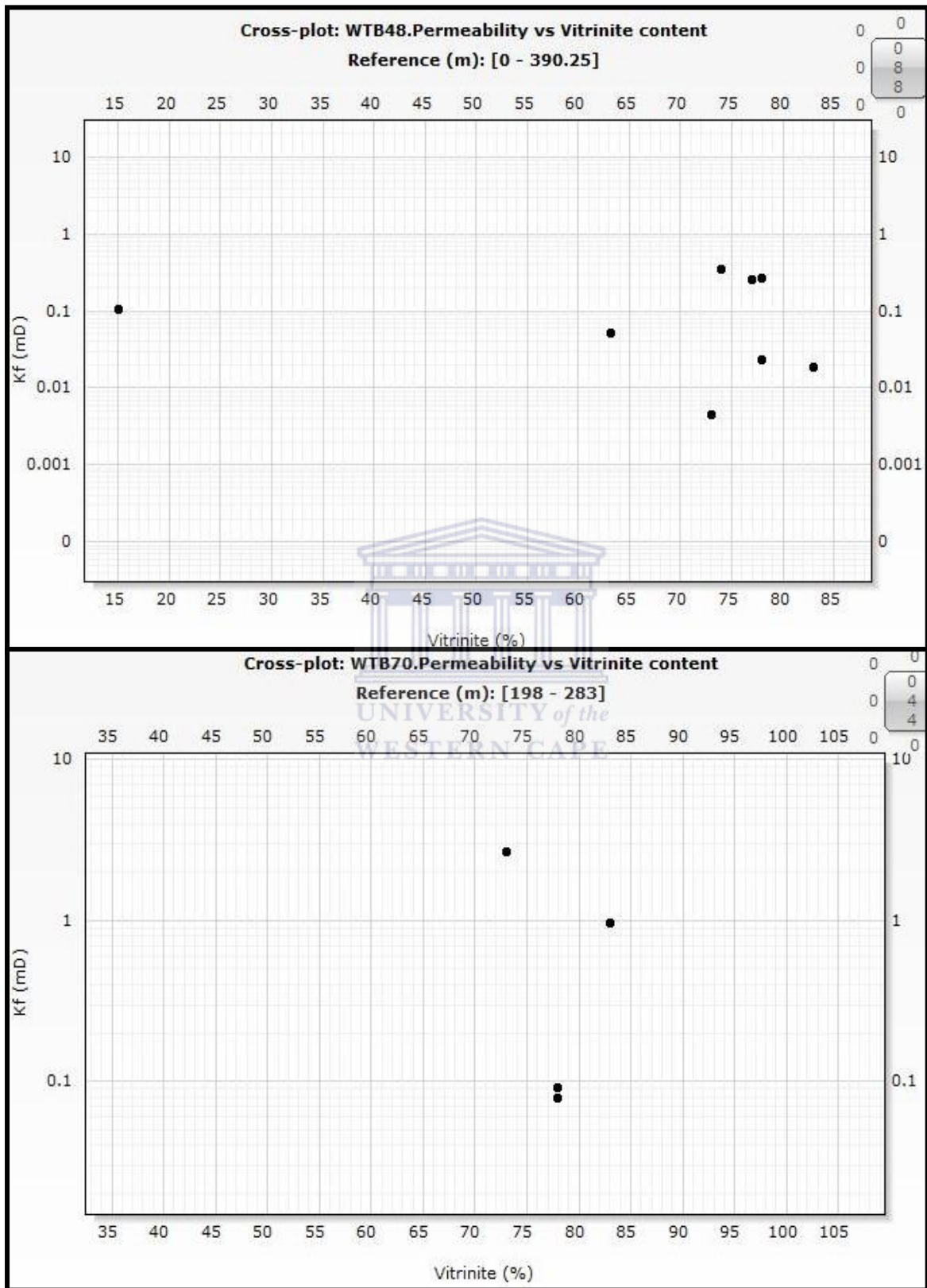


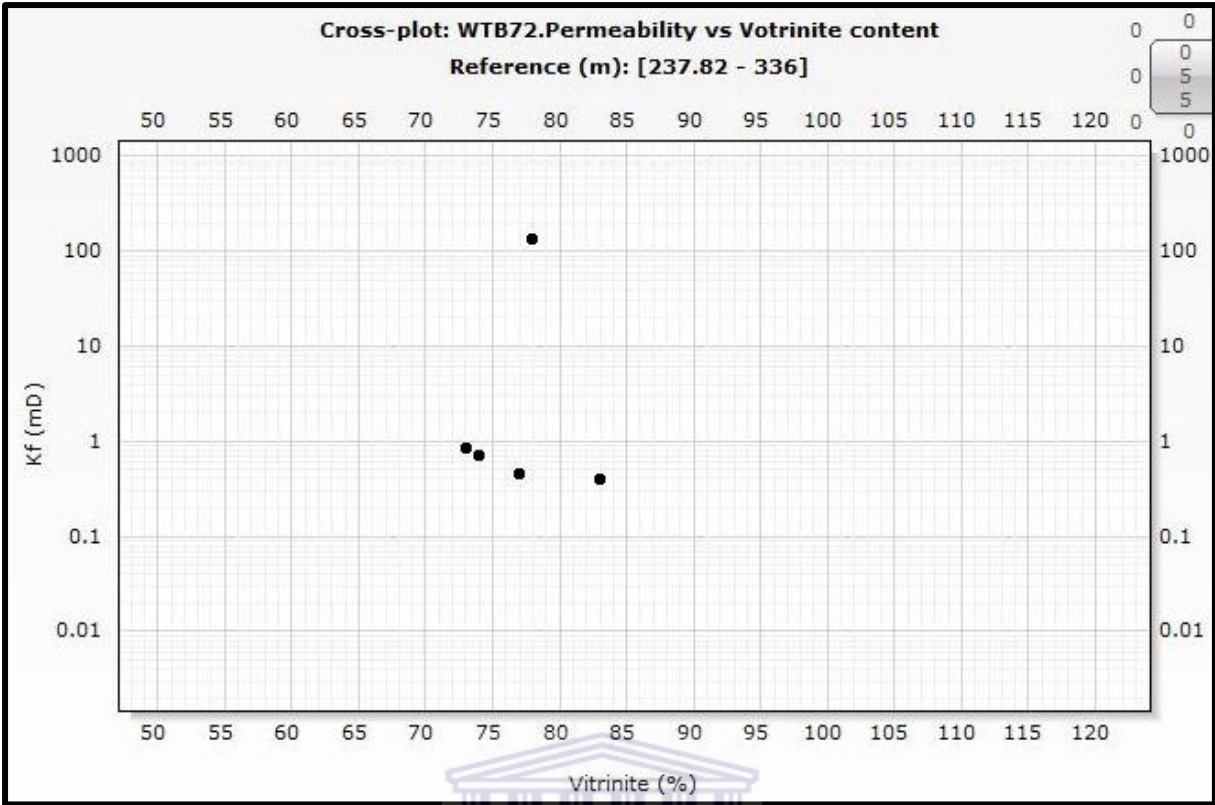


Appendix 9: Permeability vs VR plots for WTB48 and 70

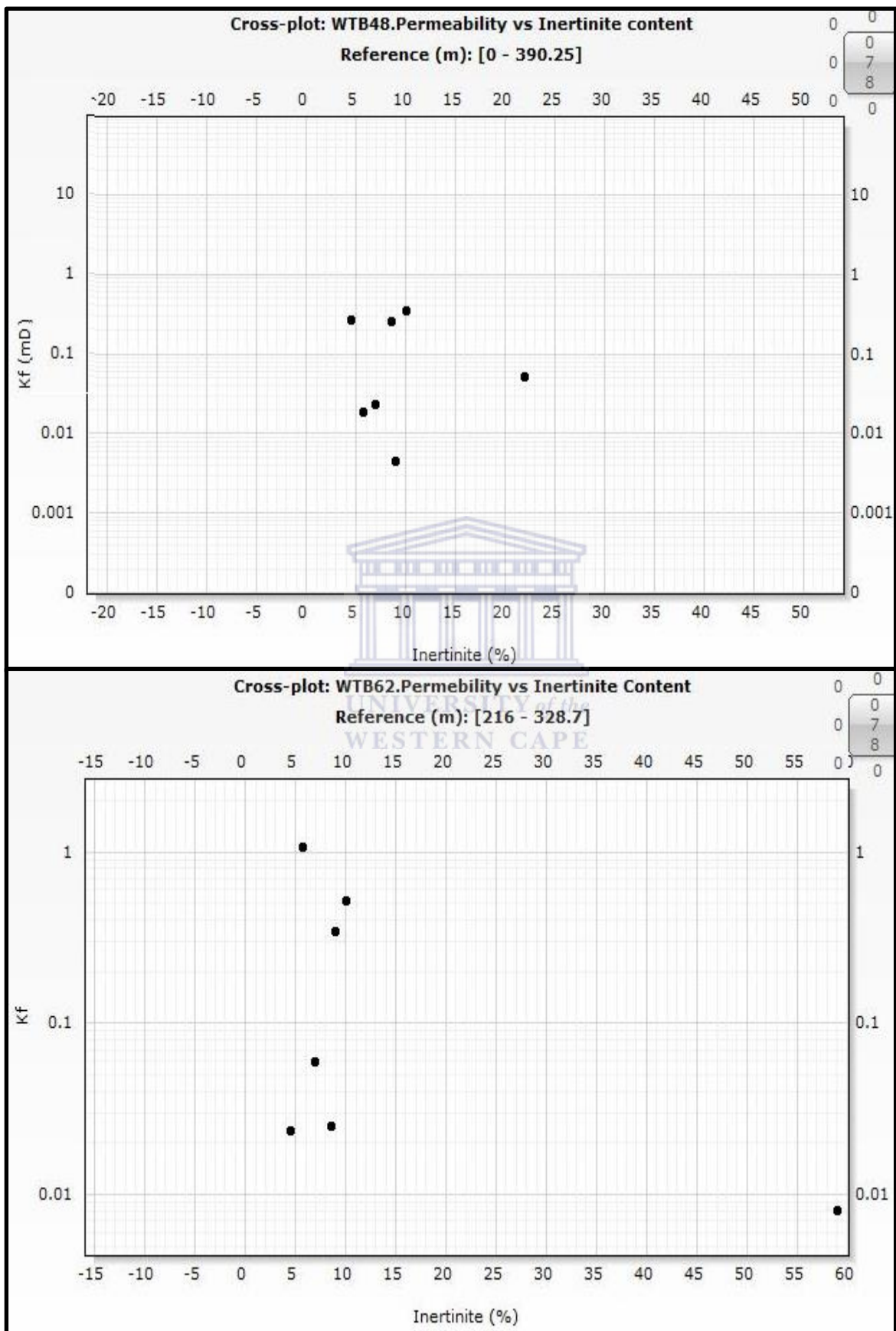


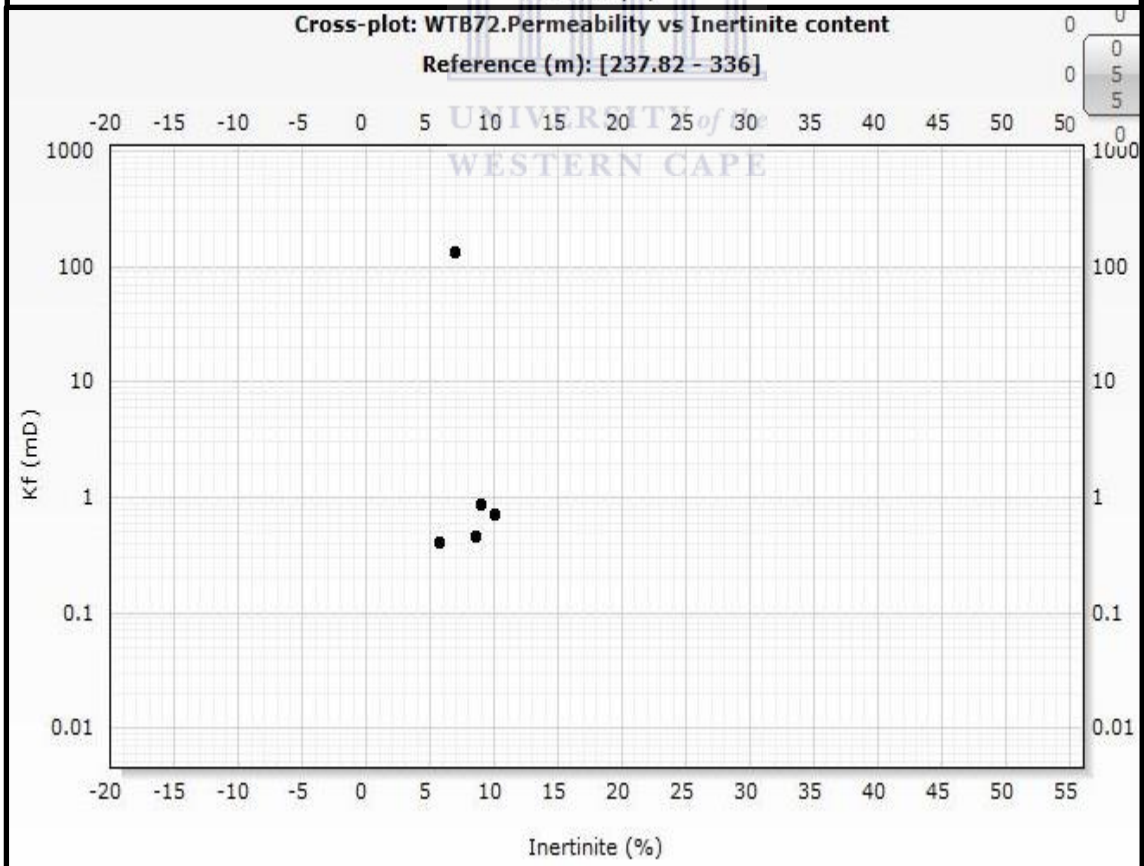
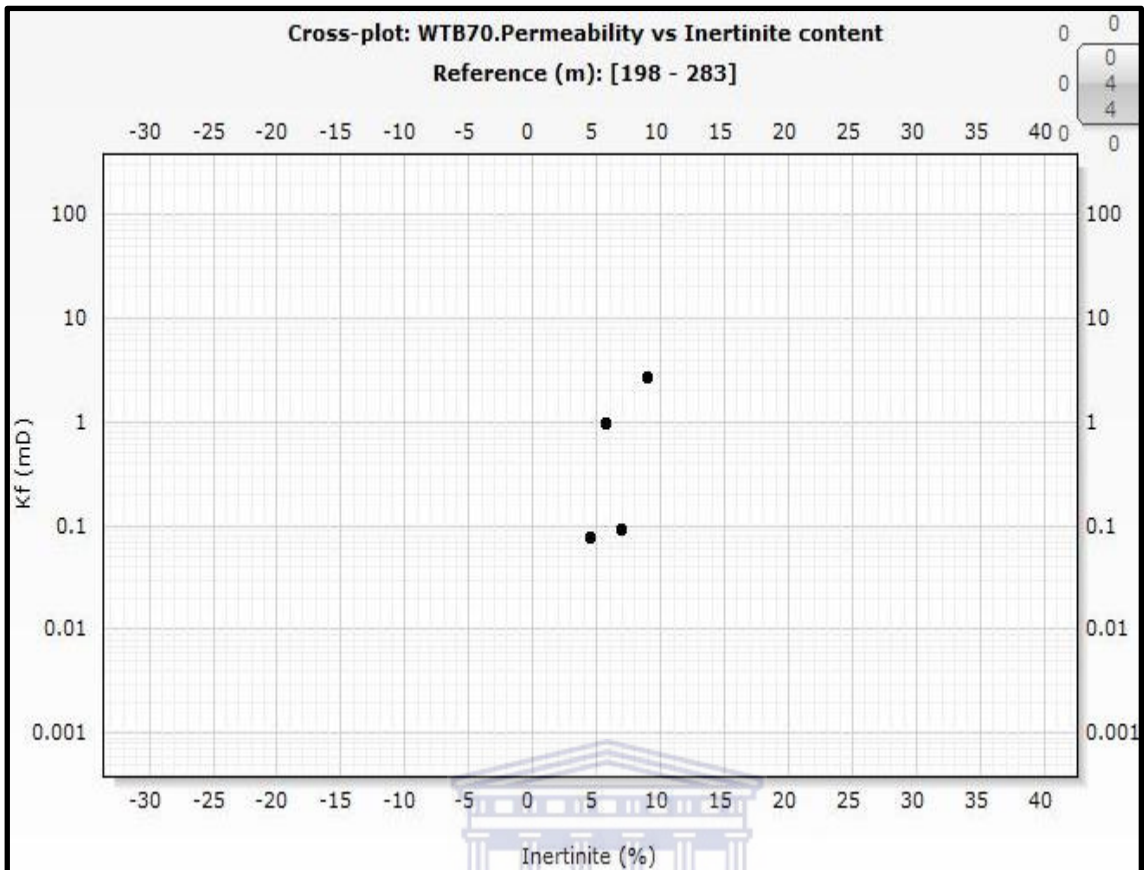
Appendix 10: Permeability vs Vitrinite content plots for WTB48, 70 and 72





Appendix 11: Permeability vs Inertinite Content Plots for WTB48, 62, 70, and 72





Appendix 12: Permeability vs Cementation Index plots for WTB45 and WTB70.

